DEVELOPMENT OF A MATHEMATICAL MODEL FOR BLOWDOWN OF VESSELS CONTAINING MULTI-COMPONENT HYDROCARBON MIXTURES

A thesis submitted to the University of London for the degree of Doctor of Philosophy

by

SHAN MENG ANGELA WONG B.Eng (Hons)

Department of Chemical Engineering
University College London
Torrington Place
London WC1E 7JE
June 1998

ABSTRACT

This thesis describes the development of a mathematical model, BLOWSIM, for simulating vapour space blowdown of an isolated vessel containing single (vapour) or two-phase (vapour and liquid) hydrocarbon mixtures based on three Cubic Equations of State (CEOS). These include Soaves Redlich-Kwong (SRK), Peng-Robinson (PR) and the recently developed Twu-Coon-Cunningham (TCC) CEOS.

The performances of the above equations are first evaluated by comparing their predictions for a range of important thermophysical properties (including vapour/liquid equilibrium data, speed of sound and fluid densities) with experimental data for single and multi-component hydrocarbon systems. These data are reported as a function of reduced pressures and temperatures in the ranges 0.00053 - 43.41 and 0.33 - 2.09 respectively. Typical systems tested include pure alkanes as well as mixtures containing methane, ethane, propane, H_2S, CO_2, N_2 and trace amounts of heavy hydrocarbons.

The above is then followed by applications of all three equations in the blowdown model and comparing the results with those obtained from a number of experiments relating to the blowdown of the various hydrocarbon systems from a maximum pressure of 120 atm and ambient temperature. Typical output include the variations of fluid pressure, temperature (both liquid and vapour), discharge rate as well as the wetted and unwetted wall temperatures with time.

Another major part of the study includes investigating the effects of different assumptions relating to the estimation of the liquid/wall heat transfer coefficient, the thermodynamic trajectory of the fluid in the vessel as well as the fluid phase at the orifice on blowdown predictions.

We find that in general all three CEOS provide a similar level of accuracy with TCC CEOS providing the best performance in terms of predicting vapour speed of sound at $P_r > 3$. However, the equation gives rise to relatively large errors in predicting liquid speed of sound at $T_r \leq 0.6$. Typical accuracy of the blowdown model in terms of predicting fluid and wall temperatures during depressurisation are $\pm$ 7 and 5 K respectively.

To my parents for their endless support,

encouragement and great understanding.

ACKNOWLEDGEMENTS

I would like to express my gratitude to the Crouch Foundation, the Society of Chemical Industry, the ORS Award scheme and the Graduate School of University College London for their financial support for this work.

My special thanks go to my supervisor, Dr Haroun Mahgerefteh for his excellent supervision, constant encouragement, and unlimited patience during the course of my research.

I would also like to thank Dr. Chorny H. Twu from Simulation Science, California, USA for many useful discussions relating to the work associated with equations of state.

Additionally, I would like to acknowledge the help with computer programming from Henry Tillotson of the Department of Information Systems at UCL.

Finally, it has been a pleasure to receive the help of many members of the Department, in particular Martin Vale and his colleagues of the electronic workshop.

LIST OF CONTENTS

CHAPTER 1

INTRODUCTION

The term blowdown refers to the rapid wanted depressurisation of a vessel. In the offshore industry for example, blowdown of vessels or sections containing hydrocarbons is a common way of reducing the failure hazard in an emergency situation.

In recent years such operations have presented process and safety engineers with a dilemma.

The primary aim of blowdown is to reduce the pressure and inventory in the least amount of time possible. However, rapid depressurisation results in a dramatic drop in the fluid temperature and also tremendous heat transfer between the fluid and the vessel wall which lead to a reduction of wall temperature. If the wall temperature falls below the ductile-brittle transition temperature of the vessel material, rupture is likely to occur. Low fluid temperatures can also lead to the formation of solid hydrates in cases where free water is present in the vessel. The presence of solid hydrate can cause great difficulties in operations [Katz & Lee, 1990].

Clearly the optimum blowdown time requires a delicate balance between the maximum permissible blowdown duration and the minimum wall and fluid temperatures that may be safely accommodated.

Consequently, in recent years there have been a number of theoretical and experimental studies addressing the above issues. The theoretical models primarily fall into two categories; those on the basis of simplified relations [API, 1990; Montgomery, 1995; Reynolds & Kays, 1958] which are either not capable of predicting wall and fluid temperatures accurately or are applicable to non-condensable gases only. In the majority of cases, these models lead to gross over estimations which will in turn require considerable capital equipment expenditure. The second category are those based on rigorous analytical procedures such as those proposed by Haque et al. [1992a] and Overa et al. [1994]. The main drawback in the

former model is associated with the use of the extended principle of corresponding states [Rowlinson & Watson, 1969] for generating fluid thermodynamic properties which as well as uncertainties associated with its accuracy, makes the simulation computationally demanding. This also presents consistency problems as in practice, cubic equations of state (CEOS) are almost universally used in process simulations. Additionally, important information relating to the formulation of the model is not available in the open literature.

On the other hand, Overa et al.[1994] assume single phase discharge (this may be inappropriate in many practical situations) as well as a constant heat transfer coefficient for the liquid phase. The effect of the latter assumption on blowdown data has not been investigated.

The purpose of the present study is to develop a mathematical simulation, named BLOWSIM based on CEOS for blowdown of vessels containing single (vapour) or two-phase (vapour and liquid) hydrocarbon mixtures. The model is computationally efficient, requires the minimum number of input parameters whilst at the same time produces good predictions with acceptable engineering accuracy as compared to experimental data. In addition, various modifications to the simulation are introduced in order to identify and quantify the importance of taking into account the different processes taking place during blowdown. An important part of the study involves a detailed evaluation of the performance of the recently developed TCC CEOS [Twu et al., 1992] which has been particularly designed to address some of the shortcomings associated with SRK [Soave, 1972] and PR CEOS [Peng & Robinson, 1976] employed in this study.

The study is divided into 7 chapters.

In chapter 2, published experimental studies on blowdown reported in the past 40 years are reviewed. These primarily identify the nature of the various processes taking place during blowdown.

In chapter 3, the most important mathematical models reported in the open literature for blowdown of isolated vessels, with no chemical reaction, under non fire situations

are reviewed. It starts with a description of commonly used industrial methods based on engineering practice for blowdown calculation and is followed by introducing simple mathematical models for blowdown of non-condensable gases. The chapter is concluded by reviewing BLOWDOWN [Haque et al., 1992a] and SPLIT FLUID MODEL [Overa et al., 1994] in detail for blowdown of condensable gases or two-phase mixtures.

Chapter 4 describes the mathematical model, BLOWSIM developed in this study for vapour space blowdown through a single orifice from the top of an isolated vessel containing single (vapour) or two-phase (vapour and liquid) hydrocarbon mixtures. In the same chapter, the model is used to identify the level of detail required for blowdown modelling as well as addressing the following issues :

1) The effects of applying various cubic equations of state on the performance of blowdown simulation in terms of predicting field data.

2) The suitability of different thermodynamic trajectories for vapour phase expansion during blowdown of hydrocarbon mixtures from elevated pressures.

3) The effects of applying different thermodynamic trajectories to the liquid phase in terms of the accuracy in predicting temperatures and pressures.

4) The effect of Overa et al.'s [1994] suggested constant heat transfer coefficients between liquid and wetted wall compared to the boiling heat flux empirical correlation employed by Haque et al. [1992a] on the accuracy of the predicted liquid and wetted wall temperatures.

5) Comparisons of the rigorous [Haque et al., 1992a] against simple discharge calculation methods (based on ideal gas assumption) in terms of predicting temperatures and pressures during blowdown.

In chapter 5, the Soave Redlich-Kwong, SRK [Soave, 1972], Peng-Robinson, PR, [Peng & Robinson, 1976] CEOS for generating the required thermodynamic properties for blowdown simulation are presented and discussed. The newly developed Twu-Coon-Cunningham, TCC, CEOS [Twu et al., 1992] aimed at

addressing some of the drawbacks of these equations is also given. This is followed by the derivation of the appropriate equations for determining specific heat capacities, speed of sound and thermal expansion coefficient based on TCC CEOS. Finally the performance of the above CEOS in predicting the required important parameters for blowdown calculation (e.g. densities and speeds of sound for vapour and liquid, as well as liquid volume percentage) for single and multi-component hydrocarbon systems are investigated by comparison with published experimental values. Mixtures containing light hydrocarbons are mainly considered as vapour space blowdown is always used for the process gas stream.

In chapter 6, the results obtained from BLOWSIM are compared against those predicted from BLOWDOWN, and published experimental data for high pressure blowdown of a full-size vessel containing various hydrocarbon mixtures. These include, non-condensable gas, condensable gas and two-phase mixtures. In each and every case, the effects of incorporating any one of the three CEOS on the results predicted by BLOWSIM are evaluated. The latter include pressure/time and temperature/time profiles for the vessel wall (both wet and dry), the bulk gas and where applicable, for the bulk liquid. Additionally, the effects of accounting for or discounting the work done by the liquid phase on the results obtained using BLOWSIM are investigated. This is followed by an investigation of the effects in applying various selected heat transfer coefficients between vessel wall and the liquid phase within the vessel on BLOWSIM's predictions. The final part of the chapter investigates the performance of BLOWSIM based on either ideal gas assumption or real fluid approach at the discharge orifice in terms of minimum temperature predictions and computational time.

Chapter 7 deals with general conclusions and suggestions for future work.

CHAPTER 2

VAPOUR SPACE BLOWDOWN PHENOMENA

2.1 INTRODUCTION

In recent years, a number of experimental studies have been conducted by various researchers to study blowdown. Table 2.1 presents a summary of these investigations carried out in the past 40 years and the corresponding experimental conditions. This chapter describes the salient features of these studies with a particular emphasis in highlighting the various processes taking place during blowdown. A review of published models for simulating blowdown is given in chapter 3 .

2.2 VAPOUR SPACE BLOWDOWN

During vapour space blowdown of a hydrocarbon mixture, the gas within the vessel initially expands rapidly and follows an isentropic path which leads to very low gas temperatures. However, substantial heat transfer takes place between the gas and vessel wall which prevents it from reaching the isentropic temperature. Condensation of heavier gaseous hydrocarbon components can still occur when the gas enters the two-phase region.

For a vessel initially containing gas phase only, condensation will lead to accumulation of liquid at the bottom of the vessel. The pool of liquid will be boiling vigorously because it is in contact with the relatively warm vessel wall [Haque et al., 1990; 1992b]. If the fluid is initially two-phase (vapour and liquid), liquid droplets will be added to the existing boiling liquid (due to reduction of pressure) within the vessel and evaporation of lighter liquid components will take place [Haque et al., 1992a]. Hence, the temperatures of liquid and vessel wall will drop.

The results of various studies [Eggers & Green, 1990; Haque et al., 1992b and Overa et al., 1994] have shown that there are significant temperature differences between different fluid phases during blowdown. This is a clear indication of non-equilibrium between phases. The temperature differences also cause non-uniform wall temperatures along the vessel. The differences in vessel wall

Table 2.1 Summary of vapour space blowdown studies in recent years.

Year	Researchers	Fluid	Vessel		Initial Conditions			Measured Parameters	Comments
			vol. (m^3)	orientation	phase	P (atm)	T (K)		
1958	Reynolds & Kays	Air	0.03785	Vertical	Gas	7.8	338.6	Variations of bulk gas temperatures and pressures with time.	Blowdown time was 20 s.
1961	Potter & Levy	Moist air (humidity were 78 and 82 %)	0.05873	Horizontal	Gas	5.4	300	Variations of bulk gas temperatures and pressures with time.	Gas temperatures were measured in four different positions along the axis of the cylinder. Blowdown times were, 16, 55 & 212 s.
1964	Byrns et al.	H_2	0.05	Horizontal	Gas	135.2	294 - 300	Variations of pressures, bulk gas and wall temperatures.	Gas temperatures were measured in two positions, at the neck and mid-height of the bottom. Wall temperatures were measured in various positions along the cylinder. Blowdown times were, 14, 30 & 480 s.

Table 2.1 Summary of vapour space blowdown studies in recent years. (Continued)

Year	Researchers	Fluid	Vessel		Initial Conditions			Measured Parameters	Comments
			vol. (m^3)	orientation	phase	P (atm)	T (K)		
1990	Haque et al.	N_2	0.089	Vertical	Gas	148	290	Variations of pressures, bulk gas and wall temperatures with time	64 thermocouples were used at various positions. Blowdown time was 100 s
		N_2 ,70 mol.%, CO_2 , 30 mol.%	0.089	Vertical	Gas	148	290	Same as above	Same as above
1990	Eggers & Green	CO_2	0.05	Vertical	86 vol. % of liquid CO_2	59.2	295	Variations of pressure, bulk gas and wall temperatures with time	Blowdown time were 400 and 3000 s.
1992b	Haque et al.	C_1 , 85.5 mol.%; C_2 , 4.5 mol.%; C_3, 10.0 mol.%	2.78	Vertical	Gas	118.4	303	Variations of pressures, bulk gas, liquid and wall temperatures with time	120 thermocouples were used at various positions. Blowdown time was 1500 s.
		C_1 , 66.5 mol.%; C_2 , 3.5 mol.%; C_3, 30.0 mol.%	2.78	Vertical	Gas	118.4	303	Same as above.	Same as above

Table 2.1 Summary of vapour space blowdown studies in recent years. (Continued)

Year	Researchers	Fluid	Vessel		Initial Conditions			Measured Parameters	Comments
			vol. (m^3)	orientation	phase	P (atm)	T (K)		
1993	Norris III	Air	0.05	Vertical	Gas	135.2	313	Variation of bulk gas temperatures with time.	Blowdown time was 125 s.
1994	Norris III	C_1, 91.51 mol.%; C_2, 5.27 mol.%; C_3, 3.22 mol.%	0.15	Vertical	Gas	101.7	300	Variation of bulk gas temperatures with time.	Blowdown time was 40 s.
1994	Overa et al.	N_2, Air	Small vessel (vol. is not specified)	Not specified	Gas	175.7	295	Variations of bulk gas and wall temperatures with time.	Blowdown time was 240 s.
		Hydrocarbon gas and unstabilized oil	0.85	Vertical	Gas and liquid	20.2	298	Variations of bulk gas and liquid temperatures with time.	Blowdown time was 1320 s.

and fluid temperatures are maintained for a significant period of time [Haque et al., 1992b; Overa et al., 1994]. The following describes the main features of heat transfer effects between vessel wall and vapour space, vessel wall and liquid space, vessel and surrounding, heat and mass transfer between fluid phases and flow through the relief valve during blowdown.

2.2.1 Heat Transfer between Vessel Wall and Vapour Space

Blowdown of non-condensable gases have been studied for a number of years as indicated in table 2.1 which also gives the pertaining experimental conditions. Reynolds and Kays [1958] for example analysed experimentally the discharge of a small air tank for a short time (ca. 20 s) by measuring the bulk gas temperatures. Their results indicated that in practice, the reduction in the bulk gas temperatures does not follow the isentropic path concluding that heat transfer between the gas and wall is significant. The authors developed a method for predicting gas temperatures by assuming natural convection taking place in the vessel. The effect of forced convection due to discharged gas was ignored. Calculated gas temperatures agreed well with the experimental values.

Potter and Levy [1961] found that during depressurisation of moist air cylinders, the gas temperatures deviated from isentropic temperatures and passed through a minimum followed by an increase near the end of the tests. Byrnes et al. [1964] conducted experiments using a small hydrogen tank for different blowdown times (see table 2.1). The eventual recovery in the temperature of the gas was considered to be due to the increasingly pronounced effect of heat transfer between the gas and vessel wall. On the bases of Reynolds and Kays' [1958] conclusion regarding natural convection, the authors developed a method for estimating gas temperatures which was capable of providing a fair agreement between calculated and measured values. These studies were mainly restricted to small scale non-hydrocarbon fluids in which natural convection was the main mode of heat transfer as opposed to forced convection. The wall temperature of hydrogen tank during blowdown was measured by Bynes et al.. In all cases, the wall temperature did not drop as low as the gas

temperatures. This was mainly attributed to the low gas heat transfer coefficient and the relatively high heat capacity of the vessel wall.

More recently, relatively high pressure blowdown experiments have been conducted for both hydrocarbons and non-hydrocarbons using different scale plant. Haque et al. [1990, 1992b] for example presented experimental data for depressurising a small vessel containing either pure nitrogen or its mixture with carbon dioxide (70 mole % nitrogen, 30 mole % carbon dioxide) and full scale vessels containing hydrocarbon gas mixtures at high pressures (see table 2.1 for initial operating conditions). Nitrogen was used as a non-condensable gas whilst the nitrogen and hydrocarbon gas mixtures represented a condensable gas. The fluid and wall temperatures were measured at various positions along the vessel using 76 thermocouples for the small vessel and 156 thermocouples for the full scale vessel.

The variations of measured bulk fluid and wall temperatures with time for nitrogen and the hydrocarbon gas mixture are shown in figures 2.1 - 2.3. The grey regions show experimental measurements whilst the solid lines show the predictions from BLOWDOWN [Haque et al., 1992a]. The pressure/time profile for the hydrocarbon gas mixture is shown in figure 2.4. Figure 2.5 shows the isotherms and flow pattern during blowdown of nitrogen.

Overa et al. [1994] presented experimental data for depressurising a vessel containing a hydrocarbon gas and unstablised oil (composition was not specified). The variations of measured bulk fluid temperatures with time is shown in figure 2.6. The solid lines represent predictions from a computer program based on the SPLIT FLUID MODEL developed by the same authors. The initial operating conditions are given in table 2.1.

Referring to figures 2.1 and 2.2, the grey regions representing the measured bulk gas temperatures are a clear indication of presence of temperature gradients which in turn give rise to density differences within the vapour phase especially after an extended period of time. Figure 2.5 on the other hand, indicates the presence of large temperature gradients near the walls of the vessel which lead to significant natural convection within the vessel. The same observation was also made by Overa et al.

[1994] who measured gas temperatures during blowdown at different elevations along the vessel and filmed the outside of the vessel with a heat sensitive film. The authors were able to map the fluid flow pattern for the vapour space during blowdown indicating the prevalence of natural convection for a variety of blowdown tests. Figure 2.7 shows the general pattern. These flow patterns are very similar to those generated by Haque et al. [1992b] as shown in figure 2.5.

Overa et al. [1994] interpreted the presence of temperature gradients in vapour phase during blowdown as a result of warming effect of cold vapour by the warmer vessel wall and accumulation of colder vapour in the bottom of the vessel. Haque et al. [1992a] also pointed out that natural convection is pronounced especially at high pressures due to low viscous effects which facilitates natural convection. The predominant effect of natural convection was also observed by Overa et al., [1994] during experiments with vessels containing substantially warmer liquid where cold gas would accumulate immediately above the liquid.

Returning to figures 2.1 and 2.2, the bulk gas temperatures pass through a minimum and rise near the end of blowdown. This has been explained by the competition of two processes; gas expansion cooling and convection heating of the gas by vessel wall. Referring to figure 2.4, at the beginning of blowdown (before 500 s), the rate of depressurisation is so high that the gas temperature drops very rapidly due to expansion as compared to relatively slow process of natural convection. After 500 s (figure 2.4), the depressurisation rate slows down and the effect of heat transfer between gas and vessel wall dominates the gas expansion cooling effects. As a result, the gas temperature rises.

Norris [1993, 1994] also made the same observation during the blowdown of high pressure vessels containing air or a hydrocarbon gas mixture. The experimental conditions can be found in table 2.1. Same mechanisms described above can be used to explain the observed bulk gas temperature profile shown in figure 2.6 by Overa et al. [1994]. Interestingly, the data indicate two local minima instead of one in the measured bulk gas temperatures. The authors attributed this to severe turbulence in

vapour phase and possibly liquid entrainment on the thermocouples which led to erratic vapour temperature measurements.

The temperature of the wall in contact with vapour as shown in figures 2.1 and 2.3 do not drop as low as that of the gas. This is mainly due to low gas heat transfer coefficient and the high heat capacity of the vessel wall. However, from figure 2.3, the lowest wall temperature is located in the regions in contact with the liquid phase.

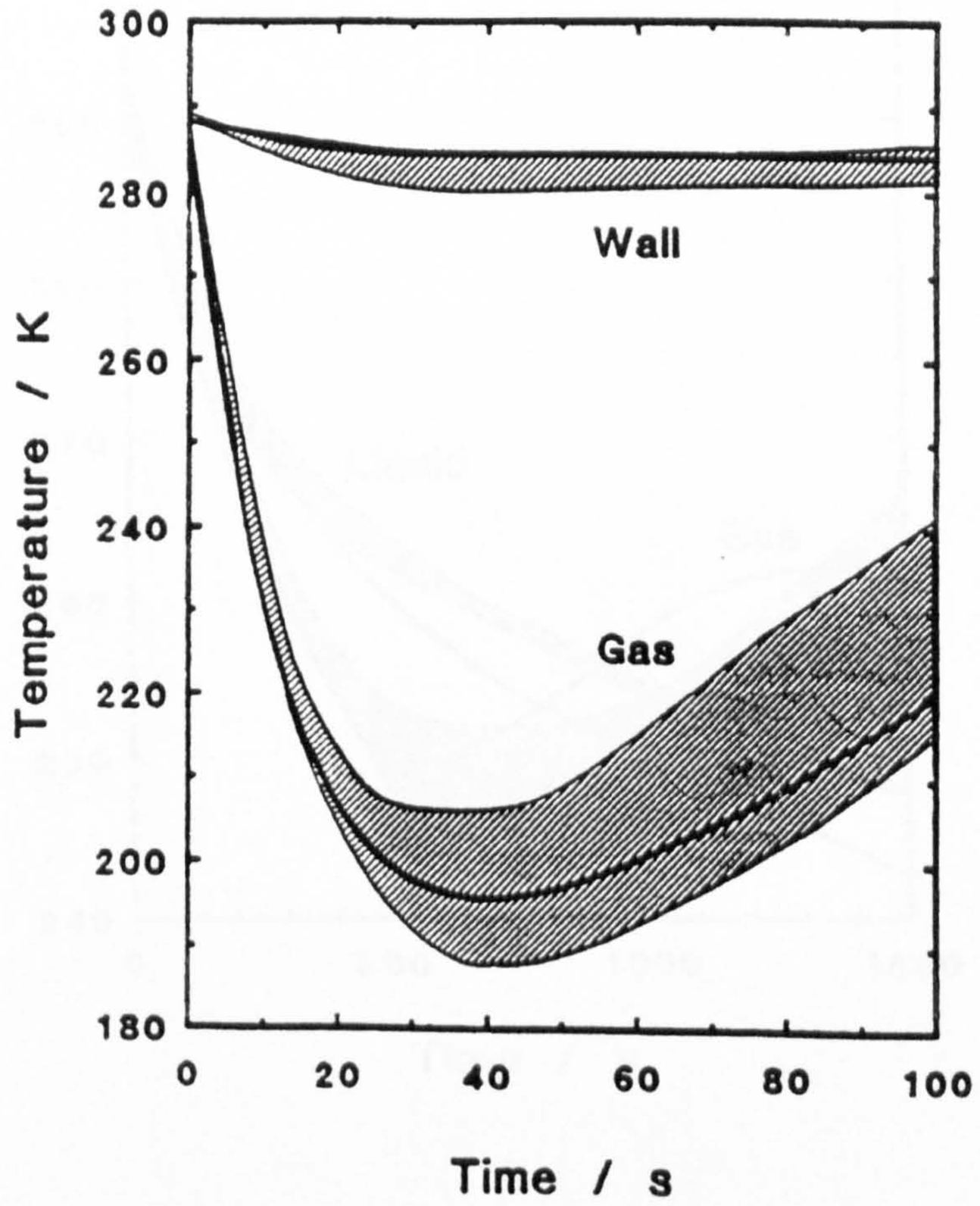

Figure 2.1 Variations of bulk gas and inside wall temperatures with time for depressurisation of nitrogen (Hatched regions span experimental measurements, solid lines are predictions from BLOWDOWN) [Haque et al. 1992b]

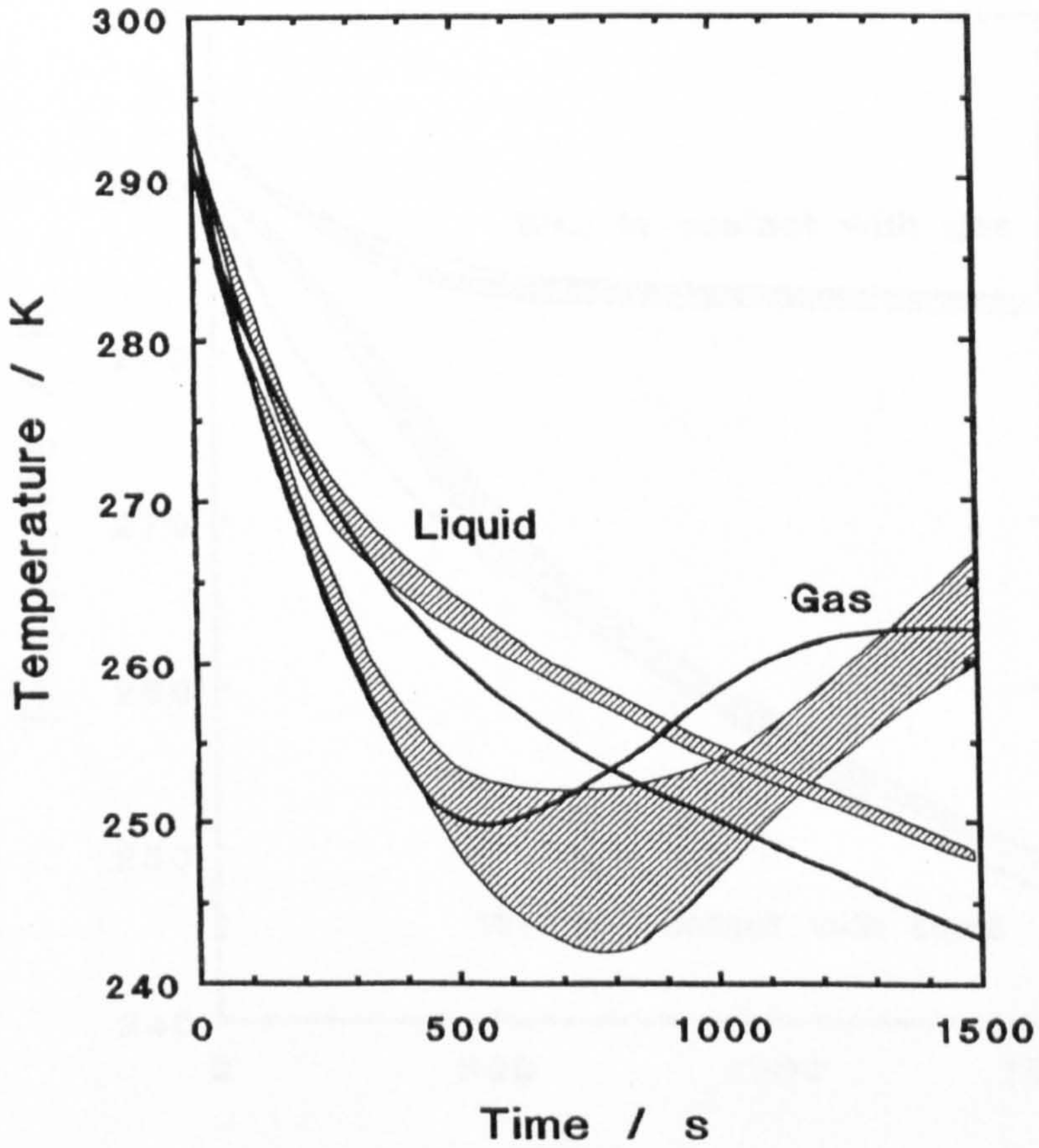

Figure 2.2 Variations of bulk gas and bulk liquid temperatures with time for depressurisation of a hydrocarbon mixture containing 66.5% mole methane, 3.5 mole % ethane, 30.0 mole % propane and traces of higher molecular weight hydrocarbons in particular of butanes (Hatched regions span experimental measurements, solid lines are predictions from BLOWDOWN) [Haque et al. 1992b]

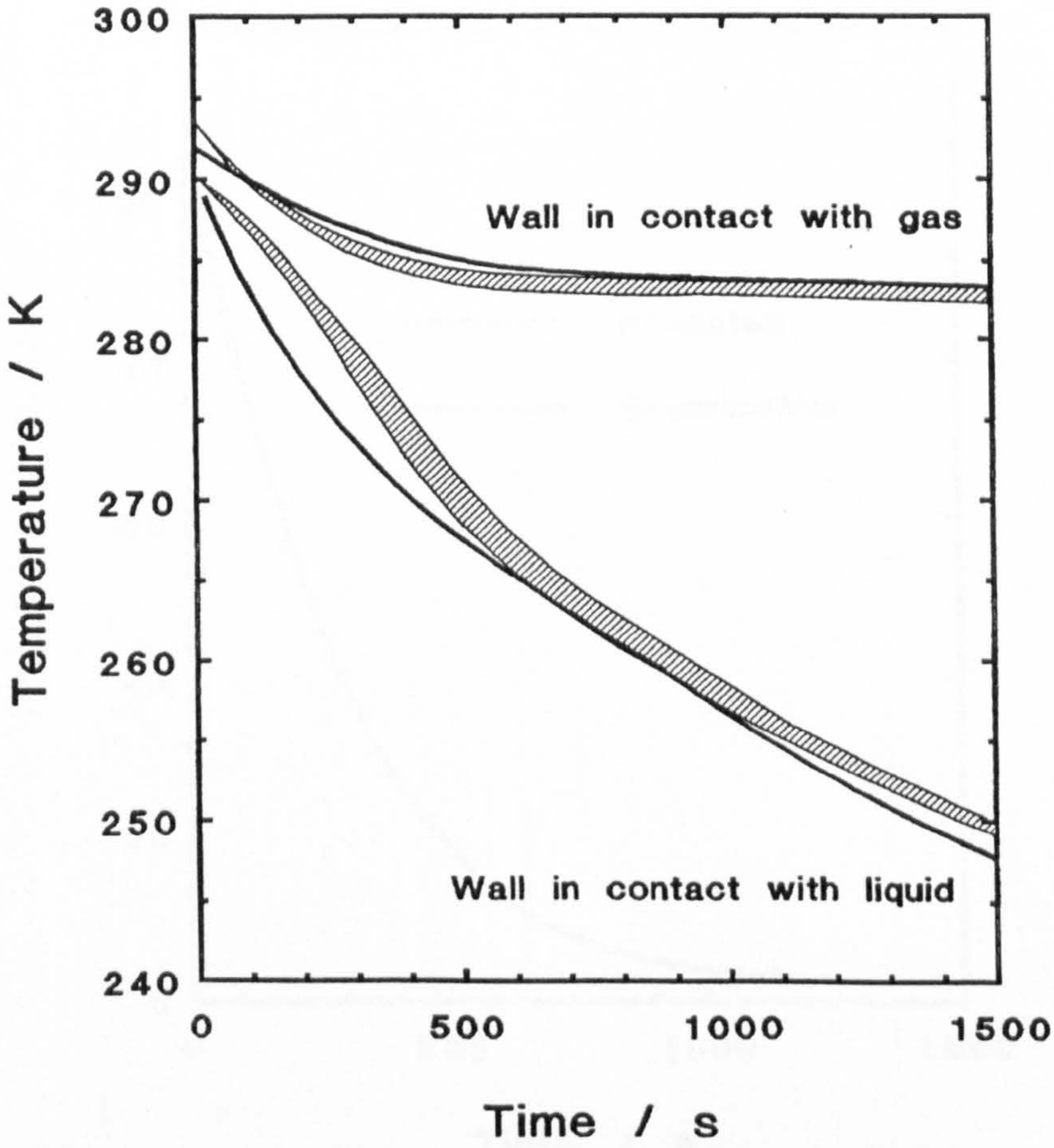

Figure 2.3 Variations of inside wall temperatures with time for depressurisation of a hydrocarbon mixture containing 66.5% mole methane, 3.5 mole % ethane, 30.0 mole % propane and traces of higher molecular weight hydrocarbons in particular of butanes (Hatched regions span experimental measurements, solid lines are predictions from BLOWDOWN) [Haque et al. 1992b]

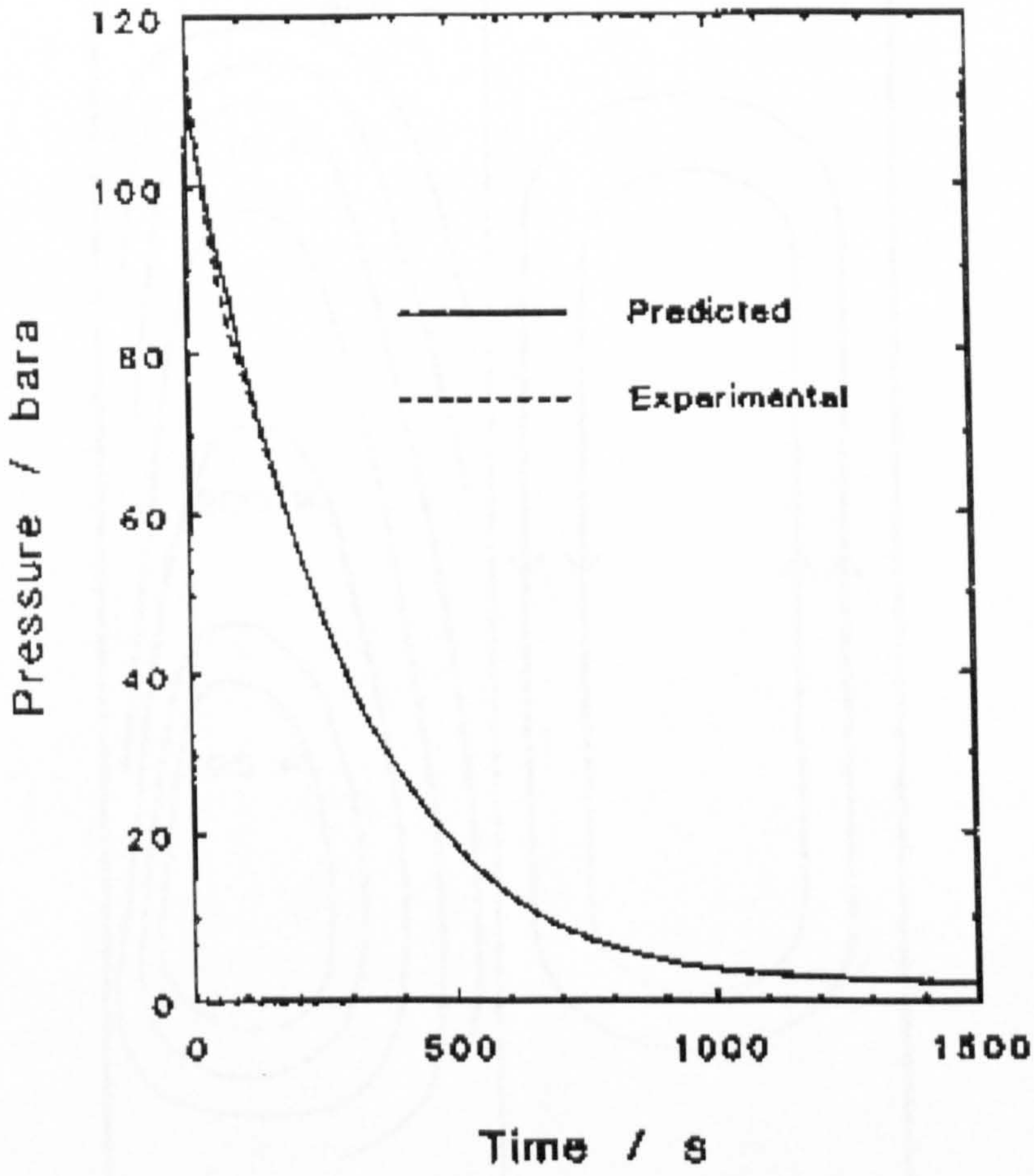

Figure 2.4 Variation of pressure with time for depressurisation of a hydrocarbon mixture containing 66.5% mole methane, 3.5 mole % ethane, 30.0 mole % propane and traces of higher molecular weight hydrocarbons in particular of butanes (Solid line is prediction from BLOWDOWN) [Haque et al. 1992b]

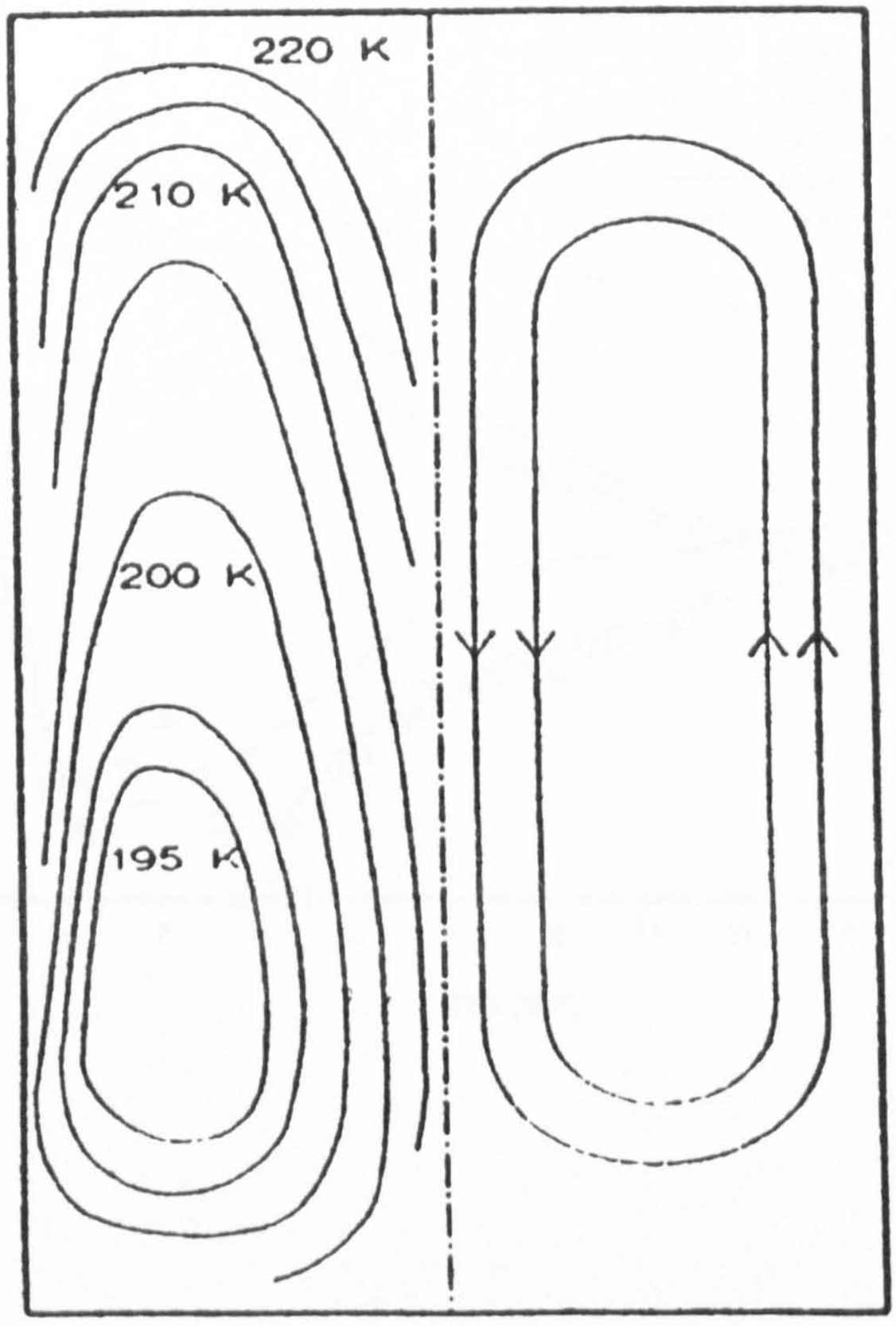

Figure 2.5 Isotherms (left-hand side) and flow pattern (right-hand side) during blowdown of nitrogen [Haque et al., 1992b]

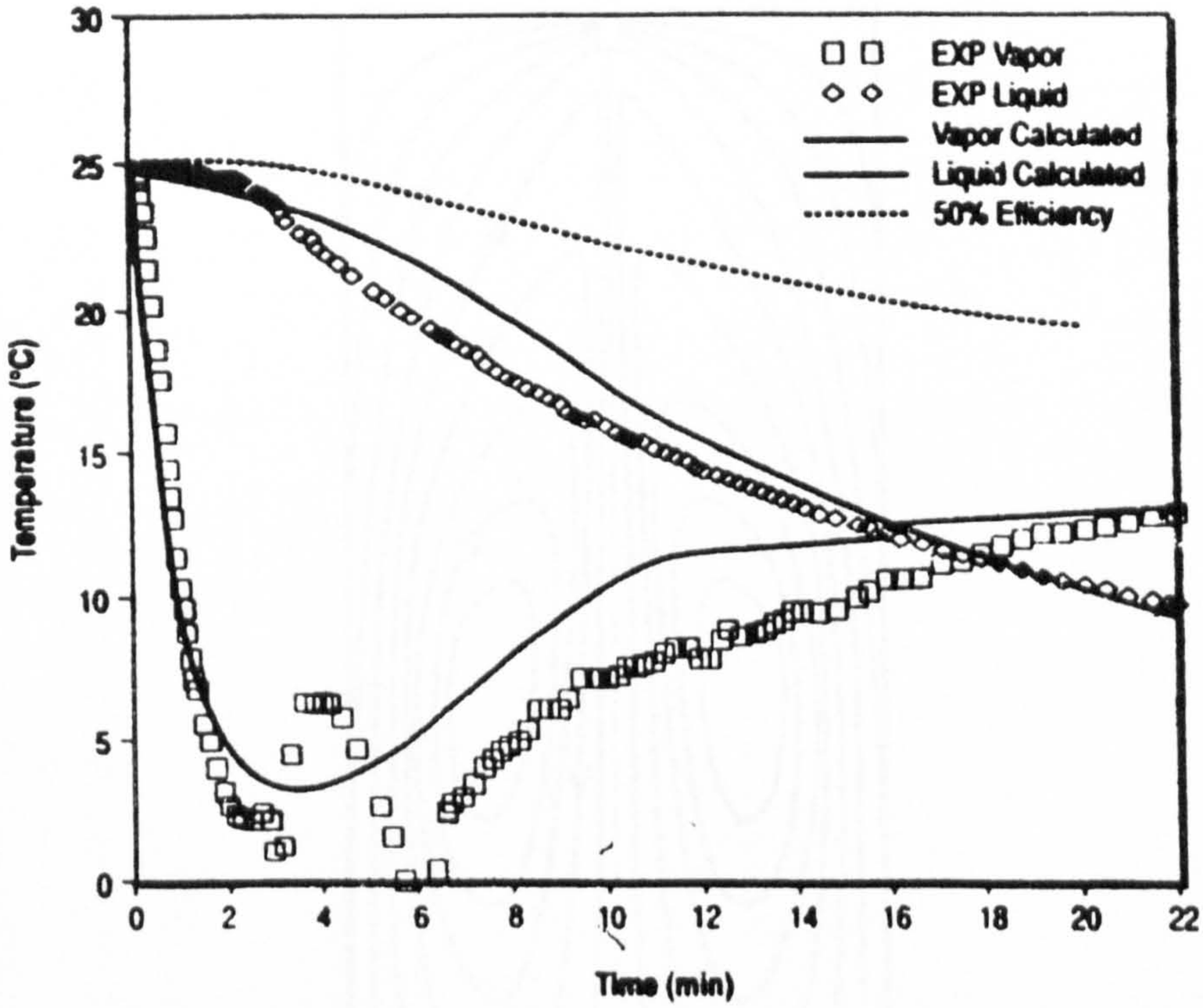

Figure 2.6 Variations of bulk gas and bulk liquid temperatures with time for depressurisation of a hydrocarbon two-phase mixture [Overa et al., 1994]

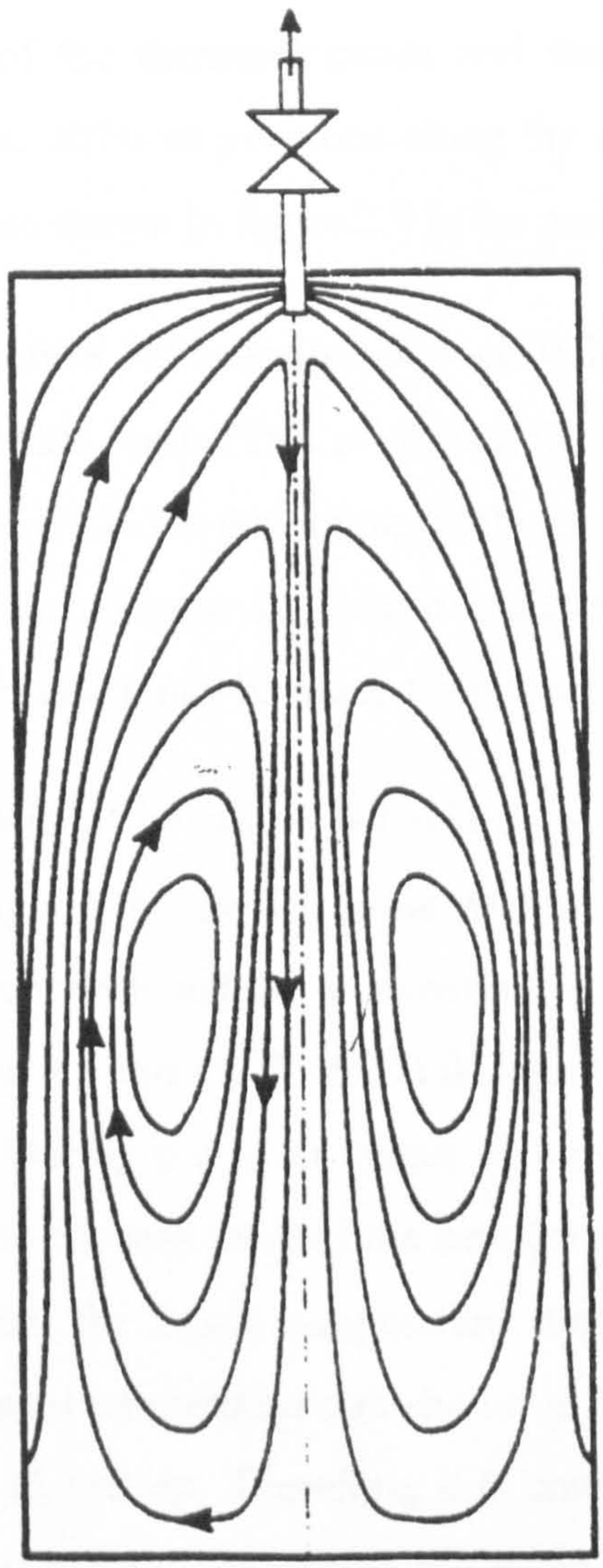

Figure 2.7 Flow pattern of gas phase in a vertical vessel during blowdown [Overa et al., 1994]

2.2.2 Heat Transfer between Vessel Wall and Liquid Space

Eggers and Green [1990] presented results of depressurising a small vessel containing 86 vol. % of liquid carbon dioxide (see table 2.1 for experimental conditions). The location of the thermoelements and the corresponding recorded temperatures/time profiles at different positions along the tank are shown in figures 2.8 and 2.9 respectively. Also shown in figure 2.9 is the pressure/time profile.

Figure 2.9 indicates that before formation of dry ice (where the pressure remains constant) the liquid temperature (curve T6) is very similar to the temperature of the inner wall by the liquid (curve T11) at the bottom of the tank. The similarity of liquid and inner wall temperatures indicates good heat transfer between the liquid and vessel wall. The same observation may be made from the data in figures 2.2 and 2.3.

Haque et al. [1992a] explained the above behaviour by attributing it to nucleate, transition and film boiling of the liquid phase which yields high heat transfer coefficients when compared with natural convection in gas phase [Welty et al., 1984]. Therefore, as shown in figure 2.2, the bulk liquid temperatures are initially higher than the bulk gas. During the latter stages of blowdown, due to the rise of vapour temperature and also because most of the heat from the vessel wall in contact with the liquid is removed, the liquid temperature drops below that of the gas. Consequently, the vessel wall temperatures as shown in figure 2.3 are lower at the bottom of the vessel than at the top. Therefore, it is common to find the minimum wall temperature located at the bottom part of the vessel where liquid (either from condensation of gas or existing liquid) is present. Note, incidentally, that, while there is some spatial variation in bulk gas temperature, there is very little spatial variation in bulk liquid temperature. This is because the intense boiling in the liquid gives rise to very rapid mixing and hence thermal equilibration.

Another interesting observation by Haque et al. [1990] relating to the blowdown of a condensable gas is a rise followed by a decrease of condensate temperature. Such data for a nitrogen and carbon dioxide mixture is shown in figure 2.10. The upper band refers to bottom zone (condensate) temperatures and the lower band to top zone (vapour) temperatures. The corresponding predictions using BLOWDOWN are also

shown. The liquid level is only a few centimetres deep compared to the vessel height of 1.5 m. The authors attributed this behaviour to the warming effect of the relatively warm vessel wall in contact with the small amount of condensate formed. The more volatile components were driven off and thereby raising the boiling temperature. During the latter stage of depressurisation, due to expansion, more and more condensate was formed in the upper part of the vessel. This fell to the bottom and as the bottom of the vessel itself was cooled, the evaporation rate fell off and a pool of liquid gradually accumulated. Since the pressure in the system was still falling, the liquid experienced evaporative cooling. It is interesting to note that the sudden increase of liquid temperatures is not found in figure 2.2 where the condensate level was reported to be appreciably higher compared to the vessel height.

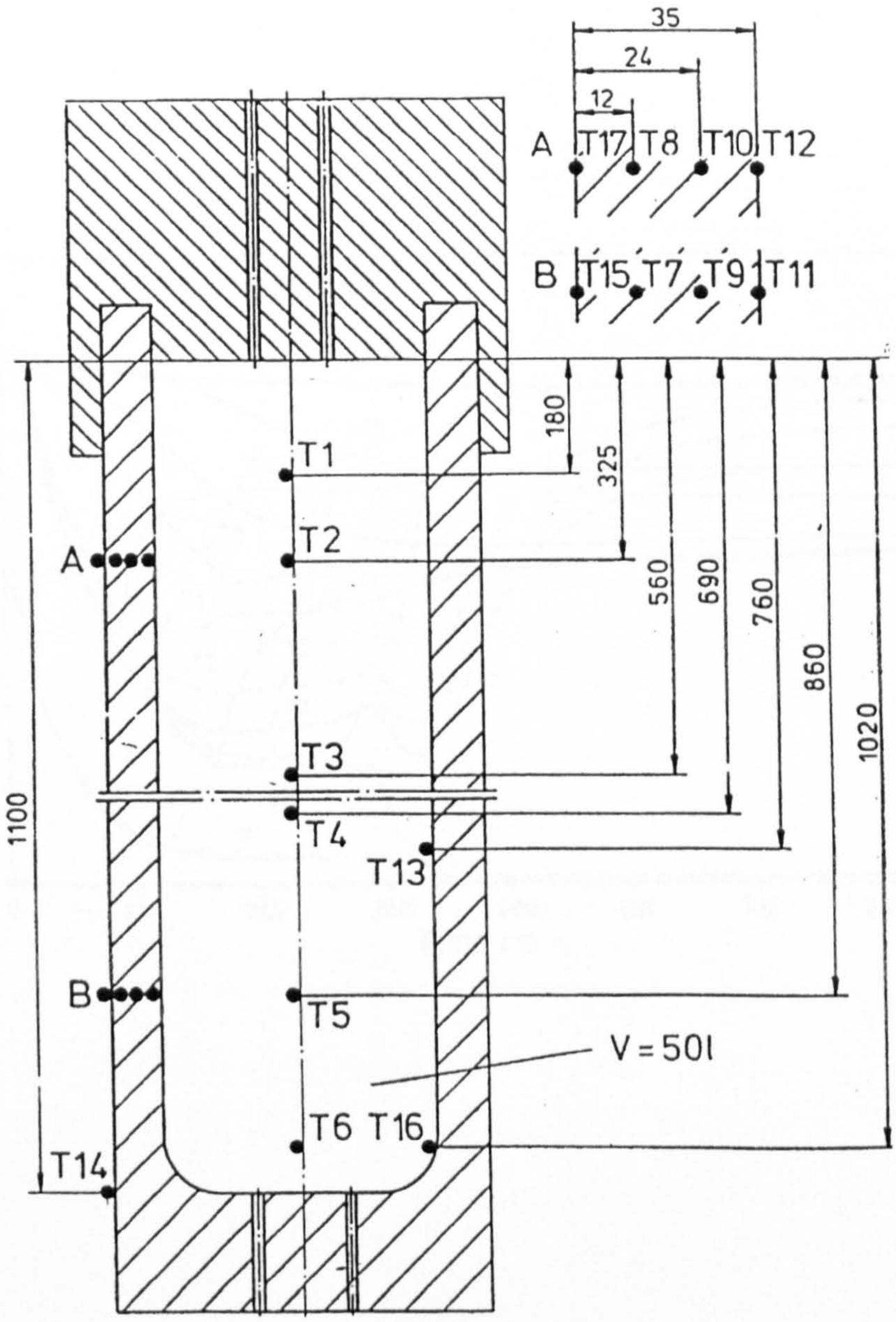

Figure 2.8 **Schedule of thermoelements positions of tank containing carbon dioxide [Eggers & Green, 1990]**

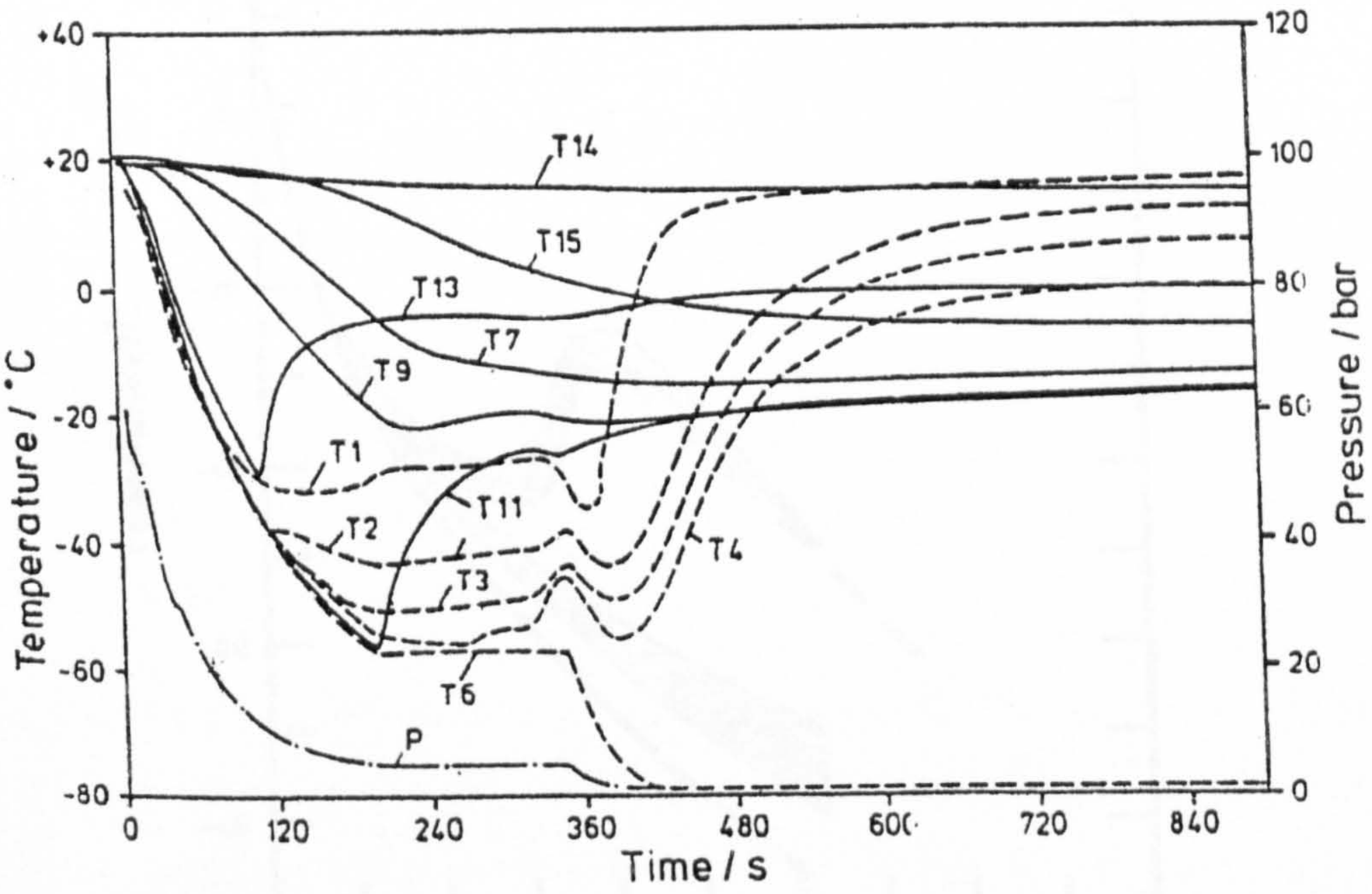

Figure 2.9 **Time profiles of pressure and fluid and wall temperatures (blowdown time is 400 s) of a carbon dioxide tank [Eggers & Green, 1990]**

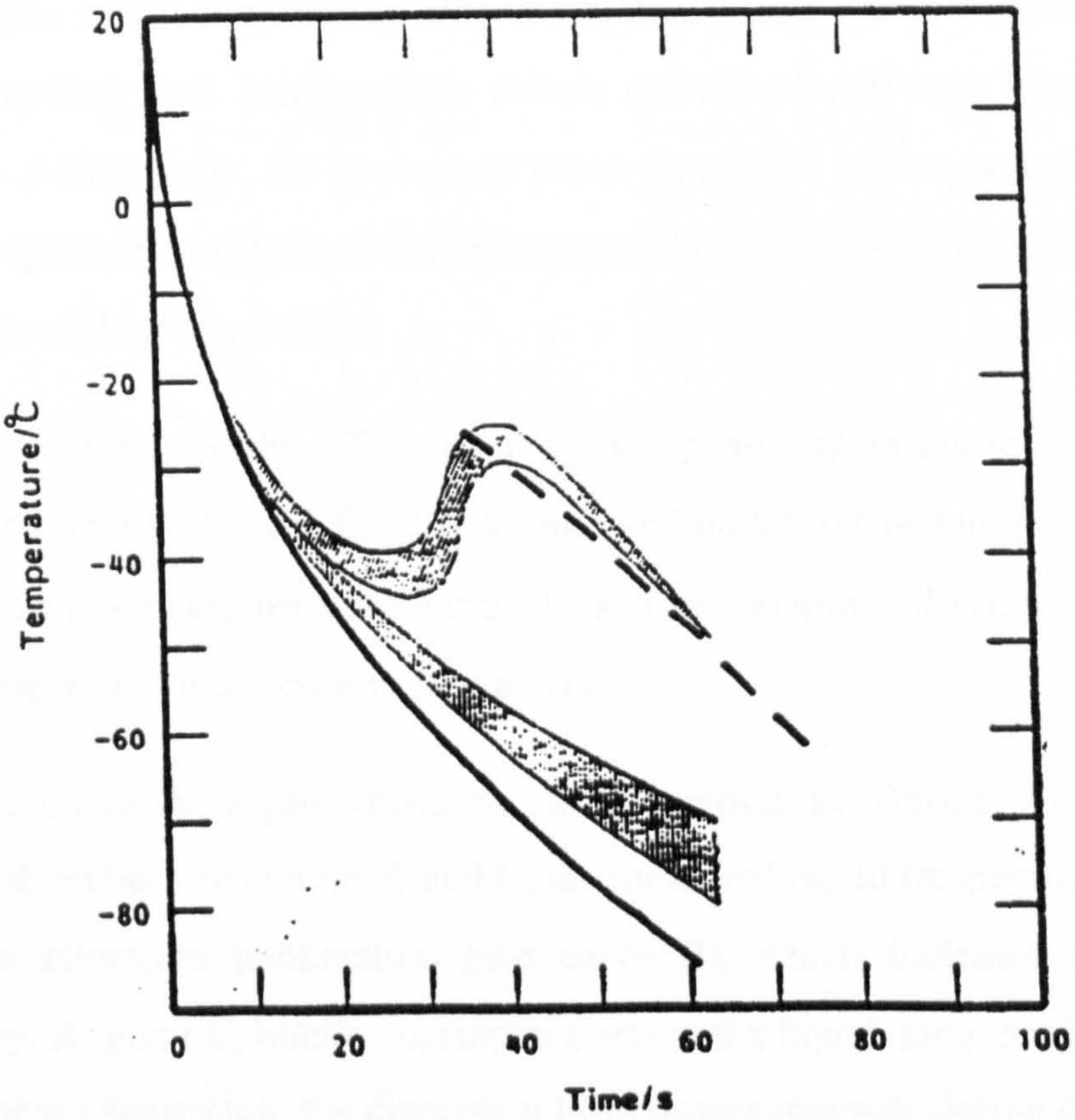

Figure 2.10 Variations of bulk gas and bulk liquid (condensate) temperatures with time for depressurisation of a vessel containing 70% mole nitrogen and 30% mole carbon dioxide (Hatched regions span experimental measurements, solid and dotted lines are predictions from BLOWDOWN) [Haque et al., 1990]

2.2.3 Heat and Mass Transfer Between Vapour and Liquid Phases

During blowdown of condensable gases or two phase mixtures, heat and mass transfer take place by evaporation and condensation due to drop in pressure and temperature. Overa et al. [1994] also considered heat transfer by convection due to temperature difference between phases. Mayinger [1982] indicated when the depressurisation rate is high during blowdown, thus giving rise to transient unstable conditions, boiling and condensation delays exist in liquid and vapour phases respectively. Additionally, the process of phase separation of evaporated liquid and condensed vapour from corresponding phases can be relatively slow when compared with high rate of depressurisation.

The author demonstrated the effects of delay and phase separation in boiling liquid by depressurising a vessel 2/3 filled with saturated liquid, refrigerant R 12, from 7.4 atm and 30°C to ambient pressure within 15 s. The variations of pressure with time and fluid temperature are shown in figure 2.11.

Referring to curve A, depressurisation starts at point B. During the very steep pressure gradient between points B and C, the measured liquid temperature markedly exceeds the saturation temperature (see curve B), which indicates considerable boiling delay. At point C, bubble formation starts in the liquid. Due to relatively slow process of phase separation, the dispersion level moves upwards during the period C-D and reaches the release valve. The vapour flow at release valve containing only traces of liquid droplets is superseded with a two-phase discharge containing large amounts of liquid. As the maximum velocity of two-phase mixture is much lower than sonic velocity of vapour, vapour formation in the vessel exceeds the volumetric discharge rate between time D and F. As a result, pressure starts to build up within the vessel until point F where the rate of flashing starts to fall and the pressure decreases steadily to point H.

2.2.4 Heat Transfer Between the Vessel and the Surrounding

The type of heat transfer between the vessel and the surrounding depends on the nature of the surrounding atmosphere. Under non-fire situations, heat transfer is by natural convection if the vessel is sheltered, for example, within an enclosed module on an offshore platform and the wind speed is low. Otherwise, heat transfer may be by forced convection.

2.2.5 Flow Through the Relief Valve

In the case of a fluid (single or two phase) approaching a relief valve, if the back-pressure is sufficiently low, the fluid will be accelerating through the orifice at it's maximum velocity. In addition, condensation may occur due to rapid rate of expansion from the upstream to orifice pressure. Haque et al. [1990] indicated that the fluid in the choke could be either in a metastable state or in thermodynamic and phase equilibrium. The authors compared predictions based on the above assumptions with experimental measurements and concluded that the latter assumptions gave better results.

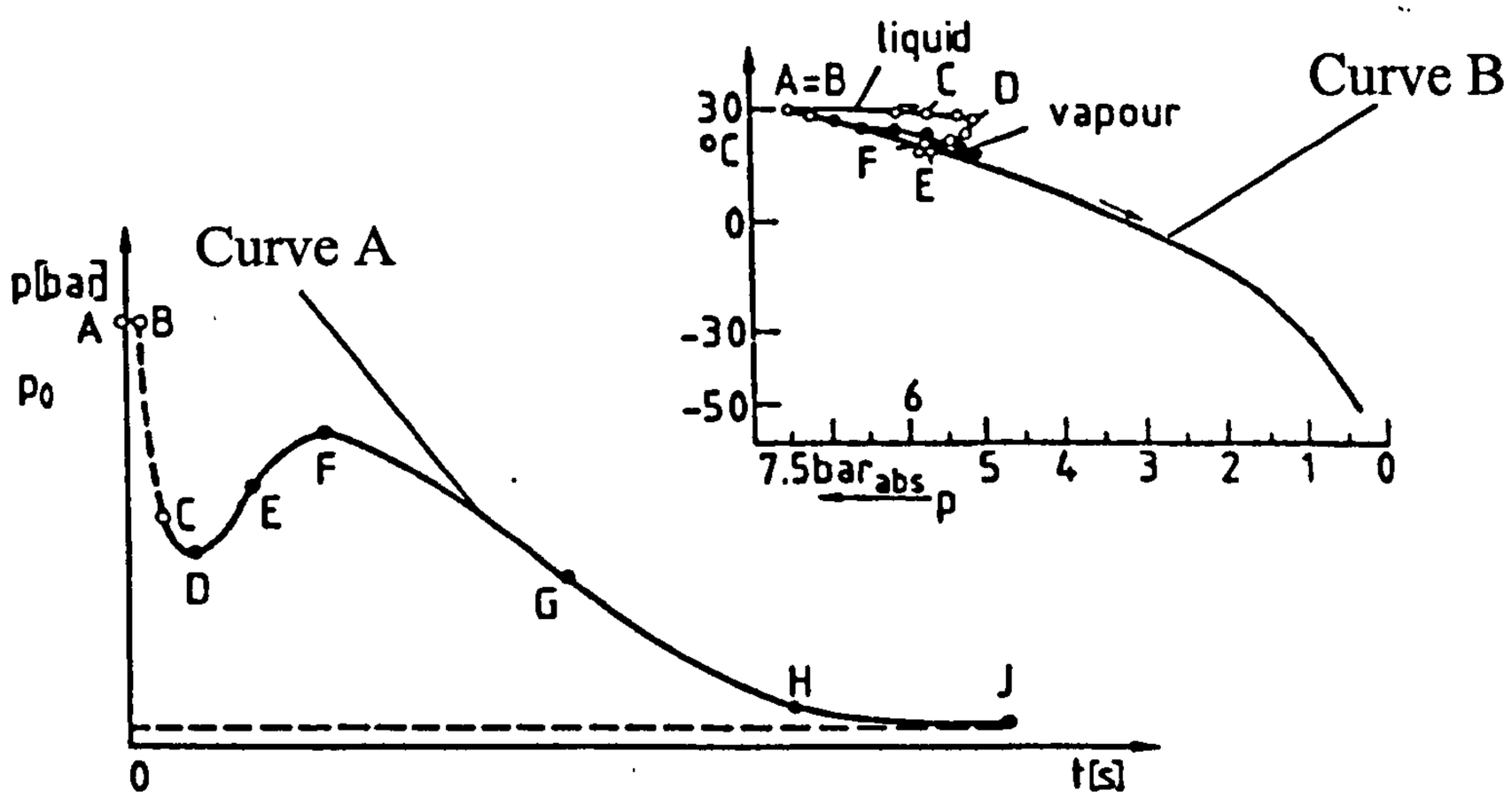

Figure 2.11 **Variations of pressure with time (curve A) and fluid temperature with pressure (curve B) for depressurisation of saturated liquid, refrigerant R 12 [Mayinger, 1982]**

2.3 CONCLUSION

On the basis of the literature reviewed so far, we can make the following important conclusions with regards to the various processes taking place during blowdown:

- The gas temperature does not drop as low as the isentropic temperature. After an extended period of time the gas temperature reaches a minimum and increases near the end of blowdown. This is due to heat transfer between gas and vessel wall.

- The presence of temperature gradients within the gas phase gives rise to density differences which in turn lead to natural convection dominating forced convection as the main heat transfer mechanism.

- The temperature of vessel wall in contact with the gas does not drop as low as the gas temperature because of low gas heat transfer coefficient and high heat capacity of the vessel wall.

- The liquid phase is superheated and boiling occurs. This results in a high heat transfer coefficient when compared to natural convection in gas phase.

- Due to rapid rate of heat transfer between vessel wall and liquid, it is common to find the minimum wall temperature located near the bottom of the vessel.

- There are significant temperature differences between different fluid phases during blowdown. Hence, equilibrium does not exist between these phases.

- Inter-phase mass and heat transfer are achieved by evaporation of lighter liquid hydrocarbon components and condensation of heavier gaseous hydrocarbons.

- During rapid depressurisation, boiling and condensation can be significant. Phase separation of evaporated liquid and condensed vapour from corresponding phases can in turn be slow when compared with the high rate of depressurisation. The above may lead to foaming and two-phase discharge and a build up of pressure within the vessel during blowdown.

- The flow (either gas or two-phase) through the discharge orifice is usually choked (at the speed of sound for gas or at it's maximum for two-phase discharge) if the back-pressure is sufficiently low. The fluid in the choke may in turn be in a metastable state or in thermodynamic and phase equilibrium.

CHAPTER 3

REVIEW OF MATHEMATICAL MODELS FOR BLOWDOWN SIMULATION

3.1 INTRODUCTION

This chapter reviews some of the most important mathematical models reported in the open literature for blowdown of isolated vessels, with no chemical reaction, under non fire situations. It starts with a description of commonly used industrial methods based on engineering practice and is followed by introducing simple mathematical models for blowdown of non-condensable gases. The chapter is concluded by reviewing mathematical models for blowdown of condensable gases or two-phase mixtures. In cases where experiments were carried out for validation of the reviewed models, the pertaining experimental conditions including the volume of vessel and measured parameters may be found in table 2.1 (chapter 2).

3.2 TRADITIONAL ENGINEERING METHODS FOR BLOWDOWN SIMULATION

A number of simple methods for blowdown are in common use in industry. These universally assume that the fluid within the vessel is homogenous. The selection of thermodynamic path for expansion of fluid that takes place during blowdown is often arbitrary. Overa et al. [1994] studied some traditional engineering methods given in table 3.1 and compared their predictions with experimental data.

Table 3.1 Traditional blowdown methods used in industry

Thermodynamic Path	Description
100% or 50% isentropic	The fluid expansion is either 100% or 50% isentropic (i.e., first isentropic, then isenthalpic with the enthalpy corrected by an efficiency) and there is no heat transfer with the vessel.
Isenthalpic	The fluid expansion is isenthalpic. No heat transfer with the vessel is assumed to take place.
Constant heat transfer coefficient	The fluid expansion is 100% isentropic, and heat transfer between fluid and vessel wall is determined by assuming constant heat transfer coefficients which are specified separately for vapour and liquid phases.

The authors compared predictions of minimum fluid and wall temperatures with blowdown experimental data of low pressure air (initially at 21.2 atm) and high pressure nitrogen (initially at 175.7 atm). For a low pressure two-phase hydrocarbon mixture (initially at 19.7 atm), comparisons were only made for the minimum vapour and liquid temperatures while the minimum wetted and unwetted wall temperatures were not reported.

Their results indicated that the predictions from the above methods greatly deviated from experimental values except for low pressure air, where the constant heat transfer method gave reasonable predictions of both gas and wall temperatures. The large errors introduced by all the above models were attributed to unrealistic assumptions of the mode of heat transfer within the vessel and also to the modelling of a two phase mixture as a single homogenous fluid.

As mentioned in chapter 2, the heat transfer effects of the fluid and non-equilibrium between phases are the major features of blowdown. Hence, correct interpretations are required for such effects in order to generate accurate predictions.

3.3 Simple Mathematical Models for Blowdown of Non-Condensable Gases

It is clear from the above that the application of a proper energy balance between vessel wall and the fluid within the vessel is required for blowdown calculation. The simplest case is blowdown of a non-condensable gas where the effects due to the presence of vapour condensate or liquid phase can be ignored. The following is a review of the pertaining mathematical models reported by various authors. These are mainly derived from the first law of thermodynamics. Heat transfer from the surrounding to the vessel is ignored.

3.3.1 Reynolds and Kays [1958]

Reynolds and Kays [1958] proposed a mathematical model which allows predictions of gas temperature and discharge rate as a function of residual mass of gas in a vessel with or without solid [1]capacitors. In some industrial applications, capacitors are

[1] In some applications, heat capacitors are deliberately inserted in the container to control temperature or store thermal energy.

deliberately placed within the vessel to control temperature during blowdown. Heat transfer between gas and the vessel or the solid capacitors is accounted for.

The major assumptions adopted in the simulation are :

1) Constant specific heat for vessel wall.
2) Constant heat transfer coefficient between the gas, vessel wall and internal solid capacitor.
3) Temperature gradient across the vessel wall or solid capacitor is ignored.
4) The gas in the vessel is ideal and well mixed.

The authors derived an energy balance in terms of dimensionless gas temperature, T*, and a dimensionless mass of gas, M* in the vessel in the form :

$$w^* M^* \frac{dT^*}{dM^*} - \left[(k-1)w^* + NTU\right]T^* + NTU\ T_c^* = 0 \qquad (3.3.1)$$

The dimensionless parameters are:

$M^* = M/M_0$

$NTU = (hA)/(C_v w_0)$

$T^* = T/T_0$

$T_c^* = T_c/T_0$

$w^* = w/w_0$

Where
- A = Heat transfer area
- h = Heat transfer coefficient between fluid and vessel wall or solid capacitor
- C_v = Gas specific heat at constant volume
- k = Ratio of specific heats of the gas
- M, M_0 = Residual mass of gas in the vessel at any instance during blowdown and at initial condition respectively
- T, T_0 = Gas temperatures at any instance during blowdown and at initial condition respectively
- T_c = Vessel wall's or capacitor's temperatures at any instance

during blowdown

w, w_0 = Discharge rates at any instance during blowdown and at initial condition respectively

The initial conditions when M* = 1 are :

$$T^* = 1 \tag{3.3.2}$$

$$T_c^* = T_{c0}^* \tag{3.3.3}$$

Where T_{c0}* is equal to T_{c0}/T_0, and T_{c0} is the vessel wall's or capacitor's temperature at initial condition.

Equation 3.3.1 is based on the first law of thermodynamics for a non-steady flow process. During blowdown through a choke, the discharge rate equals to the critical flow and the dimensionless temperatures of vessel wall or capacitor are assumed to be constant. This assumption is said to be appropriate when blowdown time is short. The dimensionless discharge rate, w*, given by the authors is :

$$w^* = M^* \left(T^*\right)^{1/2} \tag{3.3.4}$$

Hence, equation 3.3.1 is reduced to :

$$M^* \frac{dT^*}{dM^*} - (k-1)T^* + \frac{\left(T_c^* - T^*\right)NTU}{M^* T^{*1/2}} = 0 \tag{3.3.5}$$

The dimensionless vessel pressure based on ideal gas equation is :

$$P^* = M^* T^* \tag{3.3.6}$$

Where P* = P/P_0

P, P_0 = Vessel pressures at any instance during blowdown and at initial condition respectively

As equation 3.3.5 is nonlinear, it can be integrated numerically either by specifying dT* or dM*. w* and P* are then calculated from equations 3.3.4 and 3.3.6

respectively. The actual temperature, pressure and mass of gas in the vessel can be determined provided the initial conditions are known.

In order to investigate the mode of heat transfer during blowdown and to validate their model, the authors performed experiments by depressurising a low pressure vessel containing air from an initial pressure of 7.8 atm through a choke. A typical run lasted for about 20 s. Two types of thermal capacitors, vertical-strip and concentric-can were inserted into the vessel respectively. The pressures and gas temperatures were recorded for both cases. The vessel was lined internally with a thick layer of balsa wood to provide an adiabatic environment.

For any measured pressure and gas temperature, the dimensionless gas mass, M* was determined from equation 3.3.6. The results of T* against M* for a vertical-strip capacitor and a concentric-can capacitor are given in figures 3.1 and 3.2 respectively. The solid lines in the figures represent the predicted values while the data points show the measured values for two different runs. The dotted lines on the other hand are predictions on the basis of the adiabatic expansion of gas which show large deviations from experimental data.

By adjusting the values of NTU in equation 3.3.5, the authors were able to produce good predictions and also determine the heat transfer coefficients for both types of capacitors. The magnitude of calculated heat transfer coefficients suggested the dominance of natural convection in the gas phase. The authors also indicated that the Grashof number of the gas was greater than 10^9 and turbulent convection boundary layer existed in the gas during blowdown.

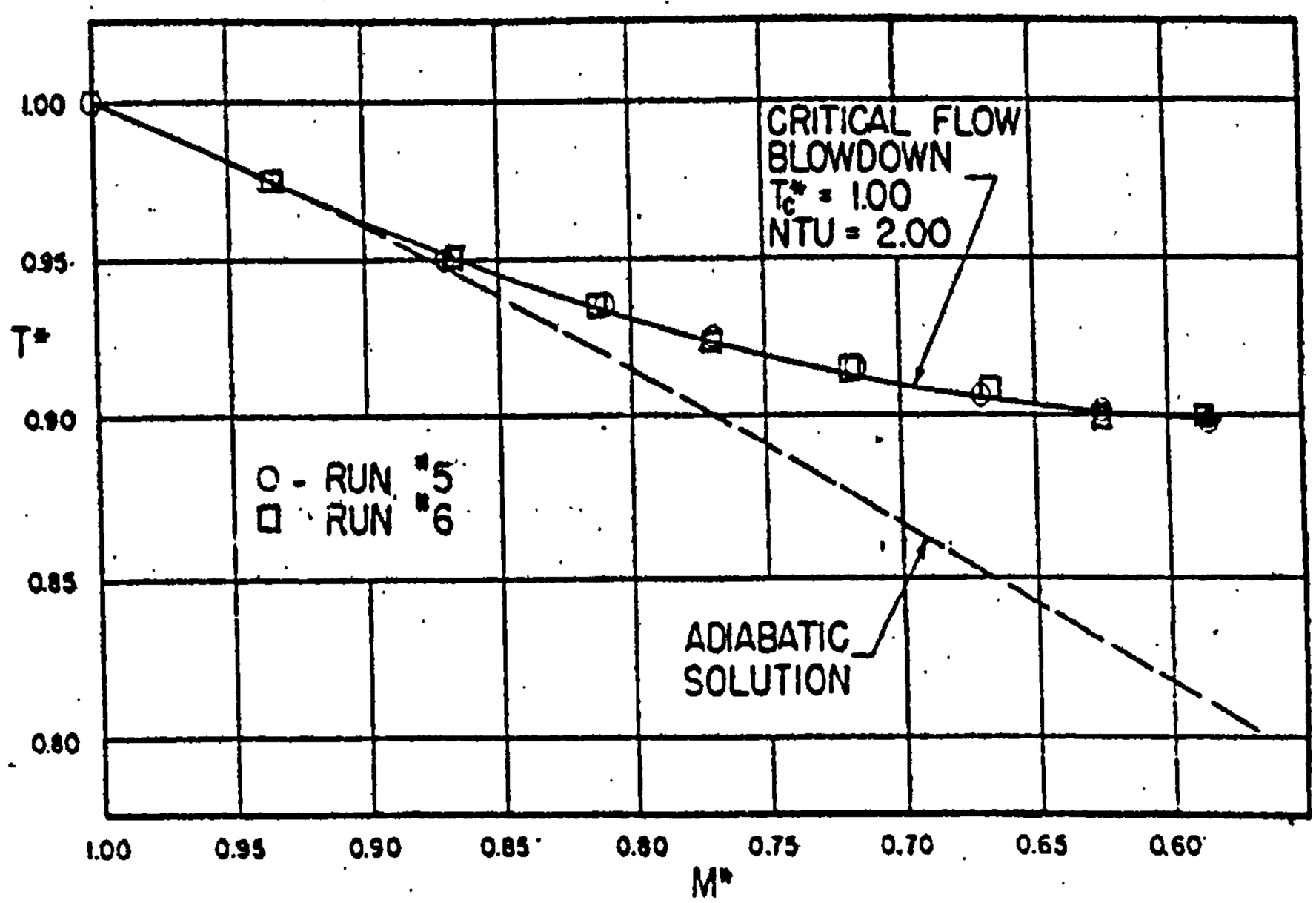

Figure 3.1 **Variation of dimensionless temperature, T*, with dimensionless mass of gas, M* for blowdown of high pressure air with vertical - strip capacitors [Reynolds & Kays, 1958]**

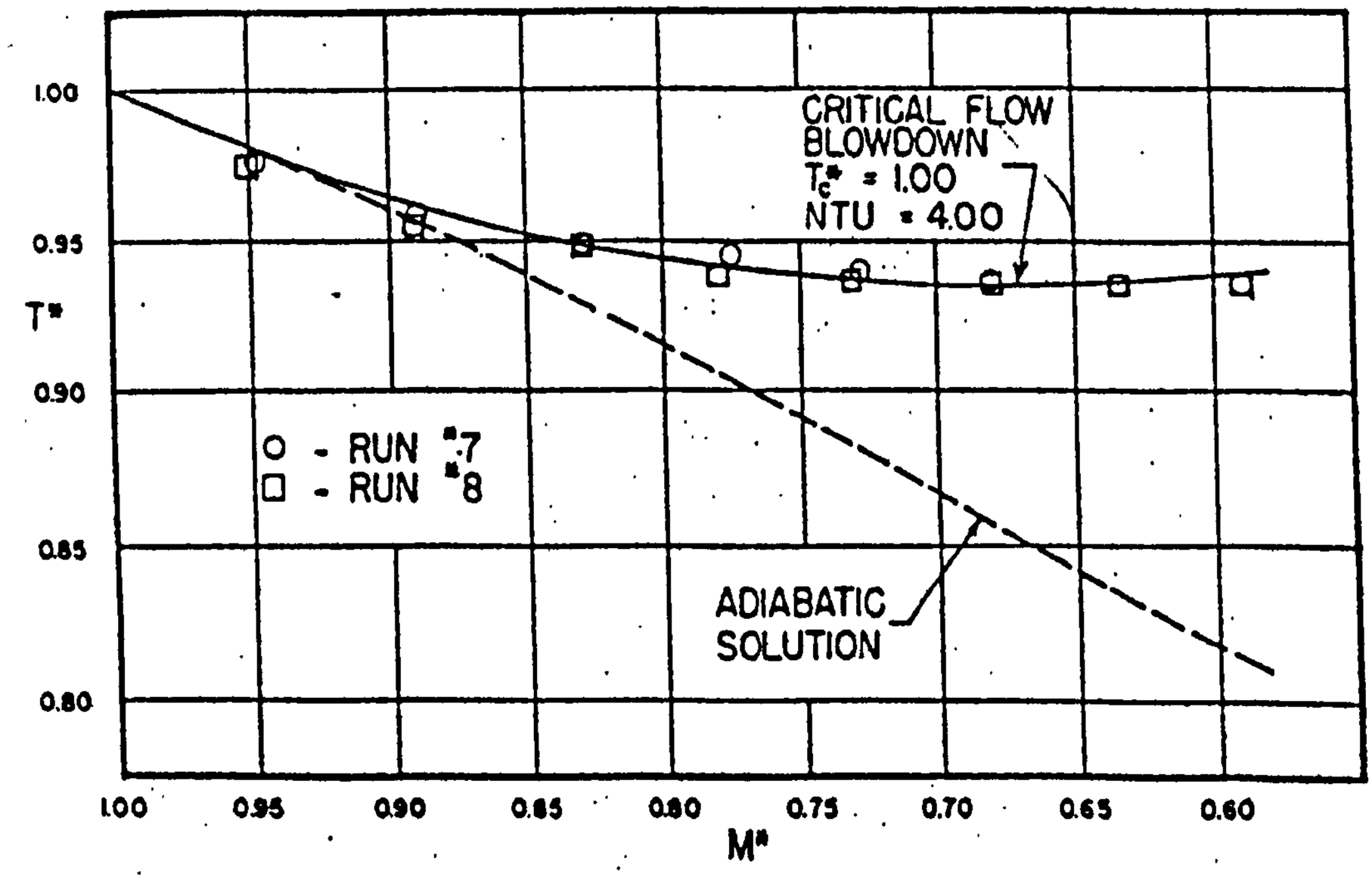

Figure 3.2 **Variation of dimensionless temperature, T*, with dimensionless mass of gas, M* for blowdown of high pressure air with concentric -can capacitors [Reynolds & Kays, 1958]**

3.3.2 Byrnes et al. [1964]

The dominance of heat transfer by natural convection also at high pressures was confirmed by Byrnes et al. [1964]. The authors used a correlation given by McAdams [1954] for predicting the heat transfer coefficient between the gas and vessel wall during natural convection to produce good agreement with experimental data.

Similar to Reynolds and Kays, Byrnes et al. assumed that the gas within the vessel to be ideal. On the basis of the first law of thermodynamics for steady flow process, the energy balance between the vessel wall and the gas was expressed as a function of time instead of the dimensionless parameters used by Reynolds and Kays. This is given by:

$$hA(T_w - T) = M C_p \frac{dT}{dt} - V\frac{dP}{dt} \tag{3.3.7}$$

The pressure-time profile is given in an exponential form provided the flow is choked across the orifice:

$$\frac{P}{P_0} = e^{-at} \tag{3.3.8}$$

Where
- a = Pressure profile parameter (fitting constant)
- C_p = Gas specific heat at constant pressure
- V = Vessel's volume
- T_w = Vessel wall temperature
- t = Time

If the pressure profile parameter, a, in equation 3.3.8 is known, equation 3.3.7 can then be solved by finite difference method where the mass of gas in the vessel, M, is assumed constant for a given time interval. The amount of discharged gas as a result of the expansion is given by the volume of fluid after expansion minus the volume of the vessel. Material balance is then performed to correct the value of 'M' for the next time interval.

For validation purposes, the authors carried out experiments by depressurising high pressure hydrogen vessels (initial pressure is 135.2 atm) with three different blowdown times, 14, 30, and 480 s. The pressure, gas and wall temperatures were measured. Figures 3.3 - 3.5 show the comparisons between experimental data and predictions from the model (solid lines represent measured values, dotted lines represent predicted values) for the three different blowdown times respectively. The predictions are based on the assumption of constant wall temperature. Reasonable agreement is observed from the above figures.

Byrnes et al. [1964] demonstrated the applicability of the perfect gas assumption for blowdown simulation of a simple gas at elevated pressures. Both mathematical models described above are simple to use and give reasonable gas temperature predictions. However, in the case of vessels containing gases at low temperatures and also when the vessel is depressurised for a significant period of time, Reynolds and Kays [1958] assumption of constant vessel wall temperature will fail to predict the low vessel wall temperatures which may be encountered in practice. On the other hand, although Byrnes et al.'s [1964] method accounts for the variation of heat transfer coefficient with time, it is not completely predictive as the pressure-time profile is needed from experiment.

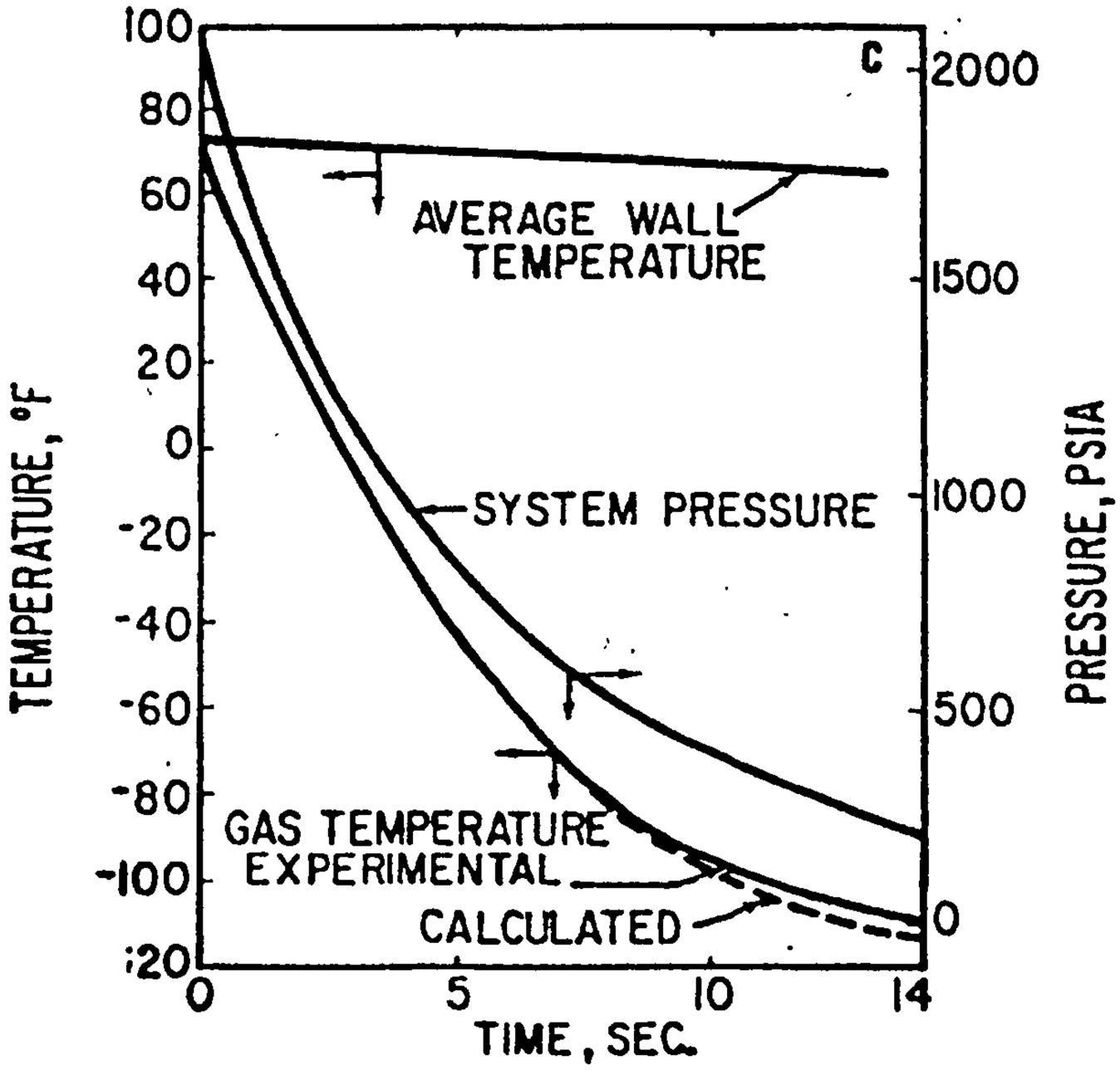

Figure 3.3 **Variations of temperatures and pressure for blowdown of high pressure hydrogen (blowdown time = 14 sec) [Byrnes et al., 1964]**

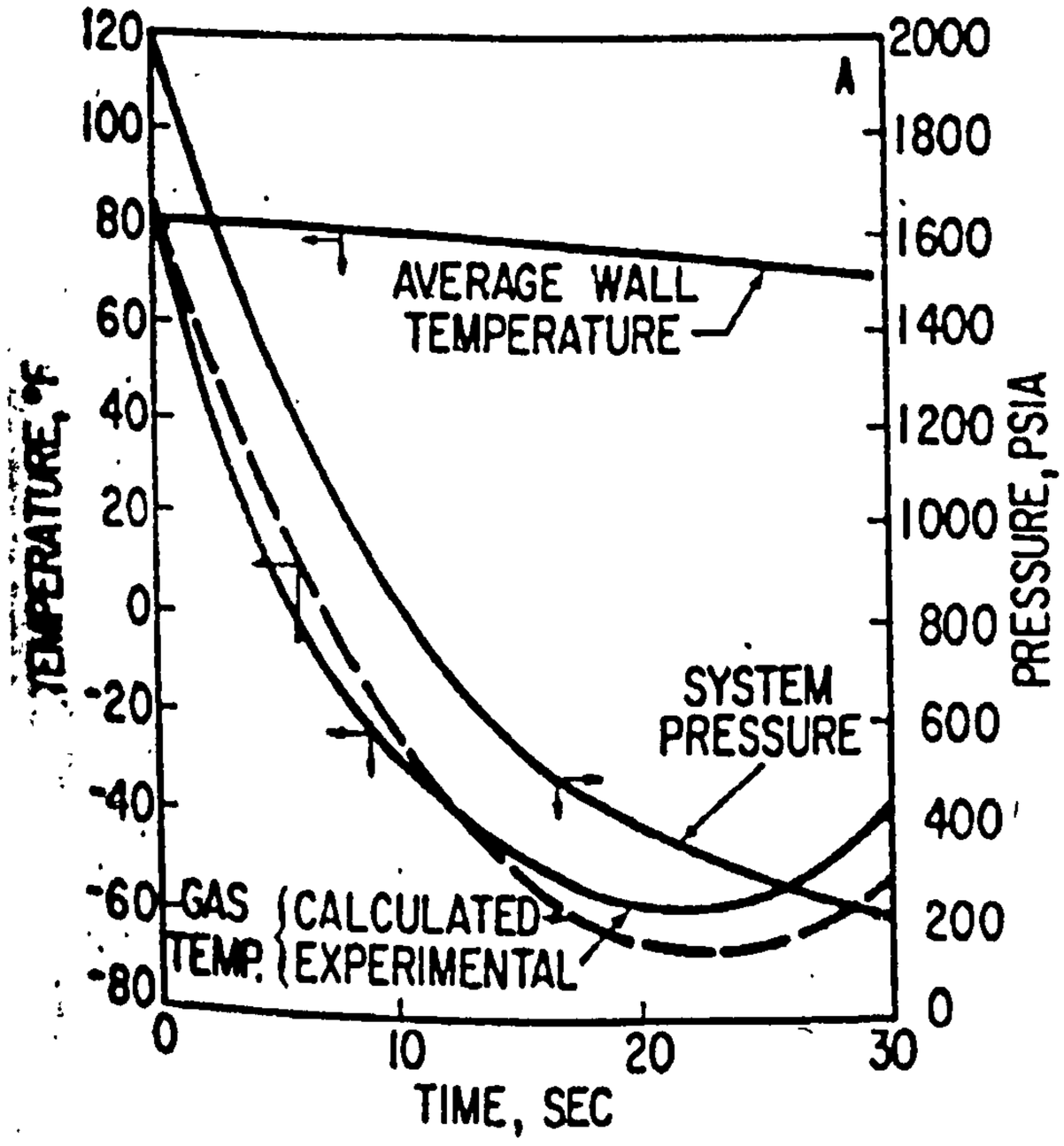

Figure 3.4 **Variations of temperatures and pressure for blowdown ofhigh pressure hydrogen (blowdown time = 30 sec) [Byrnes et al., 1964]**

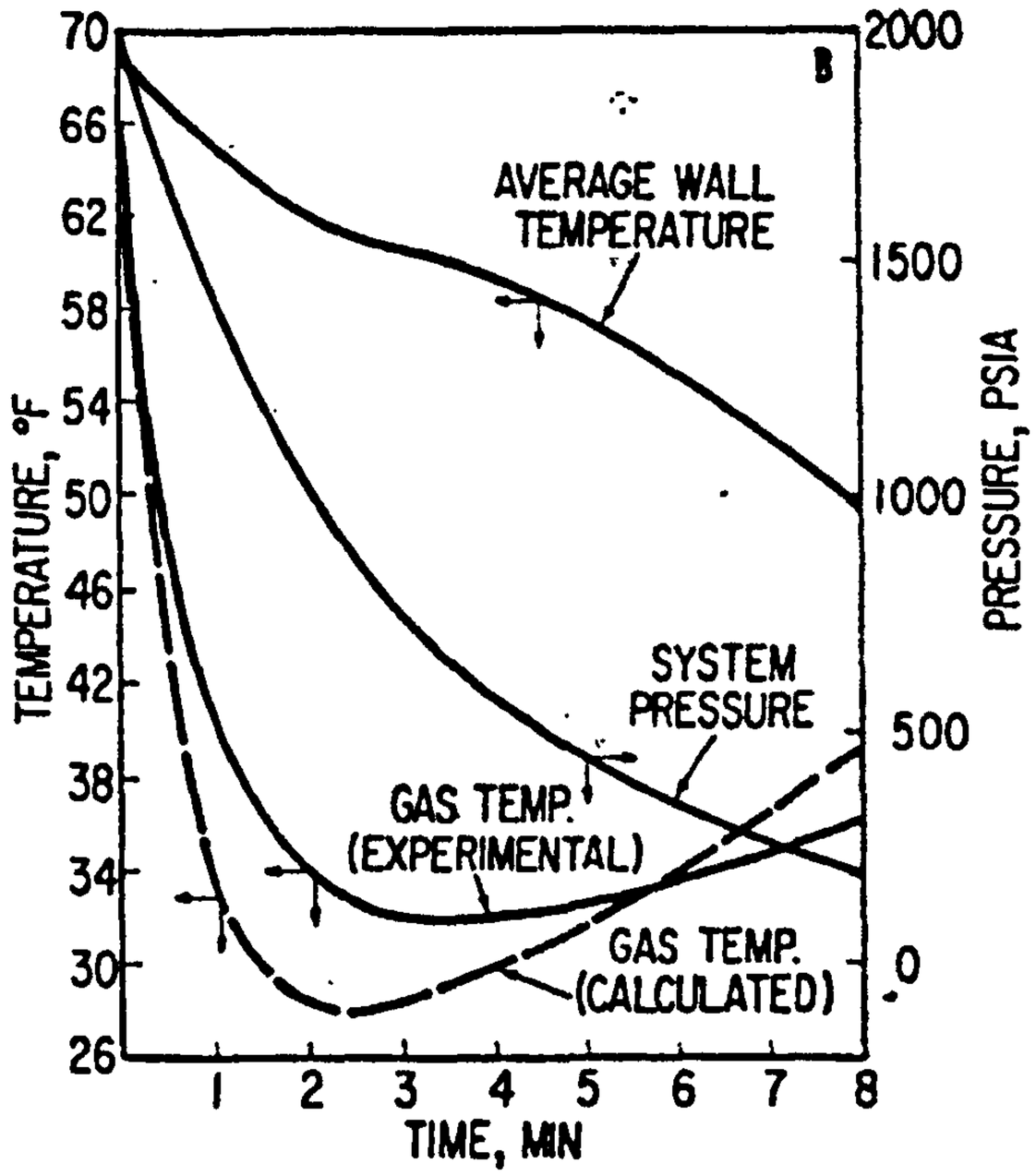

Figure 3.5 Variations of temperatures and pressure for blowdown of high pressure hydrogen (blowdown time = 480 sec) [Byrnes et al., 1964]

3.3.3 Montgomery [1995]

The above drawbacks were addressed by Montgomery [1995]. The author related the rate of energy loss in the vessel wall to the rate of energy absorbed by the fluid. The energy balance, which was based on the first law of thermodynamics of unsteady flow process, was simplified by assuming constant gas specific heat capacity and constant heat transfer coefficient between the gas and vessel wall. The corresponding pressure, wall and gas temperatures together with gas compressibility factor were then determined by solving the energy and mass balances iteratively.

The material and energy balances were based on a vessel with an arbitrary number of inlet and outlet streams as depicted in figure 3.6.

Figure 3.6 A pressurised vessel with a number of inlet and outlet streams [Montgomery, 1995]

The material balance is given by :

$$\frac{d(\rho V)}{dt} = \sum\left(\frac{dm}{dt}\right)_i \qquad (3.3.9)$$

Where ρ = Fluid density within the vessel

m = Mass of fluid

$\left(\frac{dm}{dt}\right)_i$ = Mass flowrate of stream i in or out of the vessel

The rate of change of fluid energy is given by summation of three components. The first component represents the energy transfer of the vessel due to inlet and outlet mass flows. The second component is the work done by the expanding fluid in the vessel. The third component is the energy transferred from the vessel wall to the fluid. The energy balance for the fluid is given by :

$$\frac{d(\rho V C_p T)}{dt} = \sum\left(\frac{d(mC_pT)}{dt}\right)_i + \frac{d(PV)}{dt} + hA(T_w - T) \tag{3.3.10}$$

and :

$$hA(T_w - T) = -\frac{d(M_w C_{pw} T_w)}{dt} \tag{3.3.11}$$

Where C_{pw} = Specific heat capacity of the vessel wall material at constant pressure

M_w = Mass of the vessel wall

$\left(\frac{d(mC_pT)}{dt}\right)_i$ = Enthalpy flowrate of stream i in or out of the vessel

For flow into the vessel, the specific heat, C_p, and fluid temperature, T, of stream i are determined based on the conditions of inflowing fluid. For flow out of the vessel, both parameters are based on the conditions of fluid within the vessel.

The equation to determine flowrates in and out of the vessel is given by the author in the form :

$$\frac{dm}{dt} = 0.525 Y d^2 \sqrt{\frac{\rho \Delta P}{K}} \tag{3.3.12}$$

and

$$K = \frac{fL}{D} \tag{3.3.13}$$

Where d = Internal diameter of pipe, valve or fitting (in.)

D = Internal diameter of pipe, valve or fitting (ft.)

f = Moody friction factor

L = Length of pipe or equivalent length of valve or fitting (ft)

Y = Expansion factor

ΔP = Pressure drop across pipe, valve or fitting (psia)

The expansion factor, Y, is given by :

$$Y = 1 - \left(\frac{0.515}{K^{0.747}} + 0.29\right)\left(\frac{\Delta P}{P_1}\right) \qquad (3.3.14)$$

Where P_1 the inlet pressure to pipe, valve or fitting in psia.

The author then investigated the variation of gas and vessel wall temperatures during blowdown for different heat transfer coefficients (0 - 500 btu/hr-ft^2) by applying the model to a hypothetical high pressure (initial pressure and temperature are 103.1 atm and 311 K respectively) full-size vessel (internal diameter and vessel height are 1.5 m and 4.8 m respectively). The gas was assumed to be ideal with a molecular weight of 20g/mol. The results of variations of gas and vessel wall temperatures with time for different heat transfer coefficients are given by figures 3.7 - 3.10.

Two major conclusions were drawn at the based on these studies. Firstly, as expected, the gas temperature never reaches the isentropic temperature (from figure 3.7, -175°F) during blowdown. Secondly, the vessel wall temperature does not drop as low as the gas. Although no experimental data were used to validate the model, the conclusions confirmed the experimental observations described in section 2.2.1 of chapter 2. The author also indicated that the effect of liquid vaporization could be significant. Hence, more sophisticated mathematical models are required to handle the additional effects due to presence of liquid or condensed gas.

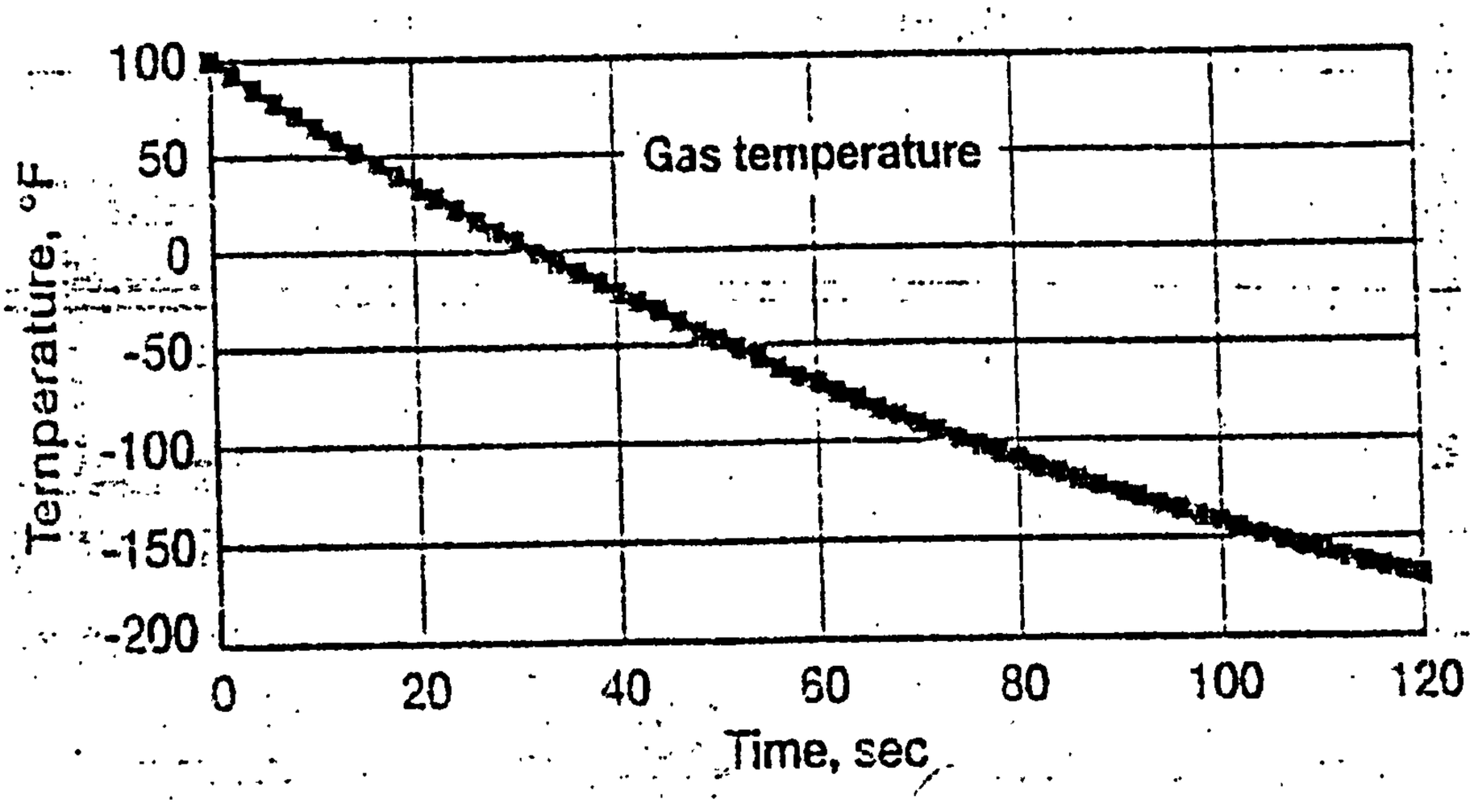

Figure 3.7 **Variation of temperature with time for gas with no heat transfer with vessel (h = 0 Btu/hr-ft^2-°F) [Montgomery, 1995]**

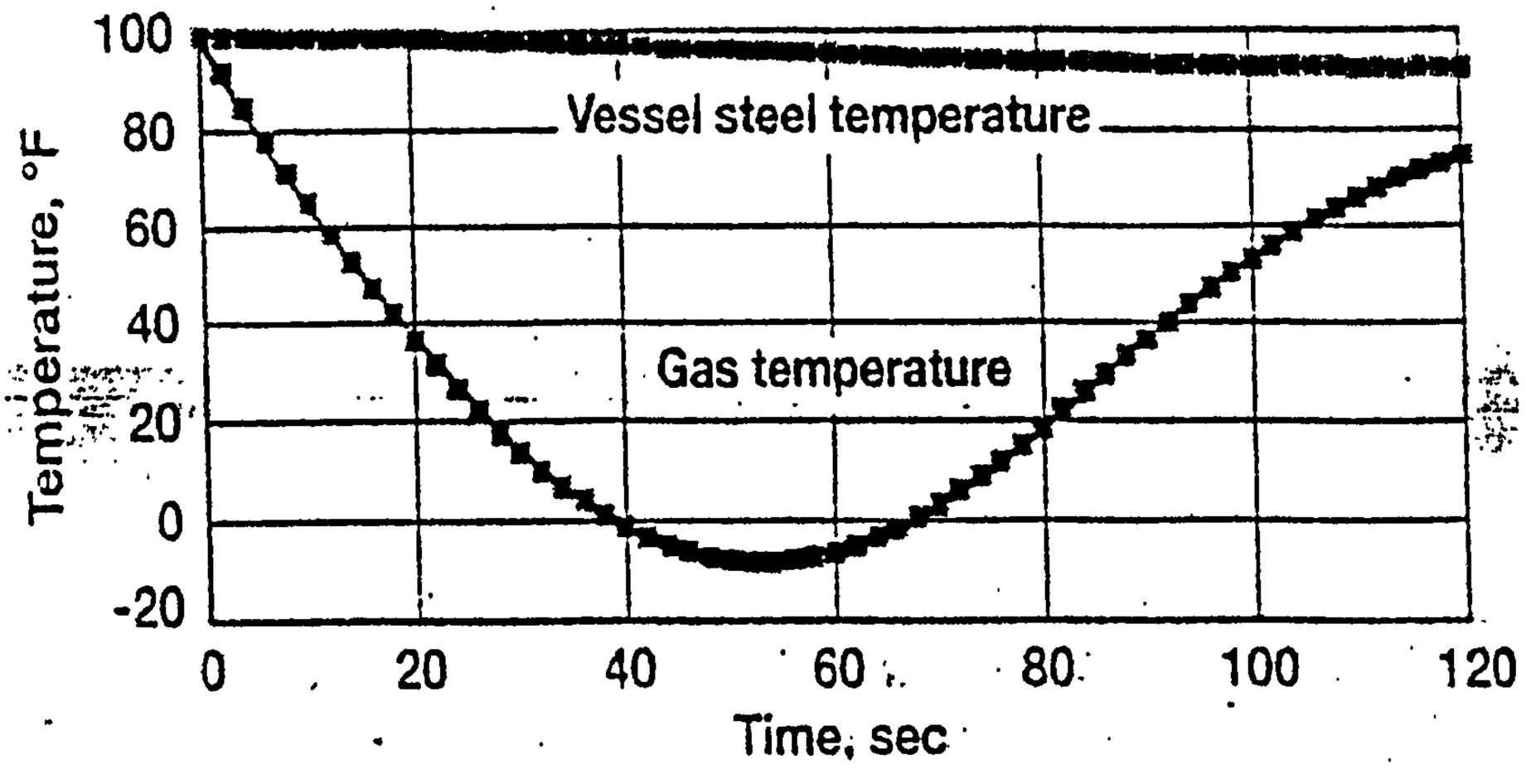

Figure 3.8 **Variations of gas and vessel wall temperatures with time for gas with heat transfer with vessel (h = 50 Btu/hr-ft^2-°F) [Montgomery, 1995]**

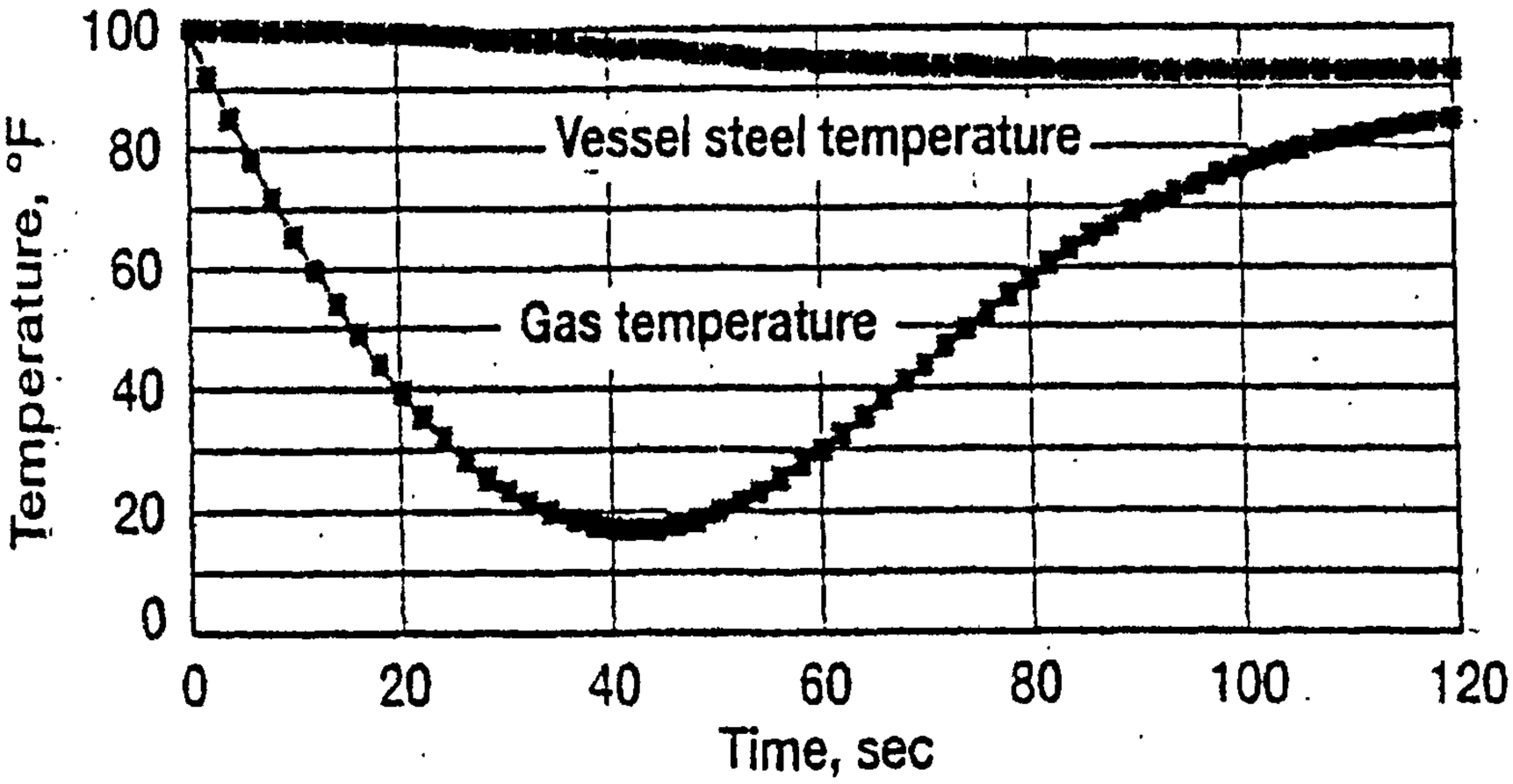

Figure 3.9 Variations of gas and vessel wall temperatures with time for gas with heat transfer with vessel (h = 100 Btu/hr-ft^2-°F) [Montgomery, 1995]

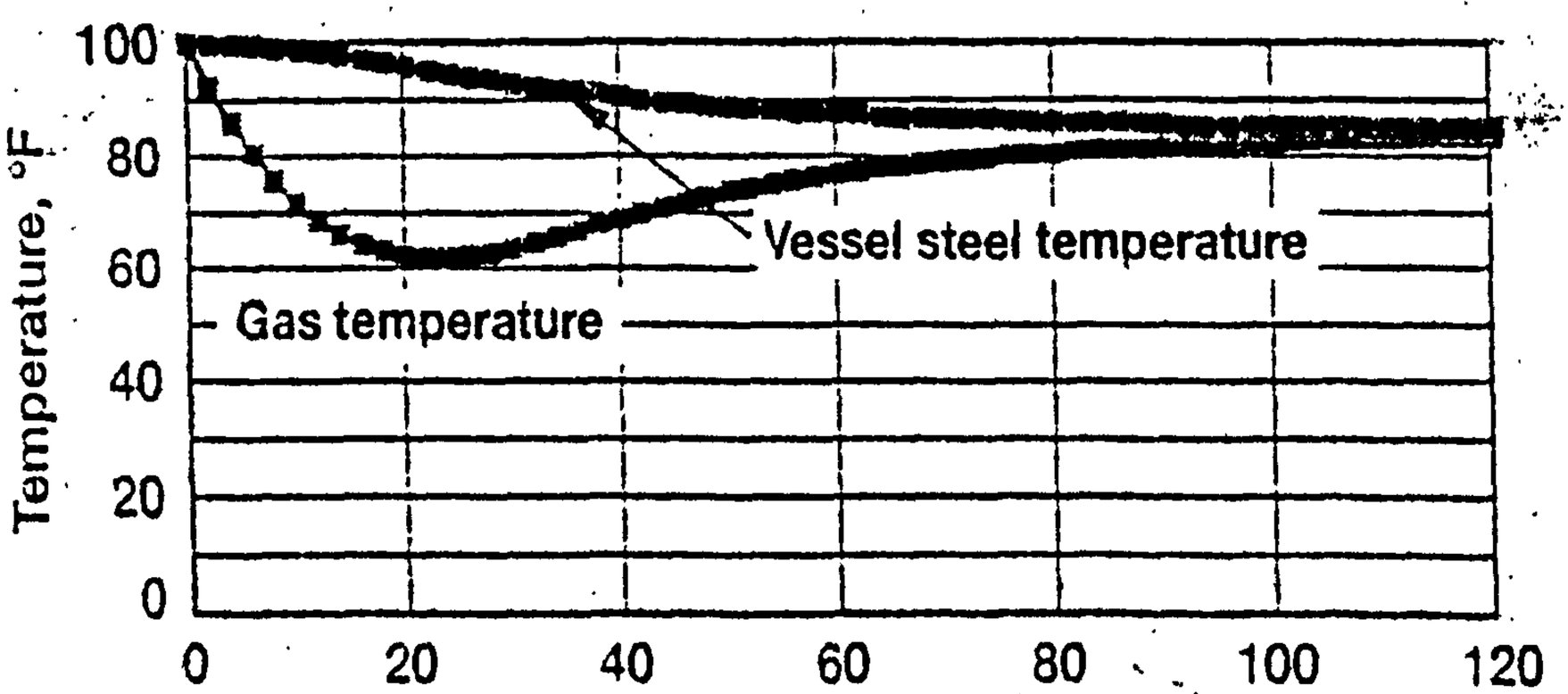

Figure 3.10 Variations of gas and vessel wall temperatures with time for gas with heat transfer with vessel (h = 500 Btu/hr-ft^2-°F) [Montgomery, 1995]

3.4 RIGOROUS MATHEMATICAL MODELS FOR BLOWDOWN

So far, two models, BLOWDOWN [Haque et al., 1990; Haque et al., 1992a] and SPLIT FLUID MODEL [Overa et al., 1994], have been reported for determination of pressure and temperature time profiles during blowdown of a vessel containing a hydrocarbon mixture. These take into account non-equilibrium effects as well as temperature differences between phases and their associated vessel wall. Both models have been validated against experimental data [Haque et al., 1992b; Overa et al., 1994]. Their main features are described in the following.

3.4.1 Blowdown [Haque et al., 1990; Haque et al., 1992a]

The mathematical model, BLOWDOWN, developed by Haque et al. [1990, 1992a] at Imperial College is aimed to provide accurate predictions of physically significant effects taking place during blowdown. It is in two versions; the earlier version [Haque et al., 1990] can handle two phases mixtures while the later version [Haque et al., 1992a] is capable of handling an additional third phase, water. The earlier version of BLOWDOWN is described briefly here while the more superior revised version, which has been validated with high pressure hydrocarbon mixtures, is reviewed in more detail.

3.4.1.1 Haque et al., 1990

The first version of BLOWDOWN [Haque et al., 1990] was developed to handle vapour space blowdown (blowdown from vessel's top) of permanent or condensable gases.

The depressurisation process is approximated by dividing it into a series of discrete pressure steps. The vessel during blowdown is assumed to be divided into two zones:

Zone1: Vapour together with any suspended liquid-phase droplets, below which is

Zone2: Condensed vapour from the top zone forming a pool on the bottom of the vessel. This zone is eliminated if liquid is not present.

Spatially uniform temperature and composition are assumed in each zone while spatially uniform pressure is assumed within the vessel. For each pressure step, the

fluid is assumed to expand isentropically followed by heat transfer from the adjacent vessel wall.

The mathematical algorithm adopted is given in the following :

1) Select a pressure decrement.
2) Perform an isentropic flash on each zone.
3) Calculate the rate of discharge through the choke.
4) Calculate the duration of the time step and the amount of fluid discharged.
5) Calculate the heat transfer coefficients for each zone.
6) Perform energy and mass balances over the contents of each zone and an energy balance over the vessel wall.
7) If depressurisation is complete, stop; otherwise repeat this process.

On the bases of experimental observation (chapter 2), natural and forced convection between Zone 1 and adjacent vessel wall are considered. While in Zone 2, nucleate and film boiling heat transfer involving higher heat transfer coefficients compared to Zone 1 are assumed. The main mode of heat transfer between vessel and surrounding is assumed to be natural convection. The corresponding correlations for predicting heat transfer coefficients and details of discharge calculation will be described later in the revised version of BLOWDOWN (section 3.4.1.2)

The authors validated the model against experimental data obtained following blowdown of a small high pressure vessel (initial pressure is 148 atm) containing either pure nitrogen or a mixture of nitrogen and carbon dioxide. The results of the comparison for nitrogen mixture were shown earlier in figure 2.10 of chapter 2.

In the case of nitrogen blowdown, the model successfully predicted the temperatures of gas and of the inner wall. While for the mixture of nitrogen and carbon dioxide, the mathematical model was able to predict when condensation occurred and also the corresponding temperatures of vapour and condensate.

3.4.1.2 Haque et al., 1992a

The revised version of BLOWDOWN incorporates two major modifications. Firstly, the isentropic expansion of the fluid is replaced by a polytropic process [Bett et al., 1975] as it allows considerably larger pressure decrements while retaining accuracy [Haque et al., 1992a]. Secondly, the model can handle an additional third phase, water, which is commonly found in offshore unit operations.

The vessel is divided into three zones prior to blowdown as shown in figure 3.11. These are :

Zone1: Gaseous hydrocarbon including evaporated water, below which is

Zone2: Liquid hydrocarbon including dissolved water, below which is

Zone3: Free water including dissolved hydrocarbons

MATHEMATICAL ALGORITHM

A polytropic process [Bett et al., 1975] is defined as that in which both heat and work are transferred. By assuming the process is reversible, it can be used to approximate an irreversible process involving a real fluid when the initial and final states of the process are known. Bett et al. [1975] indicated that such approximation usually gives remarkably accurate predictions of heat and work.

There are an infinite number of reversible polytropic paths between two states. Bett et al. proposed the following path which is physically plausible and mathematically convenient :

$$T\left(\frac{dS}{dT}\right) = C \qquad (3.4.1)$$

Where C = Polytropic constant

S = Fluid entropy

T = Fluid temperature

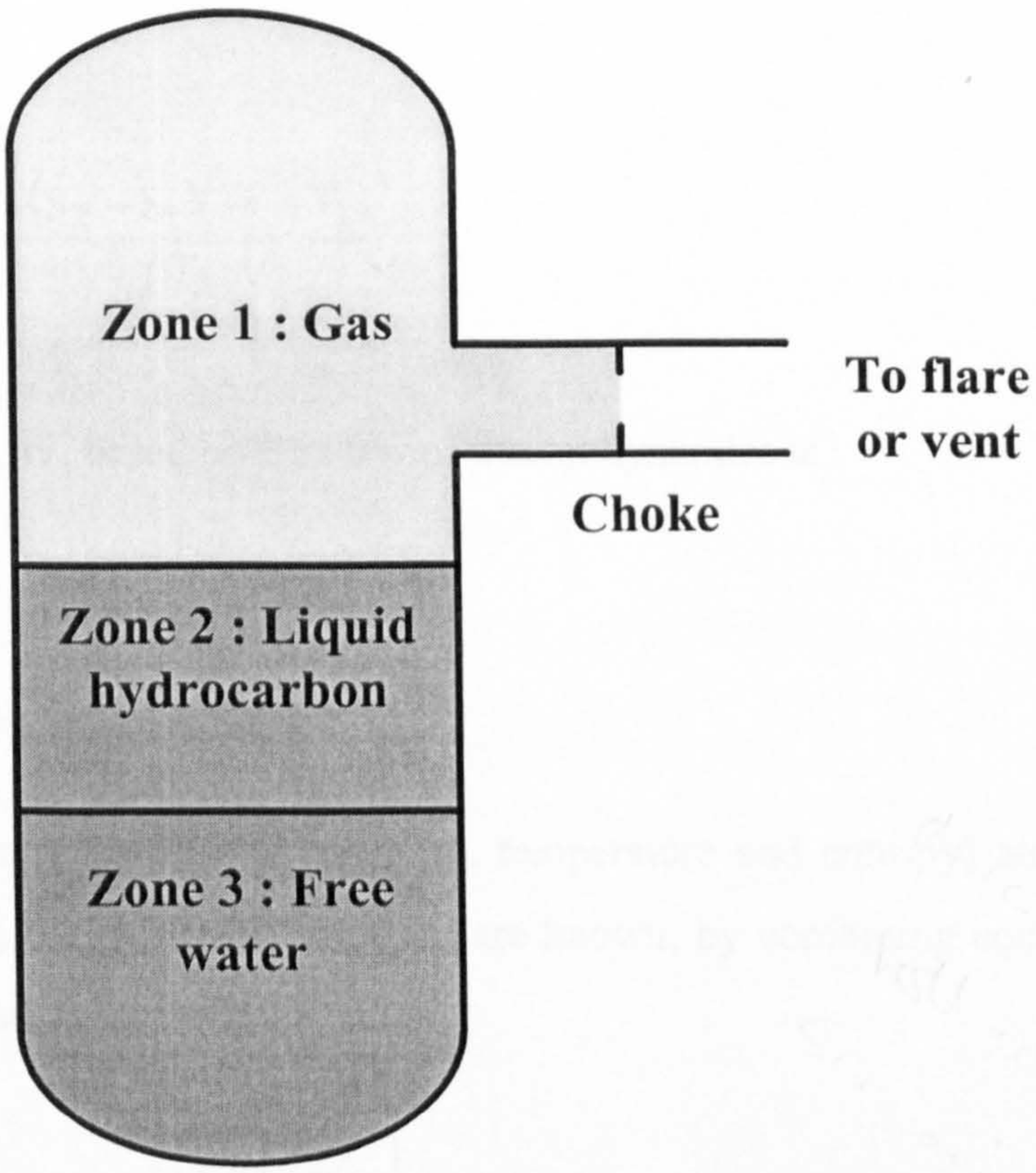

Figure 3.11 Schematic diagram of vessel with blowdown from top [Haque et al., 1992a]

The above equation is solved by assuming a linear relationship between heat and temperature. The amount of heat being transferred is given by :

$$Q = \int_1^2 TdS = C(T_2 - T_1) \tag{3.4.2}$$

Where Q = Heat being transferred

1, 2 = Initial and final states

Hence,

$$Q = \frac{(S_2 - S_1)(T_2 - T_1)}{\ln\left(T_2/T_1\right)} \tag{3.4.3}$$

and the work, W, based on first law of thermodynamics is :

$$W = (H_2 - H_1) - Q \tag{3.4.4}$$

Where H is the fluid enthalpy.

When the initial conditions (pressure, temperature and entropy) and final pressure together with the polytropic constant are known, by combining equations 3.4.2 and 3.4.3, the entropy at the final state is :

$$S_2 = S_1 + \frac{Q \times \ln\left(T_2/T_1\right)}{(T_2 - T_1)} \tag{3.4.5}$$

The fluid temperature can then be determined by performing a flash calculation at the final pressure and entropy.

The following is the mathematical algorithm adopted by Haque et al. :

1) Select a pressure decrement.
2) Expand the fluid in each zone polytropically by assuming C, and calculate the energy Q which must be transferred to the fluid.

4) Calculate the duration of the time-step corresponding to the chosen pressure step by determining the flow rate through the choke.
5) Calculate all relevant heat transfer coefficients.
6) Perform energy balances on the fluid and vessel wall and calculate the energy Q* transferred to the fluid.
7) If $Q \neq Q^*$, alter the value of C and return to step two. Otherwise proceed to step eight.
8) Perform mass balances on the fluid and calculate the quantity of liquid which condenses and settles out from the gas and the quantity of gas which evaporates out of the liquid hydrocarbon.
9) If depressurisation is complete, stop. Otherwise return to step one.

HEAT AND MASS TRANSFER EFFECTS

Heat Transfer Between Vessel Wall/Fluid/Surrounding

Heat transfer modes between zones 1 and 2 and the associated vessel wall were described in section 3.4.1.1. When a significant quantity of water is encountered during blowdown, the authors concluded that based on experimental studies (results not presented), the temperature of water varies relatively little and natural convection is dominant. The correlations used to determine heat transfer coefficients for individual phases are summarised in table 3.2. In zone 2, the maximum temperature difference between fluid and vessel wall for nucleate boiling and minimum one for film boiling are determined by standard correlations [Lienhard & Dhir, 1973; Berenson, 1961].

The overall energy balance over the contents and wall of the vessel are determined by finite-difference solution of the transient heat conduction equation [Incropera, & De Witt,1985]. This method allows description of the temperature gradient across the wall thickness. As such, it can be applied to vessel wall with [2]duplex construction. Heat transfer between the vessel wall and the surrounding is considered to be either by natural or forced convection depending on the nature of the surrounding and the corresponding standard correlations [Perry & Chilton,1973a,b; Churchill & Chu, 1975] are used.

[2] Multi-layer construction

corresponding standard correlations [Perry & Chilton, 1973a, b; Churchill & Chu, 1975] are used.

Table 3.2 Summary of heat transfer modes simulated by BLOWDOWN [Haque et al., 1992a] for each fluid zone and the associated wall region during blowdown

Zone	Heat Transfer Mode	Correlations Used to Determine Heat Transfer Coefficients or Heat fluxes
Zone 1	Natural and forced convection where natural convection dominates.	Heat transfer coefficients are predicted by : *Natural convection* : Perry & Chilton [1973a] *Forced convection* : Perry & Chilton [1973b]
Zone 2	Nucleate and film boiling	Corresponding heat fluxes are predicted by : *Nucleate Boiling* : Rohsenow [1952] *Film Boiling* : Jordan [1968] *Transition Boiling* : No correlation is used. The heat transfer coefficients are determined by linear interpolation.
Zone 3	Natural convection	Heat transfer coefficient is predicted from Perry & Chilton [1973a]

Heat and Mass Flux between Adjacent Fluid Zones

The inter-phase heat and mass fluxes between gaseous (zone 1) and liquid (zone 2) hydrocarbons are a consequence of evaporation and condensation of lighter and heavier components respectively. In order to accurately describe the fluxes between the corresponding phases and the position of liquid droplets within the gas phase, information on phase equilibrium, nucleation time and settling velocity of liquid droplets are required. The authors proposed the following empirical correlations to determine the nucleation time, τ (s), and the settling velocity of liquid droplets, v (ms^{-1}) relative to the gas, as a function of the equilibrium liquid mole fraction, x in the gas phase (zone 1):

$$\tau = \frac{1}{x} \tag{3.4.6}$$

$$v = 0.03 + 3x \tag{3.4.7}$$

The above equations are deduced for mixtures of nitrogen, carbon dioxide, methane, ethane, propane and butane at pressures up to 148 atm [Richardson, 1998]. The authors assumed negligible mass transfer between the liquid hydrocarbon (zone 2) and water (zone 3). However, heat transfer between the phases occurs because the phases are not in general, at the same bulk temperature.

The authors concluded that when the free water is warmer than the liquid hydrocarbon, heat transfer is mainly by boiling, otherwise it is by natural convection. Standard correlations are used to determine the inter-phase heat transfer coefficients [see for example Perry & Chilton, 1973a; Rohsenow, 1952; Jordan, 1968; Lienhard & Dhir, 1973; Berenson, 1961] .

DISCHARGE RATE CALCULATION

A number of possible situations of the fluid states at the entrance of and within the choke were considered. The fluid approaching the choke can be one phase (vapour) or two-phase (liquid and vapour) and the fluid in the choke can be in a metastable state or in thermodynamic and phase equilibrium. On the bases of their comparison with the experimental measurements, the best predictions were generated by assuming fluid phase equilibrium within the choke and at the entrance of the choke where the fluid could either be in one or two-phases.

The rate of discharge through the choke is determined by assuming that the fluid accelerates through the choke isentropically and the fluid velocity is equal to the local speed of sound when the back-pressure is sufficiently low. An energy balance across the choke is performed by assuming the fluid velocity approaching the choke is zero:

$$H_i = H_C + \frac{1}{2}a^2 \tag{3.4.8}$$

The local speed of sound, a, is given by :

$$a = \left[\frac{\partial P}{\partial \rho}\right]_S^{\frac{1}{2}} = \left[\frac{C_p}{C_v}\left(\frac{\partial P}{\partial \rho}\right)_T\right]^{\frac{1}{2}} \tag{3.4.9}$$

All terms in the above equation are evaluated under choked conditions. The above two equations are governed by the isentropic condition :

$$S_i = S_C \tag{3.4.10}$$

Where C_p, C_v = Specific heats at constant pressure and at constant volume respectively

H_i, H_C = Enthalpies of the fluid far upstream of the orifice and at the choke respectively

P = Pressure

S_i, S_C = Entropies of the fluid far upstream of the orifice and at the choke respectively

S = Entropy of the fluid

T = Temperature

ρ = Density

The conditions at the choke are calculated by solving equations 3.4.8 - 3.4.10 iteratively. The mass flow rate is then determined from a knowledge of orifice area and a discharge coefficient.

THERMOPHYSICAL PROPERTIES

The thermodynamic phase and transport properties are predicted by a computer package based on an extended principle of corresponding states [Rowlinson & Watson, 1969]. Briefly, this approach is based on relating the properties of the mixture to those of methane chosen as a reference substance [Saville & Szczepanski, 1982]. The authors justified the choice of the extended principle of corresponding states over the well known cubic equations of states (CEOS) as a consequence of its accurate representation of phase equilibrium, enthalpy and density, whilst the CEOS

are claimed to be much less successful in predicting the last two properties. However, the authors point out that solving the extended principle of corresponding states is more computationally demanding (ca. two folds [Richardson, 1997]) compared to solving a CEOS.

EXPERIMENTAL VALIDATION

Predictions from BLOWDOWN were compared with experimental data. Three comparisons were published, one with a small vessel containing nitrogen (initial pressure is 148 atm) and the other two with a full-size vessel containing different hydrocarbon mixtures (initial pressures ca. 118.4 atm). In all cases, the model accurately predicted the pressure/time profiles as well as the minimum average bulk fluid and minimum inside wall temperatures to 5 K. The comparisons of fluid and inner wall temperature/time profiles for nitrogen were given in figure 2.1 in chapter 2. The time profiles for the fluid and wall temperatures for a hydrocarbon mixture (66.5% mole methane, 3.5% mole ethane, 30.0% mole propane and traces of butanes) were respectively given in figures 2.2 and 2.3 in the same chapter.

The corresponding results (with the exception of the measured liquid temperatures) for another hydrocarbon mixture containing 85.5% mole methane, 4.5% mole ethane and 10.0% mole propane with traces of butanes are given in figures 3.12 and 3.13. Solid lines represent predictions from BLOWDOWN while the shaded regions show experimental data.

From the above figures, although there is no comparison for liquid temperature, the proposed model is capable of predicting the variation of inner wetted wall temperature with time accurately (see figure 3.13). The authors indicated that the fluid in the vessel was initially gas and liquid condensate started to form after about 100 s, which was sometime after entering the mixture's phase envelope. The maximum depth of liquid condensate was about 0.1 m which was very low when compared with the vessel height of 3.24 m. They attributed the delay to the relatively slow process of phase equilibration. However, it is interesting to note that figure 3.13 showing the measured and predicted temperatures of wall in contact with liquid phase indicates the presence of vapour condensate well before 100 s.

Additionally, the predicted liquid temperature (figure 3.12) initially decreases and then increases at about 100 s before it decreases again. This behaviour is very similar to the experimental observation made earlier by the authors [Haque et al., 1990] in the case of depressurisation of a nitrogen mixture (see figure 2.10 in chapter 2) where a small amount of vapour was condensed after 10 s (total blowdown time was 100 s).

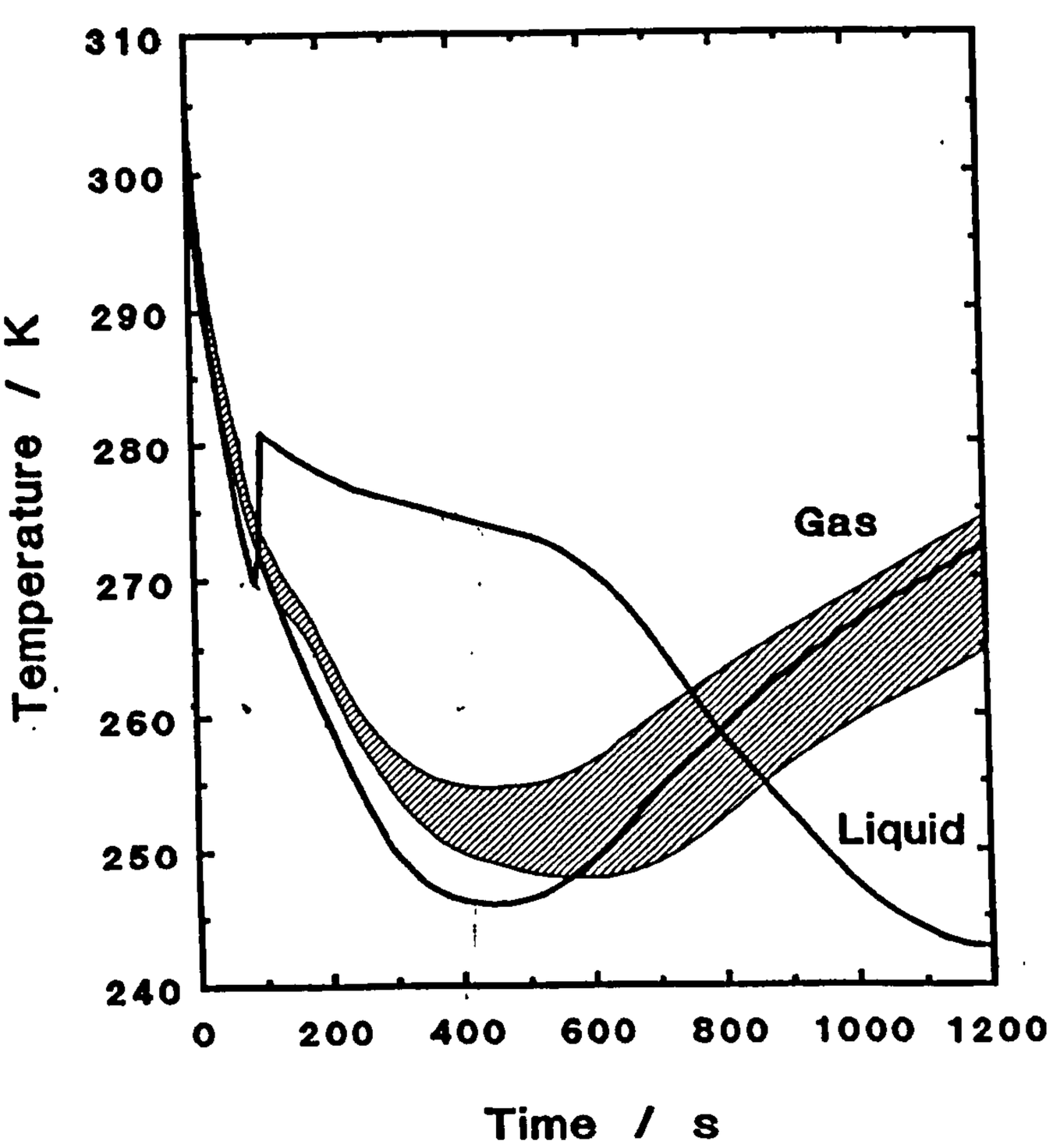

Figure 3.12 **Variations of bulk gas and bulk liquid temperatures with time for depressurisation of a hydrocarbon mixture (85.5% mole methane, 4.5 mole % ethane, 10.0 mole % propane with traces of higher molecular weight hydrocarbons in particular of butanes). Hatched regions span experimental measurements, solid lines are predictions from BLOWDOWN [Haque et al. 1992b].**

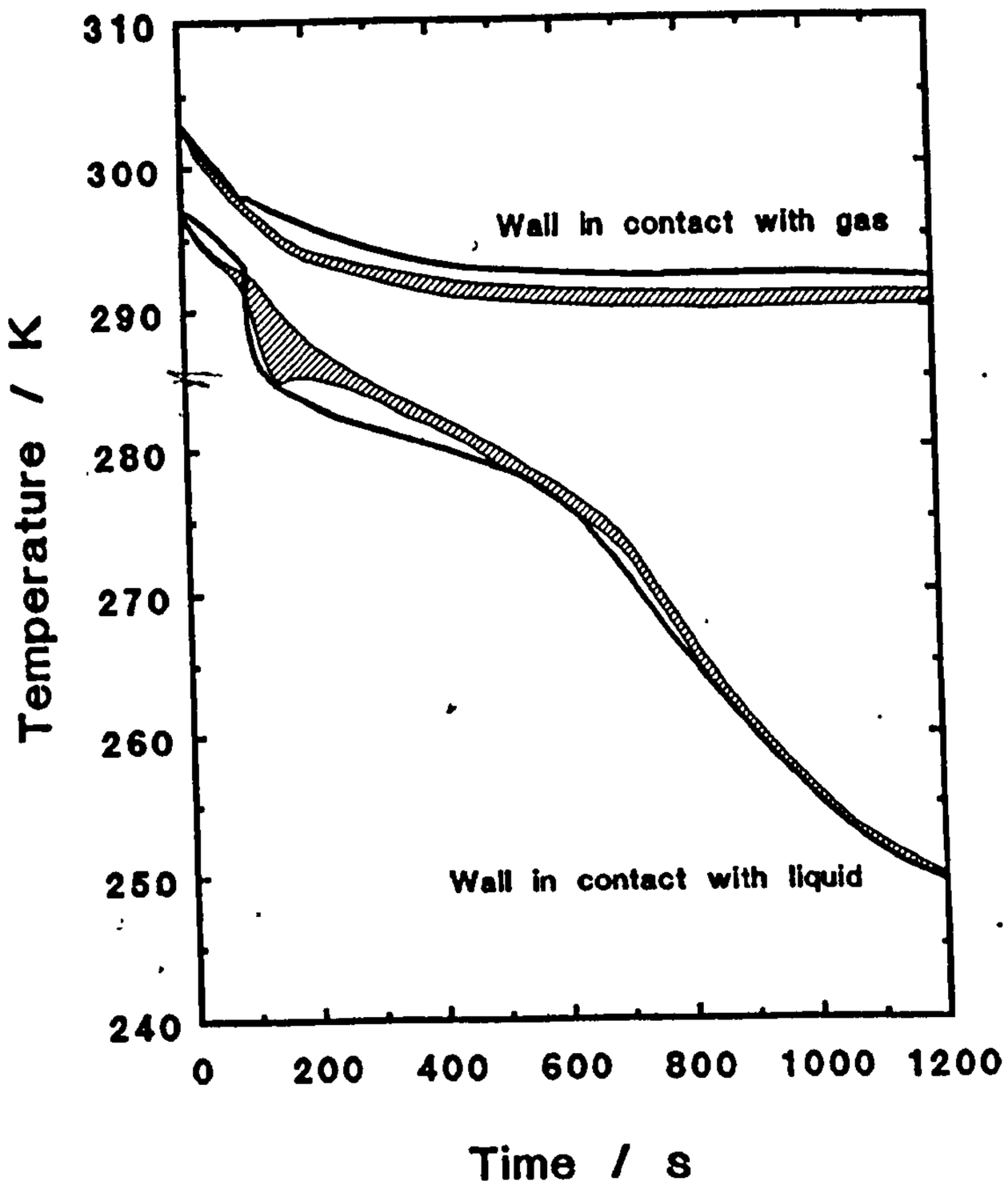

Figure 3.13 Variations of inside wall temperatures with time for depressurisation of a hydrocarbon mixture (85.5% mole methane, 4.5 mole % ethane, 10.0 mole % propane with traces of higher molecular weight hydrocarbons in particular of butanes). Hatched regions span experimental measurements, solid lines are predictions from BLOWDOWN [Haque et al. 1992b]

3.4.2 Split Fluid Model [Overa et al., 1994]

In response to the shortcomings associated with the conventional methods based on common engineering practice for blowdown (see section 3.2), Overa et al. [1994] proposed a SPLIT FLUID MODEL for blowdown of single or two-phase hydrocarbon mixtures. Figure 3.14 (page 71) is an overview of the depressurisation model and the various output parameters. Calculations are carried out using variable time steps throughout the depressurisation process.

The vessel is assumed to be at spatially uniform pressure and each fluid zone is well-mixed. Hence, there is a uniform distribution of temperature and composition in each zone. Gas only is assumed to be discharged from the vessel.

MATHEMATICAL ALGORITHM

Overa et al. [1994] divided the fluid within the vessel during blowdown into two phases: the liquid phase which comprises the existing liquid and condensed vapour from the sub-cooled vapour and the vapour phase which comprises the existing vapour and evaporated liquid from the boiling liquid. Heat transfer between the vapour and the liquid as well as the associated vessel walls are considered. The authors proposed different thermodynamic trajectories for each fluid phase.

The enthalpy change of the liquid phase during a given time interval is assumed to be due to heat transfer effects only. Hence, work done by the liquid due to expansion is ignored. Heat transfer to the liquid phase is assumed to take place from wetted wall surface. On the other hand, heat transfer from the vapour phase occurs due to the temperature difference between the two phases.

The liquid temperature, T_L, and the number of moles of evaporated liquid, N_b, at stage i+1 are determined by pressure enthalpy flash at vessel pressure. The specific enthalpy of the liquid is given by :

$$H_L^{i+1} = \frac{N_L}{N_L + N_C}\left(H_L^i - \frac{(q_L - q_{LV})\Delta t}{N_L}\right) + \frac{N_C}{N_L + N_C} H_{LC} \qquad (3.4.11)$$

Where H_{LC}, H_L = Specific enthalpies of condensed vapour and liquid respectively

N_C, N_L = Number of moles of condensed vapour and evaporated liquid respectively

q_L, q_{LV} = Rates of heat transfer between liquid and vessel or vapour

Δt = Finite time step for calculation

The evaporated liquid is added to the existing vapour and the vapour composition is updated.

The entropy change of vapour phase is determined on the basis of second law of thermodynamics by assuming that the heat transfer during a given 'small' time interval is infinitesimal and that there is no change in temperature.

The vapour temperature, T_V, vessel pressure, P, and the number of moles of condensed vapour, N_C, at stage i+1 are determined by a volume/entropy flash. The vapour volume is fixed when both the vessel and liquid volumes are known. The specific entropy of the vapour is given by :

$$S_V^{i+1} = \frac{N_V}{N_V + N_b}\left(S_V^i - \frac{\frac{(q_V + q_{LV})\Delta t}{T_V}}{N_V} \right) + \frac{N_b}{N_V + N_b} S_b \qquad (3.4.12)$$

Where S_b, S_V = Specific entropies of vaporized liquid and vapour respectively

N_b, N_V = Number of moles of vaporized liquid and vapour respectively

q_V = Rate of heat transfer between vessel and vapour

Equations 3.4.11 and 3.4.12 may be solved iteratively until the vessel pressure during a given time interval is found.

HEAT AND MASS TRANSFER EFFECTS

Heat Transfer Between Vessel Wall/Fluid/Surrounding

Overa et al. [1994] assumed negligible temperature gradient across the wall thickness. The wetted, T_{LW}^{i+1}, and unwetted, T_{VW}^{i+1}, wall temperatures at stage i+1 are respectively given by :

$$T_{LW}^{i+1} = T_{LW}^{i} + \frac{(q_L + q_0)\Delta t}{m_{LW} C_{pW}} \tag{3.4.13}$$

$$T_{VW}^{i+1} = T_{VW}^{i} + \frac{(q_V + q_0)\Delta t}{m_{VW} C_{pW}} \tag{3.4.14}$$

Where C_{pw} = Specific heat capacity of vessel wall material

m_{LW}, m_{VW} = Masses of wetted and unwetted wall respectively

q_0 = Rate of heat transfer from the surrounding

The heat capacity of vessel wall material is determined as a function of temperature. However, no correlation is specified.

The model considers natural and forced convection between vessel wall and vapour by employing standard correlations [Kreith & Black, 1980; Incropera & De Witt, 1985] to predict the appropriate heat transfer coefficients. The rate of heat transfer between vapour and unwetted wall, q_V , is given by :

$$q_V = (T_{VW} - T_V) U_V A_V \tag{3.4.15}$$

Where A_V = Surface area of unwetted inner wall

U_V = Overall heat transfer coefficient between vessel wall and vapour

The boiling heat transfer coefficient between liquid and vessel wall is assumed to be constant. The rate of heat transfer between liquid and wetted wall, q_L, is determined from equation 3.4.15 where wetted wall and liquid temperatures are used in conjunction with the appropriate heat transfer coefficient and inner wetted wall surface area.

Based on experimental data both for depressurisation of a 'real oil' and for fire exposure tests of vessels filled with liquid pressurised gas (LPG), typical values of heat transfer coefficients between wetted wall and liquid phase were determined to be in the range 1000 - 3000 W/m^2K.

Heat transfer between wall and surrounding is assumed to be by convection. For insulated vessels, this term is assumed to be zero. For uninsulated vessels, the authors used values of heat transfer coefficients in the range 5 - 30 W/m^2K. No correlation for determining the corresponding heat transfer coefficient is specified.

Heat and Mass Flux between Adjacent Fluid Zones

The SPLIT FLUID MODEL considers not only heat and mass transfer by evaporation and condensation but also takes into account the effect of natural convection between liquid and vapour due to temperature difference between the two phases. Heat transfer between liquid and vapour surface is assumed to be by laminar natural convection and a standard correlation [Incropera & DeWitt, 1985] is used to determine the appropriate heat transfer coefficient. The assumption is adopted for both warm liquid/cold vapour and vice versa. The vapour/liquid interface heat transfer rate is given by :

$$q_{LV} = (T_L - T_V) U_{LV} A_{surface} \qquad (3.4.16)$$

Where $A_{surface}$ = Vapour/liquid interfacial area

U_{LV} = Overall heat transfer coefficient between vapour and liquid

DISCHARGE RATE CALCULATION

The model allows calculation of discharge through a valve or an orifice. The calculation is applicable to both sonic and subsonic flow. However, two-phase flow discharge is not considered and the equation for discharge rate calculation has not been given.

THERMOPHYSICAL PROPERTIES

The thermophysical properties are predicted by an in house process simulator [Wilson et al., 1991]. No correlation is specified.

EXPERIMENTAL VALIDATION

Figures 2.6 in chapter 2 shows the variations of liquid and gas temperatures with time following the blowdown of a two-phase hydrocarbon mixture (no composition specified) from 19.7 atm and 25 °C. Solid lines show data predicted from the model which are in good agreement with those obtained from experiment. The SPLIT FLUID MODEL is capable of predicting temperatures to 4 K. The dashed line shows the results obtained by assuming 50% isentropic expansion of the fluid which greatly overestimates the fluid temperature. No data indicating the performance of the model in terms of predicting the pressure/time profile or the wall temperatures in contact with the liquid and vapour phases are given.

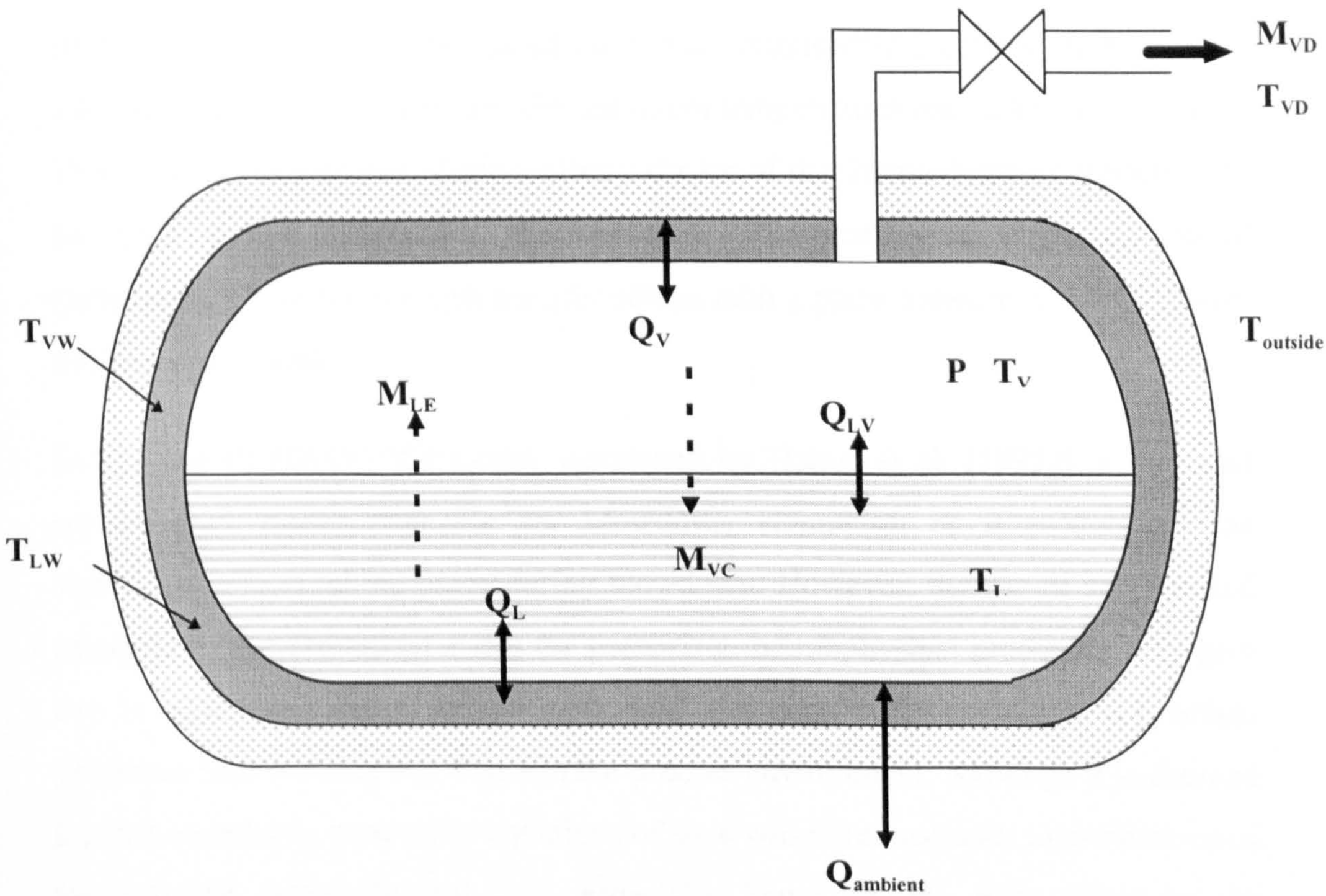

Keys :

M_{LE}	Mass of evaporated liquid	T_L	Liquid phase temperature
M_{VC}	Mass of condensed vapour	T_{LW}	Wetted wall temperature
M_{VD}	Total mass of discharged vapour	$T_{outside}$	Temperature at the surface of the vessel
P	Vessel pressure	T_V	Vapour phase temperature
$Q_{ambient}$	Heat input (or loss) to ambient	T_{VD}	Discharge gas temperature
Q_L	Heat flow between vessel and liquid	T_{VW}	Unwetted wall temperature
Q_{LV}	Heat flow between vapour and liquid		Vapour phase
Q_V	Heat flow between vessel and vapour		Liquid phase
			Metal wall layer
			Insulation wall layer

Figure 3.14 Depressurisation model for Split Fluid Model [Overa et. al., 1994]

3.5 CONCLUSION

On the basis of the literature reviewed in this chapter, it may be concluded that simple blowdown simulations based on various engineering practices are hopelessly inadequate in terms of predicting the minimum temperatures encountered in practice. This is primarily because of the arbitrary choice of the thermodynamic trajectory of the fluid during blowdown. The appropriate thermodynamic trajectory should quantitatively account for heat transfer effects taking place between the fluid phases and associated walls.

So far, the BLOWDOWN model, developed by Haque et al. [1992a] is the most sophisticated model available for blowdown simulation as it models all the significant effects taking place during blowdown. However, the use of an extended principle of corresponding states for predicting thermophysical properties may give rise to significant computational work load and consistency problems in practical situations as it is rarely employed in the process environment. Although it is claimed that the commonly used cubic equations of state will introduce error to predictions of the required thermophysical data, especially liquid density, their effect on the performance of the blowdown simulation is not known.

Despite the simplicity of Overa et al.'s [1994] blowdown model, it has not been validated at high pressures (>19.7 atm) for blowdown of hydrocarbon mixtures. Additionally, the authors use an experimentally determined heat transfer coefficient between the wetted wall and the liquid phase and hence the model is not strictly predictive. Furthermore, the model is not capable of predicting the presence of two-phase discharge at the orifice; it assumes vapour discharge only. The effects of this assumption on the predictions of temperature and pressure during blowdown especially at elevated pressures are not known.

In conclusion, it is obvious, based on mathematical models by Overa et al. [1994] and Haque et al. [1992a], that the thermodynamic trajectory for vapour phase needs to account for both work and heat. However, the authors have defined different relationships between heat and temperature. Overa et al. assume the heat transfer

during a given time interval is infinitesimal and the vapour temperature is unchanged while Haque et al. assume a linear relationship between heat and vapour temperature.

Different opinions prevail on the thermodynamic trajectory for the liquid phase. Overa et al. [1994] ignore the work done by the liquid while Haque et al. [1992a] take this into account by assuming the liquid expands polytropically. Haque et al. [1992b] demonstrated that their model agrees well with experimental measurements at elevated pressures (up to 120 atm) while Overa et al.'s model is only validated in conjunction with blowdown of a low pressure (ca. 20 atm) two-phase hydrocarbon mixture.

CHAPTER 4

THE DEVELOPMENT OF A BLOWDOWN MATHEMATICAL MODEL : BLOWSIM

4.1 INTRODUCTION

The review of the important mathematical models for blowdown, particularly BLOWDOWN [Haque et al., 1992a] and SPLIT FLUID MODEL [Overa et al., 1994], highlighted the following points which require further investigation:

1) The effects of cubic equations of state on the performance of blowdown simulation in terms of predicting field data.
2) The suitability of Overa et al.'s thermodynamic trajectory for vapour phase expansion during blowdown of hydrocarbon mixtures from elevated pressures.
3) The effects of applying different thermodynamic trajectories to liquid phase in terms of the accuracy in predicting temperatures and pressures during blowdown.
4) The effect of Overa et al.'s [1994] suggested constant heat transfer coefficients between liquid and wetted wall compared to the boiling heat flux empirical correlation employed by Haque et al. [1992a] on the accuracy of the predicted liquid and wetted wall temperatures.
5) Comparisons of the rigorous [Haque et al., 1992a] against simple discharge calculation methods (based on ideal gas assumption) in terms of predicting temperatures and pressures during blowdown.
6) The level of sophistication required in blowdown modelling.

This chapter describes the development of a mathematical model, BLOWSIM which addresses the above issues. It allows for vapour space blowdown through a single orifice from the top of an isolated vessel containing single (vapour) or two-phase (vapour and liquid) hydrocarbon mixtures. The evaluation of performance of various cubic equations of state in predicting the appropriate thermodynamic properties are described in the next chapter. An evaluation of the accuracy of the model by

comparison with experimental data and those predicted from BLOWDOWN is presented in chapter 6.

4.2 DEVELOPMENT OF BLOWSIM MATHEMATICAL MODEL

BLOWSIM accounts for the most important processes described in chapter 2 which take place during blowdown. These include non-equilibrium effects between phases, heat transfer between each fluid phase and their corresponding sections of vessel wall, inter-phase fluxes due to evaporation and condensation, and the effects of sonic flow at the orifice. Typical output include the variations of discharge rate, pressure together with fluid and wall temperatures with time.

The temperature and composition in each fluid phase are assumed to be spatially uniform (well mixed), and the pressure is assumed to be spatially uniform in the vessel. Although the results of published blowdown experiments [Haque et al., 1992b] indicate the presence of temperature gradients in both vapour and liquid phases (the effect is more pronounced in vapour phase; figure 2.2, chapter 2), Haque et al. [1992b] and Overa et al. [1994] demonstrated that their blowdown simulations based on the above assumptions gave reasonable predictions when compared with experimental data (see figures 2.1- 2.3 for Haque et al.'s validations and figure 2.6 for Overa et al.'s validation). In addition, the fluid prior to blowdown is assumed to be at equilibrium and the vessel wall temperature equal to the fluid temperature.

The detailed assumptions regarding heat and mass transfer together with discharge calculations are described later in sections 4.2.2 - 4.2.5.

4.2.1 Application of Finite Difference Method to Blowdown Calculation

The equations to be solved in blowdown calculation are mainly non-linear and functions of both pressure and time. It is more practical to solve these equations by finite difference method instead of integration. In this study, we approximate the depressurisation process by a series of variable pressure increments. The advantages of employing pressure increments are it s thermodynamic convenience and computational efficiency when compared to choosing time intervals (employed by Overa et al.'s model [1994]) which are thermodynamically irrelevant.

The pressure increment, ΔP_i, and vessel pressure, P_i, at stage i are determined by the following equations :

$$\Delta P_i = P_{i-1} \times r \tag{4.2.1}$$

$$P_i = P_{i-1} - \Delta P_i \tag{4.2.2}$$

Where r is the constant ratio between pressure increment and vessel pressure during blowdown. In this study r is chosen to be equal to 0.05.

The accuracy of blowdown predictions by the finite difference method strongly depends on the magnitude of the required duration to depressurise the vessel through a given pressure increment. As the vessel pressure declines exponentially with time (see figure 2.4 and figures 3.3 - 3.5), the depressurising duration for a constant pressure increment increases exponentially with time. Consequently large errors can be introduced when using the same depressurisation increment, especially during the later stages of blowdown. Therefore, equation 4.2.1 is established to prevent the possibility of introducing the above errors by decreasing the pressure increment exponentially with declining pressure.

It is important to note that when the depressurisation process is approximated by a series of pressure increments, it is necessary to assume the vessel pressure decreases monotonically with time. Otherwise, time intervals approximation should be used. An example of non-monotone behaviour in depressurisation is described in section 2.2.3 of chapter 2 where there is a sudden increase in vessel's pressure due to the effects of liquid swelling and high liquid level prior to blowdown (see figure 2.11 of chapter 2). However, the above behaviour is usually prevented in process industry by limiting the liquid level below half of the height of the vessel prior to blowdown.

4.2.2 Fluid Phase Material Balances

In section 2.2.3 of chapter 2, the inter-phase mass and energy fluxes during blowdown is shown to be a consequence of condensation (in sub-cooled vapour) and evaporation (in boiling liquid). In order to derive the appropriate material balance for each fluid phase and account for the above effects, the fluid in the vessel during blowdown is divided into two zones :

Zone1: Sub-cooled vapour and condensed vapour

Zone2: Liquid or condensed vapour from zone 1.

The phase distribution is shown in figure 4.1 (see page 79). If the mixture is single phase (vapour only), zone 1 contains pure vapour whilst zone 2 is eliminated. The appropriate assumptions and the material balances for both zones are described separately in the following.

4.2.2.1 Zone 1 : Condensation in Sub-Cooled Vapour

Until now, Haque et al.'s mathematical model [1992a] is the only one which accounts for condensation delay and the finite efficiency of phase separation in the sub-cooled vapour by predicting the nucleation time and settling velocity of liquid droplets. These parameters are determined using empirical correlations simply expressed as a function of the equilibrium liquid fraction in vapour phase (see equations 3.4.6 and 3.4.7 respectively in chapter 3). However, there is some uncertainty associated with their use in conjunction with mixtures other than those tested by the authors.

In this study, the delay in formation of liquid droplets is assumed to be negligible when compared with depressurising duration for a given pressure increment. Additionally, the condensed vapour is assumed to be at equilibrium with the vapour phase. For a given pressure interval, the condensed vapour is assumed to settle immediately at the bottom of the vessel or above the existing liquid phase.

Based on the above assumptions, for a given pressure increment, the material balance for zone 1 is given by :

$$N_{i-1,V} + N_{i,EL} = N_{i,V} + N_{i,CV} + N_{i,D} \qquad (4.2.3)$$

Where $N_{i,CV}$ = No. of mole of condensed vapour in zone 1 at stage i

$N_{i-1,V}$, $N_{i,V}$ = No. of moles of vapour in zone 1 at stages i-1 and i respectively

$N_{i,D}$ = No. of mole of discharged material at stage i

$N_{i,EL}$ = No. of mole of evaporated liquid from zone 2 at stage i

For vessel containing vapour only, $N_{i,CV}$ and $N_{i,EL}$ are equal to zero.

The volume of discharged material (either vapour or vapour and liquid) is determined from the volume of fluid in both zones 1 and 2 after expansion minus the vessel volume. The mass of discharged material is given by the product of density and volume. The corresponding density is dependent on the phase of fluid approaching the orifice. If single phase, density of vapour is applied, otherwise the bulk density is used.

4.2.2.2 Zone 2 : Evaporation in Boiling Liquid

No mathematical models accounting for the delay in boiling and also for determining the efficiency of phase separation in the boiling liquid during blowdown of hydrocarbon mixtures exist. On the other hand, the liquid level prior to blowdown is usually maintained at a low level. Hence, any swelling of the liquid which is characterised by such delays and accompanied by a substantial increase in pressure can be ignored.

Similar to zone 1, the process of boiling during blowdown is simplified by assuming the bubbles rise rapidly and separate freely from the boiling liquid which is at equilibrium with evaporated vapour. The latter is assumed to be well mixed with the zone 1 fluid.

The material balance for zone 2 is given by :

$$N_{i-1,L} + N_{i-1,CV} = N_{i,L} - N_{i,EL} \qquad (4.2.4)$$

Where $N_{i-1,L}$ and $N_{i,L}$ are number of moles of liquid in zone 2 at stages i-1 and i respectively.

It is noted that the above assumption may not be appropriate when there is a sudden increase in liquid level during blowdown. This may happen, for example, when a supercritical vapour is rapidly depressurised and enters the two-phase region from the bubble point boundary instead of the dew point boundary. The amount of liquid formed is much larger in the former case and can lead to high levels of liquid where the effects of liquid swelling may become important.

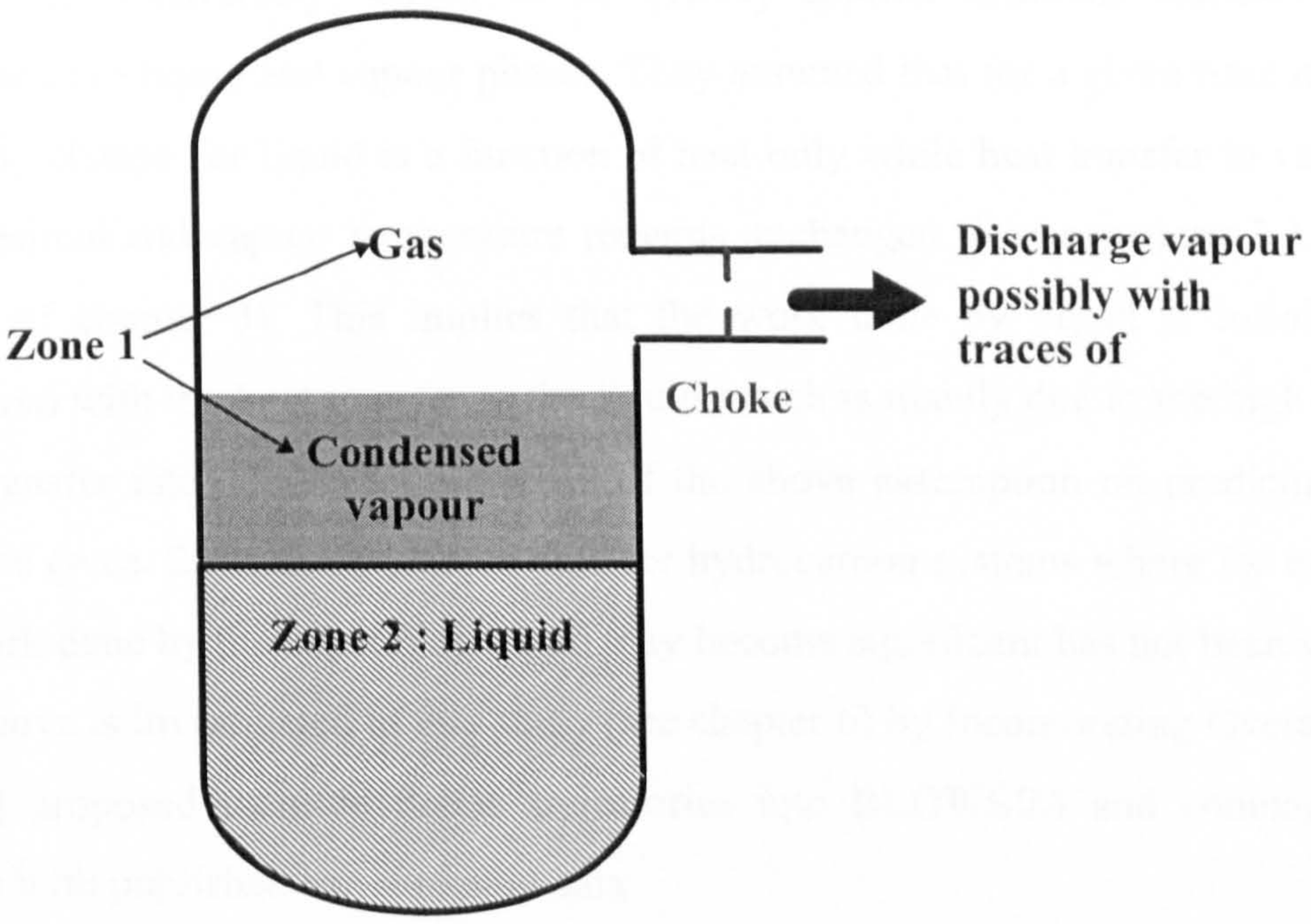

Figure 4.1 Fluid phase distribution within the vessel modelled by BLOWSIM during blowdown

4.2.3 Thermodynamic Trajectories for Fluid Phases

The rates of mass and energy transfer in each fluid zone are governed by an appropriate thermodynamic trajectory. Haque et al. [1992a] applied the same thermodynamic trajectory to all phases by assuming a linear relationship between heat and temperature over a given pressure increment during blowdown (see equation 3.4.2 of chapter 3). The authors were able to generate accurate blowdown predictions of hydrocarbon mixtures at high pressures (see their validations in figures 2.1 - 2.4 of chapter 2). Conversely, Overa et al. [1994] applied different thermodynamic trajectories to liquid and vapour phases. They assumed that for a given time interval, enthalpy change for liquid is a function of heat only while heat transfer to vapour is infinitesimal and vapour temperature remains unchanged. (see equations 3.4.11 and 3.4.12 of chapter 3). This implies that the work done by liquid is infinitesimal compared with the heat transfer to the liquid which is mainly due to the high boiling heat transfer rate. However, the effect of the above assumption on predicting high pressure (> ca. 20 atm) blowdown data for hydrocarbon systems where for example, the work done by the expanding liquid may become significant has not been verified. The above is investigated in this study (see chapter 6) by incorporating Overa et al.'s [1994] proposed thermodynamic trajectories into BLOWSIM and comparing the results with published experimental data.

The thermodynamic trajectories in BLOWSIM and the corresponding enthalpy or entropy balances for each fluid zone are given in the following.

4.2.3.1 Thermodynamic Trajectory for Zone 1

In chapter 3, we concluded that the thermodynamic trajectory for vapour phase needs to account for both work and heat (polytropic process). Some simple mathematical models for blowdown of single component non-condensable gases, described in section 3.3, relate enthalpy change of vapour to heat and work using the first law of thermodynamics. However, for a multi-component real fluids, work done by the fluid due to expansion, and hence the change of enthalpy cannot be easily defined especially once the two-phase region is entered. An alternative way adopted in this

study is to apply the second law of thermodynamics which relates entropy to heat and subsequently solve the first law of thermodynamics for work done by the fluid.

The entropy change for a reversible expansion of a fluid is given by :

$$\Delta S = \int \frac{dQ_{REV}}{T} \tag{4.2.5}$$

Where Q_{REV} = Heat transfer by reversible process

S = Entropy

T = Temperature

An assumed relationship between heat and temperature is required to determine ΔS. Overa et al. [1994] assumed that the amount of heat transfer to the vapour during a given 'small' time interval is infinitesimal and the vapour temperature remains unchanged (see equation 3.4.12 of chapter 3).

Hence, equation 4.2.5 becomes :

$$\Delta S = \frac{Q_{REV}}{T} \tag{4.2.6}$$

Based on the above equation and using the material balance given by equation 4.2.3, for a given pressure increment, the specific entropy in zone 1, $S_{i,Z1}$, for a vessel containing either vapour or two-phase mixture are given by equations 4.2.8 and 4.2.9 respectively.

Vapour only :

$$S_{i,Z1} = S_{i-1,Z1} + \frac{Q_{i,Z1}}{T_{i,Z1}\, N_{i-1,Z1}} \tag{4.2.7}$$

Two-phase mixture :

$$S_{i,Z1} = \frac{T_{i,Z1}\left[\left(S_{i-1,V}\right)N_{i-1,V} + \left(S_{i,EL}\right)N_{i,EL}\right] + Q_{i,Z1}}{T_{i,Z1}\left(N_{i-1,V} + N_{i,EL}\right)} \tag{4.2.8}$$

Where $N_{i-1,Z1}$ = Total no. of mole of zone 1 fluid in the vessel at stage i-1

$Q_{i,Z1}$ = Total heat transfer to zone 1 fluid at stage i

$S_{i-1,V}$ = Specific entropy of vapour at stage i-1

$S_{i-1,Z1}$ = Specific entropy of fluid in zone 1 at stage i-1

$S_{i,EL}$ = Specific entropy of evaporated liquid from zone 2 at stage i

$T_{i,Z1}$ = Fluid temperature in zone 1 at stage i

The mole fraction of condensed vapour and fluid temperature, $T_{i,Z1}$, are determined by pressure/entropy flash calculation at vessel pressure, P_i, and $S_{i,Z1}$. The composition, Y_n, used for the corresponding flash calculation is determined from :

$$Y_n = \frac{y_{i-1,V,n} \times N_{i-1,V} + y_{i,EL,n} \times N_{i,EL}}{N_{i-1,V} + N_{i,EL}} \qquad (4.2.9)$$

Where $y_{i-1,V,n}$ = Composition of component n in vapour at stage i-1

$y_{i,EL,n}$ = Composition of component n in evaporated liquid at stage i

4.2.3.2 Thermodynamic Trajectory for Zone 2

The effect of assuming that the work done by the liquid is negligible on blowdown data is investigated in this study (see chapter 6) by applying Overa's proposed thermodynamic trajectories for vapour (accounts for both heat and work) and liquid phases (discounting work) respectively to zone 2 and comparing results with published experimental data. The appropriate energy balances are derived in the following.

Applying Overa et al.'s liquid thermodynamic trajectory to zone 2 fluid and assuming the process is reversible, the first law of thermodynamics gives :

$$\Delta H = Q_{REV} \qquad (4.2.10)$$

On the basis of the above equation and material balance given by equation 4.2.4, for a given pressure increment, the specific enthalpy in zone 2, $H_{i,Z2}$, for a vessel containing two-phase mixture is given by :

$$H_{i,Z2} = \frac{(H_{i-1,L})N_{i-1,L} + (H_{i-1,CV})N_{i-1,CV} + Q_{i,Z2}}{N_{i-1,L} + N_{i-1,CV}} \quad (4.2.11)$$

Where $N_{i-1,CV}$ = No. of mole of condensed vapour from zone 1 at stage i-1

$N_{i-1,L}$ = No. of mole of liquid in zone 2 at stage i-1

$H_{i-1,CV}$ = Specific enthalpy of condensed vapour at stage i-1

$H_{i-1,L}$ = Specific enthalpy of liquid in zone 2 at stage i-1

$Q_{i,Z2}$ = Total heat transfer to zone 2 fluid at stage i

Similarly, applying Overa et al.'s vapour thermodynamic trajectory, equation 4.2.6, and material balance given by equation 4.2.4, for a given pressure increment, the specific entropy in zone 2, $S_{i,Z2}$, for a vessel containing two-phase mixture is given by:

$$S_{i,Z2} = \frac{T_{i,Z2}\left[(S_{i-1,L})N_{i-1,L} + (S_{i-1,CV})N_{i-1,CV}\right] + Q_{i,Z2}}{T_{i,Z2}(N_{i-1,L} + N_{i-1,CV})} \quad (4.2.12)$$

Where $S_{i-1,L}$ = Specific entropy of liquid at stage i-1

$S_{i-1,CV}$ = Specific entropy of condensed vapour from zone 1 at stage i

$T_{i,Z2}$ = Fluid temperature in zone 2 at stage i

The mole fraction of evaporated liquid and $T_{i,Z2}$ are determined by pressure/enthalpy (equation 4.2.11) or pressure/entropy (equation 4.2.12) flash calculations at vessel pressure, P_i. The composition, X_n, used for both flash calculations is determined from :

$$X_n = \frac{x_{i-1,L,n} \times N_{i-1,L} + x_{i-1,CV,n} \times N_{i-1,CV}}{N_{i-1,L} + N_{i-1,CV}} \quad (4.2.13)$$

Where $x_{i-1,L,n}$ = Composition of component n in liquid at stage i-1

$x_{i-1,CV,n}$ = Composition of component n in condensed vapour at stage i-1

The computer programme used to perform pressure/enthalpy and pressure/entropy flash is described in section 4.4.

4.2.4 Heat Transfer between Vessel Wall and Fluid Phases

In chapter 2, the published experimental observations reviewed show the prevalence of convection and boiling heat transfer between vessel wall/vapour and vessel wall/liquid respectively. These are also the key features of Haque et al.'s [1992a] and Overa et al.'s [1994] mathematical models. Although Overa et al. also accounted for convection heat transfer between phases due to temperature difference (see equation 3.4.16 in chapter 3), in this study, we assume that the above effect is negligible when compared with the other modes of heat transfer. In addition, the following assumptions are applied :

1) Heat transfer between the vessel and surrounding is negligible when compared with other modes of heat transfer within the vessel under non-fire or mild weather conditions.

2) The effects of heat transfer due to presence of insulation or [1]duplex construction are ignored. Heat transfer is only considered between the fluid and the layer of vessel wall adjacent to the fluid within the vessel.

3) Vessel wall temperature in contact with each fluid zone is assumed to be uniform along the vessel surface and temperature gradient across the thickness of the wall is negligible.

4) The rate of heat transfer between each fluid zone and corresponding section of vessel wall is constant during a given pressure increment.

In the above, the second assumption will produce conservative average vessel wall temperature predictions (lower than the actual temperature) as it reduces the effective vessel's heat capacity and hence the amount of heat transferred to the fluid. This in turn increases the drop in the average wall temperature in contact with the fluid during blowdown. If temperatures of other wall layers are required, the finite-difference solution of the transient heat conduction equation [Incropera & DeWitt,

[1] Multi-layer construction

1985], may be used to determine the temperature gradient across different wall layers.

The third assumption mentioned above is based on experimental observations by Haque et al. [1992b] as shown in figure 2.3 of chapter 2. On the other hand, the temperature gradient across the wall thickness may be considered to be negligible by assuming that the conduction resistance within the vessel wall is very small when compared with the heat transfer resistance between the wall and each fluid phase. Otherwise, the finite-difference solution of the transient heat conduction equation [Incropera & DeWitt, 1985] may be used to determine the temperature change across the wall thickness.

The last assumption given above is a consequence of the application of finite difference method which approximates variations of all variables with time by a series of step changes.

On the basis of the above assumptions, the energy balance between each zone and corresponding section of vessel wall is given by :

$$Q_{i,Zx} = \left(T^{i}_{W,Zx} - T_{Zx}\right) U_{Zx} A_{Zx} \Delta t = M_{W,Zx} C_{pW} \left(T^{i-1}_{W,Zx} - T^{i}_{W,Zx}\right) \quad (4.2.14)$$

Where x = Zone number, either 1 or 2

A_{Zx} = Internal area of vessel wall in contact with zone x

C_{pW} = Specific heat capacity at constant pressure of vessel wall material

$M_{W,Zx}$ = Mass of section of vessel wall in contact with zone x

$T^{i-1}_{W,Zx}, T^{i}_{W,Zx}$ = Average wall temperatures adjacent to zone x at stages i-1 and i respectively

U_{Zx} = Overall heat transfer coefficient between zone x and corresponding section of vessel wall

Although C_{pW}, is usually a function of temperature, in this study, it is assumed to be constant as its variation with temperature under 400 K is considered to be small for carbon steel and stainless steel [Incropera & DeWitt, 1996c]. The corresponding

assumptions and correlations for predicting heat transfer coefficient and heat flux between vessel wall and each fluid zone are given in the following.

4.2.4.1 Heat Transfer between Vessel Wall and Zone 1

As natural convection dominates forced convection in the vapour space especially at high pressures during blowdown (see section 2.2.1 of chapter 2), in this study, in contrast to Haque et al. [1992a] and Overa et al. [1994], we assume that forced convection induced by the discharging material is negligible.

The heat transfer coefficients between fluid and vessel wall are given by empirical correlations (see later) which are functions of vessel geometry and thermophysical properties of the fluid. At a given pressure increment, assuming that the amount of condensed vapour in zone 1 (see figure 4.1) is small enough so that its effect on heat transfer with associated section of vessel wall may be ignored, the thermophysical properties are calculated for vapour only. These are in turn determined at the film temperature, $T_f = \left(T_{W,Z1} + T_{Z1}\right)/2$. Hence, U_{Zx} in equation 4.2.14, where x is equal to 1, is a function of both $T_{W,Z1}$ and T_{Z1}. In order to determine $T_{W,Z1}$, for a given T_{Z1}, equation 4.2.14 is solved by iteration using Brent's method [Press et al., 1992]. The methods for predicting the required transport properties are given at the end of this section.

A correlation for predicting the natural convection heat transfer coefficient for an enclosed fluid in an isothermal container is not available. In this work, a vertical vessel is approximated by ignoring the effects of curvature on rate of heat transfer and treating the cylindrical section as a vertical plane with the same inner surface area. The two ends on the other hand are approximated by two horizontal planes.

The overall heat transfer coefficient, U_{Z1}, in equation 4.2.14 is determined by :

$$U_{Z1} = \left(h_{Tend,} + h_{Bend}\right)\left(\frac{A_{end}}{A_{Z1}}\right) + h_{cyc,Vap}\left(\frac{A_{cyc,Z1}}{A_{Z1}}\right) \qquad (4.2.15)$$

Where A_{end} = Inner surface area of vessel end

$A_{cyc,Z1}$ = Inner surface area of cylindrical part of the vessel in contact with zone 1 fluid

A_{Z1} = Total inner surface area in contact with zone 1 fluid

h_{Bend}, h_{Tend} = Heat transfer coefficients between vapour and bottom or top end of the vessel wall

$h_{cyc,Vap}$ = Heat transfer coefficient between vapour and the corresponding cylindrical section of vessel wall

For a domed end vessel, both ends are assumed to be part of a sphere.

Churchill and Chu's correlation [Incropera & DeWitt, 1996a] is applied to cylindrical section of the vessel wall in contact with vapour. This is given by :

$$Nu_{cyc,Vap} = \left\{ 0.835 + \frac{0.387 Ra_{Vap}^{1/6}}{\left[1 + \left(0.492/Pr_{Vap}\right)^{9/16}\right]^{8/27}} \right\}^2 \qquad (4.2.16)$$

The dimensionless groups are defined as

$$Nu_{cyc,Vap} = \frac{h_{cyc,Vap} L_{cyc}}{k_{Vap}}$$

$$Ra_{cyc,Vap} = Gr_{cyc,Vap} \, Pr_{Vap}$$

$$Gr_{cyc,Vap} = \frac{L_{cyc}^3 \rho_{Vap}^2 g \beta_{Vap} \left(T_{W,Z1} - T_{Z1}\right)}{\mu_{Vap}^2}$$

$$Pr_{Vap} = \frac{C_{p\,Vap} \mu_{Vap}}{k_{Vap}}$$

Where $Nu_{cyc,Vap}$ = Nusselt number of vapour in contact with cylindrical section of the vessel

$Ra_{cyc,Vap}$ = Rayleigh number of vapour in contact with cylindrical section of the vessel

$Gr_{cyc,Vap}$ = Grashof number of vapour in contact with cylindrical

section of the vessel

Pr_{Vap} = Prandlt number of vapour

C_{pVap} = Specific heat capacity of vapour at constant pressure

g = Gravitational acceleration

k_{Vap} = Vapour thermal conductivity

$L_{cyc,Vap}$ = Characteristic length corresponding to vapour in contact with cylindrical section of the vessel

μ_{Vap} = Vapour viscosity

ρ_{Vap} = Vapour density

The vapour thermal expansion coefficient, β_{Vap}, is given by [Incropera & DeWitt, 1996a] :

$$\beta_{Vap} = -\frac{1}{\rho_{Vap}}\left(\frac{\partial \rho}{\partial T}\right)_P \qquad (4.2.17)$$

The term $\left(\frac{\partial \rho}{\partial T}\right)_P$ can be determined by differentiating an equation of state.

For a vessel containing vapour only, the characteristic length, $L_{cyc,Vap}$ is equal to tan-to-tan length for domed end vessel or vessel height for a flat end vessel. When zone 1 enters the two-phase region at any instant, $L_{cyc,Vap}$ is given by:

$$L_{cyc,Vap} = L_{Vessel} - L_{Dome} - L_{Liq} \qquad (4.2.18)$$

Where L_{Dome} = Internal height of the domed end (zero for a flat end vessel)

L_{Liq} = Liquid level

L_{Vessel} = Total internal height of the vessel

The advantage of the above heat transfer correlation over those used by Haque et al. [1992a] and Overa et al. [1994] (see section 3.4 of chapter 3 for corresponding references) is its applicability to the entire range of Rayleigh number [Incropera & De Witt, 1996a] thereby it covering both laminar and turbulent flows.

The heat transfer coefficients, $h_{end,Vap}$ between vapour and both ends of the vessel is calculated from McAdams's correlation [Incropera & De Witt, 1996a],

$$Nu_{end,Vap} = d\, Ra_{end,Vap}^{b} \tag{4.2.19}$$

The dimensionless groups are defined as

$$Nu_{end,Vap} = \frac{h_{end,Vap}\, L_{end}}{k_{Vap}}$$

$$Ra_{end,Vap} = Gr_{end,Vap}\, Pr_{Vap}$$

$$Gr_{end,Vap} = \frac{L_{end}^3\, \rho_{Vap}^2\, g\beta_{Vap}\left(T_{W,Z1} - T_{Z1}\right)}{\mu_{Vap}^2}$$

Where b, d = Correlation constants given in table 4.1

$h_{end,Vap}$ = Heat transfer coefficients between vapour and bottom or top end of the vessel

$L_{end,Vap}$ = Characteristic length corresponding to vapour in contact with vessel end

Values for the parameters b, and d are given in table 4.1 for upper and lower surface of heated plates at different range of Rayleigh numbers [Incropera & De Witt, 1996a]. As the vapour temperature during blowdown is always lower than the average wall temperature, the parameters for "Hot surface facing down" should be used for top end of the vessel. If zone 2 is not present, the parameters for "Hot surface facing up" is used for bottom end.

Table 4.1 McAdams parameters for natural convection from horizontal plates [Incropera and De Witt, 1996a]

Type of Flow	*d*	*b*	Ra Range
Hot surface facing down (Laminar flow)	0.27	1/4	10^5 - 10^{10}
Hot surface facing up (Laminar flow)	0.54	1/4	10^4 - 10^7
Hot surface facing up (Turbulent flow)	0.15	1/3	10^7 - 10^{11}

If the calculated Ra falls outside the specified range, the maximum or minimum valves are used depending on whether Ra is above or below the range.

For flat end vessel, the characteristic length, L_{end}, is determined from the following equation [Bejan, 1995a]:

$$L_{end} = \frac{D_{Vessel}}{4} \tag{4.2.20}$$

Where D_{Vessel} is the internal diameter of the vessel.

In order to apply equation 4.2.20 to a domed end vessel, the equivalent diameter of the inner surface area of the domed end, D_{Dome}, is given by :

$$D_{Dome} = 2\sqrt{\frac{A_{Dome}}{\pi}} \tag{4.2.21}$$

Where A_{Dome} is the inner surface area of the domed end.

The characteristic length, L_{end}, is then determined by replacing D_{Vessel} in equation 4.2.20 by D_{Dome}.

The vapour thermal conductivity and viscosity used for calculating Nusselt, Grashof and Prandlt numbers are determined by Ely and Hanley's method [Ely & Hanley, 1981 and 1983] which is based on the principle of corresponding states by using methane as the reference fluid. Assael et al. [1996c] point out that it is one of the few schemes which is able to predict with any accuracy the viscosity and thermal conductivity of a large number of non-polar components and their mixtures in both liquid and vapour phases over a wide range of conditions. However, in BLOWSIM, this method is only used for vapour phase as a more appropriate method is used for liquid phase (see later).

The main advantage of this method is that only the critical constants and the acentric factor are required for the mixture transport property calculation. The accuracy of this method in predicting viscosity and thermal conductivity is in the region of 10 to 20 per cent [Ely & Hanley, 1981 and 1983]. However, the disadvantage is it s

incapability in predicting transport properties near the critical region [Assael et al., 1996c] and a complex methodology is required in this region [Assael et al., 1996b]. In this study, it is assumed that the possible errors introduced by employing Ely and Hanley's method near the critical region does not have significant effects on blowdown predictions.

4.2.4.2 Heat Transfer between Vessel Wall and Zone 2

Heat transfer between liquid and the adjacent wall is governed by boiling heat transfer (see section 2.2.2 of chapter 2). In the following, different modes of boiling heat transfer are first described followed by the assumptions and the correlation used for predicting the corresponding heat flux.

The nature of boiling heat transfer is governed by the excess temperature, defined as the temperature difference between saturated liquid and the solid surface. The variation of heat flux with excess temperature is determined by the boiling curve for the liquid. Figure 4.2 presents the boiling curve for water at 1 atm [Welty et al., 1984] on a horizontal wire. Similar trends are observed with other fluids [Incropera & DeWitt, 1996b].

Referring to figure 4.2, in regime I, the wire surface temperature is a few degrees higher than the surrounding saturated liquid and natural convection currents circulate the superheated liquid. Regimes II and III relate to nucleate boiling. The bubbles initially form at certain surface sites, where vapour bubble nuclei are present, which rise and condense before reaching the free liquid surface. When wire surface temperature increases, larger and more numerous bubbles form, and rise to reach the free surface. Beyond the peak of the curve is the transition boiling regime, region IV where a vapour film collapses and reforms around the wire in an unstable manner. The vapour film provides a considerable resistance to heat transfer, thus the heat flux decreases. Region V is the stable film regime, where the vapour film around the wire becomes stable. In region VI where the excess temperature is above 540 ^{o}C, radiant energy transfer takes part, and the heat flux curve rises again.

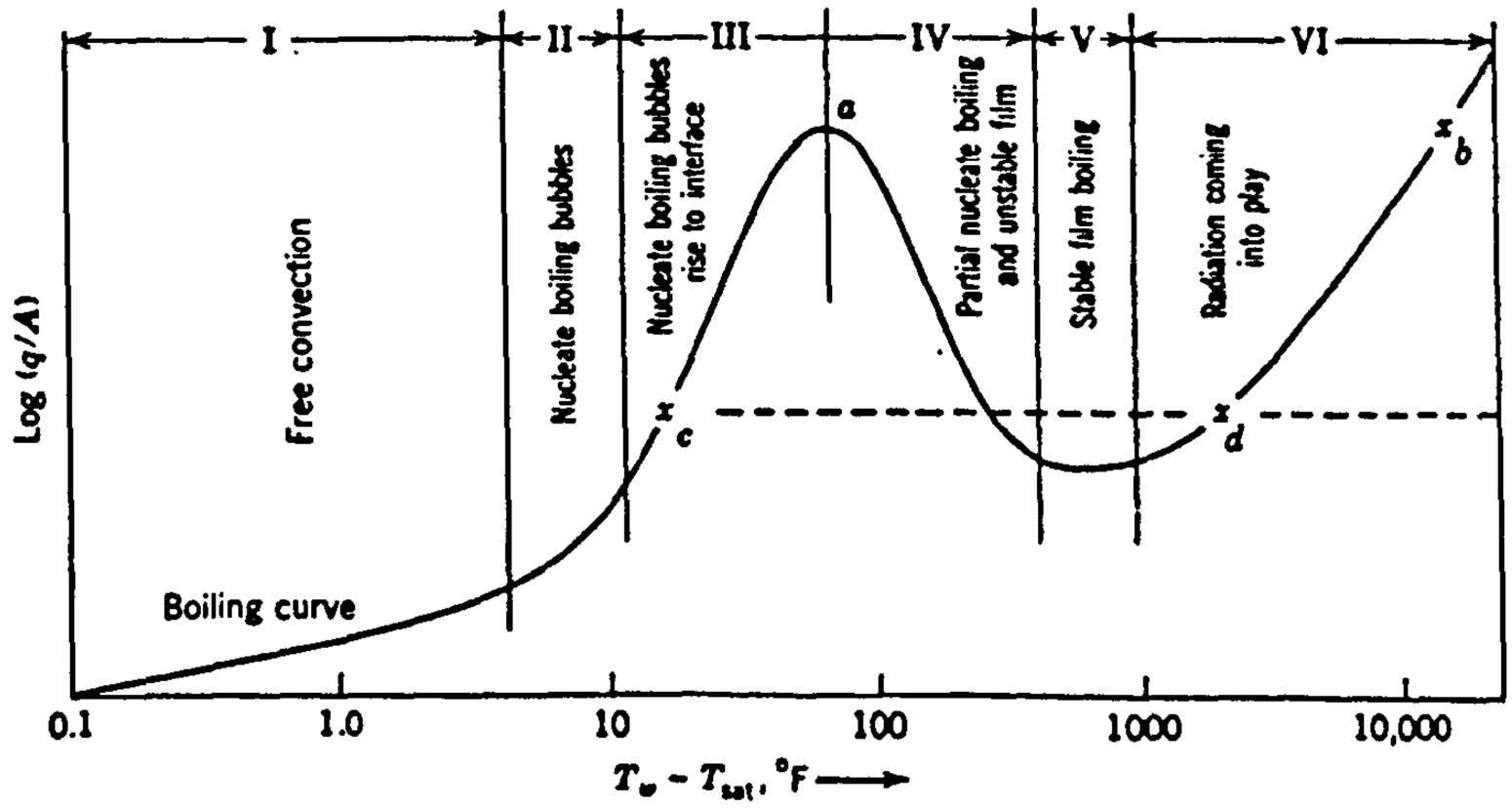

Figure 4.2 **Boiling curve of water on a horizontal wire at atmospheric pressure [Welty et al., 1984]**
q is the rate of heat transfer, A is the area, T_w is the temperature of the wire and T_{sat} is the saturated liquid temperature.

Haque et al.'s mathematical model [1992a] predicts heat fluxes for nucleate, and film boiling by some standard correlations (see table 3.2 of chapter 3). It also predicts the excess temperature at maximum and minimum heat fluxes by empirical correlations (see "*Heat and mass transfer effects*" in section 3.4.1.2). Conversely, Overa et al.'s model [1994] assumes the corresponding boiling heat transfer coefficient is constant during blowdown.

As a very high excess temperature would be required to reach the transition and film boiling regimes, these modes of heat transfer are more likely to exist in the boiling liquid during blowdown only under fire conditions.

In addition, no satisfactory correlations exist for predicting heat flux in the transition boiling regime [Welty et al., 1984]. Haque et al. [1992a] estimate this heat flux by linear interpolation between the maximum and minimum heat fluxes. The accuracy of the correlation [Berenson, 1961] used for determining the minimum heat flux is as low as 50% for most fluids at moderate pressures and provides even poorer estimates at higher pressures [Incropera & De Witt, 1996b]. Consequently, the heat flux between liquid and vessel wall can be greatly over or under estimated. This may in turn affect the prediction of minimum wall temperature if this temperature is located at the wetted wall section.

Nucleate boiling is most likely to be dominant during blowdown under non-fire situations as the differences in wall and liquid temperature are usually small to moderate (see Haque et al.'s measured liquid and wetted wall temperatures during blowdown in figures 2.2 and 2.3). Therefore, in this study we consider nucleate boiling heat transfer only. We estimate the corresponding heat flux using the widely recommended [Bejan, 1995b; Burmeister, 1993; Incropera & DeWitt, 1996b] Rohsensow's correlation [Incropera & De Witt, 1996b]. This is given by :

$$q_{Z2} = \mu_{Liq}\, h_{fg} \left[\frac{g\left(\rho_{Liq} - \rho_{EL}\right)}{\sigma}\right]\left(\frac{C_{p\,Liq}\,\Delta T_e}{C_s h_{fg}\,Pr_{Liq}^{n}}\right)^3 \qquad (4.2.22)$$

The total heat input to zone 2 at stage i, is then given by:

$$Q_{i,Z2} = q_{Z2} \times A_{Z2} \times \Delta t \tag{4.2.23}$$

The dimensionless group is :

$$Pr_{Liq} = \frac{C_{pLiq}\,\mu_{Liq}}{k_{Liq}}$$

Where A_{Z2} = Inner surface area of the vessel in contact with zone 2 fluid

C_s, n = Parameters given later in table 4.2 for different surface-liquid combinations.

$C_{P\,Liq}$ = Specific heat capacity of liquid at constant pressure

h_{fg} = Latent heat of vaporisation for liquid

ρ_{EL} = Density of evaporated liquid

ρ_{Liq} = Density of liquid

μ_{Liq} = Viscosity of liquid

σ = Surface tension of liquid

The viscosity, μ_{Liq}, and thermal conductivity, k_{Liq}, for liquid mixtures containing alkanes (methane to n-dodecane) are determined by a semi-empirical scheme proposed by Dymond and Assael [Assael, et al., 1996c]. The range of application is generally from about 280 to 400 K with pressures from saturation up to 986.9 atm. The uncertainty of the correlations is not greater than 5 per cent [Assael, et al., 1996c]. 2000 experimental values of viscosity and thermal conductivity were employed to optimise the coefficients used in the scheme. For mixtures containing different classes of compounds, correlations proposed by DIPPR (Design Institute for Physical Property Data) [ChemCAD III user guide, 1993] are applied due to their simplicity.

The surface tension, σ, is predicted by Macleod-Sugden correlation [Reid et al., 1986] which is applicable to polar and non-polar systems. A typical accuracy is claimed to be ca. $\pm$ 5 - 10 % [Reid et al., 1986].

It is unclear how Haque et al. [1992a] determined the pseudo latent heat, h_{fg}, in equation 4.2.22 for multi-component mixtures where the composition of the vapour is different from that of the liquid. In our model, h_{fg}, is simply taken as the difference between specific enthalpies of liquid and evaporated liquid. The parameters, C_s and *n*, are dependent on the type of fluid/solid surface system. These are mainly available for water, n-pentane and alcohol [Bejan, 1995b; Incropera & DeWitt, 1996b] in contact with different types of surfaces. The values used by Haque et al. [1992a] are not given in their publication. As light hydrocarbon mixtures (mainly methane) usually have an average molecular weight similar to that of water and the vessel is usually constructed from stainless steel (or carbon steel), the parameters associated with water and stainless steel are used in this study. No values for C_s and *n* are available for carbon steel .

The corresponding values for C_s and *n* for different types of stainless surfaces are presented in table 4.2.

Table 4.2 Values of C_s and *n* associated with water and different types of stainless steel in Rohsenow's correlation [Incropera & DeWitt, 1996b]

Stainless steel surface in contact with water	C_s	*n*
Chemically etched	0.013	1.0
Mechanically polished	0.013	1.0
Ground and polished	0.006	1.0

In this study, the corresponding values for C_s and *n* for "ground and polished" surface are used. This will result in the highest predicted heat flux (see equation 4.2.22) thus leading to a more conservative estimation (lower) of the wall temperature in contact with the liquid.

It is important to note that the Rohsenow's correlation applies only for clean surfaces. Incropera and DeWitt [1996b] claim that in practice, the correlation can give rise to as much as ±100 % error in the calculated heat flux. It is interesting to note that despite the above together with the uncertainties associated with the correct

choice of the parameters C_s and n, as well as the pseudo latent heat, h_{fg}, Haque et al.'s [1992b] blowdown results show a reasonable agreement with experimental data.

Overa et al. [1994], simply assume (see section 3.4.2, chapter 3) a constant heat transfer coefficient (1000 - 3000 W/m^2K) between liquid and wall during blowdown. In this way, the total heat transfer to the liquid from the wall at a given pressure increment can be determined from equation 4.2.14, where, x is equal to 2.

In this study, the effects of employing both Rohsensow's correlation and Overa et al.'s suggested values of constant heat transfer on the blowdown predictions are evaluated by comparison with experimental data. The results are shown in chapter 6.

4.2.5 Discharge Calculation

During blowdown, either gas or a two-phase fluid is discharged from the orifice. In this section, we first describe the nature of the processes taking place through the discharge orifice followed by the derivation of appropriate equations for discharge calculations.

Figure 4.3 represents a simple case relating to single phase gas flow from a vessel at pressure, P_v through an orifice. P_d is the downstream pressure and P_o is the pressure at the orifice. When the pressure difference between P_v and P_d is moderate, the orifice pressure, P_o is equal to the downstream pressure and the gas travels at subsonic velocity. When P_d decreases further and reaches the critical pressure, P_c, the gas velocity increases to it s maximum which is equal to the local speed of sound and the gas is said to be choked. Any further decreases in downstream pressure, P_d, will not increase the gas velocity and the orifice pressure, P_o, will remain at P_c .

Two-phase flow through an orifice results in similar phenomena as in the case of a gas, except the maximum fluid velocity at the orifice is given by critical two-phase flow rather than choked flow [Haque et al., 1992a].

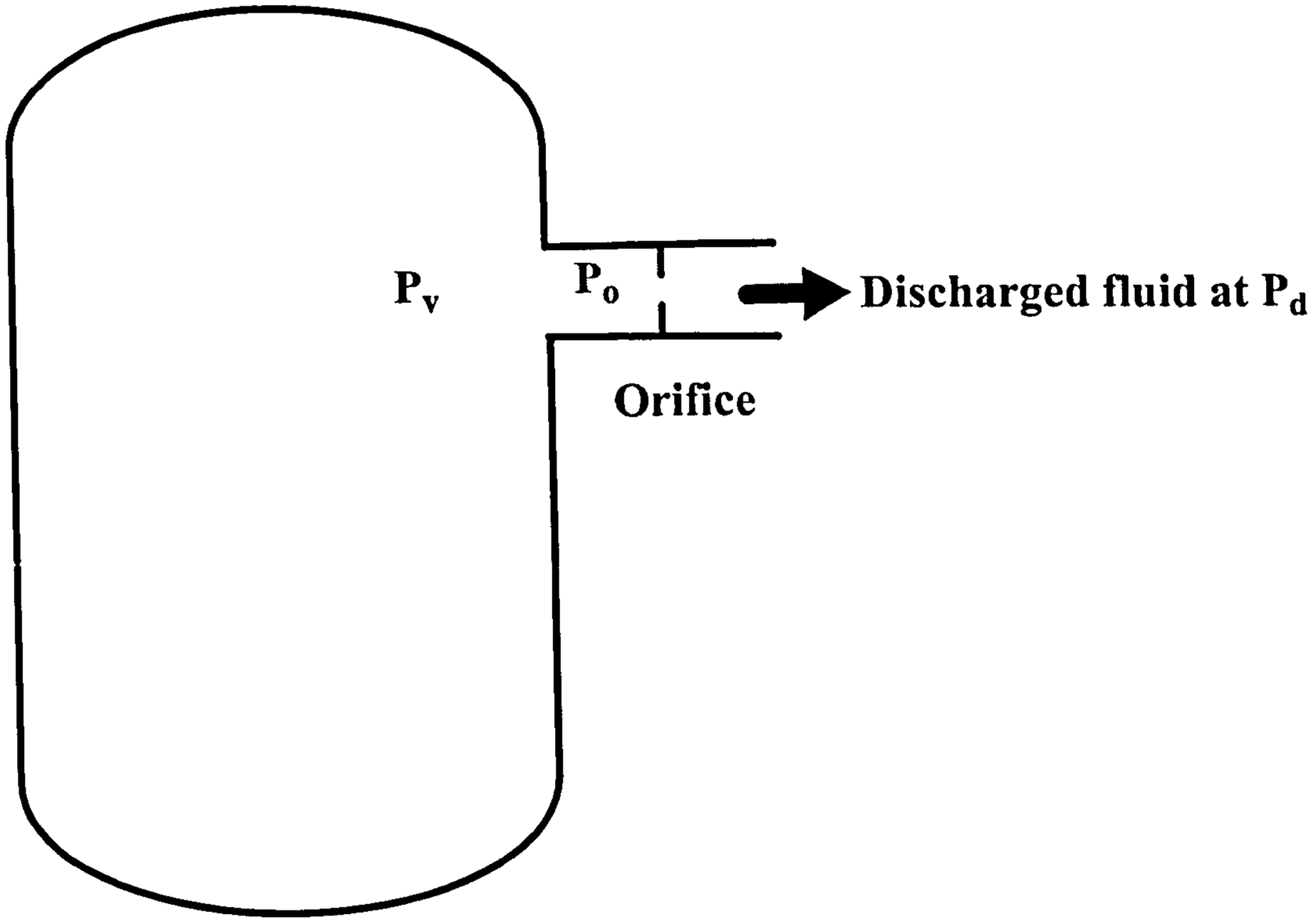

Figure 4.3 Schematic diagram showing pressures at varies positions during blowdown of a vessel containing vapour

As the inner surface area of the orifice is very small and the fluid is travelling at high speed, heat transfer to the fluid at the orifice is negligible. In addition, as the fluid expands rapidly through the orifice, the flow may be assumed to be isentropic. However, in practice, friction at the orifice results in irreversibility and hence non isentropic conditions. Therefore, the actual flow rate is smaller than the isentropic flow rate and the ratio between both flow rates is given by the discharge coefficient, C_d.

When C_d is equal to 1, the flow is isentropic. The discharge coefficient is function of shape of the orifice, Reynolds number and pressure ratio between upstream and downstream [Shapiro, 1953]. In this study, we assume a constant value for the discharge coefficient. The energy balance across the orifice is given by:

$$h_u + \frac{1}{2}v_u^2 + gz_u = h_o + \frac{1}{2}v_o^2 + gz_o \qquad (4.2.23)$$

Where g = Gravitational acceleration

h_u, h_o = Enthalpies per unit mass of fluid at upstream away from and within the orifice respectively

v_u, v_o = Velocities of fluid at upstream away from and within the orifice respectively

z_u, z_o = Heights from datum level to upstream and to the orifice respectively

Equation 4.2.23 is simplified by assuming the change in potential energy is small compared with the kinetic-energy and enthalpy terms (i.e., the terms g_{zu}, g_{zo} are neglected). Additionally assuming that the upstream velocity, v_u is negligible compared to the fluid velocity at the orifice we have:

$$h_u = h_o + \frac{1}{2}v_o^2 \qquad (4.2.24)$$

The above equation is governed by (see section 2.2.5, chapter 2)

1) The state of fluid within the choke which can either be in a metastable state or in thermodynamic and phase equilibrium.

2) The phase of fluid approaching the relief valve which can either be single (vapour) or two-phase (vapour and liquid).

Based on experimental measurements, Haque et al. [1992a] justify thermodynamic and phase equilibrium for the state of the fluid within the choke. The same assumption is adopted in the BLOWSIM simulation.

The fluid phase approaching the relief valve depends on the state of fluid in zone 1 within the vessel. However, when simulating blowdown in the process industry, it is common practice to assume single phase gas release through the orifice. The effect of non ideal fluid is taken into account by using the ideal gas equation in conjunction with a compressibility factor.

An alternative is to derive the discharge equation on the basis of a real fluid. This approach allows consideration of two-phase flow prior to and within the choke by solving equation 4.2.24 in conjunction with a suitable equation of state iteratively. Inevitably, the calculations are more complicated and less computationally efficient compared with the ideal gas approach. Both methods of discharge rate calculation are described in the following.

4.2.5.1 Ideal Gas Method

By applying the ideal gas law to equation 4.2.24 and assuming specific heat capacity of gas, C_p, is constant.

Equation 4.2.24 becomes :

$$C_p T_u = C_p T_o + \frac{1}{2} v_o^2 \qquad (4.2.25)$$

Where T_u and T_o are the fluid temperatures at upstream and within the orifice respectively.

When the gas is choked, T_o is equal to choke temperature, T_c, and the gas velocity is equal to the speed of sound, a given by :

$$a = \left(\frac{\partial P}{\partial \rho}\bigg|_S \right)^{1/2} = \left(k \frac{\partial P}{\partial \rho}\bigg|_T \right)^{1/2} \tag{4.2.26}$$

Where k = Ratio of specific heat

P = Pressure

S = Entropy

T = Temperature

ρ = Density

For a perfect gas, equation 4.2.26 becomes :

$$a = (kRT)^{1/2} \tag{4.2.27}$$

Where R is the gas constant.

By applying the isentropic assumption and combining equations 4.2.25 and 4.2.27 together with the ideal gas law, the choke pressure, temperature and discharge rate are respectively given by :

$$P_c = P_u \left(\frac{2}{1+k} \right)^{\frac{k}{k-1}} \tag{4.2.28}$$

$$T_c = T_u \left(\frac{2}{1+k} \right) \tag{4.2.29}$$

$$G = \left[\left(\frac{2}{k+1} \right)^{\frac{k+1}{k-1}} k P_u \rho_u \right]^{1/2} A_o C_d \tag{4.2.30}$$

Where A_o = Cross section area of orifice

C_d = Discharge coefficient

G = Mass flowrate of vapour

P_u, P_c = Upstream and choke pressures respectively

ρ_u = Vapour density at upstream

The real gas specific heat ratio and density at upstream conditions are used in the above equations. Equations 4.2.28 - 4.2.30 show the choke conditions are functions of upstream properties only. The gas is choked when the downstream pressure, P_d, is equal to or below the choke pressure, P_c. Otherwise, P_o is equal to P_d and the discharge velocity, v_o is determined by rearranging equation 4.2.25 which gives :

$$v_o = \sqrt{2C_p\left(T_u - T_o\right)} \tag{4.2.31}$$

C_p at upstream condition is used. The equations based on the isentropic perfect gas assumption for evaluating T_o and fluid density at the orifice, ρ_o, are given by equations 4.2.32 and 4.2.33 respectively.

$$T_o = T_u\left(\frac{P_d}{P_u}\right)^{\frac{k-1}{k}} \tag{4.2.32}$$

$$\rho_o = \rho_u\left(\frac{P_d}{P_u}\right)^{\frac{1}{k}} \tag{4.2.33}$$

The corresponding discharge rate is given by the product of the discharge velocity, the orifice area, the discharge coefficient and the fluid density at the orifice.

4.2.5.2 Real Fluid Method

For real fluids, equations 4.2.28 - 4.2.30 are no longer valid at the choke conditions of a gas. The energy balance given by equation 4.2.24 together with the isentropic equation need to be solved iteratively for the critical condition at the orifice. This method allows consideration of two-phase flow prior to and within the orifice. The equations for solving the critical and non-critical conditions at the orifice are presented here. This is followed by the description of the corresponding mathematical algorithm.

DETERMINATION OF CRITICAL AND NON-CRITICAL CONDITIONS

The fluid phase and conditions at the orifice are governed by the isentropic expansion through the orifice and the energy balance given by equation 4.2.24. If the fluid within the orifice is single phase, the velocity term, v_o, in equation 4.2.24, is replaced by local speed of sound, a, and becomes :

$$h_u = h_o + \frac{1}{2}a^2 \qquad (4.2.34)$$

The thermodynamic definition of, a is given by equation 4.2.26 and both k and $\left.\frac{\partial P}{\partial \rho}\right|_T$ can be determined analytically for a given equation of state. In the case of a two-phase fluid approaching the orifice, h_u is given by the bulk enthalpy of the mixture.

If a two-phase mixture exists within the orifice, Richardson and Saville [1996] recommended the homogeneous equilibrium model should be used to determine the corresponding velocity. The model assumes thermodynamic and phase equilibrium between both phases and thus both phases travelling at the same velocity. Hence, the critical velocity is equal to the speed of sound of the two-phase mixture and equation 4.2.34 is applicable.

However, the speed of sound, a, in equation 4.2.34 cannot be solved analytically as k and $\left.\frac{\partial P}{\partial \rho}\right|_T$ or $\left.\frac{\partial P}{\partial \rho}\right|_S$ in equation 4.2.26 are difficult to define. Consequently, the numerical procedure recommended by Picard and Bishnoi [1987] is used by expressing equation 4.2.26 into the following form :

$$a^2 = \left(\left.\frac{\Delta P}{\Delta \rho}\right|_S\right) \qquad (4.2.35)$$

A small pressure drop from P_c to P_c-ΔP is introduced by performing pressure entropy flash calculation at P_c-ΔP and fluid entropy at upstream, S_u. The corresponding bulk density difference, $\Delta\rho$, is then determined. In BLOWSIM, the ratio between ΔP and

P_c is set to be 1×10^{-6}. By solving equation 4.2.34, assuming isentropic flow together with the appropriate speed of sound equation, the critical pressure, temperature, velocity and number of phases at the orifice can be determined.

If the downstream pressure, P_d, is greater than the critical pressure, P_c, the orifice pressure is equal to downstream pressure and the orifice temperature is evaluated by performing a pressure entropy flash calculation at P_d and the upstream entropy, S_u. Subsequently, the fluid enthalpy at the orifice is determined and equation 4.2.24 can be solved for v_o.

MATHEMATICAL ALGORITHM FOR DISCHARGE CALCULATION

The logic flow diagram for determination of orifice conditions is given in figure 4.4 The calculation procedure is as follows.

Step 1

Guess the critical pressure, P_c, and perform pressure entropy flash at P_c and S_u to determine the number of phases, bulk enthalpy per unit mass, h_c, and critical temperature, T_c.

Step 2

If the fluid is single phase, the speed of sound, *a*, is determined from equation 4.2.26, otherwise, by equation 4.2.35 which is solved numerically.

Step 3

Substitute h_c and *a* in equation 4.2.34. If this equation is not satisfied, repeat steps 1-3 until it is converged.

Step 4

If the downstream pressure, P_d, is less than or equal to the calculated critical pressure, P_c, the fluid is at it s maximum speed. Otherwise, the fluid temperature, T_o within the orifice, and bulk fluid enthalpy, h_o , are determined by pressure-entropy flash at P_d and S_u. Subsequently, the fluid velocity, v_o, is determined by solving equation 4.2.24.

The Brent's iteration method [Press et al., 1992] is used to solve for the critical pressure, P_c. When the discharge velocity, v_o,is known, the discharge rate, G, can be determined.

The mass of discharge material, M_D during a time increment, Δt is given by :

$$M_D = G \times \Delta t \qquad (4.2.36)$$

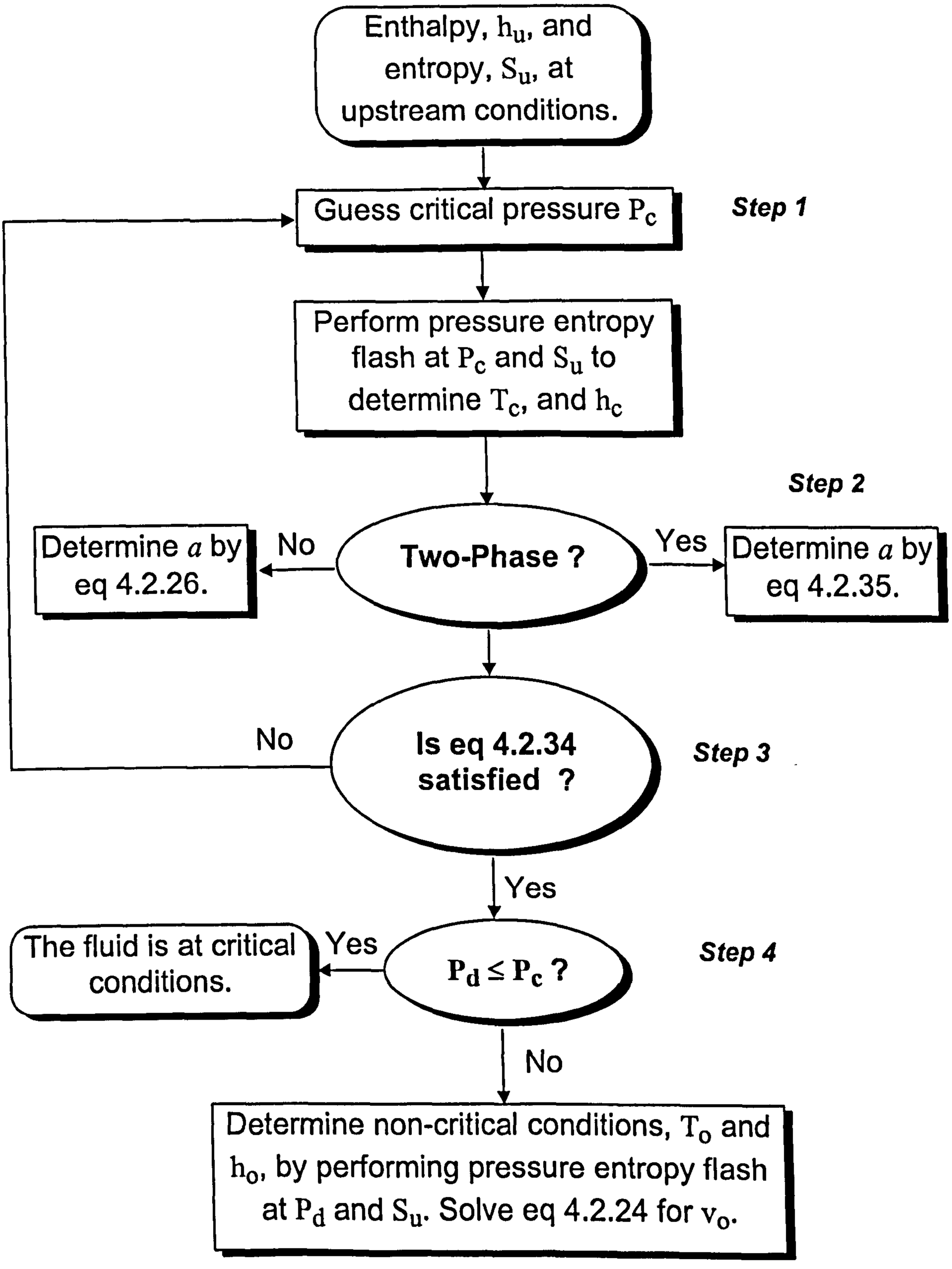

Figure 4.4 Logic flow diagram for determination of orifice conditions

4.3 MATHEMATICAL ALGORITHM FOR BLOWDOWN CALCULATION

The required inputs for BLOWSIM are :

1) Initial conditions of the vessel :
   - Vessel's pressure, fluid temperature and composition
2) Vessel dimensions
   - Internal diameter
   - Vessel height and tan to tan length (for domed end vessel only)
   - Vessel wall thickness (if wall thickness at cylindrical part is different from the vessel end, the former value is used)
   - Vessel end shape (either domed or flat end)
3) Blowdown conditions
   - Downstream pressure
   - Orifice diameter
   - Discharge coefficient
   - Ratio of pressure increment over vessel pressure, r
4) User's options
   - Thermodynamic trajectory for zone 2 with (pressure entropy flash) or without (pressure enthalpy flash) consideration of work done by the fluid due to expansion.
   - Estimation of total heat transfer between zone 2 and vessel wall either by predicting boiling heat flux using Rohsensow's correlation (see equation 4.2.22 of section 4.2.4.2) or assuming constant heat transfer coefficient and applying Overa et al.'s [1994] suggested values in equation 4.2.14.
   - Determination of discharge rate and orifice conditions either by ideal gas or real fluid method.
5) Choice of the cubic equation of state and methods for predicting fluid transport properties.

The appropriate general flow logic diagram for BLOWSIM is given in figure 4.5.a (see page 109). An isothermal flash at initial operation conditions is first performed to determine the densities and compositions of vapour and liquid (if any) and hence

the appropriate fluid state. If the fluid is single phase (all vapour), the single phase algorithm shown in figure 4.5.b (see page 110) is adopted. Otherwise the two-phase mixture (gas-liquid) algorithm shown in figure 4.5.c (see page 113) is used. The pressure at the next interval is then determined from equations 4.2.1 and 4.2.2. The above is repeated until blowdown is completed. Details of single and two-phase calculation algorithms are given in the following sections.

4.3.1 Single Phase Algorithm (Figure 4.5.b)

The variations of temperature and pressure with time are governed by the specific entropy in zone 1, $S_{i,Z1}$ given by equation 4.2.7. As the total heat transfer to the fluid, $Q_{i,Z1}$, in equation 4.2.7 is a function of discharge duration, Δt, and fluid temperature, $T_{i,Z1}$, the equation needs to be solved iteratively and simultaneously with the discharge equation 4.2.36.

Equation 4.2.7 can be solved efficiently if an appropriate initial estimation is available for $S_{i,Z1}$, $Q_{i,Z1}$ or $T_{i,Z1}$. The simplest way for the initial guess is to employ the corresponding value from the previous pressure stage (at P_{i-1}). As $Q_{i,Z1}$ is not available for stage 0 (at zero time) and the variation of $T_{i,Z1}$ for a given pressure increment is large especially at the beginning of blowdown, $S_{i,Z1}$ is chosen for iteration purposes due to it s relative insensitivity to pressure.

Similarly, an initial guess for Δt_i is required. For stage 1, an initial guess taken as that equal to the discharge duration when the fluid is expanded isentropcially from P_0 to P_1. For successive stages, the corresponding initial guess for Δt_i is given by :

$$\Delta t_i = \frac{\Delta P_i}{\Delta P_{i-1}} \Delta t_{i-1} \qquad (4.3.1)$$

The procedures for solving equations 4.2.7 (single phase entropy balance) and 4.2.36 (discharged mass) are given in the following. The corresponding calculation flow logic diagram is given in figure 4.5.b.

Step 1a Determination of Zone 1 Fluid Temperature

The fluid temperature, $T_{i,Z1}$ and thermophysical properties are determined by pressure-entropy flash at P_i and $S_{i,Z1}$'. The volume of discharge fluid is equivalent to volume difference between vessel and fluid after expansion. The mass of discharge fluid, M_D', is the product of discharge volume and vapour density.

Step 2a Determination of heat input from vessel wall and average wall temperature

If vapour condensate is formed, it is assumed to settle immediately at the bottom of the vessel and thermal equilibrium is immediately established between vapour condensate and wetted wall. Hence, the average wetted wall temperature, $T^i_{W,Z2}$, is equal to temperature of condensed vapour, $T_{i,Z1}$.The total heat input, $Q_{i,Z1}$ and average unwetted wall temperature, $T^i_{W,Z1}$, are determined by solving equation 4.2.14. The heat transfer coefficient between wall and fluid is given in section 4.2.4.1. The calculated $Q_{i,Z1}$ and $T_{i,Z1}$ from step 1a are substituted into equation 4.2.7 to determine $S_{i,Z1}$.

Step 3a Determination of discharge rate and mass of vapour discharged

The discharge calculation is performed to determine the orifice conditions and discharge rate, G, together with mass of discharged fluid, M_D (equation 4.2.36). The discharge rate can be determined by using the ideal gas or real fluid methods given in sections 4.2.5.1 and 4.2.5.2 respectively.

Step 4a Determination of amount of vapour and condensed vapour within vessel

If $S_{i,Z1}$ and M_D are not equal to $S_{i,Z1}$' and M_D' respectively, repeat steps 1a - 3a with new estimations of $S_{i,Z1}$' and Δt. Otherwise, by knowing the mass of discharged vapour and the corresponding number of mole, equation 4.2.3 can be solved to determine the number of moles of vapour and condensed vapour within the vessel.

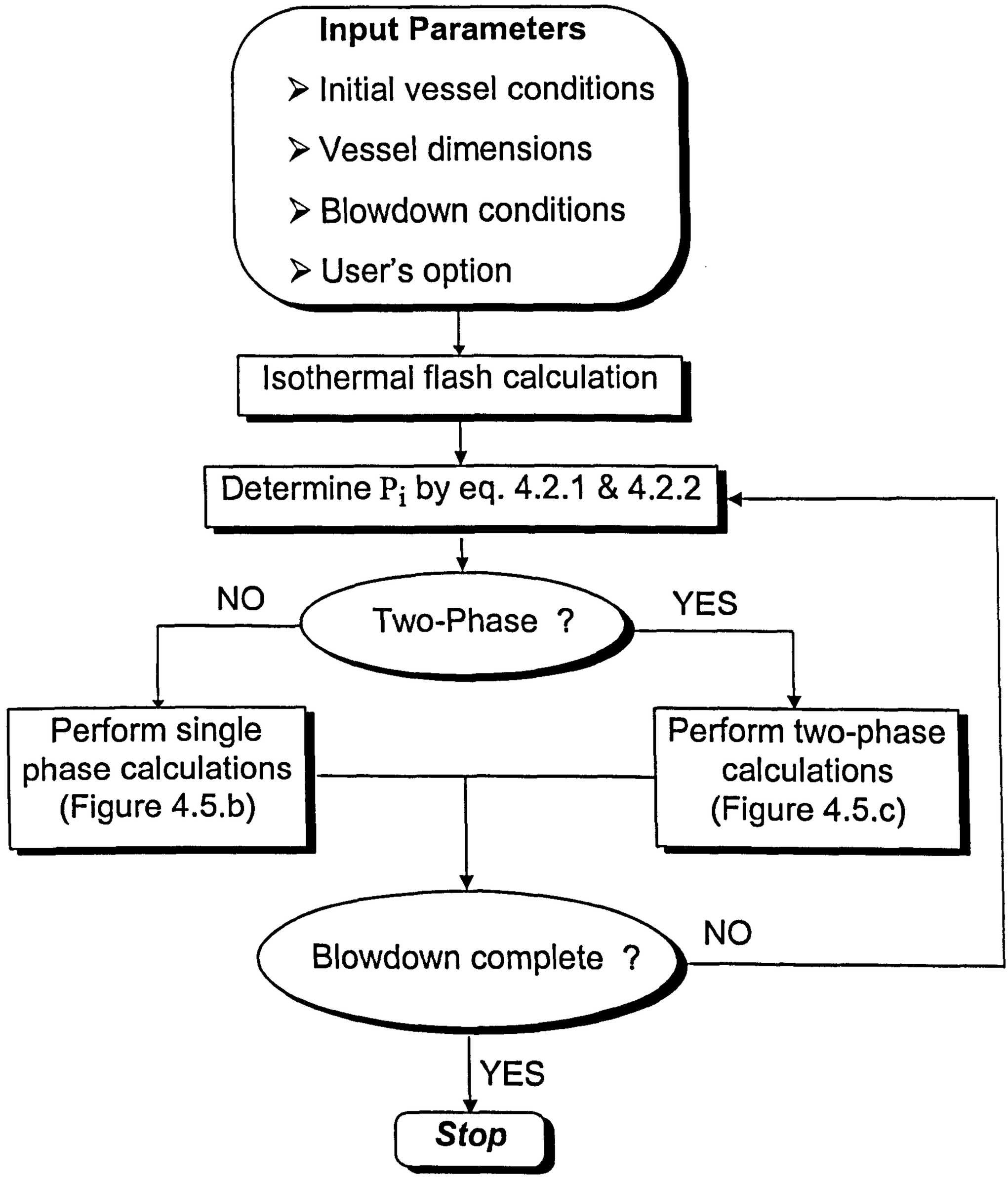

Figure 4.5.a Logic diagram of BLOWSIM

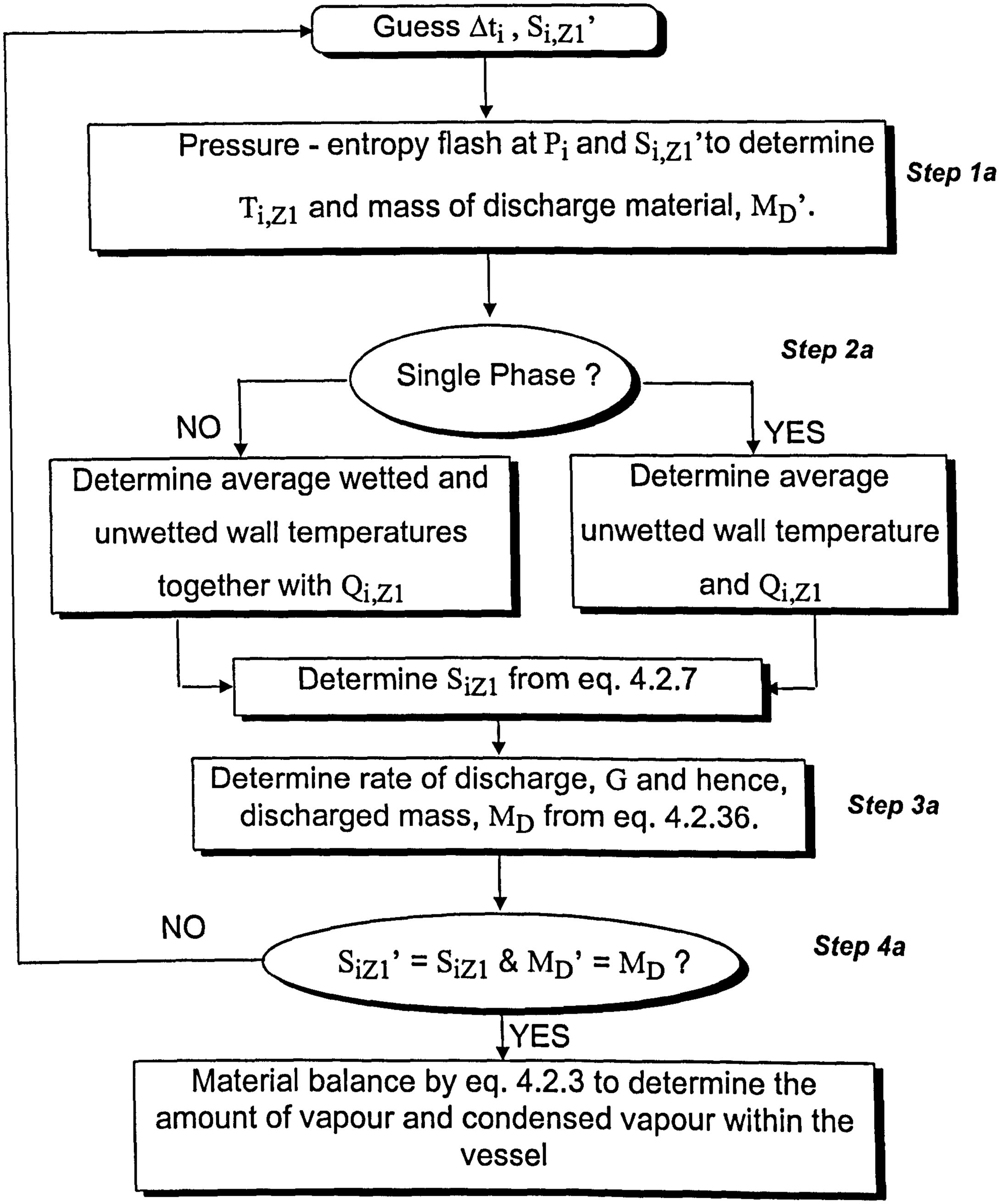

Figure 4.5.b Logic diagram for single phase algorithm of BLOWSIM

4.3.2 Two-Phase Algorithm (Figure 4.5.c)

Similar to single phase algorithm, the variations of temperature and pressure with time are governed by the specific entropy $S_{i,Z1}$ (equation 4.2.8) in zone 1, and specific enthalpy, $H_{i,Z2}$(equation 4.2.11), or entropy, $S_{i,Z2}$ (equation 4.2.12) in zone 2. In the same way as the single phase algorithm, the above equations need to be solved iteratively and simultaneously with the discharge equation (equation 4.2.36).

The initial estimations of $S_{i,Z1}$ and $H_{i,Z2}$ or $S_{i,Z2}$ are based on their corresponding values in the previous stage. The same procedures described in single phase algorithm are used to determine an initial guess for Δt_i. The methodology for solving equations 4.2.8 plus 4.2.11 or 4.2.12 are given in the following. The corresponding calculation flow logic diagram is given in figure 4.5.c.

Step 1b Determination of fluid temperature in zone 2 and amount of evaporated liquid

The fluid temperature, $T_{i,Z2}$, the specific entropy, $S_{i,EL}$, of evaporated liquid together with the mole fraction of evaporated liquid, n_{EL}, are determined by either pressure/enthalpy (at P_i and $H_{i,Z2}$') or pressure/entropy (at P_i and $S_{i,Z2}$') flash at the fluid composition given by equation 4.2.13. The number of moles of evaporated liquid is given by :

$$N_{i,EL} = n_{EL}\left(N_{i-1,L} + N_{i-1,CV}\right) \tag{4.3.2}$$

Step 2b Determination of average wetted wall temperature and heat input to zone2

If constant heat transfer coefficient based on Overa et al. [1994] suggested range of values is used, equation 4.2.14 can be rearranged to solve for $T^{i}_{W,Z2}$ and hence $Q_{i,Z2}$. Otherwise, Rohsensow's correlation given by equation 4.2.22 together with equation 4.2.23 are solved to determine $Q_{i,Z2}$. Subsequently, $T^{i}_{W,Z2}$ is calculated from equation 4.2.14. $H_{i,Z2}$ or $S_{i,Z2}$ is then evaluated from equation 4.2.11 or 4.2.12, depending on the choice of the thermodynamic trajectory.

Step 3b Determination of fluid temperature in zone 1

The fluid temperature in zone 1, $T_{i,Z1}$, the specific enthalpy, $H_{i,CV}$, or entropy, $S_{i,CV}$, of condensed vapour (depending on the choice of the thermodynamic trajectory for zone 2) together with the mole fraction of condensed vapour, n_{CV}, are determined by pressure-entropy flash at P_i and $S_{i,Z1}$' at fluid composition given by equation 4.2.9. The volume of discharged fluid is equivalent to the volume difference between vessel and fluid (zones 1 & 2) after expansion. The mass of discharge fluid, M_D', is the product of bulk density (vapour density if ideal gas discharge method is used) and volume of discharge fluid.

Step 4b Determination of average unwetted wall temperature and heat input to zone 1

The total heat input, $Q_{i,Z1}$ and average unwetted wall temperature, $T^{i}_{W,Z1}$, are determined by solving equation 4.2.14. The heat transfer coefficient between wall and fluid is given in section 4.2.4.1. Subsequently, $S_{i,Z1}$ is evaluated from equation 4.2.8.

Step 5b Determination of discharge rate and mass of discharge vapour

The orifice conditions and discharge rate, G, together with mass of discharged fluid, M_D (equation 4.2.36) are determined in the same way as in step 3a from the single phase algorithm.

Step 6 Determination of amount of vapour and condensed vapour within vessel

If :

$$S_{i,Z2} \neq S_{i,Z2}' \text{or } H_{iZ2} \neq H_{iZ2}'$$

and

$$S_{i,Z1} \neq S_{i,Z1}' \; M_D \neq M_D'$$

repeat steps 1b - 5b with new estimations of the $S_{i,Z2}$' or H_{iZ2}', $S_{i,Z1}$' and Δt. Otherwise, similar to step 4a from the single phase algorithm, equation 4.2.3 is solved to determine the number of moles of vapour and condensed vapour.

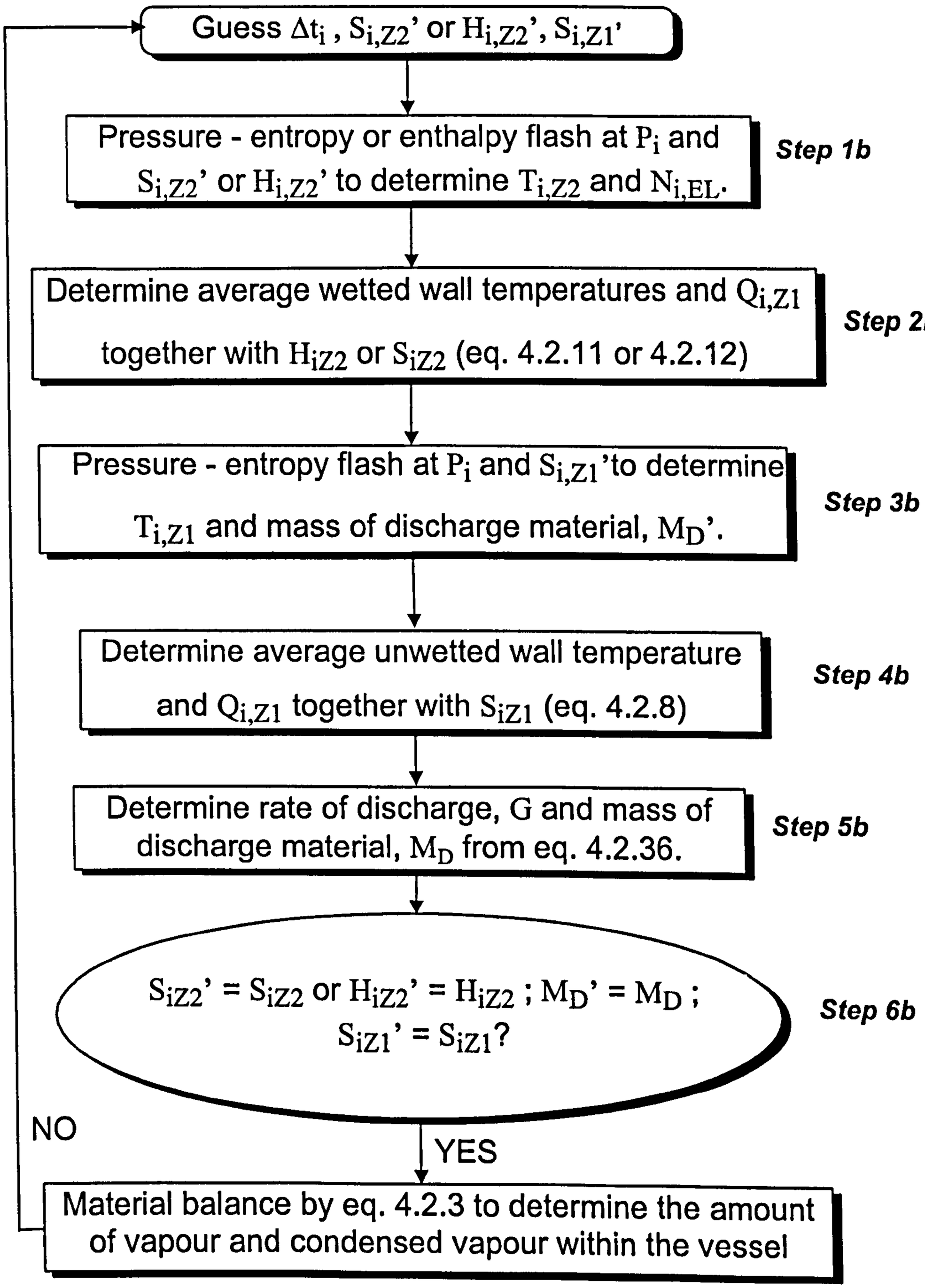

Figure 4.5.c Logic diagram for two-phase algorithm of BLOWSIM

4.4 THE COMPUTER PROGRAMME, BLOWSIM

The computer programme, BLOWSIM, is DOS based written in Fortran 77. The Nag Fortran Library routine, C05NDF is used for solving simultaneous equations for both single and two-phase algorithms. The flash calculation subroutine is a modification of a computer programme THSFLASH developed by M.L.Michelsen from Technical University of Denmark in 1983. It is part of IVC-SEP computer package for use in designing separation processes.

THSFLASH can handle up to two phases (vapour and liquid) and incorporates both Soave Redlich-Kwong, SRK [Soave, 1972], and Peng-Robinson, PR, [Peng & Robinson, 1976] cubic equations of state (CEOS). The programme first determines the number of phases in the mixture by performing a stability test [Michelsen, 1982] and is followed by either isothermal (P,T), adiabatic (P,H) or isentropic (P,S) flash calculation depending on the choice of the thermodynamic trajectory. In addition to equilibrium data (fluid temperature for PH and PS flash calculations, compositions of both phases and overall vapour mole fraction), it also determines fluid compressibility, as well as residue enthalpy and entropy for each fluid phase.

Three major modifications are made in THSFLASH prior to its implementation in BLOWSIM :

1) The addition of the newly developed Twu-Coon-Cunningham, TCC [Twu et al., 1992] CEOS. The advantages of this equation as compared to SRK and PR CEOS will be described in chapter 5.
2) Implementation of the appropriate equations for determining additional properties such as speed of sound, specific heat capacity and thermal expansion coefficient.
3) The ideal gas heat capacity polynomial correlation [Reid et al., 1977] used in THSFLASH is replaced by a correlation proposed by Aly and Lee [1981]. This is claimed [Twu, 1997a] to lead to more accurate determinations of enthalpy, entropy and speed of sound.

The input parameters are read by BLOWSIM from an ASCII file named "BLOW.INP". The output parameters for each pressure step are given by three output files which are in ASCII form. These are:

BLOW.OUT

- Time, average wall temperatures and fluid temperatures.
- Mass and number of moles of:
  - * discharged material,
  - * fluid remained in the vessel,
  - * condensed vapour and vapour in zone 1.
- Discharge rate in kg/s, number of phases at the orifice and the fluid velocity (sonic or subsonic).

CHAPTER 5

EVALUATION OF PERFORMANCE OF CUBIC EQUATIONS OF STATE

5.1 INTRODUCTION

In this chapter, the Soave Redlich-Kwong, SRK [Soave, 1972] and Peng-Robinson, PR, [Peng & Robinson, 1976] CEOS employed in this study for generating the required thermodynamic properties for blowdown simulation are presented and discussed. The newly developed Twu-Coon-Cunningham, TCC CEOS [Twu et al., 1992] aimed at addressing some of the drawbacks of these equations is also given. This is followed by the derivation of the appropriate equations for determining specific heat capacities, speed of sound and thermal expansion coefficient based on TCC CEOS.

The performance of the above CEOS in predicting the required important parameters for blowdown calculation (e.g. densities and speed of sound for vapour and liquid, and liquid volume percentage) for multi-component mixtures containing mainly hydrocarbons and pure alkanes (liquid speed of sound only) are then investigated by comparison with published experimental data. Mixtures containing light hydrocarbons are mainly considered as vapour space blowdown is always used for the process gas stream.

5.2 PREDICTION OF THERMODYNAMIC PROPERTIES BY CUBIC EQUATIONS OF STATE

The cubic equations of state are based on the van der Waals CEOS which takes into account the attractive and the repulsive forces in terms of the constant a, and b respectively. A well-known two-parameter CEOS is the Redlich-Kwong (RK) equation [1949], which greatly improves the van der Waals equation. However, it is limited to a few rather simple fluids [Assael et al., 1996a]. The equation is given by :

$$P = \frac{RT}{V-b} - \frac{a}{V(V+b)\sqrt{T}} \tag{5.2.1}$$

Where P = Pressure

R = Gas constant

T = Temperature

V = Molar volume

Parameters a and b are functions of critical constants.

There have been several attempts to improve the RK CEOS. The best known modifications were presented by Soave (SRK) [1972] and Peng and Robinson (PR) [1976]. Both CEOS are presented as follows :

SRK CEOS is given by :

$$P = \frac{RT}{V-b} - \frac{a}{V(V+b)} \tag{5.2.2}$$

PR CEOS is given by :

$$P = \frac{RT}{V-b} - \frac{a}{V(V+b)+b(V-b)} \tag{5.2.3}$$

Where

$$b = \sum_{i}^{N} x_i b_i \tag{5.2.4}$$

$$b_i = B_{Ci} \frac{RT_{Ci}}{P_{Ci}} \tag{5.2.5}$$

$$a = \sum_{i}^{N}\sum_{j}^{N} x_i\, x_j\, a_{ij} \tag{5.2.6}$$

$$a_{ij} = \left(a_i a_j\right)^{1/2}\left(1-k_{ij}\right) \tag{5.2.7}$$

$$a_i = a_{Ci}\,\alpha_i \tag{5.2.8}$$

$$a_{Ci} = A_{Ci} \frac{\left(RT_{Ci}\right)^2}{P_{Ci}} \tag{5.2.9}$$

$$\alpha_i^{0.5} = 1 + m_i\left(1 - T_{ri}^{0.5}\right) \tag{5.2.10}$$

m_i for SRK CEOS is given by :

$$m_i = 0.48 + 1.574\omega_i - 0.176\omega_i^2 \tag{5.2.11}$$

m_i for PR CEOS is given by :

$$m_i = 0.37646 + 1.54116\omega_i - 0.26992\omega_i^2 \tag{5.2.12}$$

Where k_{ij} = Binary interaction parameter

P_{Ci} = Critical pressure of component i

T_{Ci} = Critical temperature of component i

T_{ri} = Reduced temperature of component i

ω_i = Acentric factor of component i

x_i = Mole fraction component i

i,j = Component i, j

A_{Ci} (in equation 5.2.9) for SRK and PR CEOS are 0.42747 and 0.45724 respectively while B_{Ci} (in equation 5.2.5) for SRK and PR CEOS are 0.08664 and 0.07780 respectively.

Both CEOS are widely used in the process industry due to their simplicity and ability in predicting reasonably accurate thermodynamic properties for vapour and very accurate vapour-liquid equilibrium data (VLE) for systems containing non-polar components. In addition, the binary interaction parameter, k_{ij} in equation 5.2.7 which represents the deviation of a_{ij} from the geometric mean is close to zero for most hydrocarbon systems. Tsonopoulos and Heidman [1986] who investigated the ability of CEOS in predicting VLE for high pressure systems concluded that the above equations describe most adequately the high-pressure VLE of hydrocarbon systems with k_{ij} assumed to be zero. However, there are certain problems associated with these equations.

For example, the prediction of liquid density is very sensitive to critical compressibility, Z_C [Twu, 1997b]. As Z_C given by SRK CEOS for all components is 0.333 whereas for most real substances, Z_C is in the range of 0.2 to 0.3 [Danesh et al., 1991], the SRK CEOS is inadequate in predicting liquid densities for most components. To address this limitation, Peng and Robinson (PR) [1976] modified the volume function of SRK CEOS to reduce Z_C to 0.307 which generally improves liquid density predictions. However, on the basis of comparison between experimental and calculated saturated single component liquid densities of both CEOS [Twu et al., 1992], SRK CEOS gives more accurate predictions for small molecules (e.g. C_1 and C_2) while PR CEOS performs better for larger molecules (C_3 and above). Both CEOS are still rather poor in predicting liquid densities as their Z_C are quite different from values of real fluids which leads to poor liquid enthalpy and entropy predictions.

A further problem associated with SRK and PR CEOS is their inability in predicting vapour pressure for heavy hydrocarbons. This is because the correlation for m_i (equation 5.2.11) in SRK CEOS was derived from calculated vapour pressure at reduced temperature equal to 0.7 for acentric factors up to 0.5 [Soave, 1971] while for correlation for m_i (equation 5.2.12) in PR CEOS, the vapour pressures of a limited number of hydrocarbons up to an acentric factor of 0.5 were used [Peng & Robinson, 1976]. Hence, it is unlikely that both equations will suffice for higher acentric factors (i.e. heavy hydrocarbons). In addition, as their alpha functions are non-linear functions of acentric factor, extrapolation for heavy hydrocarbons is unreliable.

Furthermore, both CEOS fail to accurately predict vapour pressure at low reduced temperatures [Twu et al., 1995a and b]. This is because the present form of alpha function (equation 5.2.10) is not flexible enough to cover the vapour pressure predictions from the triple point to the critical point [Twu, 1997a]. Twu et al. [1991] also point out that the alpha function given by equation 5.2.10 becomes zero at finite temperature and then rises again with increasing temperature, which is contrary to the temperature behaviour of the attractive force.

Modifications of alpha function based on equation 5.2.10 have been made to compensate for the above weaknesses (see review by Twu et al.[1995a and b]). However, as long as the same type of alpha function is used, its inherent weaknesses will not be overcome [Twu et al., 1995b].

Twu et al. [1991] point out that an appropriate α function should fulfil the following requirements :

1) be finite and positive for all temperatures.
2) be equal to unity at the critical point
3) must approach a finite value as the temperature approaches infinity.

In order to compensate the weaknesses of SRK and PR CEOS, Twu et al. [1992] proposed a new three-parameter Twu-Coon-Cunningham (TCC) CEOS which is presented in the following section. It predicts a substance-dependent critical compressibility factor and incorporates a new alpha function which fulfils the above requirements by abandoning the original form used by SRK and PR CEOS.

5.2.1 Twu-Coon-Cunningham (TCC) Cubic Equations of State [Twu et al., 1992]

The TCC CEOS is given by :

$$P = \frac{RT}{V-b} - \frac{a}{V(V+4b)+c(V+b)} \tag{5.2.13}$$

or

$$Z^3 + (3B + C - 1)Z^2 + \left(A - 4B - C - 4B^2\right)Z - (A + BC + C)B = 0 \tag{5.2.14}$$

Parameters a, and b are determined by equations 5.2.6 and 5.2.4 respectively. The new alpha function is given as follows :

$$\alpha_i = T_{ri}^{N(M-1)} e^{L\left(1-T_{ri}^{NM}\right)} \tag{5.2.15}$$

Parameter, c is given by the following equation :

$$c = \sum_{i}^{N} x_i c_i \tag{5.2.16}$$

$$c_i = C_{Ci} \frac{RT_{Ci}}{P_{Ci}} \tag{5.2.17}$$

Parameters A_{Ci}, and C_{Ci} in equations 5.2.9 and 5.2.17 are given by :

$$C_{Ci} = 1 - 3(Z_{Ci} + B_C) \tag{5.2.18}$$

$$A_{Ci} = 3Z_{Ci}^2 + B_{Ci} + (1 - 3Z_{Ci}) + 4B_{Ci}^2 \tag{5.2.19}$$

B_{Ci} in both equations 5.2.18 and 5.2.19 is the smallest positive real root of the following cubic equation :

$$B_{Ci}^3 - (3Z_{Ci} + 1)B_{Ci}^2 + \left(3Z_{Ci}^2 - 6Z_{Ci} + 2\right)B_{Ci} - Z_{Ci}^3 = 0 \tag{5.2.20}$$

Parameters A, B and C in equation 5.2.14 are given by :

$$A = \frac{Pa}{R^2T^2} \tag{5.2.21}$$

$$B = \frac{Pb}{RT} \tag{5.2.22}$$

$$C = \frac{Pc}{RT} \tag{5.2.23}$$

The fugacity coefficient for component, i is given by :

$$\ln\phi_i = \frac{B_i}{Z-B} - \ln(Z-B) + \frac{A}{W}\left\{\theta_i - \frac{1}{a}\left[\sum x_j\left(a_{ij} + a_{ji}\right)\right]\right\}\ln\Phi + \left(\frac{1}{Z-B} - 1\right)\left\{\frac{1}{2}(4B_i + C_i) - \Theta_i\left[Z + \frac{1}{2}(4B + C)\right]\right\} \tag{5.2.24}$$

Parameters W, Θ_i, Φ_i in the above equation are determined from :

$$W = \left(16B^2 + 4BC + C^2\right)^{1/2} \tag{5.2.25}$$

$$\Phi = \frac{2Z + 4B + C + W}{2Z + 4B + C - W} \tag{5.2.27}$$

The parameters A_{Ci}, B_{Ci}, and C_{Ci} are all functions of Z_{Ci}, which is the apparent compressibility factor instead of the actual value. Twu et al. [1992] optimised Z_{Ci} for component, i by best fitting equation 5.2.14 to saturated liquid density data from triple point to the critical temperature. Subsequently, the calculated values of α_i were used to regress the parameters, L, M, and N of component, i in equation 5.2.15. The table of values of Z_{Ci}, L, M and N for thirty components (hydrocarbons and non-hydrocarbons) is given in the same publication. The [1]AAD% (average absolute deviation percentage) between measured and experimental values in predicting single component vapour pressures and saturated liquid densities of the published thirty components for reduced temperature less than 0.7 are generally within 0.5 % and 1.5 % respectively. The overall AAD% of density predictions for reduced temperatures up to unity are 3.3% for TCC, 18.3% for SRK and 10.4% for PR CEOS.

5.2.2 Determination of Specific Heat Capacities, Speed of Sound and Thermal Expansion Coefficient from Twu-Coon-Cunningham Cubic Equation of State

In order to incorporate TCC CEOS in the computer programme THSFLASH (see section 4.4 of chapter 4), equation 5.2.13 is re-written in the following form :

$$\frac{P}{T} = \frac{1}{V'-b'} - \frac{a'}{V'(V'+4b') + c'(V'+b')} \tag{5.2.28}$$

Where $$a' = \frac{a}{R^2T} \tag{5.2.29}$$

$$b' = \frac{b}{R} \tag{5.2.30}$$

$$c' = \frac{c}{R} \tag{5.2.31}$$

[1] $\text{AAD\%} = (100/n)\sum_{i=1}^{n}|Exp_i - Cal_i/Exp_i|$ where n is the number of experimental points, Exp and Cal are the experimental and calculated values respectively.

$$V' = \frac{V}{R} \tag{5.2.32}$$

For multi-component mixtures, a' is given as follows :

$$a' = \sum_{i}^{n}\sum_{j}^{n}\left(x_i x_j a'_i a'_j \left(1 - k_{ij}\right)\right) \tag{5.2.33}$$

Where
$$a'_i = \left[T_{ri}^{\frac{N(M-1)}{2}} e^{L/2\left[1-T_{ri}^{NM}\right]}\right]\frac{A_{Ci}}{P_{Ci}}^{1/2}\frac{T_{Ci}}{\sqrt{T}} \tag{5.2.34}$$

The following equations for determining specific heat capacities, speed of sound and thermal expansion coefficient are derived based on equation 5.2.28.

5.2.2.1 Specific Heat Capacities

The specific heat capacity at constant volume, C_V is defined as :

$$C_V = C_{Vi} + \Delta C_V \tag{5.2.35}$$

Where C_{Vi} = Ideal specific heat capacity at constant volume

ΔC_V = Residual specific heat capacity at constant volume

C_{Vi} is given by the following equation :

$$C_{Vi} = C_{Pi} - R \tag{5.2.36}$$

The ideal specific heat capacity at constant pressure, C_{Pi}, is determined by a correlation proposed by Aly and Lee [1981] which is a function of temperature.

ΔC_V is defined as follows :

$$\Delta C_V = RT\int_{\infty}^{V}\left[T\left(\frac{\partial^2 Z}{\partial T^2}\right)_V + 2\left(\frac{\partial Z}{\partial T}\right)_V\right]\frac{dV}{V} \tag{5.2.37}$$

By transforming the above two derivatives in terms of P, V, and T, they can then be determined by differentiating equation 5.2.28 and substituted back into the above equation. Hence, the integrated form of the equation is given by :

$$\Delta C_V = -RT\left[\frac{T\cdot\left(d^2a'/dT^2\right)}{\sqrt{\Psi}}\ln\left(\frac{4b'+c'+2V'-\sqrt{\Psi}}{4b'+c'+2V'+\sqrt{\Psi}}\right)+2\frac{da'/dT}{\sqrt{\Psi}}\ln\left(\frac{4b'+c'+2V'-\sqrt{\Psi}}{4b'+c'+2V'+\sqrt{\Psi}}\right)\right] \tag{5.2.38}$$

Where $\Psi = 4^2 b'^2 + c'^2 + 4b'c'$ (5.2.39)

Similar to C_V, the specific heat capacity at constant pressure, C_P is defined as :

$$C_P = C_{Pi} + \Delta C_P \tag{5.2.40}$$

The residual specific heat capacity at constant pressure, ΔC_P is given by :

$$\Delta C_P = -\Delta C_V - R - T\left(\frac{\partial P}{\partial T}\right)_V^2\left(\frac{\partial P}{\partial V}\right)_T^{-1} \tag{5.2.41}$$

By determining the above two derivatives from equation 5.2.28 and substituting equation 5.2.38 for ΔC_V, the above equation becomes :

$$\Delta C_P = -T\left[\left(\frac{T\cdot d^2a'/dT^2}{\sqrt{\Psi}}\right)\ln\left(\frac{4b'+c'+2V'-\sqrt{\Psi}}{4b'+c'+2V'+\sqrt{\Psi}}\right)-2\left(\frac{-da'/dT}{\sqrt{\Psi}}\right)\ln\left(\frac{4b'+c'+2V'-\sqrt{\Psi}}{4b'+c'+2V'+\sqrt{\Psi}}\right)\right]$$

$$-1-\frac{\left[T\left(\frac{-da'/dT}{V'(V'+4b')+c'(V'+b')}\right)+\frac{P}{T}\right]^2}{-\left(\frac{P}{T}+\frac{a'}{V'(V'+4b')+c'(V'+b')}\right)^2+\frac{a'(2V'+4b'+c')}{\left[V'(V'+4b')+c'(V'+b')\right]^2}} \tag{5.2.42}$$

In order to determine $\frac{da'}{dT}$ and $\frac{d^2a'}{dT^2}$ in equations 5.2.38 and 5.2.42, the first and second derivatives of a'_i (see equation 5.2.34) with respect to T are determined :

$$\frac{da'_i}{dT} = \frac{a'_i}{2T}\left[N\left(M-1-LM\cdot T_{ri}^{NM}\right)-1\right] \tag{5.2.43}$$

$$\frac{d^2a'_i}{dT^2} = \frac{da'/dT}{2T}\left[N\left(M-1-LM\cdot T_{ri}^{NM}\right)-1\right]- \frac{a'_i}{2T^2}\left[N\left(M-1-LM\cdot T_{ri}^{NM}\right)-1+LM^2N^2T_{ri}^{NM}\right] \tag{5.2.44}$$

Hence, $\frac{da'}{dT}$ can be written as :

$$\frac{da'}{dT} = \sum_{i=1}^{N}\left\{\frac{x_i}{2}\left[2a'_i\left(\sum_{j=1}^{N}\frac{da'_j}{dT}\right)+2\frac{da'_i}{dT}\left(\sum_{j=1}^{N}a'_j\right)-2\frac{da'_i}{dT}\vartheta_i\right.\right. \left.\left.-2a'_i\,\phi_i\right]\right\} \tag{5.2.45}$$

Where

$$\vartheta'_i = \sum_{j=1}^{N}x_j a'_j k_{ij} \tag{5.2.46}$$

$$\phi'_i = \vartheta_i + \sum_{j=1}^{N}x_j\frac{da'_j}{dT}k_{ij} \tag{5.2.47}$$

Subsequently, $\frac{d^2a'}{dT^2}$ can be determined by differentiating equation 5.2.45 with respect to T.

5.2.2.2 Speed of Sound

The definition of speed of sound, $\hat{a}$, is given earlier by equation 4.2.26 in chapter 4. It is then transformed into the following form :

$$\hat{a} = \frac{C_P}{C_V}\left(\frac{\partial P}{\partial V}\right)_T\left(\frac{-V^2}{MW_{Avg}}\right) \tag{5.2.48}$$

Where MW_{Avg} = Average molecular weight

The equations based on TCC CEOS for determining C_P and C_V are given in the previous section. $\left(\frac{\partial P}{\partial V}\right)_T$ is derived in conjunction with equation 5.2.28 to obtain :

$$\left(\frac{\partial P}{\partial V}\right)_T = \frac{T}{R}\left[\frac{-1}{(V'-b')^2} + \frac{a'(2V'+4b'+c')}{[V'(V'+4b')+c'(V'+b')]^2}\right] \tag{5.2.49}$$

5.2.2.3 Thermal Expansion Coefficient

The thermal expansion coefficient, β, is defined as follows :

$$\beta = \frac{1}{V}\left(\frac{\partial V}{\partial T}\right)_P \tag{5.2.50}$$

Hence, β, derived in conjunction with equation 5.2.28 is given by :

$$\beta = \frac{\left[-\frac{T}{R}\frac{da'}{dT} + \frac{P}{T}\right]^2}{\left(\frac{\partial P}{\partial V}\right)_T R} \tag{5.2.51}$$

$\frac{da'}{dT}$ and $\left(\frac{\partial P}{\partial V}\right)_T$ are given by equations 5.2.45 and 5.2.49 respectively.

5.3 Evaluation the Performance of CEOS in Terms of Predicting Fluid Densities and Percentage of Liquid Volume for a Multi-component Hydrocarbon Mixture

Although it has been established that TCC CEOS [Twu et al., 1992] is much superior than SRK and PR CEOS in predicting saturated liquid densities for pure components (see section 5.2.1), the equation has not been validated against experimental data for multi-component mixtures.

Kalra and Robinson [1979] measured equilibrium densities and percentage of liquid volume for two-phase multi-component hydrocarbons at elevated pressures by

measuring refractive index of each fluid phase. In this study, their data are used to test the performance of the TCC CEOS.

5.3.1 Experimental Conditions and Measurement Accuracy

Kalra and Robinson [1979] measured the pressure, temperature, percentage volume of liquid, VLE, and refractive index of each fluid phase at eight different equilibrium conditions over the temperature and pressure ranges 185.95 - 235.90 K and 27 - 79.3 atm respectively. The particular system examined included a mixture containing different compositions of C_1, C_2, C_3, N_2, CO_2 and H_2S. Equilibrium was assumed when the pressure and temperature were stable for at least half an hour. The experimental conditions approach the critical region of the feed at 235.90 K and 79.3 atm. As the feed compositions are not given, these are estimated in this study from the appropriate VLE data measured by the authors.

The measured pressures, temperatures and liquid volumes of the system are claimed to be accurate to ± 0.25%, ± 0.05K and ± 0.2 cm^3 respectively. The fluid phase compositions are measured to ± 0.005 mole fraction for all components except propane which has an accuracy within ± 2% of the reported composition. However, the accuracy of measured feed compositions has not been stated. The vapour and liquid densities for each condition are determined by employing a set of equations (see publication) which relate fluid phase density to measurements of refractive index, phase composition and pressure.

The authors ensured reliable measurements of percentage volume of liquid by comparing the corresponding experimental data with values calculated by overall or component material balances. Reasonable agreements were obtained. The authors calculated values of percentage volume of liquid based on component material balances are used in this study to determine the feed compositions for all cases using the following equation :

$$z_i = \frac{V}{L+V}\left(y_i + \frac{L}{V}x_i\right) \qquad (5.3.1)$$

Where L = No. of moles of liquid

V = No. of moles of vapour

x_i, y_i = Mole fractions of component i in liquid and vapour phases respectively

z_i = Mole fraction of component i in the feed

The calculated densities based on the measured refractive indices together with measured compositions of both fluid phases are inserted in the above equation. The calculated feed compositions for all eight conditions are given in table 5.1. It is notable that the feed compositions for all cases are very similar. The conditions for case 8 are reported to be close to the critical region.

Table 5.1 Kalra and Robinson [1979] experimental conditions and calculated (equation 5.3.1) feed compositions

P (atm)	**27**	**37.4**	**40.8**	**43.8**	**54.4**	**61.3**	**68**	**79.3**
T (K)	**185.95**	**199.80**	**200.20**	**213.75**	**213.70**	**227.60**	**227.60**	**235.85**
Case	**1**	**2**	**3**	**4**	**5**	**6**	**7**	**8**
C_1	0.6983	0.7114	0.7077	0.7067	0.7024	0.7050	0.7013	0.6991
C_2	0.0670	0.0657	0.0666	0.0673	0.0686	0.0688	0.0676	0.0675
C_3	0.0294	0.0282	0.0287	0.0295	0.0288	0.0280	0.0280	0.0286
N_2	0.0876	0.0766	0.0739	0.0749	0.0770	0.0754	0.0808	0.0841
CO_2	0.0199	0.0188	0.0200	0.0194	0.0201	0.0200	0.0200	0.0196
H_2S	0.0979	0.0993	0.1032	0.1022	0.1031	0.1028	0.1024	0.1010

P = Pressure; T = Temperature

5.3.2 Results

The equilibrium vapour and liquid densities together with percentages of liquid volume for all eight mixtures reported by Kalra and Robinson [1979] are determined by flash calculation based on SRK, PR or TCC CEOS at the conditions given in table 5.1. The binary interaction parameters are assumed to be zero as the amount of H_2S is relatively small. For each case, the reported experimental data and the corresponding predicted values for vapour and liquid densities together with

percentage of liquid volumes are plotted in figures 5.1 to 5.3 respectively. The absolute deviation percentages between measured and predicted vapour and liquid densities for case 8 (near the critical region of the fluid) are given in table 5.2. The average absolute deviation percentage (AAD%) between reported and predicted densities based on all three CEOS for all eight cases are given in table 5.3.

In vapour phase, the main component is C_1. It's predicted mole fractions for all cases are between 0.74 and 0.85. In the liquid phase on the other hand, the major components are C_1 and H_2S. The predicted mole fractions of the former are between 0.49 and 0.59 while for the latter are between 0.18 and 0.25. The above predictions are in fair agreement with the published experimental measurements reported by Kalra and Robinson [1979].

Table 5.2 Absolute percentage deviation between experimental and predicted vapour and liquid densities based on SRK, PR and TCC CEOS for case 8 (near the critical region of the mixture)

	Percentage deviation for vapour density	Percentage deviation for liquid density
SRK	14.67	6.76
PR	7.94	18.79
TCC	3.59	13.17

Table 5.3 AAD% between experimental and predicted vapour and liquid densities based on SRK, PR, and TCC CEOS

	AAD% of vapour density	AAD% of liquid density
SRK	5.59	2.40
PR	2.55	11.71
TCC	3.52	5.58

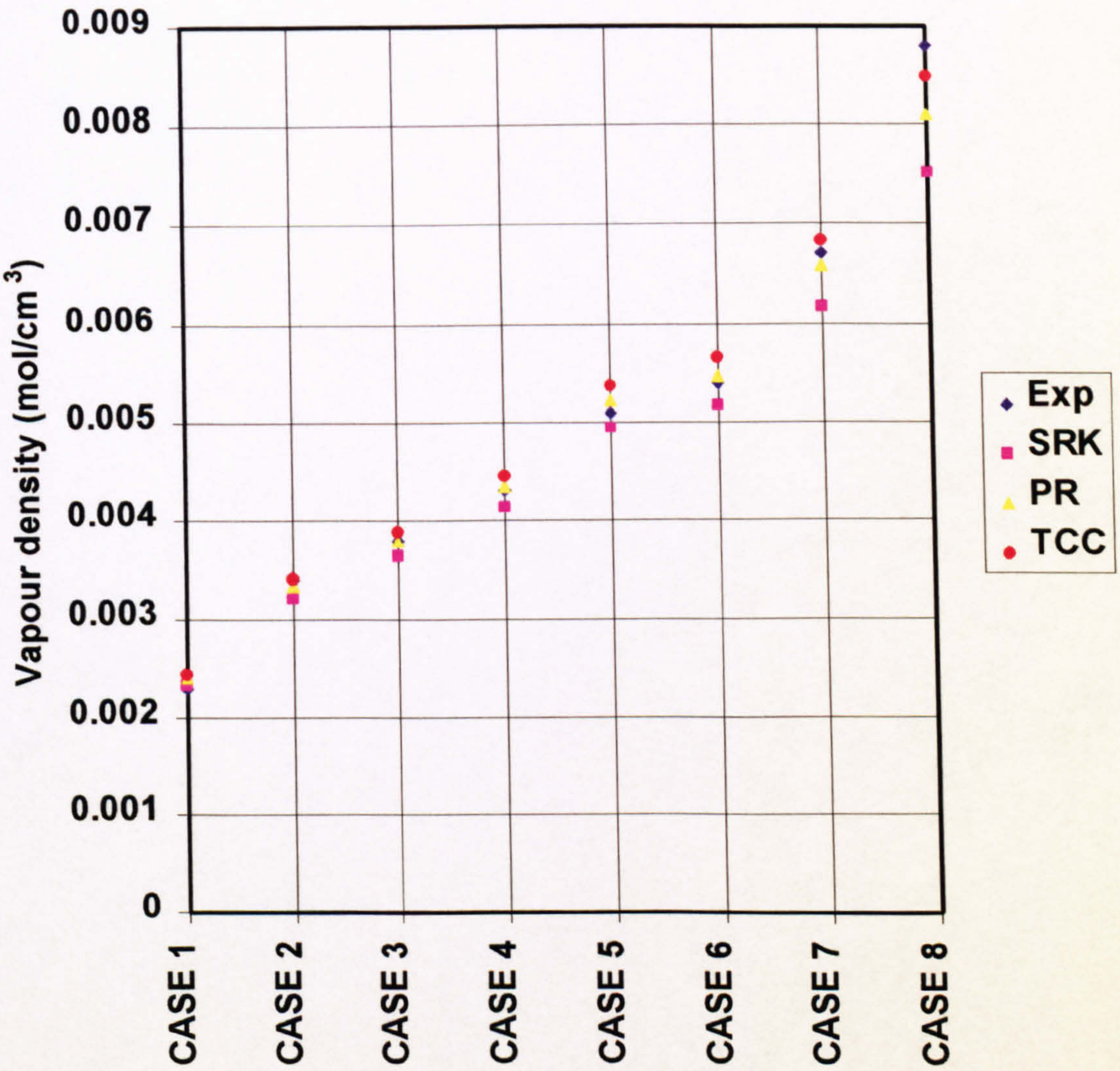

Figure 5.1 Comparison between measured (Exp) and predicted vapour densities based on SRK, PR and TCC CEOS. See table 5.1 for appropriate compositions and conditions relating to each case.

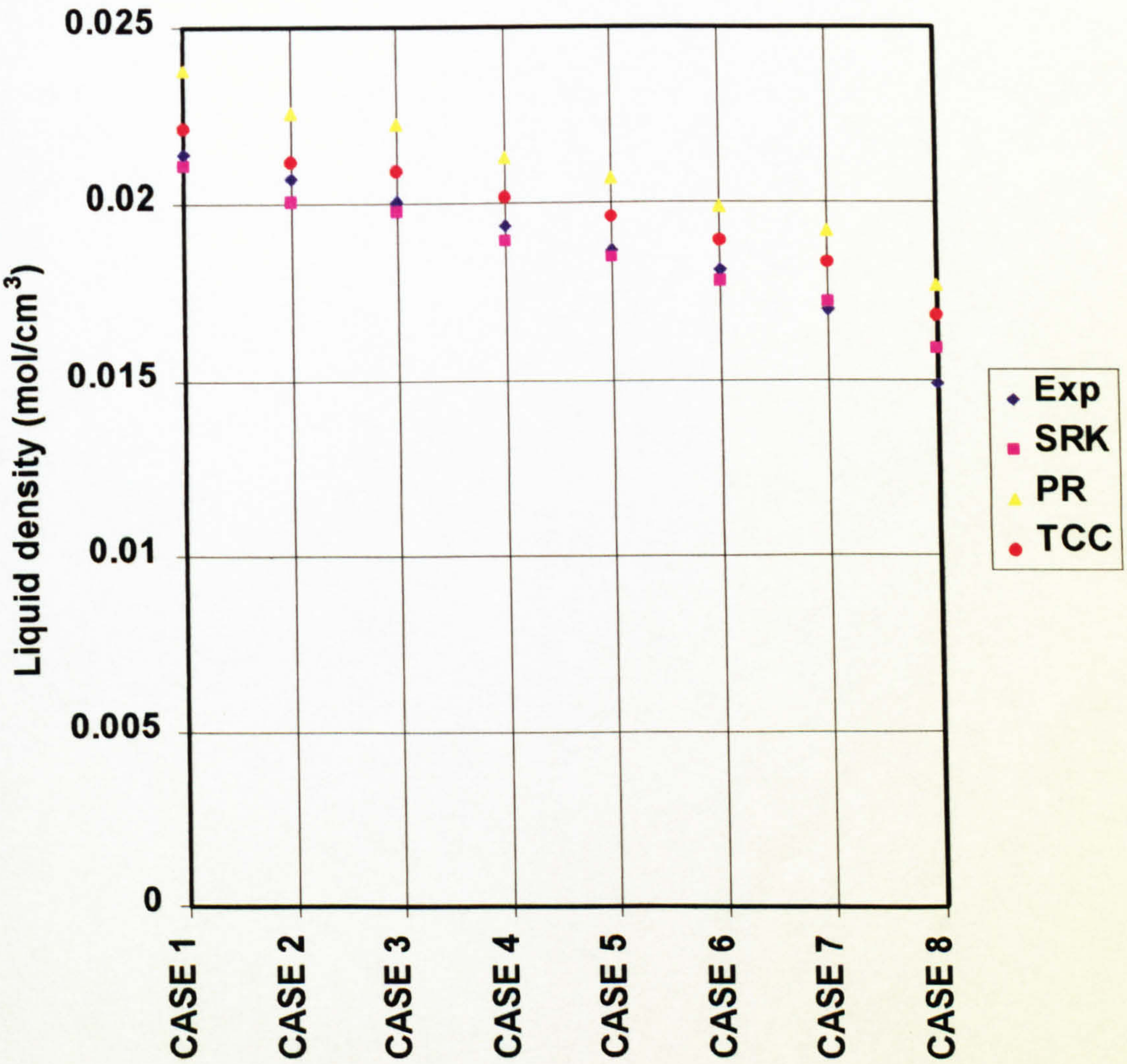

Figure 5.2 **Comparison between measured (Exp) and predicted liquid densities based on SRK, PR and TCC CEOS. See table 5.1 for appropriate compositions and conditions relating to each case.**

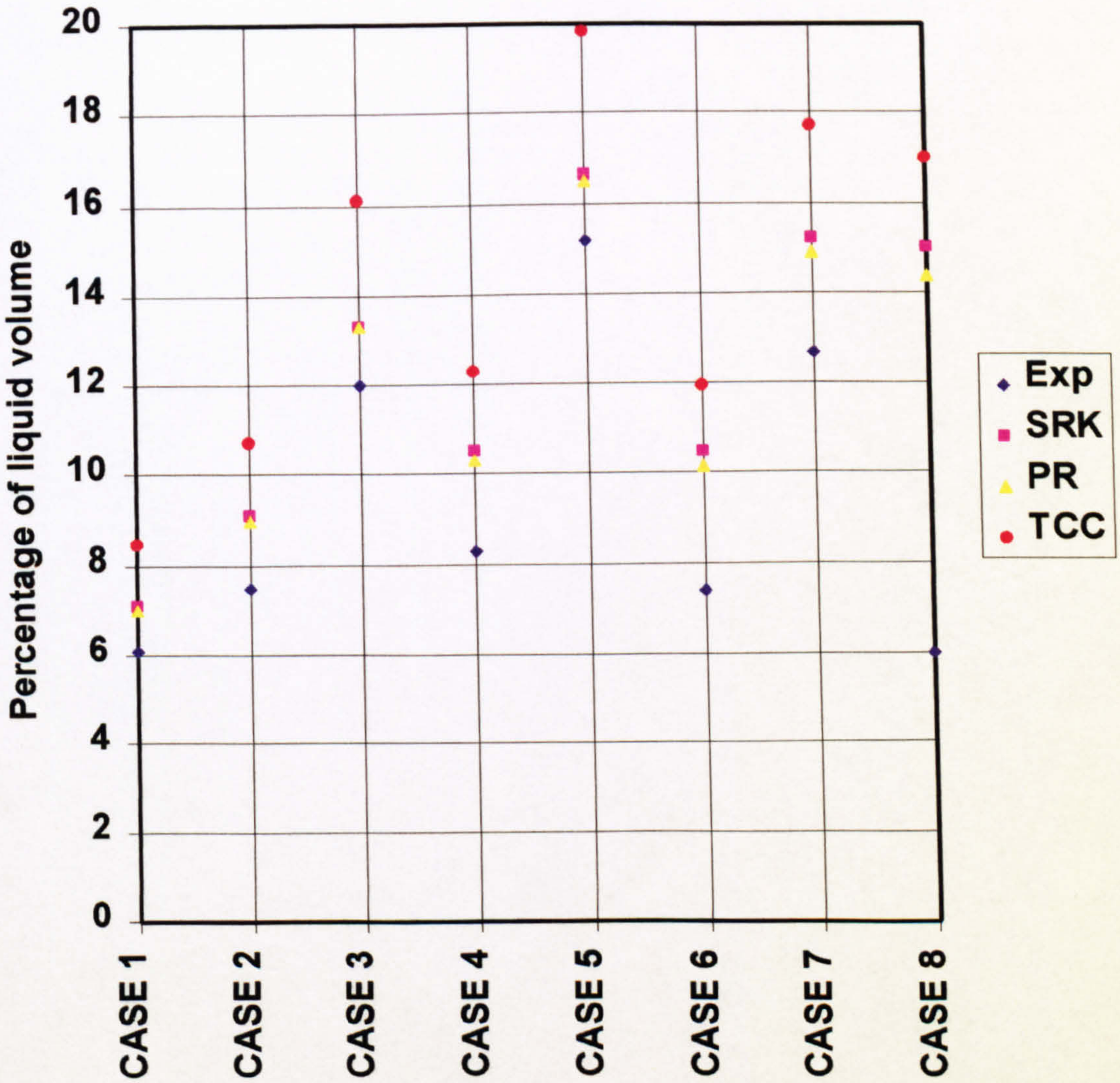

Figure 5.3 Comparison between measured (Exp) and predicted percentage of liquid volume based on SRK, PR and TCC CEOS. See table 5.1 for appropriate compositions and conditions relating to each case.

Referring to figure 5.1 showing the comparison between experimental and predicted vapour densities based on all three CEOS, it may be observed that all predictions follow the same trend as the experimental data while TCC CEOS gives the best performance for case 8 (see table 5.2). It is also interesting to note that SRK CEOS underestimates vapour densities for all cases while TCC CEOS over estimates them except in case 8. From table 5.3 it is clear that all the CEOS perform well in predicting vapour densities without the use of binary interaction parameters while PR CEOS gives slightly better results than the rest.

It is well-known [Millat et al., 1996] that the above CEOS are applicable to slightly polar systems; the predicted and measured mole fraction for H_2S in the vapour phase for all cases examined in this study are less than 0.1. Although SRK CEOS usually gives better predictions for vapour pressure and saturated vapour volumes for alkanes from C_1 up to C_{10} [Millat et al., 1996] compared with PR CEOS, table 5.3 indicates the best predictions are given by PR CEOS. As differences of AAD% between all three CEOS in predicting vapour densities are small, the above is likely to be the result of uncertainties associated with the density measurement technique rather than a true reflection of the equations' performance.

Figure 5.2 presents the comparison between measured and calculated liquid densities. Again, all predictions follow the same trend as the experimental data and the best results for case 8 is given by SRK CEOS (see table 5.2). Both TCC and PR CEOS generally over estimate liquid densities while the predictions from the latter deviate more from the experimental data. In addition, the AAD% in table 5.3 shows that both SRK and TCC CEOS give reasonable estimations for liquid density while the former is slightly superior than the latter. The worst performance is given based on PR CEOS.

The AAD% between measured and predicted liquid densities based on PR CEOS is significantly higher than those from the other CEOS (see table 5.3). This is probably because of the equation's inability to accurately predict saturated liquid densities for small molecules as compared to SRK and TCC CEOS. It is interesting to note that

SRK and TCC CEOS give reasonably good accuracy in predicting liquid densities despite the assumption of zero binary interaction parameter.

The comparison between experimental and calculated percentages of liquid volume is given in figure 5.3. For cases 1 - 7, both SRK and PR CEOS over-estimate the volume percentages by 1 to 3 % while TCC CEOS over-predicts these values by 2 to 5 %. Although all predictions follow the same trend as the experimental data, large derivations are observed between measured and estimated values in case 8 for all three CEOS. The corresponding deviations are 9% for both SRK and PR and 11% for TCC CEOS.

Both SRK and PR CEOS perform similarly and better than TCC CEOS in predicting percentages of liquid volume. However, as the predictions of the volume percentage are more sensitive to feed compositions than densities and the uncertainties associated with estimated feed compositions are not known, more experimental data for VLE would be required for validation purposes.

5.4 Evaluation the Performance of CEOS in Predicting Vapour and Liquid Speed of Sound at High Pressures for Single and Multi-component Hydrocarbon Systems

Ye et al. [1992] determined AAD% between measured and predicted speed of sound for pure liquid alkanes (n-C_3 to n-C_{16}) based on SRK and PR CEOS over a wide range of conditions. Lagourette et al. [1995] on the other hand performed a similar study for a hydrocarbon gas mixture (0.880 C_1; 0.100 n-C_3 and 0.020 n-C_8). However only the average performance, expressed in terms of average absolute deviation percentage (AAD%) based on each CEOS over a range of temperatures and pressures are reported; information on performance relating to specific temperatures and pressures are not given.

In this study, AAD% between measured and predicted speed of sound based on all three CEOS for pure liquid alkanes from C_1 to n-C_9 together with some hydrocarbon mixtures (liquid as well as vapour) over a wide range of pressures ($\leq$ 986.9 atm) and temperatures are determined. In addition, the variations of absolute deviation

percentage for speed of sound for some selected fluids against T_r and P_r are presented in order to evaluate the limitations of the three CEOS with respect to temperature and pressure. Most experimental measurements used in this study are at the reservoir conditions.

5.4.1 Experimental Conditions and Measurement Accuracy for Speed of Sound

The fluid compositions and experimental conditions (expressed in terms of reduced temperatures, T_r, and pressures, P_r) for speed of sound measurements used in this study for comparison purposes are given in table 5.4. Most conditions are either below or above saturation points except for liquid alkanes from n-C_3 to n-C_5 in which the speed of sound were measured at both compressed and saturated conditions. The source of the original data as well as the number of data points for each system are also given in the same table. As the measured critical temperatures and pressures in the case of the mixtures are not reported, in this study, these are estimated from SRK CEOS and are given in table 5.5. The claimed accuracy for the measured speed of sound data is generally within 1%. The measured temperatures and pressures have uncertainties below 0.1 K and 0.5 % respectively. The reported purity for all systems studied is above 99% mole.

Table 5.4 Fluid compositions and experimental conditions for speed of sound for various hydrocarbon mixtures

Component, mole fraction	T_r range	P_r range	No. of data points	Source
C_1, 0.685; C_2, 0.315 (V)	1.02 - 1.43	0.06 - 1.56	113	Younglove & Frederick, 1990
C_1, 0.900; n-C_3, 0.100 (V)	1.17 - 1.83	1.29 - 9.02	265	Lagourette et al., 1994
C_1, 0.980; n-C_8, 0.020 (V)	1.64 - 2.09	8.00 - 31.99	78	Same as above
C_1, 0.880; n-C_3, 0.100; n-C_8 0.020 (V)	1.42 - 1.81	3.70 - 14.81	144	Lagourette et al., 1995
C_1 (L)	0.53 - 1.58	0.36 - 7.57	61	Strarty, 1974
C_2 (L)	0.33 - 1.06	0.73 - 7.55	154	Tsumura & Strary, 1977
n-C_3 (L+SL)	0.54 - 0.92	0.0047 - 14.26	241	Niepmann, 1984
n-C_4 (L+SL)	0.47 - 0.88	0.00053 - 15.91	249	Same as above
n-C_5 (L+SL)	0.62 - 0.67	0.029 - 29.11	9	Belinskii & Ikramov, 1973
n-C_6 (L)	0.50 - 0.66	0.033 - 33.03	30	Boelhouwer, 1967
n-C_7 (L)	0.47 - 0.84	0.037 - 36.59	48	Same as above
n-C_8 (L)	0.45 - 0.69	0.041 - 40.27	48	Same as above
n-C_9 (L)	0.42 - 0.69	0.044 - 43.41	69	Same as above
C_1, 0.617; n-C_3, 0.145; n-C_8 0.238 (L)	0.64 - 0.81	1.55 - 6.18	144	Daridon& Lagourette, 1996

L = Compressed liquid; SL= Saturated liquid, V =Vapour

Table 5.5 Predicted critical temperatures (T_C) and pressures (P_C) based on SRK CEOS for the hydrocarbon mixtures given in table 5.4.

Mixtures	T_C (K)	P_C (atm)
C_1+ C_2 (V)	244.08	68.71
C_1+ n-C_3 (V)	225.33	76.59
C_1+ n-C_8 (V)	178.56	30.85
C_1+ n-C_3 + n-C_8 (V)	206.19	66.63
C_1+ n-C_3 + n-C_8 (L)	460.63	159.62

5.4.2 Determination of AAD %

The AAD% between measured and predicted values of speed of sound for all the components presented in table 5.4 based on the various CEOS are given in table 5.6. The equation for calculating speed of sound based on TCC CEOS was given in section 5.2.2. Although the fluids used in this study are single phase, the stability test (section 4.4) is applied to all cases in order to ensure that the number of phases are predicted correctly by all three CEOS. When multiple solutions are encountered in solving CEOS for molar volume, the root which gives the lowest excess Gibbs energy is used (largest root represents vapour like fluid while smallest root represents liquid like fluid).

For comparison purposes, table 5.7 shows AAD% between measured and predicted speed of sound as determined in this study for liquid alkanes n-C_3 to n-C_9 (table 5.6) as compared with values determined by Ye et al. [1992]. The same table also shows the results of the same comparison for a vapour mixture of C_1, n-C_3 and n-C_8 (see table 5.4 for composition). The literature values for AAD% in this case are from Lagourette et al. [1995]. The comparison excludes an evaluation of performance based on TCC EOS as other than the AAD% obtained in this study no other published data are available in order to allow this exercise.

Table 5.6 AAD% between measured and predicted speed of sound based on TCC, PR and SRK CEOS for the systems presented in table 5.4.

Fluid	AAD %		
	TCC	PR	SRK
C_1+ C_2 (V)	3.8	2.6	4.5
C_1+ n-C_3 (V)	2.7	8.9	5.0
C_1+ n-C_8 (V)	1.9	8.9	4.1
C_1+ n-C_3 + n-C_8 (V)	2.2	9.3	4.4
C_1 (L)	9.3	11.4	8.8
C_2 (L)	12.9	13.8	12.1
n-C_3 (SL+L)	8.6	17.3	16.6
n-C_4 (SL+L)	13.1	15.2	14.9
n-C_5 (SL+L)	21.9	17.4	18.4
n-C_6 (L)	15.6	10.9	12.0
n-C_7 (L)	13.0	10.9	11.4
n-C_8 (L)	16.0	14.6	15.6
n-C_9 (L)	17.1	16.3	17.1
C_1 + n-C_3 + n-C_8 (L)	3.8	5.3	3.0

SL = Saturated liquid, L = Liquid, V = Vapour

Table 5.7 **Comparison between reported and calculated AAD% (table 5.6) of speed of sound for liquid alkanes from n-C_3 to n-C_9 and a vapour mixture of C_1, n-C_3 and n-C_8 (see conditions in table 5.4)**

	Reported AAD %		AAD % from table 5.6	
Fluid	**SRK**	**PR**	**SRK**	**PR**
n-C_3	23.9	14.9	16.6	17.3
n-C_4	17.6	10.8	14.9	15.2
n-C_5	15.1	11.4	18.4	17.4
n-C_6	12.2	11.1	12.0	10.9
n-C_7	11.6	11.1	11.4	10.9
n-C_8	14.8	14.6	15.6	14.6
n-C_9	16.2	16.3	17.1	16.3
C_1 + n-C_3 + n-C_8 (V)	16.0	10.8	4.4	9.3

Note : The reported AAD% for the vapour mixture is from Lagourette et al. [1995].
The reported AAD% for other fluids are from Ye et al. [1992].

Referring to table 5.6, for vapour mixture of C_1 and C_2, similar accuracy is obtained from all three CEOS with best results given by PR CEOS. For other vapour mixtures, TCC CEOS performs better than the other CEOS while PR CEOS gives the worst performance. This is likely due to the fact that SRK CEOS gives more accurate predictions of saturated vapour volumes for alkanes from C_1 up to n-C_{10} compared to PR CEOS. [Millat et al., 1996]. While for TCC CEOS, the ability to predict component dependent critical compressibility factor and the use of a new alpha function are likely to improve the volume predictions over the other two CEOS. It is interesting to note (see table 5.4) that except for the C_1 and C_2 vapour mixture, the experimental conditions for other vapour mixtures are well above the critical pressures and temperatures of the fluids.

In the case of the pure liquid alkanes, C_1 and C_2 given in table 5.6, TCC and SRK CEOS perform comparatively well, whilst best overall performance for n-C_3 and n-C_4, is obtained based on TCC CEOS.

The worst performance for the above liquids are associated with PR CEOS. Conversely, for alkanes from n-C_5 to n-C_9, PR CEOS gives the best overall performance while TCC CEOS gives the worst performance except for n-C_9 in which the AAD% is the same as that from SRK CEOS. For the liquid mixture, all three CEOS perform reasonably well with SRK CEOS providing the best performance.

From table 5.7, it is surprising to note the comparatively large differences between the reported AAD% and those obtained in this study for liquid alkanes from n-C_3 to n-C_5 (which include both saturated and compressed liquid) and the vapour mixture. This is despite the fact that although in this study an analysis of the correct fluid state (liquid or vapour) involving the calculation of the Gibbs free energy (see section 5.4.2) is applied in each and every case, there is no indication of the same procedure having been applied by the authors. Clearly, an incorrect prediction of the appropriate phase particularly at the saturation conditions is expected to give rise to a pronounced effect on the data. For other pure liquid alkanes, it is postulated that the

slight differences in the AAD% are due to the application of different methods for calculating ideal heat capacities.

In order to explain the discrepancies between reported and calculated AAD% for liquid alkanes from n-C_3 to n-C_5 (see table 5.7) and investigate the performance of TCC CEOS at both compressed and saturated conditions, the AAD% for speed of sound for all three CEOS at compressed and saturated conditions are determined separately. The results are shown in tables 5.8 and 5.9.

By comparing values between both tables, the exceptionally high AAD% associated with saturated liquid alkanes for all tested CEOS (table 5.9) are mainly attributed to predicted vapour like behaviour at some saturated conditions. Consequently, the above give rise to the different AAD% for SRK and PR CEOS as observed in this study compared to those reported.

Returning to table 5.8, TCC CEOS gives the best overall performance for compressed liquid n-C_3 and n-C_4 and worst performance for n-C_5. On the other hand, from table 5.9, TCC CEOS gives the best overall performance in predicting speed of sound for saturated liquids for n-C_3 and n-C_4. This is mainly due to the comparatively better capability of TCC CEOS in predicting the correct fluid state. All three CEOS give similar AAD% for saturated liquid n-C_5.

Referring back to table 5.7, it is difficult to offer a conclusive explanation regarding the large discrepancy between reported and calculated AAD% based on SRK CEOS in conjunction with the vapour mixture (C_1 + n-C_3 + n-C_8). A possible explanation could be due to errors in the reported value of AAD%.

Table 5.8 AAD% between measured (see table 5.4) and predicted speed of sound based on TCC, PR, and SRK CEOS for compressed liquid alkanes from n-C_3 to n-C_5

Fluid	No. of data points	TCC	PR	SRK
n-C_3	220	6.93	13.76	13.13
n-C_4	230	8.82	9.51	9.77
n-C_5	8	14.66	9.65	10.76

Table 5.9 AAD% between measured (see table 5.4) and predicted speed of sound based on TCC, PR and SRK CEOS for saturated liquid alkanes from n-C_3 to n-C_5

Fluid	No. of data points	TCC	PR	SRK
n-C_3	21	25.76	54.05	52.92
n-C_4	19	55.87	74.99	67.76
n-C_5	1	79.65	79.63	79.60

5.4.3 Absolute Percentage Deviation as a Function of T_r and P_r for Vapour Mixtures

Figures 5.4 a - c show three dimensional plots of absolute percentages deviation between experimental and predicted values of vapour speed of sound based on various CEOS (TCC, PR and SRK CEOS respectively) against T_r and P_r for the C_1 and C_2 mixture (table 5.4). Similar plots for other vapour mixtures, C_1 + n-C_3, C_1 + n-C_8 and C_1 + n-C_3 + n-C_8 (table 5.4) are given in figures 5.5 to 5.7 respectively.

Returning to figures 5.4 a - c, all three CEOS perform equally well at most conditions (maximum error <5%) except near the critical region ($T_r = P_r = 1$) where the absolute percentage deviations are in the range 17-22 %. Furthermore, the absolute percentage deviation based on TCC and PR CEOS near the critical region (figures 5.4.a and b respectively) are smaller than values generated by SRK CEOS (figure 5.4.c). This is likely to be due to the over estimation of component independent critical compressibility based on SRK CEOS while the predicted values based on the other two equations are closer to real fluids (see section 5.2). On the basis of the above observations, we postulate that the inaccuracy in predicting speed of sound near or at the critical region is an inherent problem with CEOS. Nevertheless, as this is the only vapour mixture used in this study for which the conditions are near the critical region, further experimental data in such regions are required in order to reach a more generalised conclusion.

Figures 5.5.a - c, 5.6.a - c and 5.7.a - c present the variations of absolute deviation percentage between measured and predicted values of speed of sound based on the three CEOS plotted against T_r and P_r . The data are for three vapour mixtures; C_1 + n-C_3, C_1 + n-C_8 and C_1 + n-C_3 + n-C_8. All conditions are specifically chosen to be above critical temperatures and pressures.

On the basis of the above figures, it is clear that TCC CEOS consistently performs better than the other CEOS for all tested conditions while PR CEOS gives the worst performance. This is also reflected by the AAD% for the above mixtures as shown in table 5.6. The possible reasons regarding the above observations are given in section

5.4.2. For the time being, it is interesting to note that the superior performance of TCC CEOS over the other CEOS does not appear to apply to the C_1 and C_2vapour mixture which is at lower reduced pressures compared with other vapour mixtures (see table 5.4). This indicates that the particular features embodied in TCC CEOS mentioned in section 5.2.1 are more effective for vapour hydrocarbon mixtures at high reduced pressures.

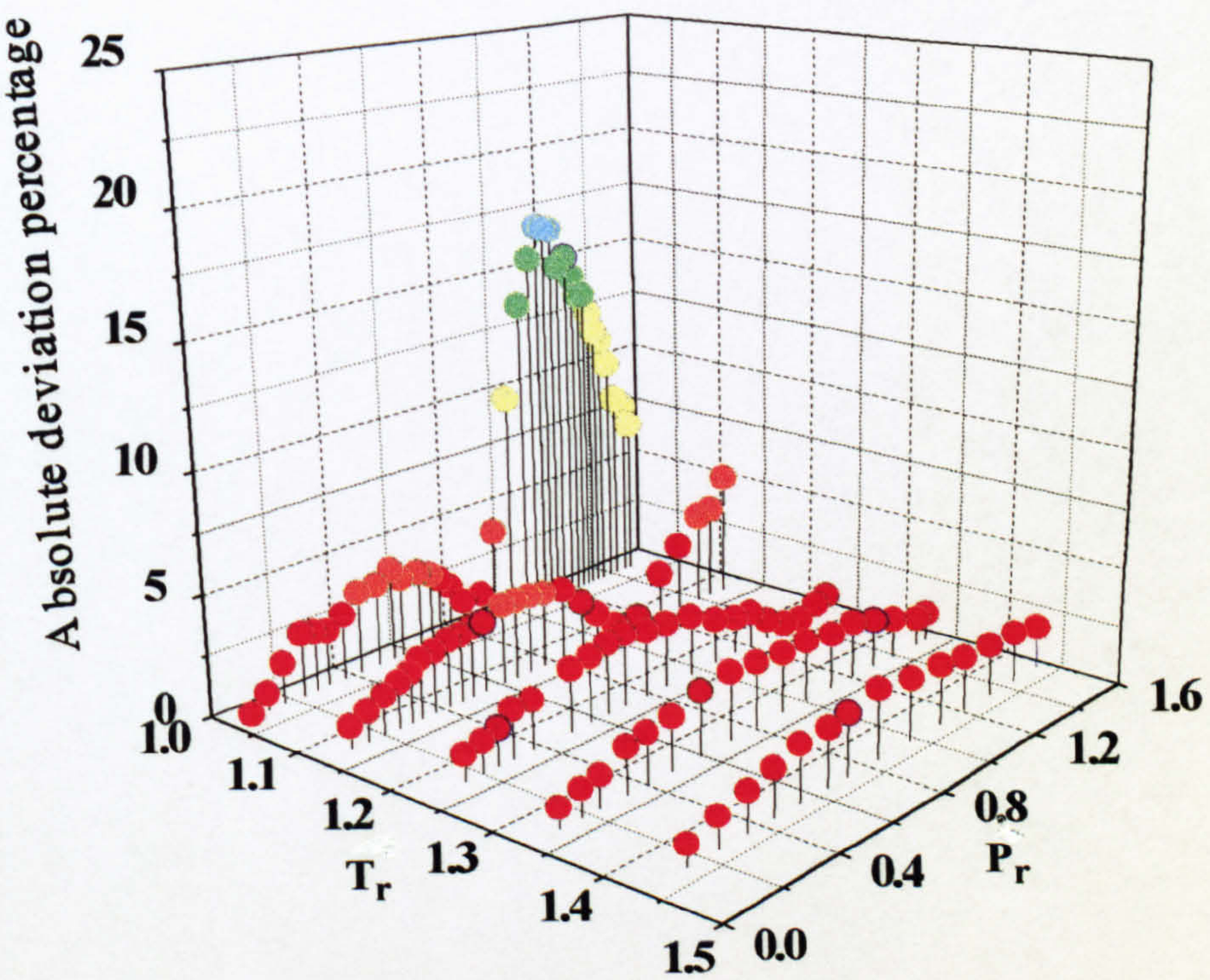

Figure 5.4.a Absolute percentage deviation between measured and predicted vapour speed of sound based on TCC CEOS against T_r and P_r for a hydrocarbon mixture containing 68.5 mole % C_1 and 31.5 mole % C_2 (table 5.4).

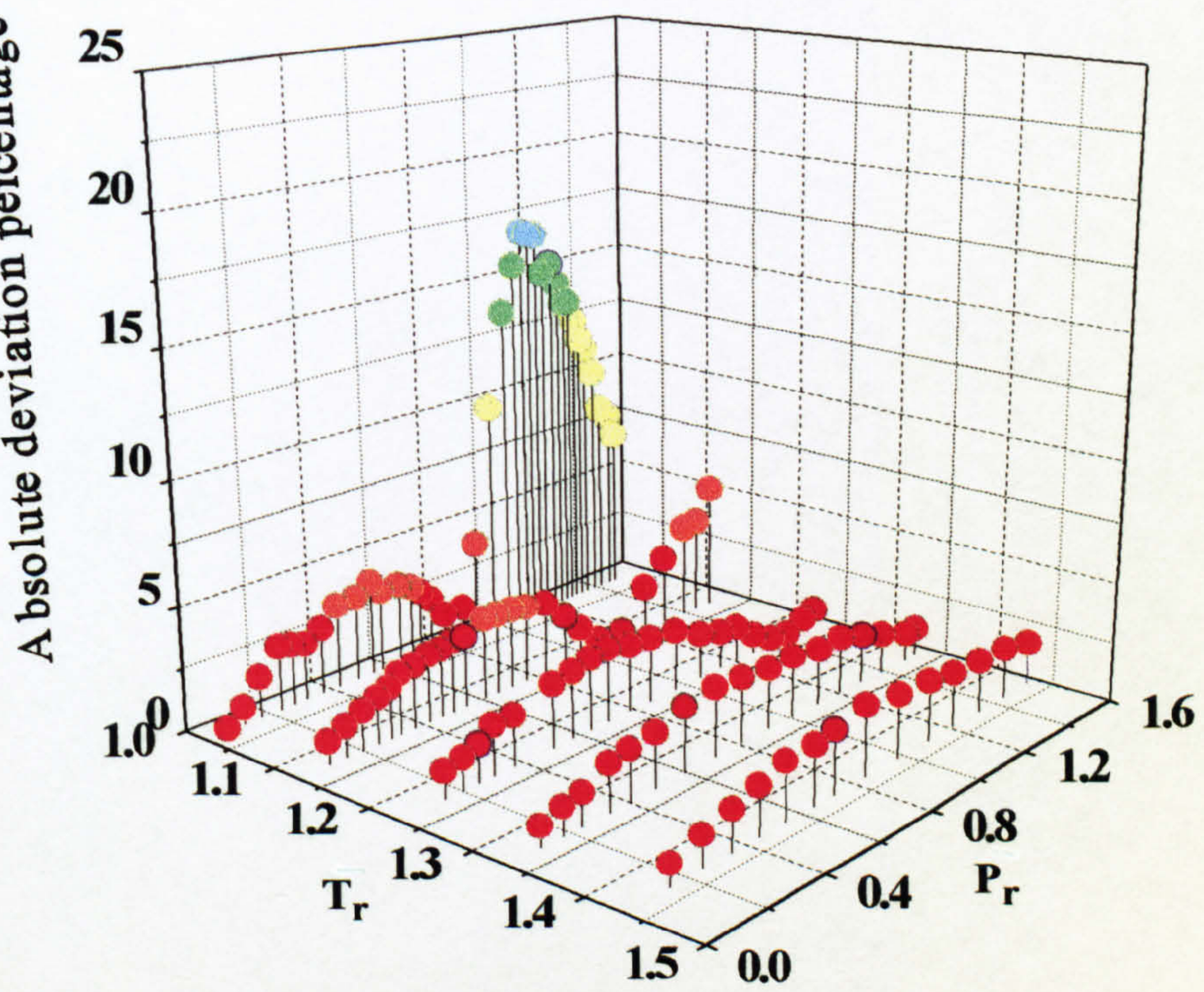

Figure 5.4.b Absolute percentage deviation between measured and predicted vapour speed of sound based on PR CEOS against T_r and P_r for a hydrocarbon mixture containing 68.5 mole % C_1 and 31.5 mole % C_2 (table 5.4).

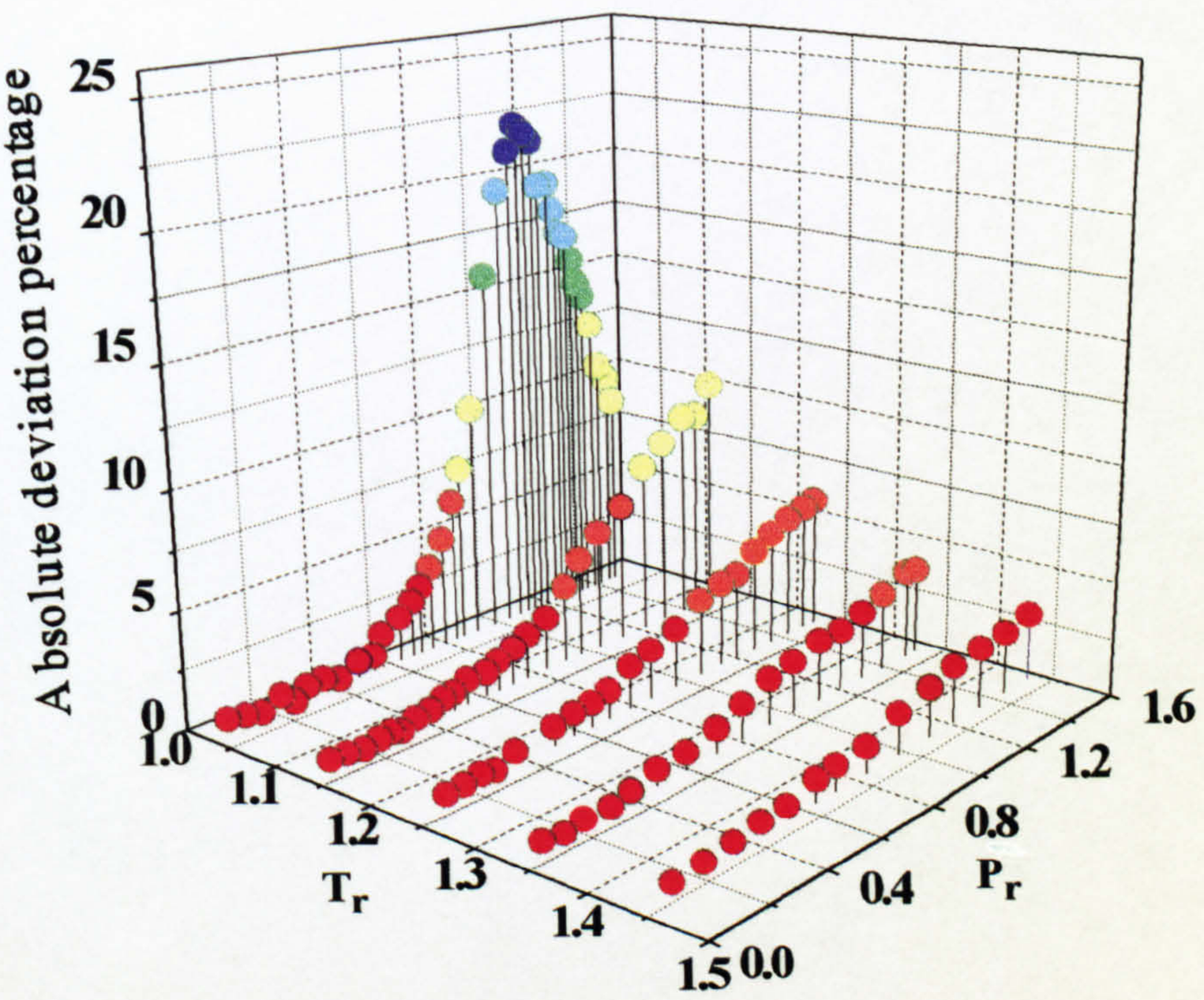

Figure 5.4.c Absolute percentage deviation between measured and predicted vapour speed of sound based on SRK CEOS against T_r and P_r for a hydrocarbon mixture containing 68.5 mole % C_1 and 31.5 mole % C_2(table 5.4).

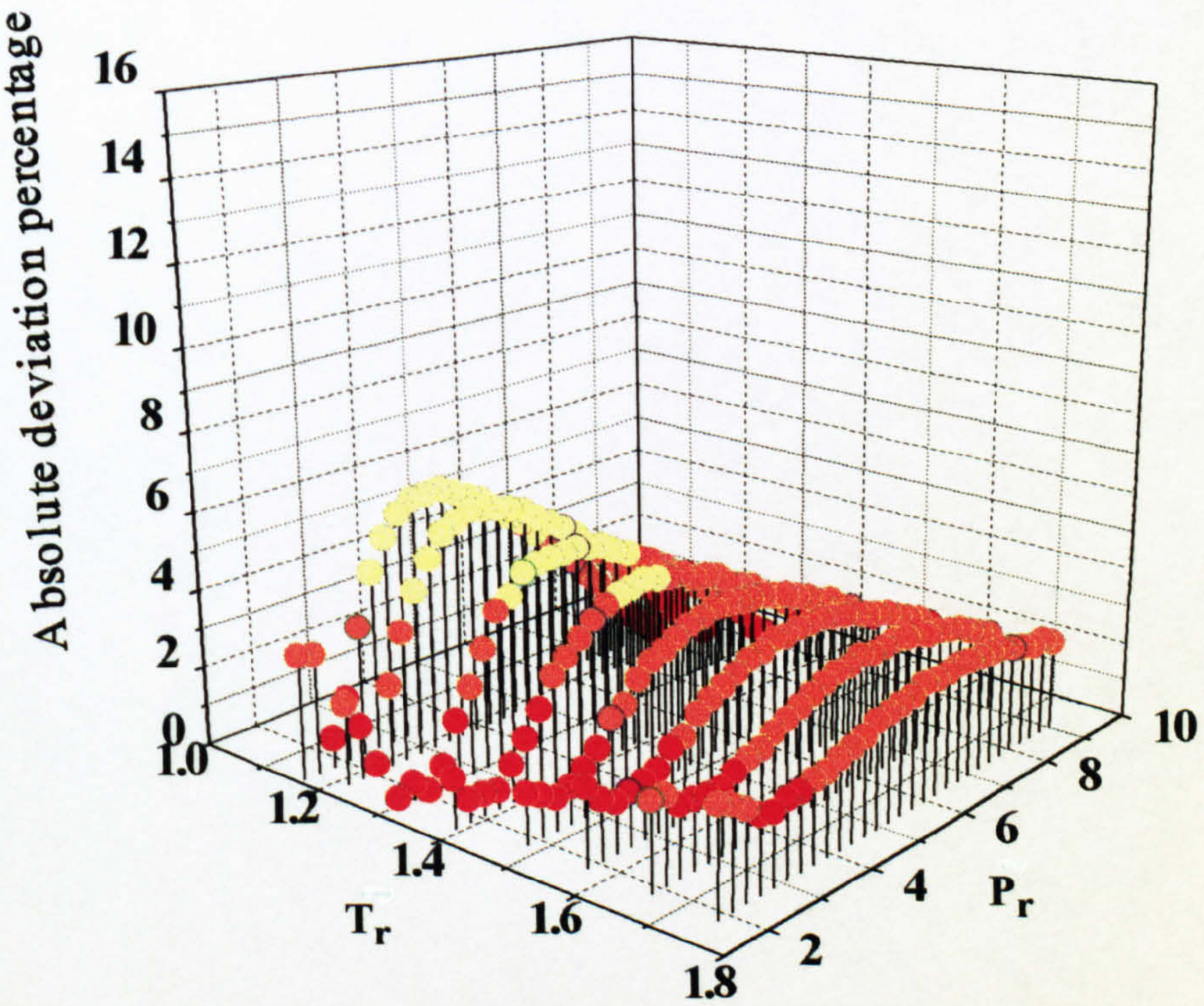

Figure 5.5.a Absolute percentage deviation between measured and predicted vapour speed of sound based on TCC CEOS against T_r and P_r for a hydrocarbon mixture containing 90.0 mole % C_1 and 10.0 mole % n-C_3 (table 5.4).

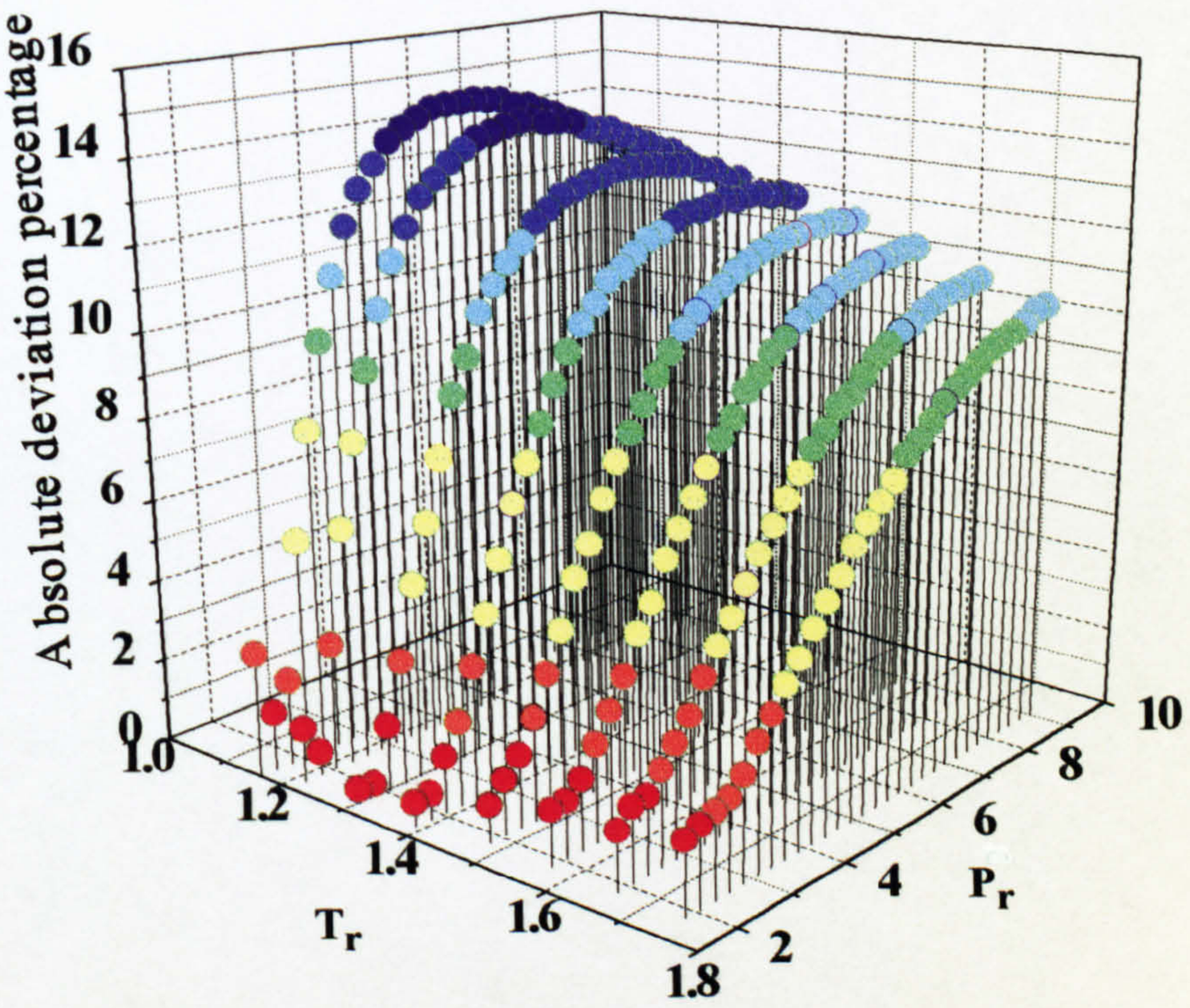

Figure 5.5.b Absolute percentage deviation between measured and predicted vapour speed of sound based on PR CEOS against T_r and P_r for a hydrocarbon mixture containing 90.0 mole % C_1 and 10.0 mole % n-C_3 (table 5.4).

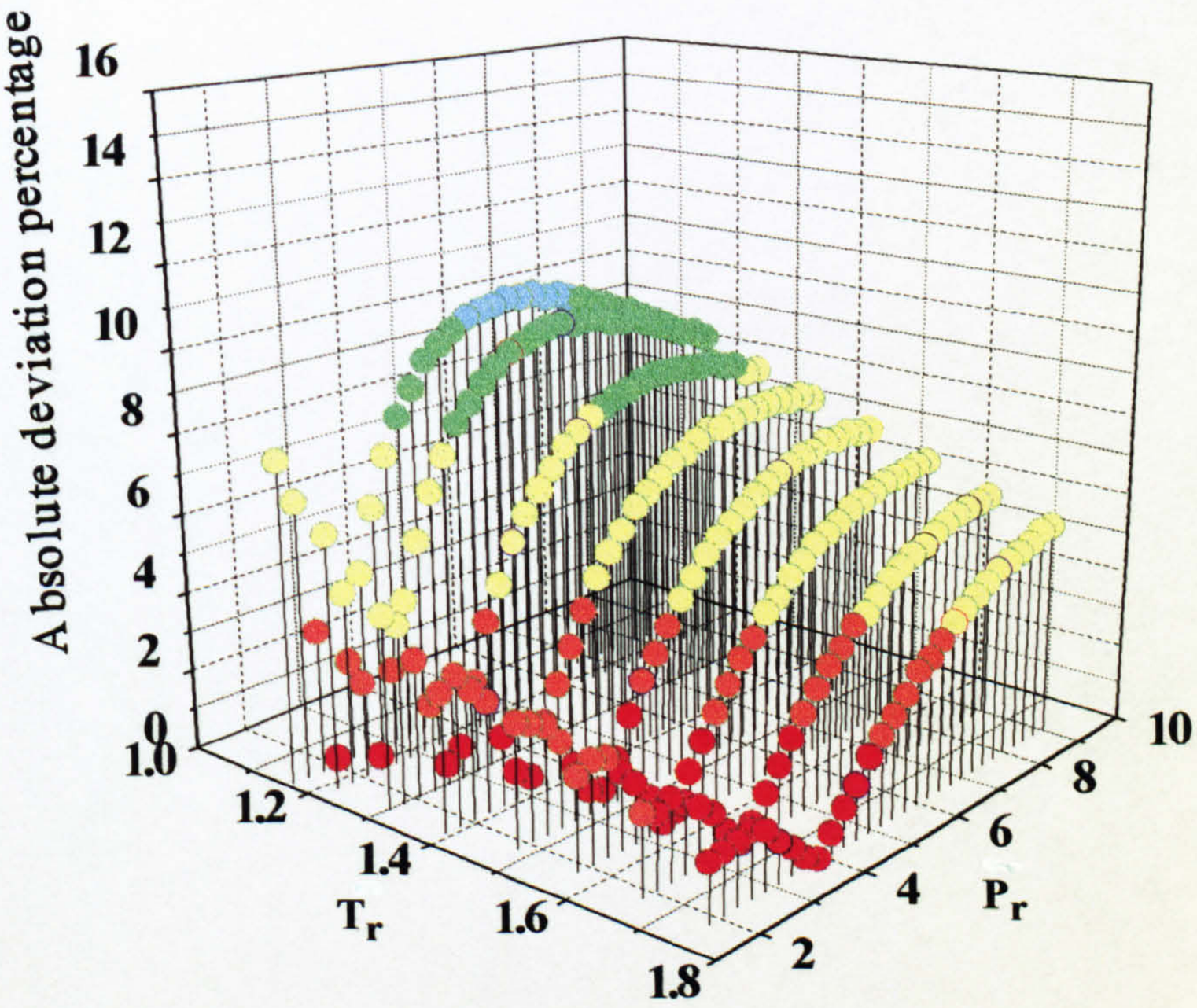

Figure 5.5.c Absolute percentage deviation between measured and predicted vapour speed of sound based on SRK CEOS against T_r and P_r for a hydrocarbon mixture containing 90.0 mole % C_1 and 10.0 mole % n-C_3 (table 5.4).

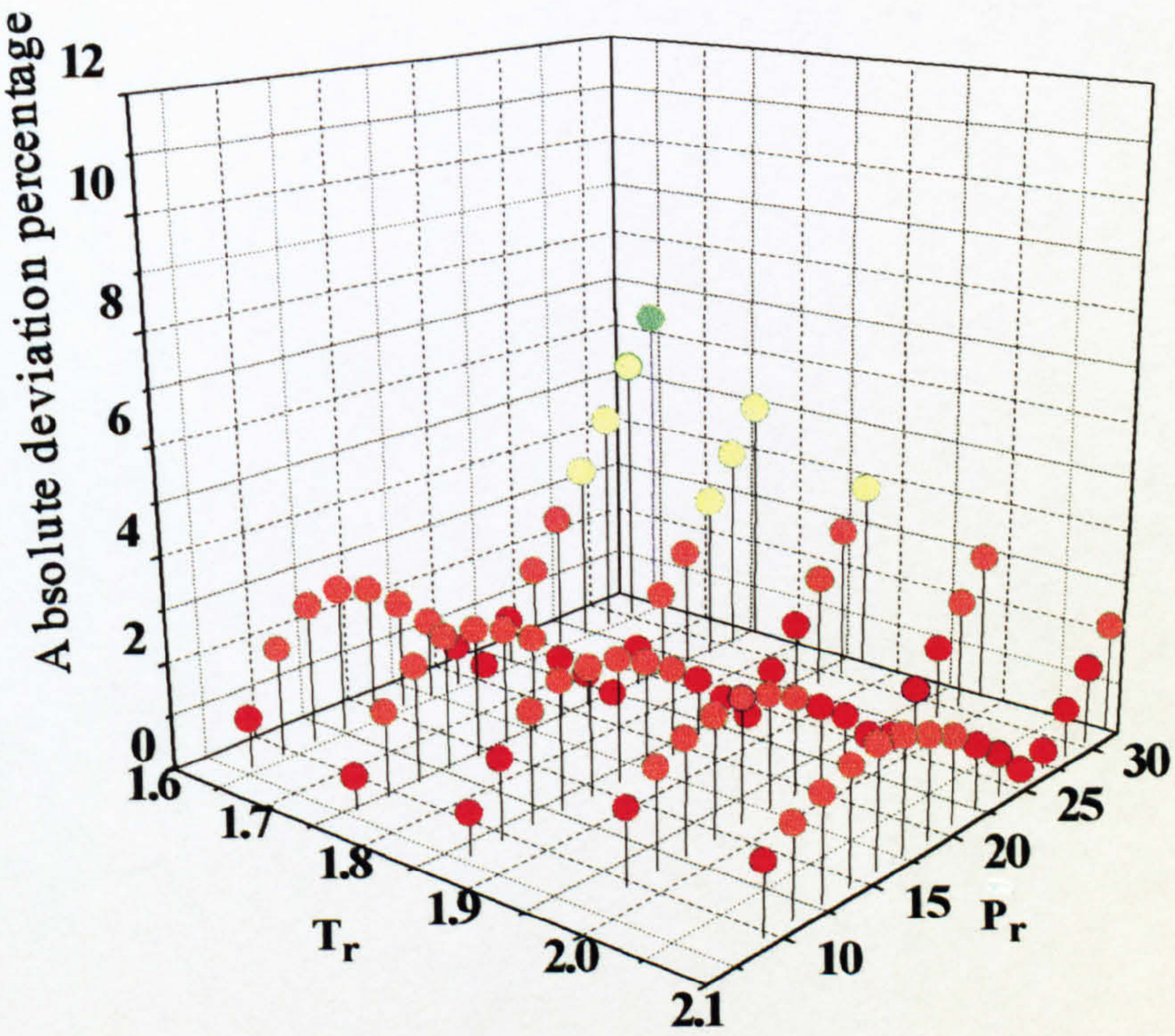

Figure 5.6.a Absolute percentage deviation between measured and predicted vapour speed of sound based on TCC CEOS against T_r and P_r for a hydrocarbon mixture containing 98.0 mole % C_1 and 2.0 mole % n-C_8 (table 5.4).

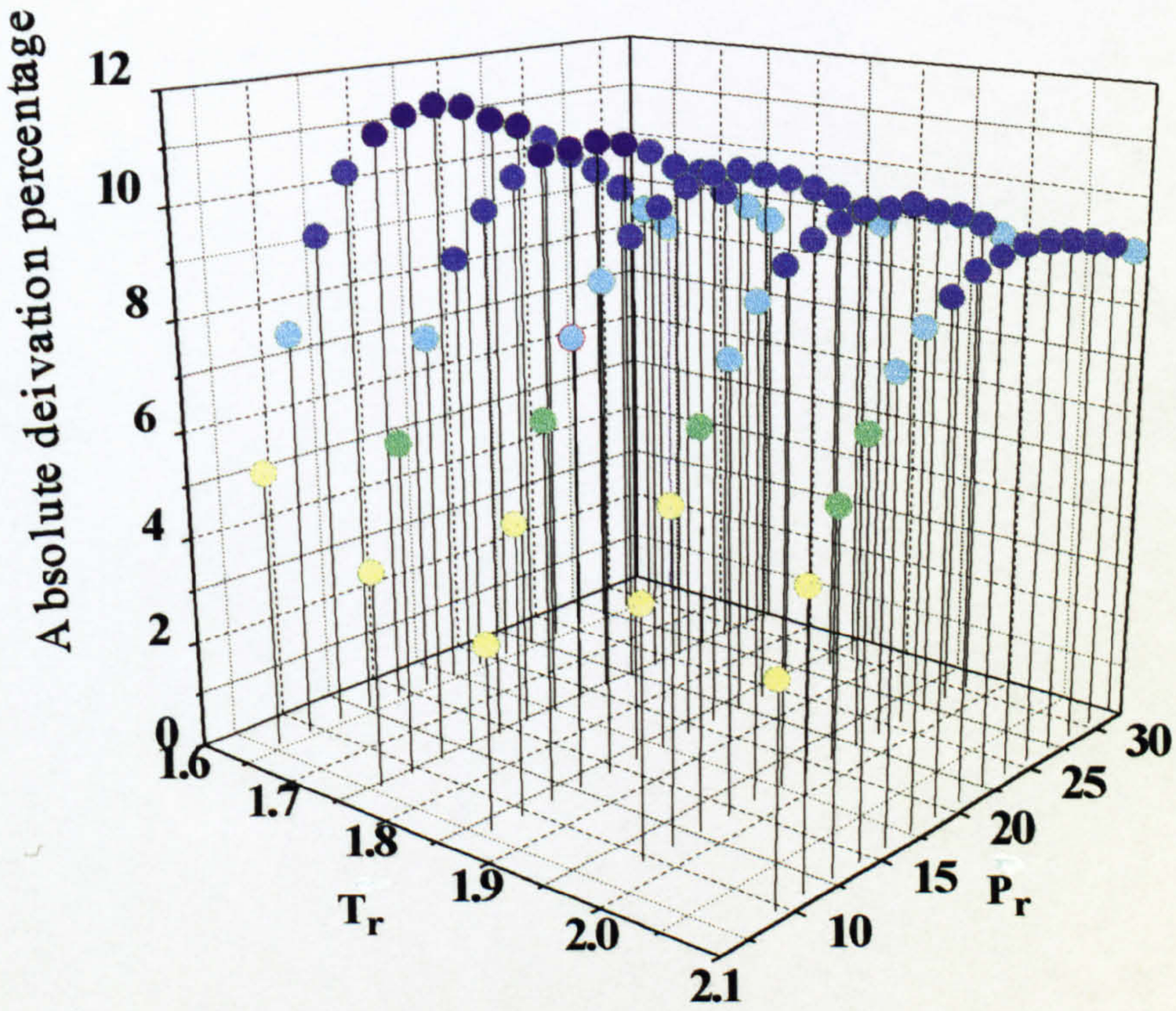

Figure 5.6.b Absolute percentage deviation between measured and predicted vapour speed of sound based on PR CEOS against T_r and P_r for a hydrocarbon mixture containing 98.0 mole % C_1 and 2.0 mole % n-C_8 (table 5.4).

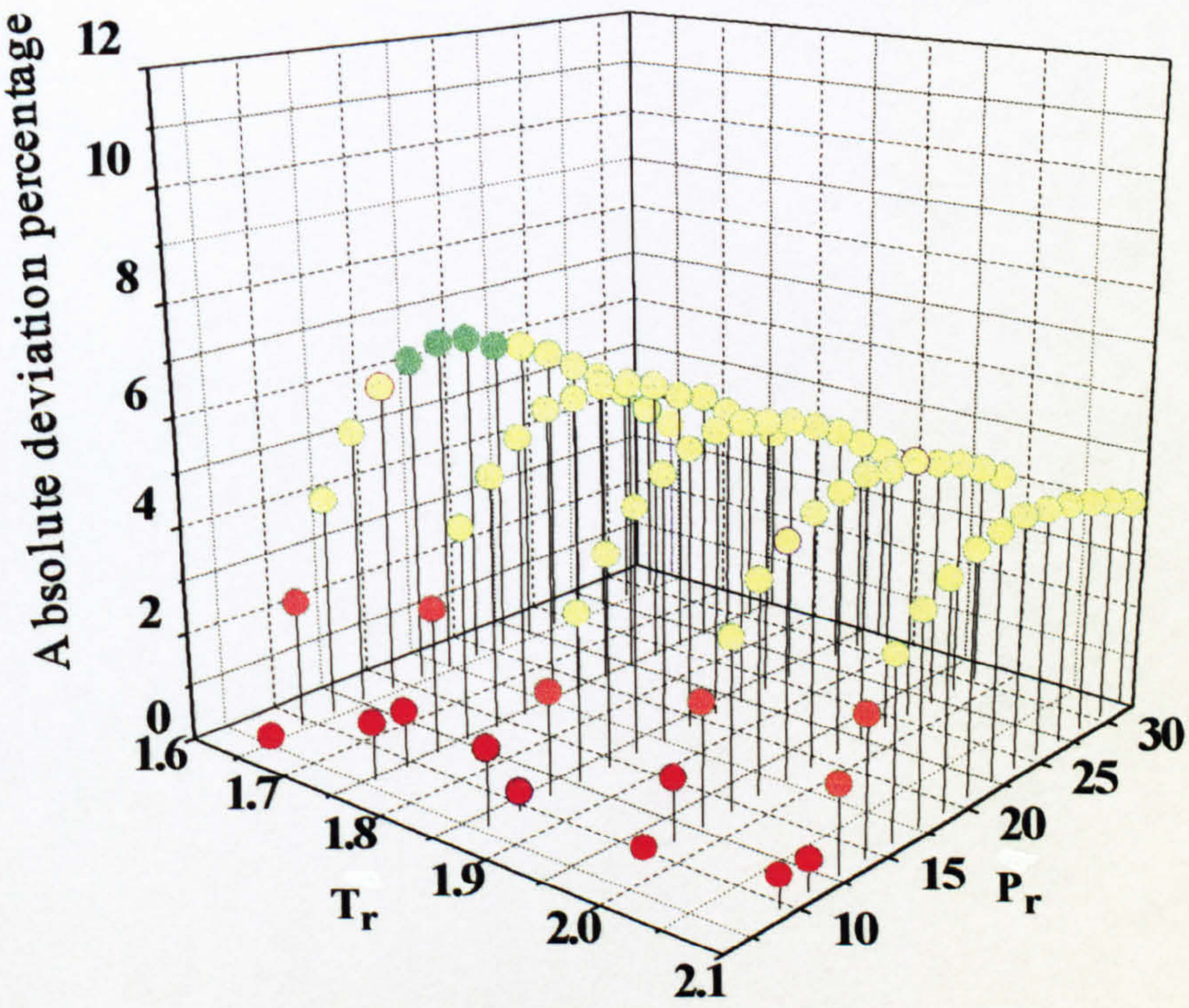

Figure 5.6.c Absolute percentage deviation between measured and predicted vapour speed of sound based on SRK CEOS against T_r and P_r for a hydrocarbon mixture containing 98.0 mole % C_1 and 2.0 mole % n-C_8 (table 5.4).

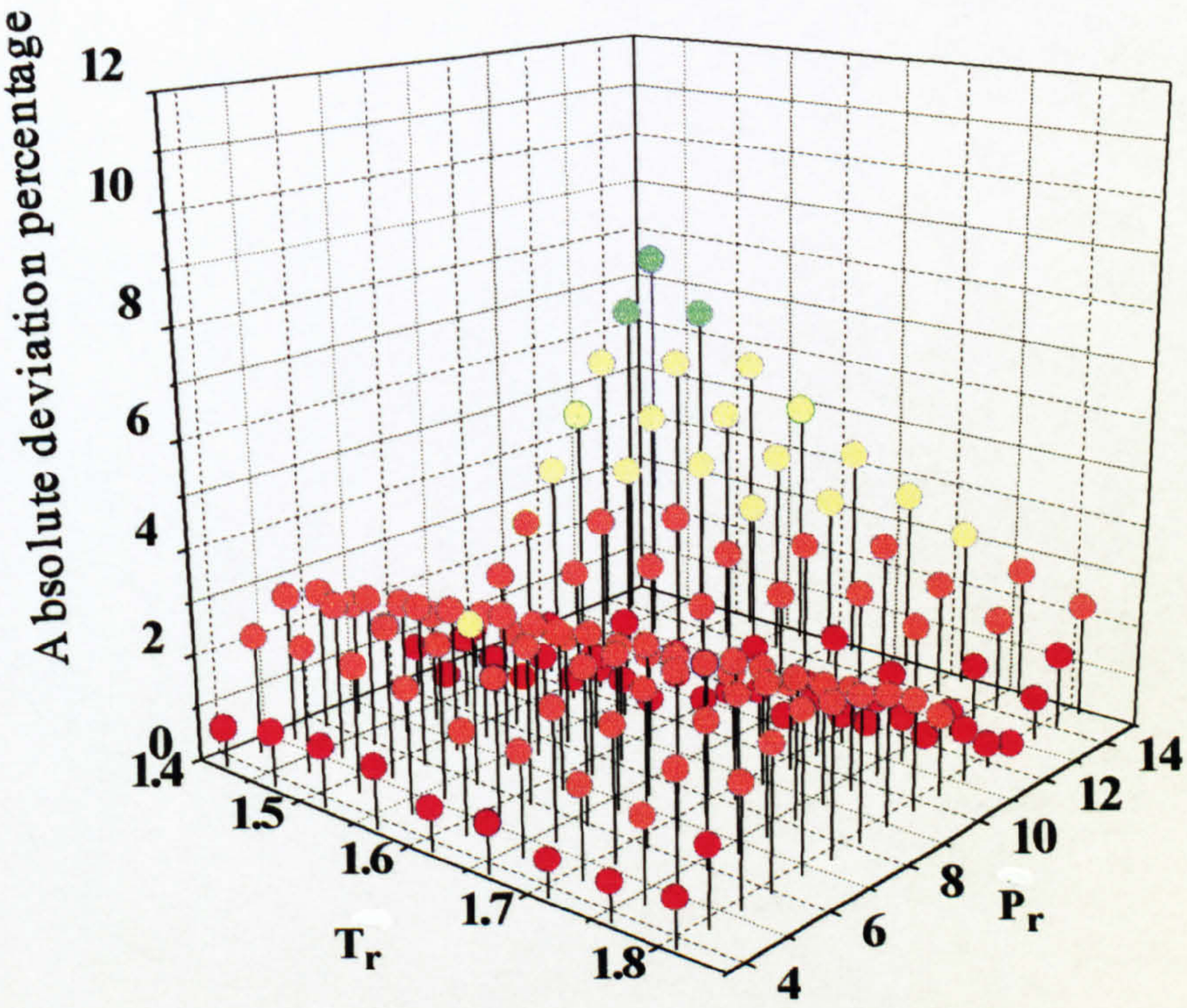

Figure 5.7.a Absolute percentage deviation between measured and predicted vapour speed of sound based on TCC CEOS against T_r and P_r for a hydrocarbon mixture containing 88.0 mole % C_1, 10.0 mole % n-C_3, and 2.0 mole % n-C_8(table 5.4).

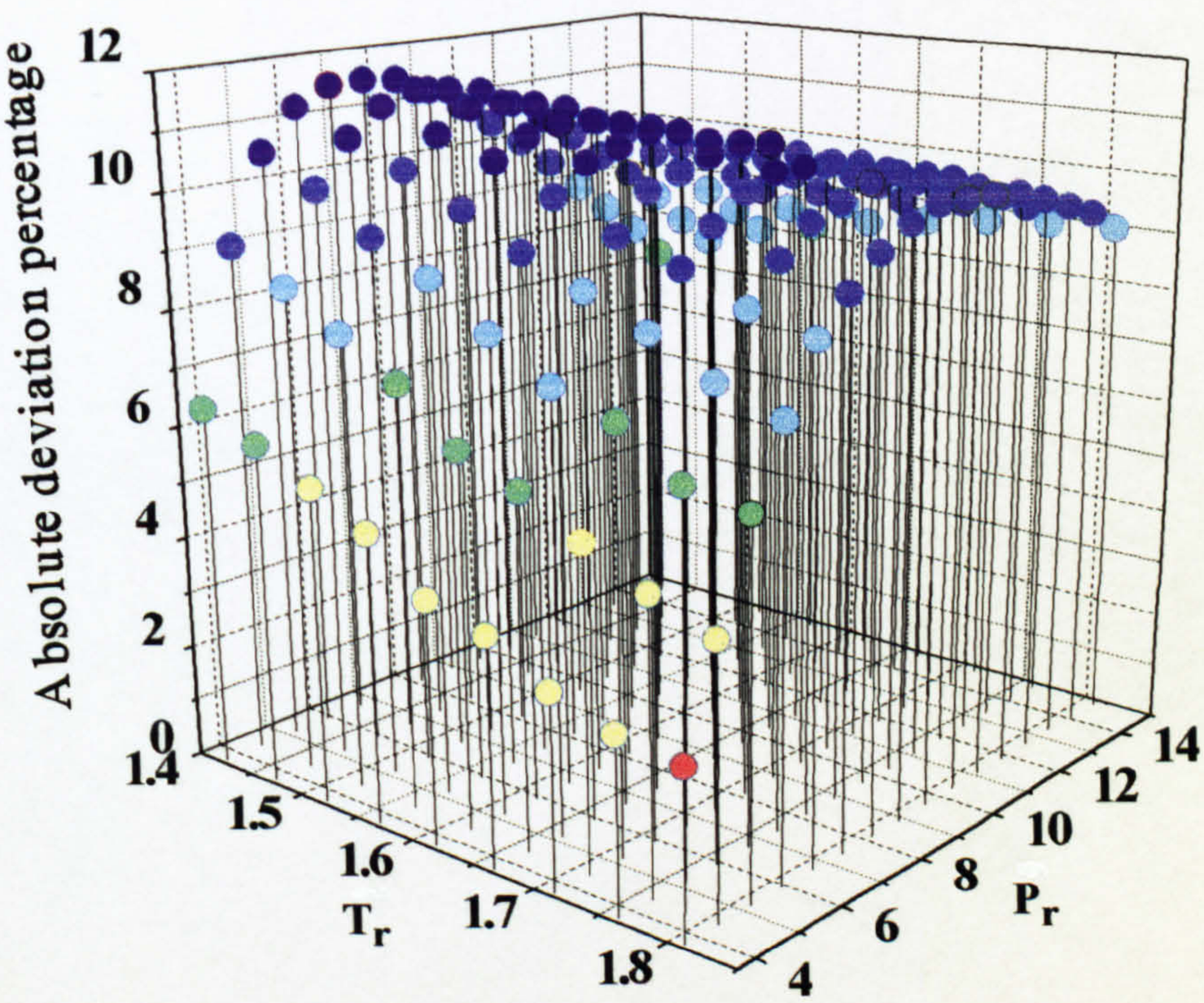

Figure 5.7.b Absolute percentage deviation between measured and predicted vapour speed of sound based on PR CEOS against T_r and P_r for a hydrocarbon mixture containing 88.0 mole % C_1, 10.0 mole % n-C_3, and 2.0 mole % n-C_8 (table 5.4).

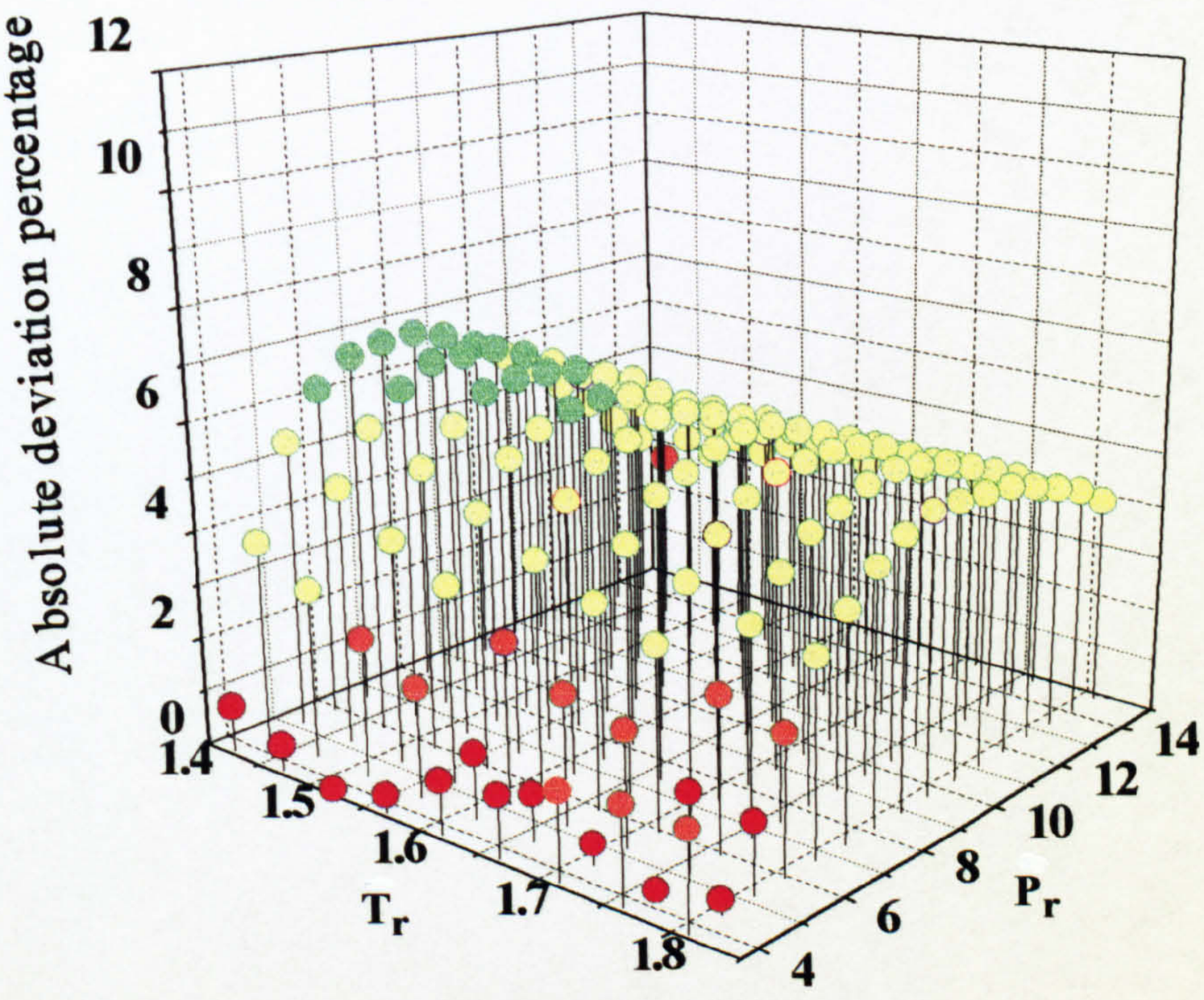

Figure 5.7.c Absolute percentage deviation between measured and predicted vapour speed of sound based on SRK CEOS against T_r and P_r for a hydrocarbon mixture containing 88.0 mole % C_1, 10.0 mole % n-C_3, and 2.0 mole % n-C_8 (table 5.4).

5.4.4 Absolute Percentage Deviation as a Function of T_r and P_r for Compressed Liquid

Figures 5.8.a - c show the variations of absolute deviation percentage between measured and predicted speed of sound with T_r and P_r for compressed liquid C_2 based on TCC, PR and SRK CEOS respectively. Similar plots for compressed liquid n-C_4 and the liquid hydrocarbon mixture containing C_1, n-C_3 and n-C_8 (see table 5.4) are given in figures 5.9 and 5.10 respectively.

As the performance of the CEOS for compressed C_2 as shown in figures 5.8 a - c are very similar to that for compressed C_1, the corresponding data are not shown here in order to avoid congestion. Referring to the figures, relatively large deviations (up to 60%) between theory and experiment are apparent based on TCC CEOS at $T_r \leq 0.6$ compared with those based on the other CEOS. However, at $T_r > 0.6$, predictions based on TCC CEOS are generally about 50% better than those based on the other CEOS. The performance of the various CEOS appears to be relatively insensitive to the ranges of P_r tested.

Similar trends in terms of performance for the three CEOS in predicting the speed of sound as a function of T_r and P_r are observed in conjunction with compressed liquid n-C_3 and n-C_4. Figures 5.9.a - c show the data for the latter. Once again, the TCC CEOS performs poorly at $T_r \leq 0.6$. However, this time the superior performance of the same equation at $T_r > 0.6$ is more evident. Also, the absolute percentage deviation is a marked function of P_r although no obvious trends are evident. The results of similar analysis indicate that the weakness of TCC CEOS in predicting accurate values of speed of sound at low T_r (usually below 0.6) applies to other compressed liquid alkanes (n-C_5 - n-C_9), however, the effect becomes less significant with increasing carbon number. While for conditions corresponding to $T_r > 0.6$, all three CEOS give similar performance for the other compressed liquid alkanes (n-C_5 - n-C_9).

The performance of various CEOS in predicting speed of sound for a compressed liquid hydrocarbon mixture of C_1, n-C_3 and n-C_8 are given in figures 5.10.a - c. Although the AAD % in table 5.6 indicates both TCC and SRK CEOS perform equally well, figures 5.10.a - c indicate that TCC CEOS gives very accurate predictions at $P_r \leq 4$ compared with other CEOS while SRK CEOS gives better performance at $P_r > 4$.

The CEOS performance in terms of predicting speed of sound is mainly dictated by its accuracy in estimating molar volume and $\left(\frac{\partial P}{\partial v}\right)_T$ (see equation 5.2.48). In order to investigate the reason for the poor performance of TCC CEOS at low T_r, the variations of $\left(\frac{\partial P}{\partial v}\right)_T$ with T_r on the basis of the three CEOS for all compressed liquid alkanes are plotted. Figure 5.11 shows the corresponding data for C_2. The figure indicates that values of $\left(\frac{\partial P}{\partial v}\right)_T$ predicted from TCC CEOS are too large at $T_r \leq$ ca 0.6 when compared with those calculated from the other CEOS. Similar trends are observed in conjunction with the other pure liquid alkanes. In table 5.10, the AAD% for the various CEOS in predicting compressed liquid densities for C_1 and C_2 are shown. The data for the two liquid alkanes are used as the densities for other alkanes in table 5.4 are not available. The claimed uncertainties for measured densities of compressed liquid C_1 and C_2 are within ± 0.1% and ± 0.2% respectively.

It is notable that TCC CEOS performs well at all ranges of T_r tested including $T_r \leq$ ca 0.6. Its poor performance in predicting the speed of sound in this region is therefore not due to its limitations in predicting fluid density. It is also interesting to note that according to the same table, SRK CEOS provides reasonably accurate predictions at $T_r \leq$ ca 0.6 whilst PR CEOS provides the worst performance compared to the other CEOS at the ranges of T_r tested.

Hence, the poor performance of TCC CEOS in predicting speed of sound at low reduced temperatures (ca. ≤ 0.6) for C_1 and C_2 is mainly because the predicted values

of $\left(\frac{\partial P}{\partial v}\right)_T$ are too large when compared with the corresponding values calculated from the other CEOS. This is also very likely to be the main source of error attributed to poor performance of TCC CEOS at low T_r in conjunction with other liquid alkanes.

Table 5.10 AAD% between measured (see table 5.4) and predicted densities based on TCC, PR and SRK CEOS for compressed liquid C_1 and C_2

Fluid	T_r range	TCC	PR	SRK
C1	0.52 - 0.63	1.31	12.51	0.27
	0.79 - 1.57	1.20	6.00	4.12
C2	0.33 - 0.59	2.37	7.59	3.99
	0.65 - 1.06	2.75	6.03	7.10

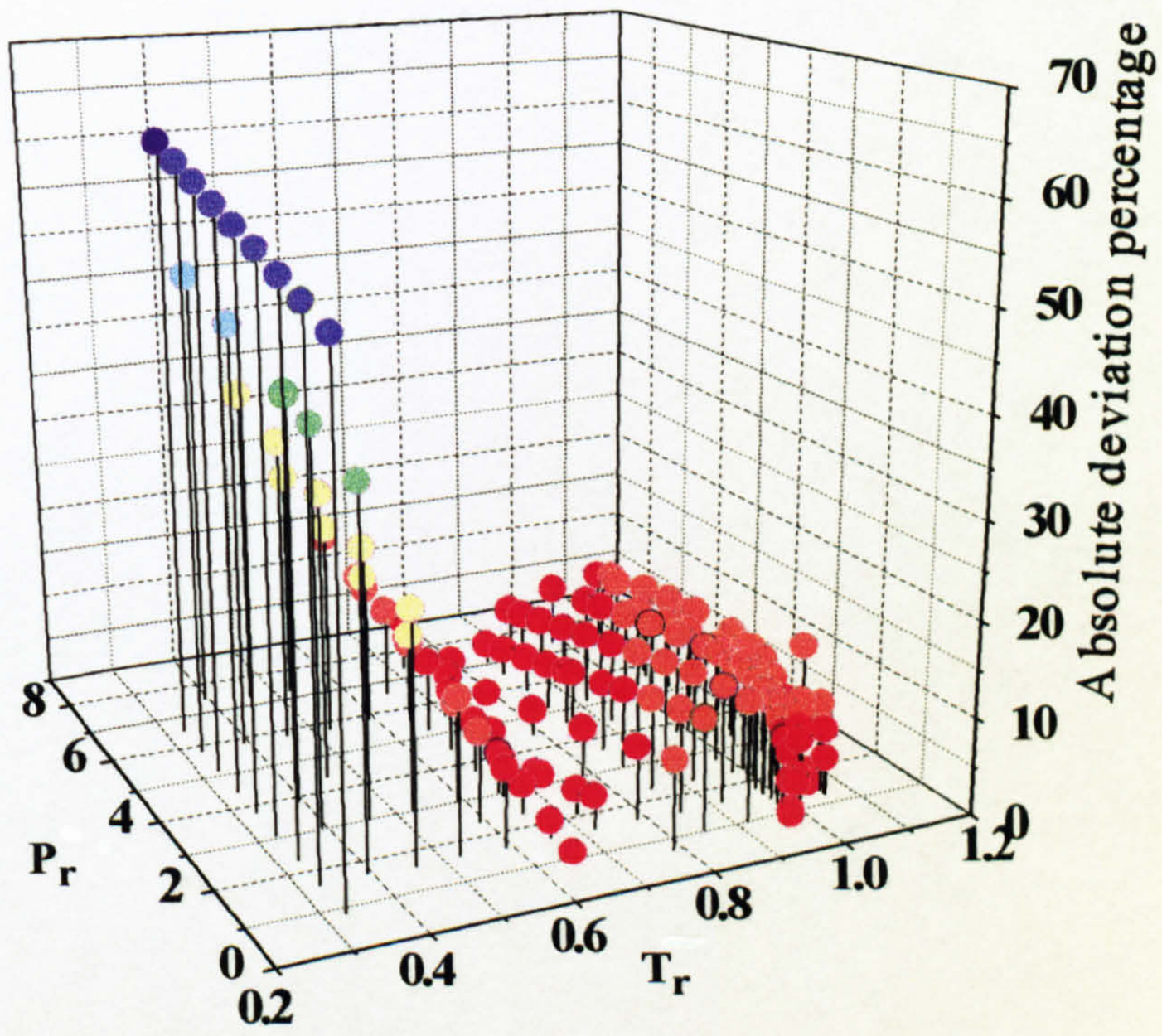

Figure 5.8.a Absolute percentage deviation between measured and predicted liquid speed of sound based on TCC CEOS against T_r and P_r for compressed liquid C_2.

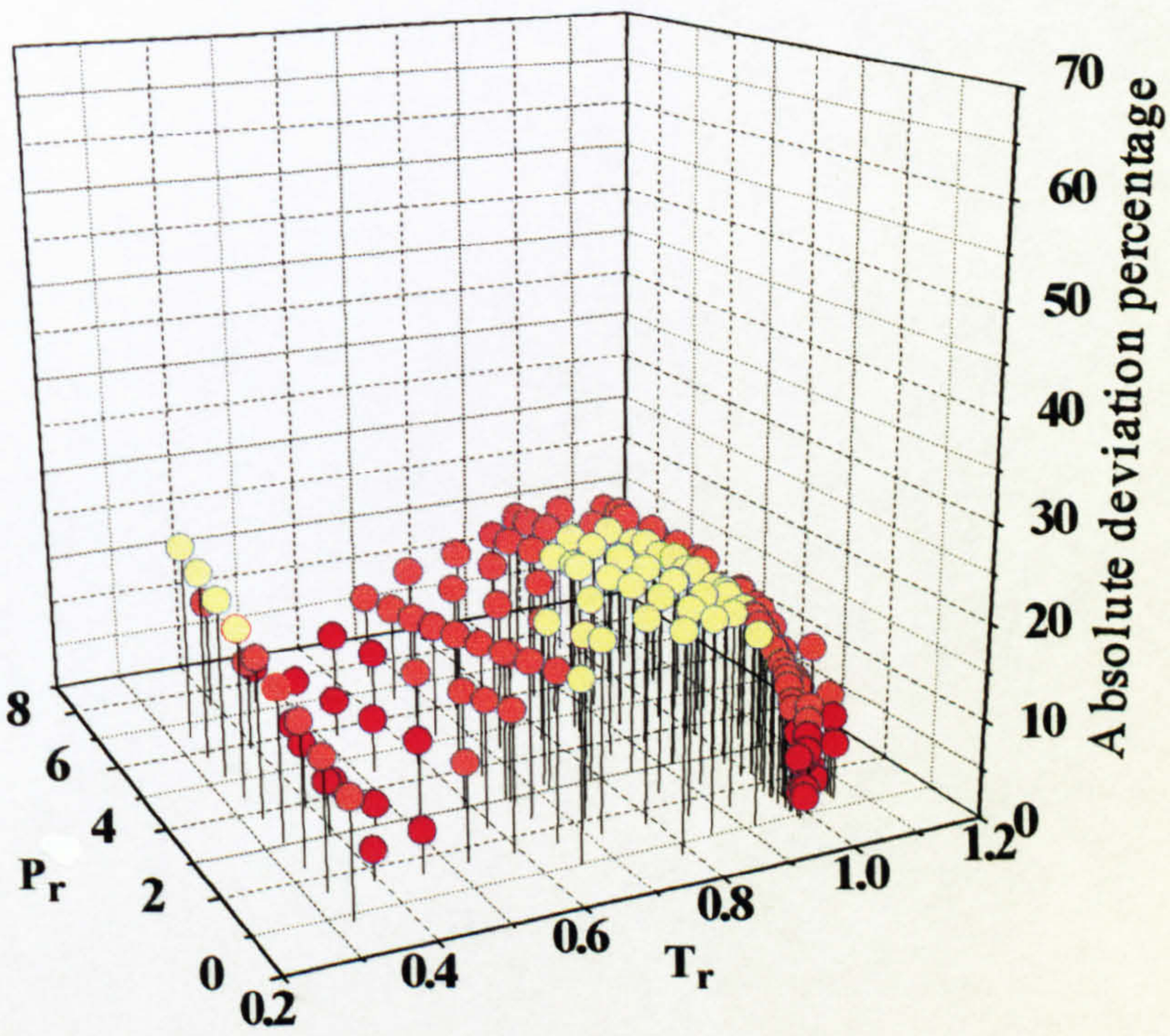

Figure 5.8.b Absolute percentage deviation between measured and predicted liquid speed of sound based on PR CEOS against T_r and P_r for compressed liquid C_2.

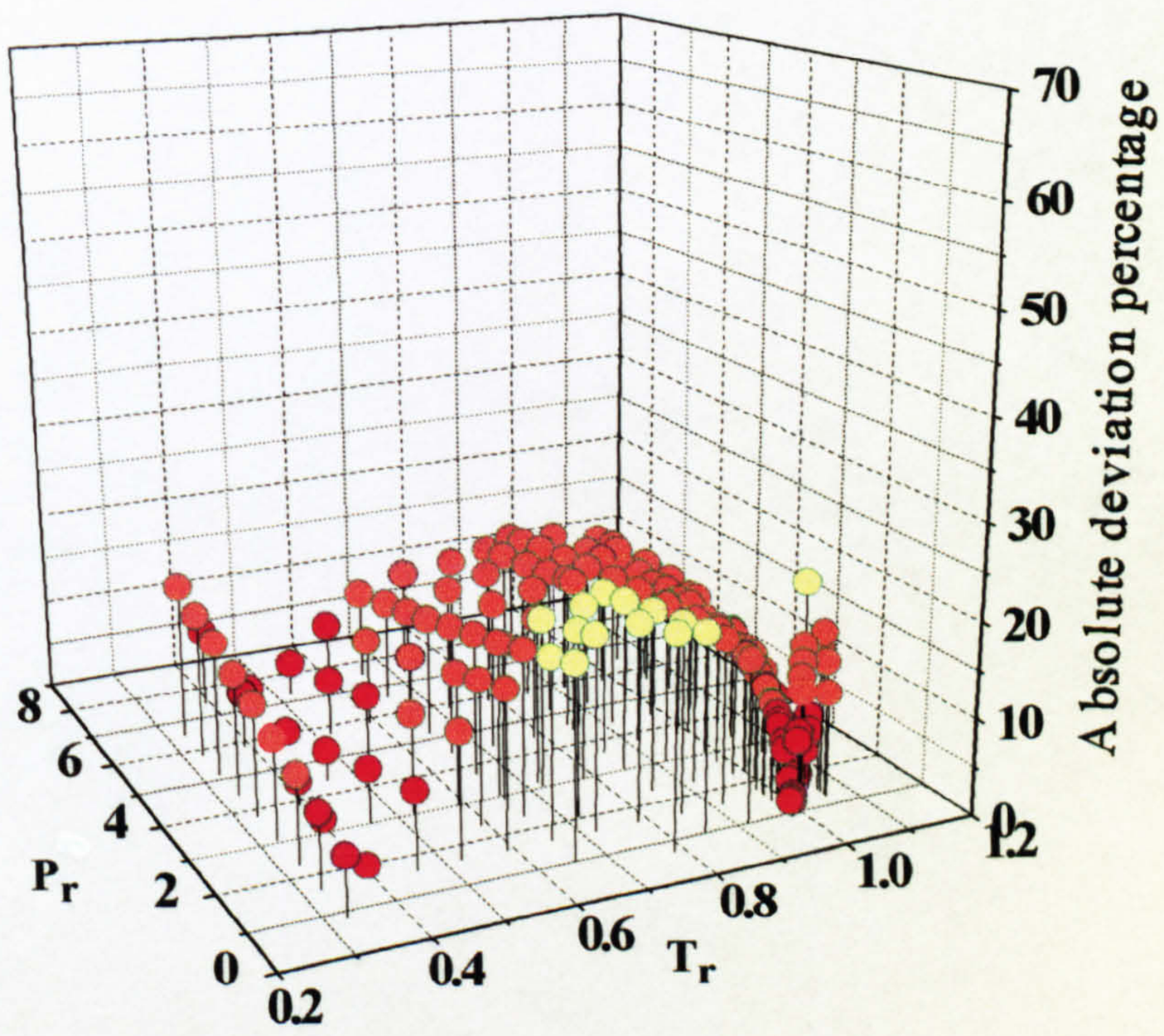

Figure 5.8. c Absolute percentage deviation between measured and predicted liquid speed of sound based on SRK CEOS against T_r and P_r for compressed liquid C_2.

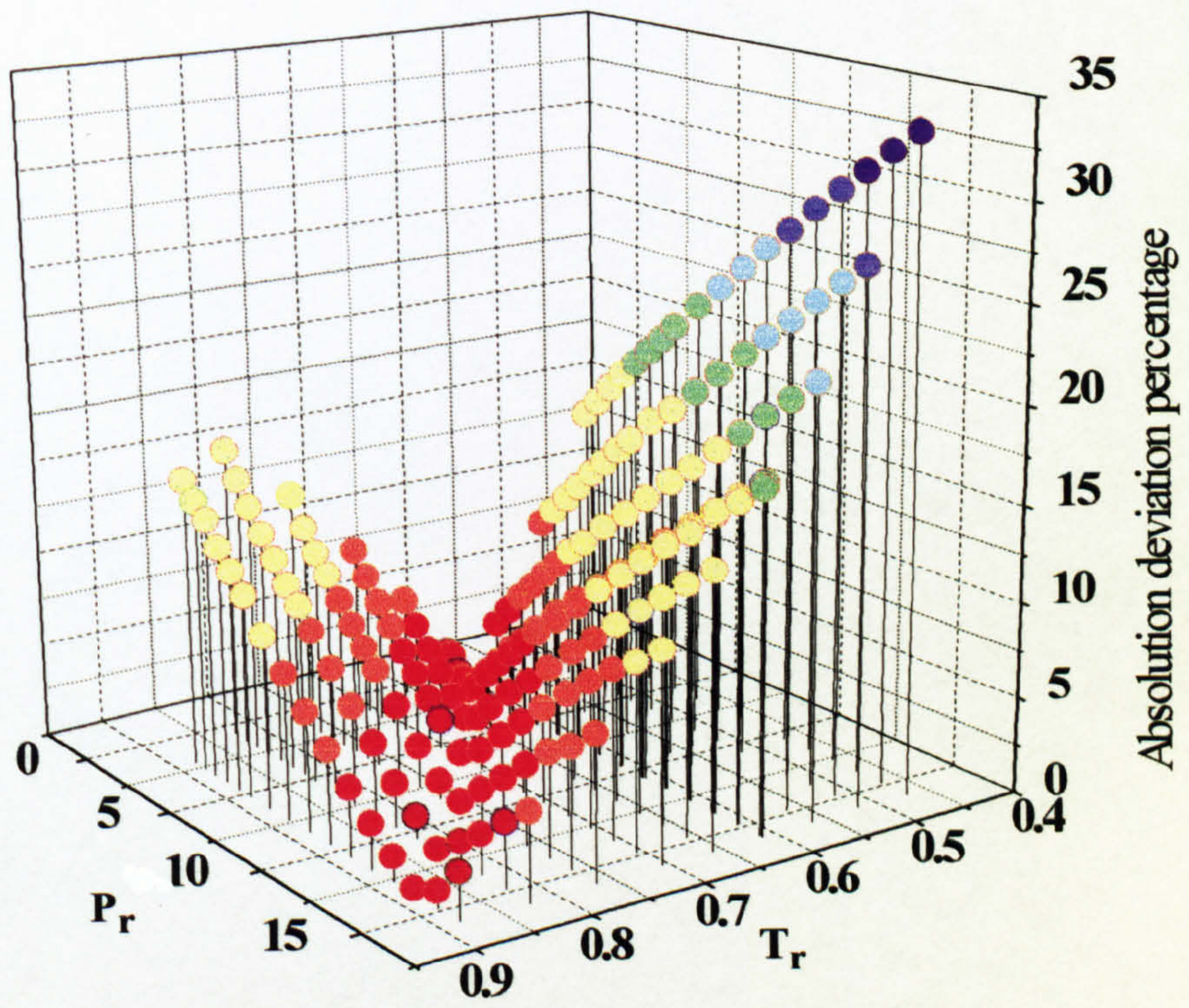

Figure 5.9.a Absolute percentage deviation between measured and predicted liquid speed of sound based on TCC CEOS against T_r and P_r for compressed liquid n-C_4.

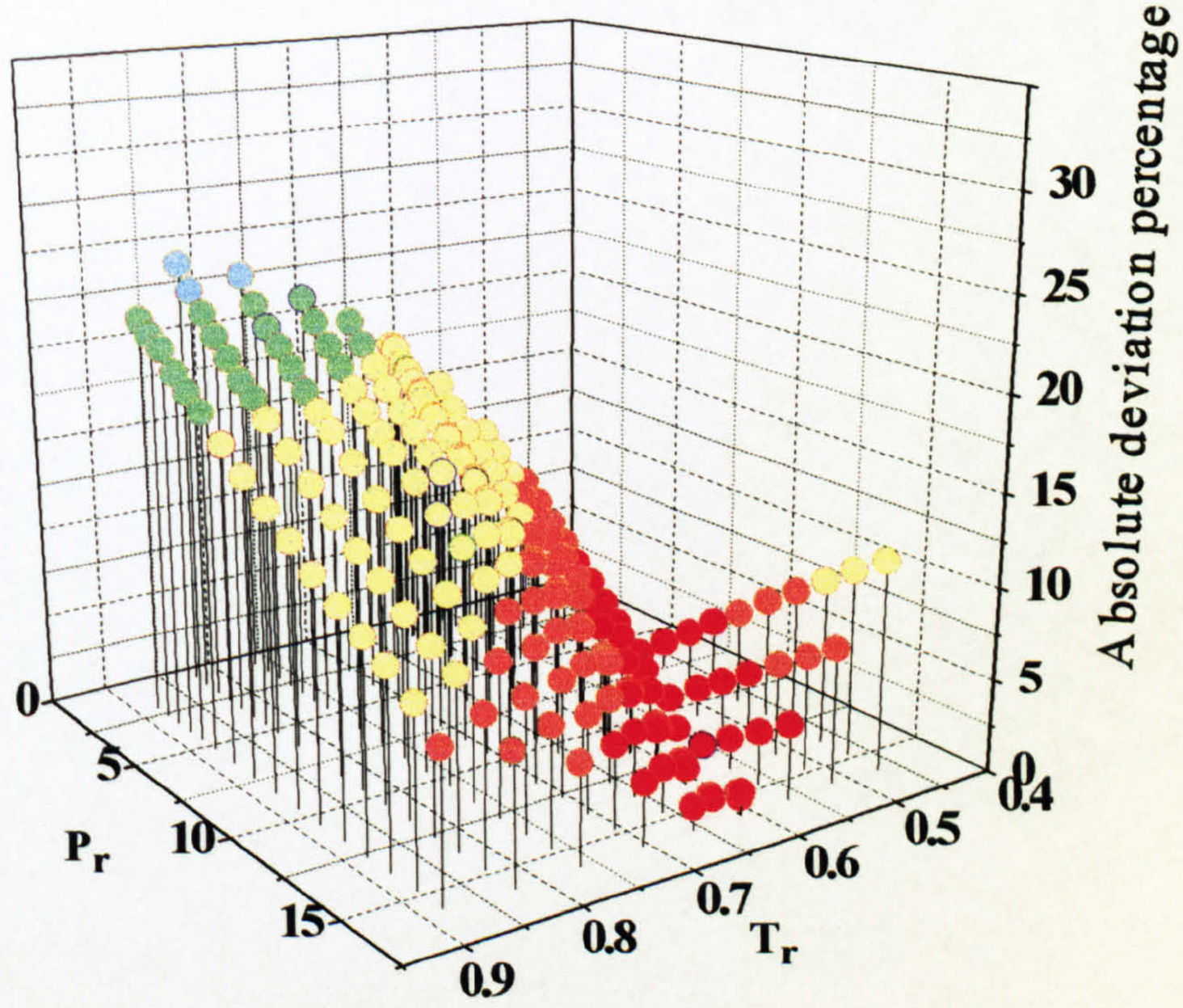

Figure 5.9.b Absolute percentage deviation between measured and predicted liquid speed of sound based on PR CEOS against T_r and P_r for compressed liquid n-C_4.

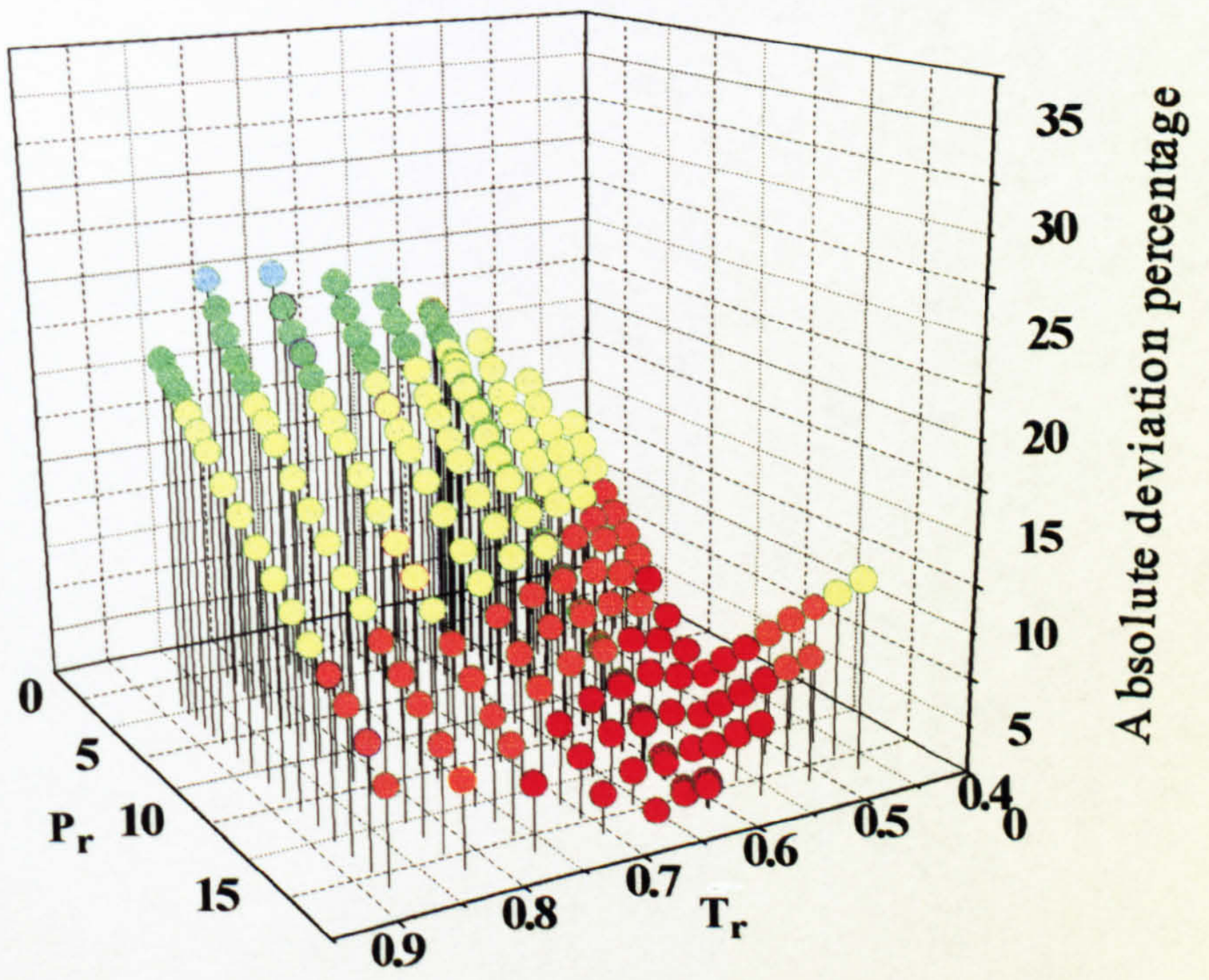

Figure 5.9.c Absolute percentage deviation between measured and predicted liquid speed of sound based on SRK CEOS against T_r and P_r for compressed liquid n-C_4.

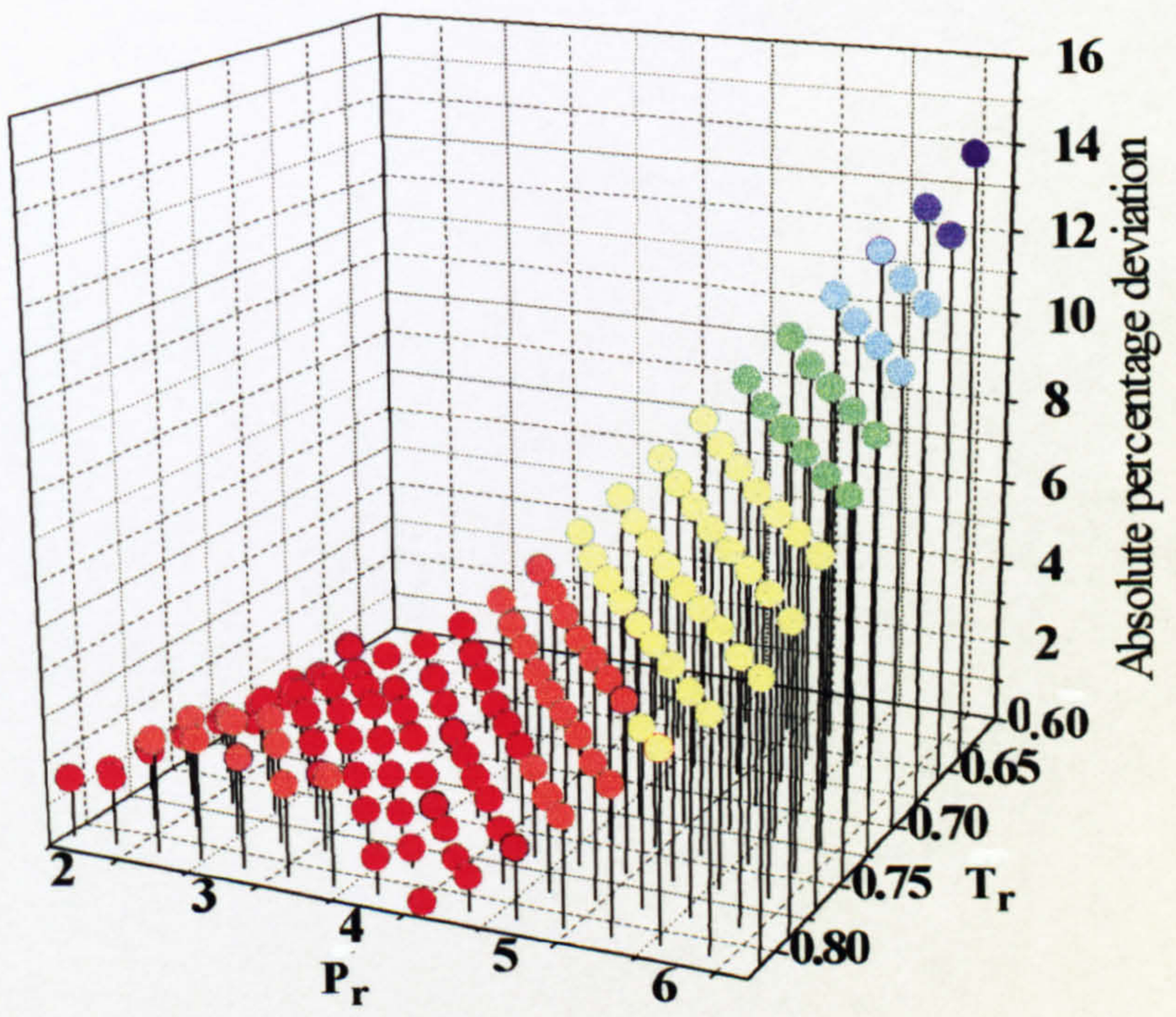

Figure 5.10.a Absolute percentage deviation between measured and predicted liquid speed of sound based on TCC CEOS against T_r and P_r for a hydrocarbon mixture containing 61.7 mole % C_1, 14.5 mole % n-C_3, and 23.8 mole % n-C_8 (table 5.4).

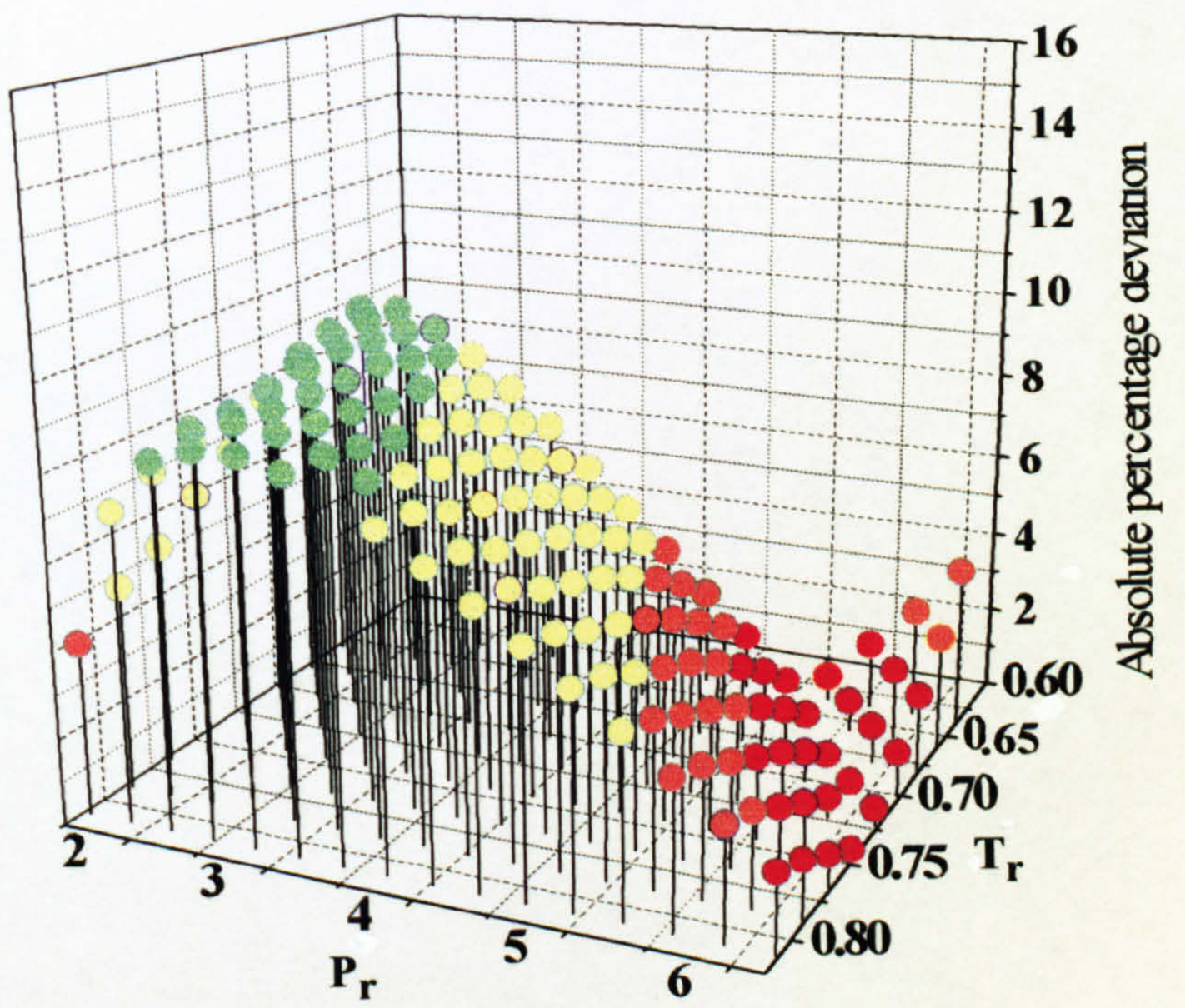

Figure 5.10.b Absolute percentage deviation between measured and predicted liquid speed of sound based on PR CEOS against T_r and P_r for a hydrocarbon mixture containing 61.7 mole % C_1, 14.5 mole % n-C_3, and 23.8 mole % n-C_8 (table 5.4).

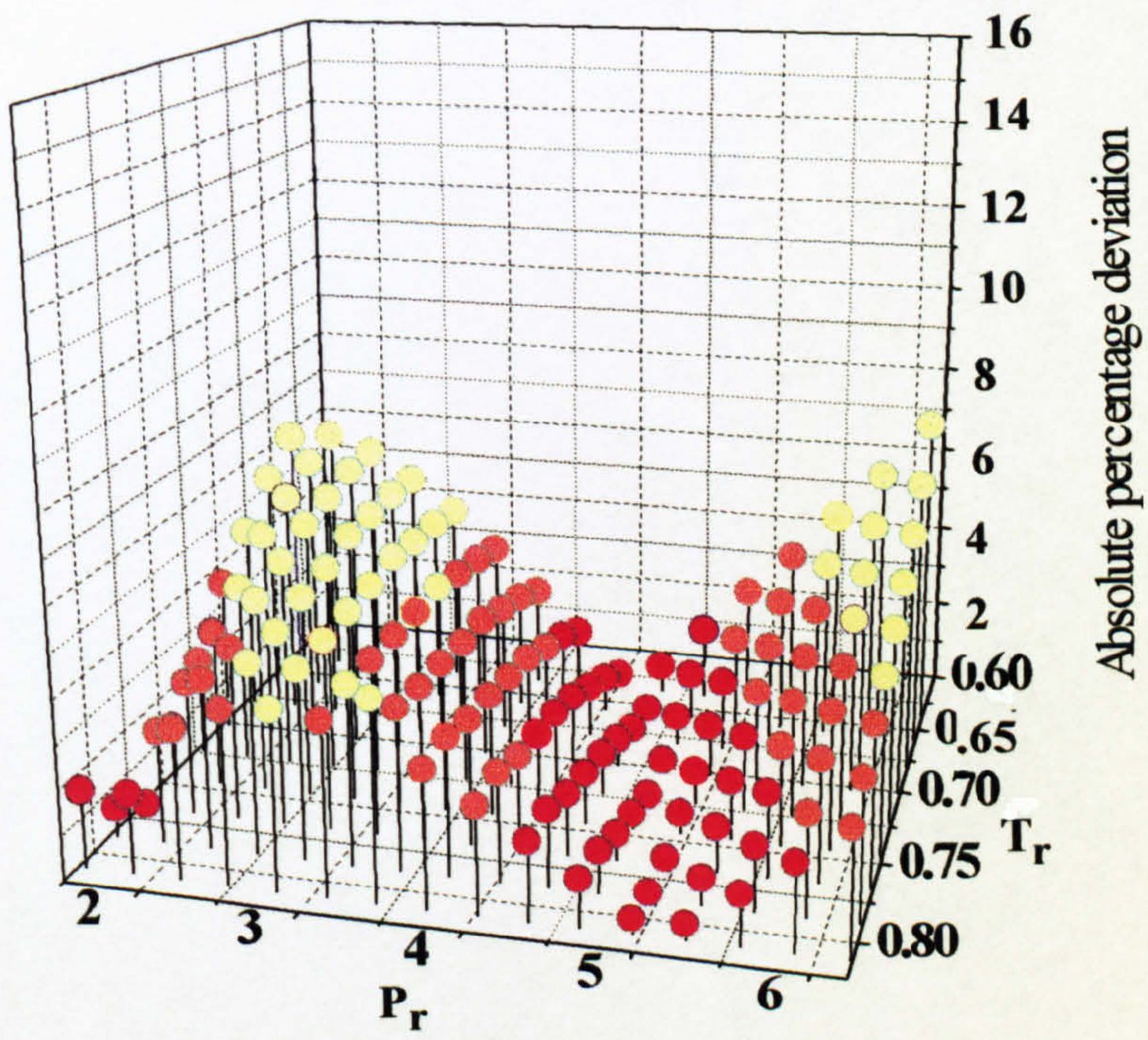

Figure 5.10.c Absolute percentage deviation between measured and predicted liquid speed of sound based on SRK CEOS against T_r and P_r for a hydrocarbon mixture containing 61.7 mole % C_1, 14.5 mole % n-C_3, and 23.8 mole % n-C_8 (table 5.4).

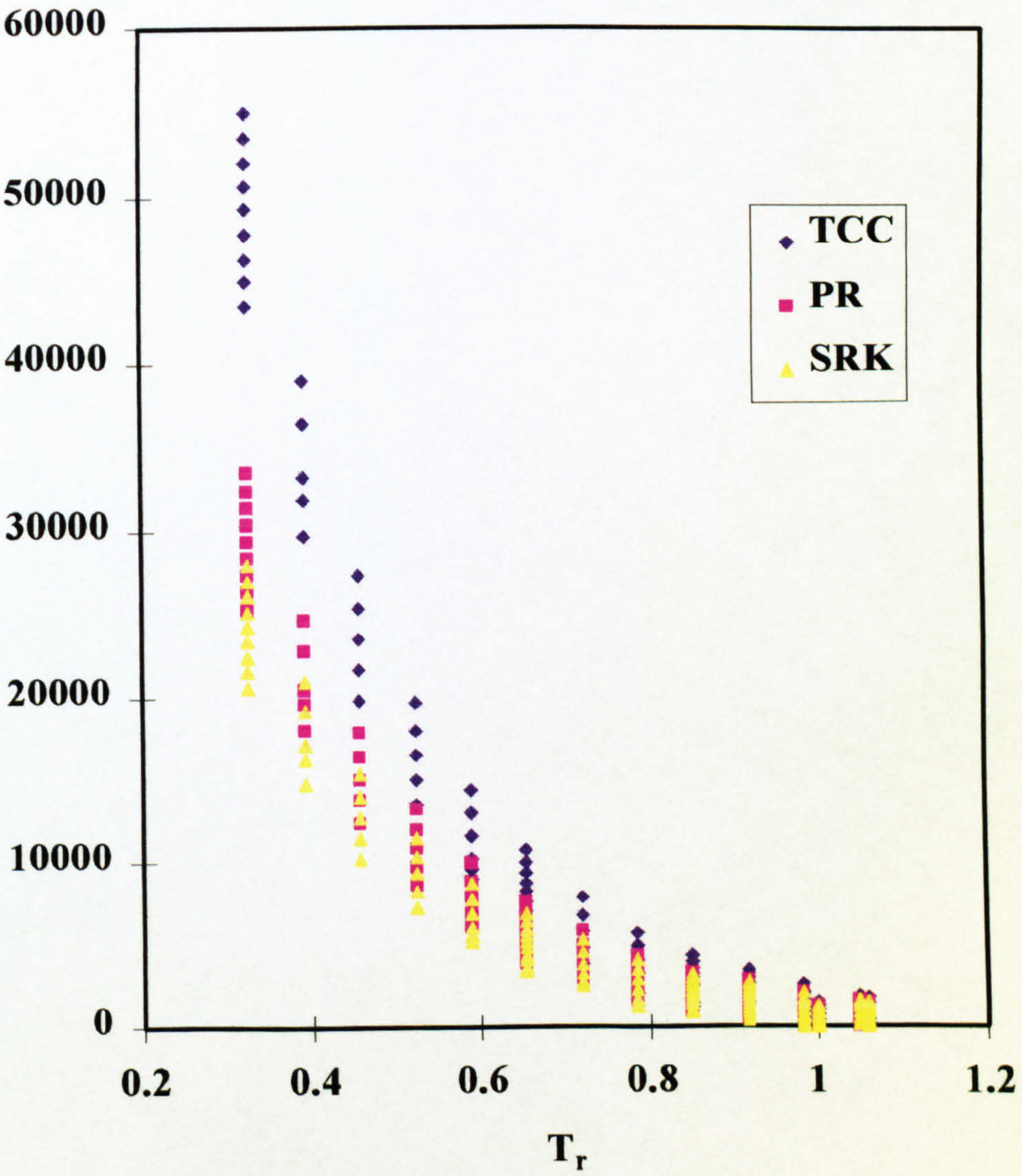

Figure 5.11 $\left(\frac{\partial P}{\partial v}\right)_T$ **predicted from SRK, PR, TCC CEOS against** T_r **for compressed** C_2 **.**

5.5 CONCLUSION

As indicated in chapter 4, an important factor governing the accuracy of blowdown simulation is the choice of a suitable equation of state. In this chapter we evaluated the performance of three CEOS, namely PR, SRK and TCC by comparing their predictions with available published experimental data at a range of temperatures and pressures.

The important findings of evaluations are:

☞ **VAPOUR AND LIQUID DENSITIES AND LIQUID VOLUME PERCENTAGE FOR TWO-PHASE MULTI-COMPONENT SYSTEMS MAINLY CONTAINING C_1 WITH SMALL AMOUNT OF H_2S**

All three CEOS perform well in predicting vapour densities without the use of binary interaction parameters while PR CEOS gives slightly better results than the rest. Around the critical region, TCC CEOS gives the best overall performance.

By assuming binary interaction parameters are equal to zero, both TCC and SRK CEOS give reasonable estimations for liquid densities while the latter is slightly superior than the former. The worst performance is given based on PR CEOS. This is probably because of the equation's inability to accurately predict saturated liquid densities for small molecules as compared to SRK and TCC CEOS. Around the critical region, SRK CEOS gives the best performance.

Both SRK and PR CEOS perform similarly and better than TCC CEOS in predicting percentages of liquid volume. At the condition near the critical region, large deviations are observed between measured and estimated values for all three CEOS. As the predictions of the volume percentage are more sensitive to feed compositions than densities and the uncertainties associated with estimated feed compositions are not known, more VLE experimental data would be required in order to draw any definitive conclusions.

☞ **SPEED OF SOUND FOR :**

i. VAPOUR HYDROCARBON MIXTURES MAINLY CONTAINING C_1 AT CONDITIONS AT OR ABOVE CRITICAL TEMPERATURES OF THE MIXTURES

All three CEOS give rise to large errors near or at critical region. This appears to be an inherent problem associated with CEOS. However, additional experimental data at such conditions are required in order to arrive to a more definitive conclusion.

At conditions $P_r > 3$, TCC CEOS consistently performs better than the other CEOS for all tested conditions while PR CEOS gives the worst performance. On the other hand, at conditions outside the above region, all three CEOS perform equally well. This indicates that TCC CEOS is more effective at high reduced pressures for vapour hydrocarbon mixtures.

ii. Liquid alkanes from C_1 to n-C_9 together with a liquid hydrocarbon mixture

For compressed liquid alkanes from C_1 to n-C_4, both SRK and TCC CEOS generally perform reasonably well with PR CEOS giving the worst performance. Conversely, for n-C_5 - n-C_9, PR CEOS performs the best while TCC CEOS gives the worst performance.

For saturated liquid alkanes (n-C_3 - n-C_5), TCC CEOS gives the best overall performance for n-C_3 and n-C_4. This is mainly due to the comparatively better capability of TCC CEOS in predicting the correct fluid state. All three CEOS give similar accuracy by predicting vapour-like behaviour for saturated liquid n-C_5.

Regarding the performance of CEOS as a function of reduced temperature (T_r), TCC CEOS gives rise to relatively large errors at $T_r \leq 0.6$ for all compressed liquid alkanes. For C_1 and C_2, this is because the predicted values of $\left(\frac{\partial P}{\partial v}\right)_T$ are too large compared with the corresponding values calculated from other CEOS.

This is also very likely to be the main source of error attributed to poor performance of TCC CEOS at low T_r for other liquid alkanes.

For the liquid mixture, all three CEOS perform reasonably well with SRK CEOS providing the best overall performance. As regards to the performance of CEOS as a function of reduced pressure, P_r, TCC gives very accurate predictions for $P_r < 4$ compared with other CEOS while SRK CEOS gives better performance for $P_r > 4$.

It should be noted that the above conclusions are on the basis of the limited amount of experimental data available which are at present mainly confined to mixtures of light hydrocarbons. Although these would be of relevance to offshore processing operations, a useful extension of this study would be undertaking of a similar exercise in conjunction with heavy hydrocarbons.

So far, the results of our study indicate that the effect of the modifications introduced in TCC CEOS in order to address the shortcomings of the PR and SRK CEOS is particularly evident in terms of improving the prediction of vapour speed of sound for hydrocarbon mixtures at conditions above critical temperatures and pressures. Clearly, were the appropriate experimental data available, it would be useful to investigate the validity of the same argument at conditions below the critical temperatures and pressures. Also within the ranges tested, the TCC CEOS provides the best performance in terms of predicting compressed liquid densities for pure hydrocarbons.

CHAPTER 6

VALIDATION OF BLOWSIM

6.1 INTRODUCTION

In chapter 4, the mathematical model, BLOWSIM, was developed for simulating vapour space blowdown of a vessel. In this chapter, the results obtained from the model are compared against those predicted from BLOWDOWN [Haque et al., 1992a] and published experimental data for high pressure blowdown of a full-size vessel containing various hydrocarbon mixtures. These include, non-condensable gas, condensable gas and two-phase mixtures. In each and every case, the effects of incorporating any one of three cubic equations of state (mentioned in chapter 5) on the results predicted by BLOWSIM are evaluated. The latter include pressure/time profiles, and temperature/time profiles for the vessel wall (both wet and dry), the bulk gas and where applicable, the bulk liquid.

Additionally, the effects of accounting for or discounting the work done by the liquid phase on the results obtained using BLOWSIM are investigated. This is followed by an investigation of the effects in applying the various chosen heat transfer coefficients between vessel wall and the liquid phase within the vessel on BLOWSIM's predictions. The final part of this chapter investigates the performance of BLOWSIM based on either ideal gas assumption or real fluid approach at the discharge orifice in terms of minimum temperature predictions and computational time.

6.2 VALIDATION OF THE COMPUTER MODEL, BLOWSIM

6.2.1 Selection of Experimental Data

Haque et al. [1992b] conducted a series of blowdown experiments on a full-size vessel at the British Gas test site in Spadeadam. The scale of their experiments reported are the largest compared to other published experimental studies (Table 2.1, chapter 2) and hence form a useful basis for comparison. These tests were conducted on hydrocarbon mixtures with various compositions mainly containing methane,

ethane and propane with trace amount of heavier hydrocarbons, in particular, butane. The vessel pressures, fluid and vessel wall temperatures were measured during the blowdown process. These data were in turn used to validate BLOWDOWN. The results of comparisons for a selection of mixtures were published together with the appropriate normal fluid compositions, excluding the mole fraction of trace amounts of butane in the mixtures, as well as the vessel dimensions.

Although the amounts of butane in the mixtures are claimed to be small, figure 6.1 shows that even the presence of small quantities may give rise to a significant effect on the mixtures' phase envelop and hence the blowdown results. The data show the effect of adding 1 and 2 mole % of n-butane to the published [Haque et al., 1992b] normal feed composition comprising 85.5 mole % methane, 4.5 mole % ethane and 10.0 mole % propane. The phase envelopes are based on SRK CEOS which has been shown [Tsonopoulos & Heidman, 1986] to give accurate VLE predictions for hydrocarbon systems.

On the basis of the above figure, it is clear that the dew point rather than the bubble point predictions are very sensitive to the amount of n-butane. At any given pressure below 80 atm, the addition of 1 and 2% mole of n-butane leads to an increase in dew point temperatures by 10K and 20K respectively. Hence, in the absence of a more precise knowledge of the actual fluid composition, the data published by Haque et al. [1992b] are inappropriate for validation purposes.

Szczepanski [1994] presented a selection of Haque et al.'s blowdown data (both measured and predicted data) with the exact fluid compositions for a two-phase mixture, condensable and non-condensable gases. Both condensable gas and two-phase mixture contain 2% mole of n-butane prior to blowdown. These data are used in this study to evaluate the performance of BLOWSIM.

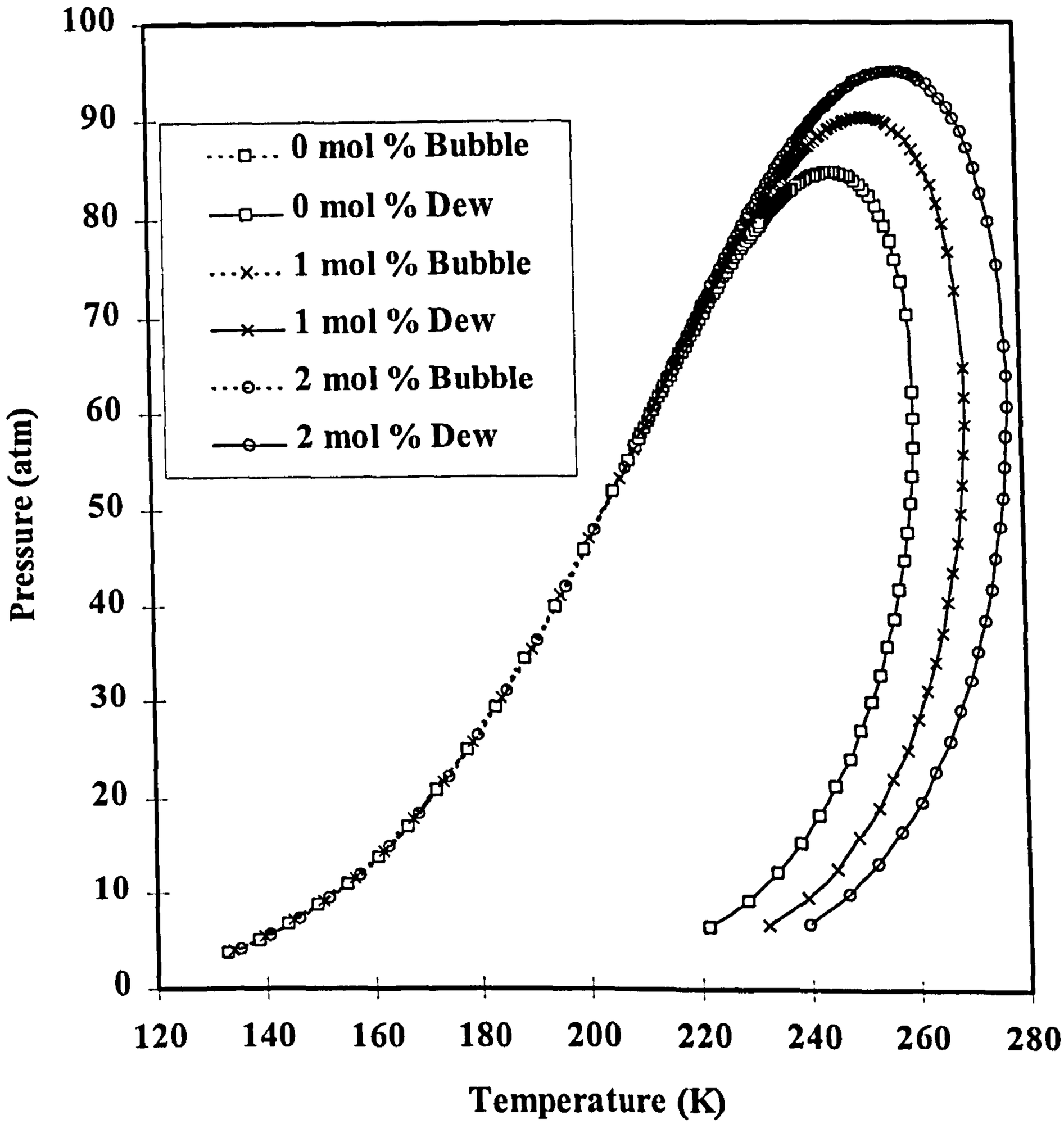

Figure 6.1 The effect of additional 1 and 2 mole % of n-butane on the phase envelope of a mixture containing 85.5 mole % methane, 4.5 mole % ethane and 10.0 mole % propane

Bubble : Bubble point

Dew : Dew point

6.2.2 Experimental Conditions and Measurement Accuracy

The vessel is a full-size suction scrubber for a gas compressor which has a total volume of 2.78 m^3, with length and inside diameter of 3.240 m (2.75 m tan-to-tan) and 1.130 m respectively. The wall thickness is 59 mm. The vessel's material of construction has not been given. In this study, it is assumed to be carbon steel.

Haque et al. [1992b] measured the fluid and vessel wall temperatures during blowdown using 156 thermocouples mounted at various positions along the vessel wall. The claimed uncertainties associated with the measurements of vessel temperature and pressure were reported to be ± 0.5 K and ± 0.2 atm respectively.

The equivalent choke diameters, feed conditions and compositions prior to blowdown for the various hydrocarbon systems are given in table 6.1. The vessel was oriented vertically in all cases.

Table 6.1 Experimental conditions for three hydrocarbon mixtures prior to blowdown and equivalent choke diameters [Szczepanski, 1994]

Fluid	Composition (% mole)	P (atm)	T (K)	d_C (mm)
Non-condensable gas	91 C_1, 9 C_2	120	303	6.35
Condensable gas	64 C_1, 6 C_2, 28 n-C_3, 2 n-C_4	116	293	10.00
Two-phase mixture	Same as above	42	293	10.00

P = Pressure; T = Temperature; d_C = Equilivent choke diameter

The following is a detailed analysis of the blowdown results obtained in conjunction with each hydrocarbon system. The measured and predicted wall temperatures based on BLOWDOWN refer to the inner wall temperatures whereas BLOWSIM's predictions represent the average values as the temperature gradient across the thickness of the wall is assumed to be negligible.

6.2.3 Non-condensable Gas

Figure 6.2 shows the predicted depressurisation rates based on BLOWSIM in conjunction with SRK, PR and TCC CEOS as compared to experimental data and BLOWDOWN predictions for the non-condensable gas mixture. It is clear that all simulations produce very accurate predictions of the pressure/time profile with the choice of the CEOS having an insignificant effect on the results.

Figures 6.3 shows the estimated variations of bulk vapour temperature based on both models against experimental data. The corresponding performance of BLOWSIM is shown to be reasonable. The maximum deviation from experimental data as indicated by the shaded area, representing the presence of temperature gradients within the fluid, is about 3K. It is clear that in general, BLOWSIM predicts lower temperatures than BLOWDOWN. This is likely attributed to the combination effects of thermodynamic trajectory and CEOS used in the former model.

Figure 6.4, shows a comparison of the predicted vessel wall temperature/time profiles based on the two models against experimental data. According to the data, the performance of BLOWSIM although reasonable (over estimates the wall temperatures by maximum 3K) is relatively insensitive to the type of CEOS used. On the other hand, BLOWDOWN which accounts for the temperature gradient across the vessel wall gives very accurate predictions of the vessel wall temperature throughout the discharge process.

Based on the above data and within the ranges tested, the Overa et al.'s thermodynamic trajectory for the vapour phase appears to be applicable to blowdown simulation of vessels containing hydrocarbon gas mixtures from elevated pressures. Furthermore, the assumption in BLOWSIM neglecting forced convection within the vapour phase and zero heat transfer between the vessel and the surrounding seems to be appropriate. However, under extreme conditions (e.g. under fire or extreme weather conditions), the heat flux between the vessel and the surrounding should be considered.

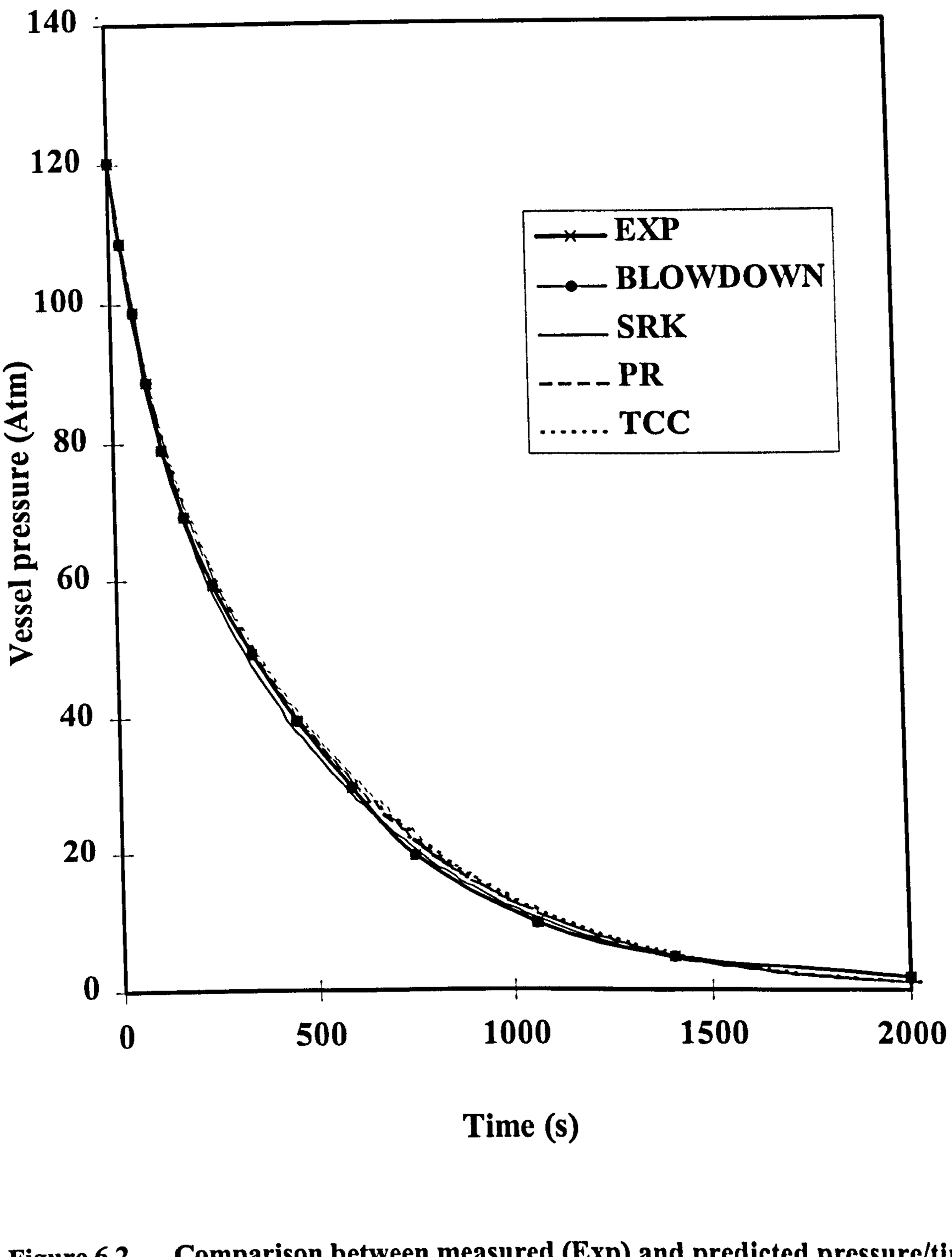

Figure 6.2 **Comparison between measured (Exp) and predicted pressure/time profiles from BLOWDOWN and BLOWSIM based on SRK, PR and TCC CEOS for non-condensable gas mixture (91 mole % C_1 and 9 mole % C_2)**

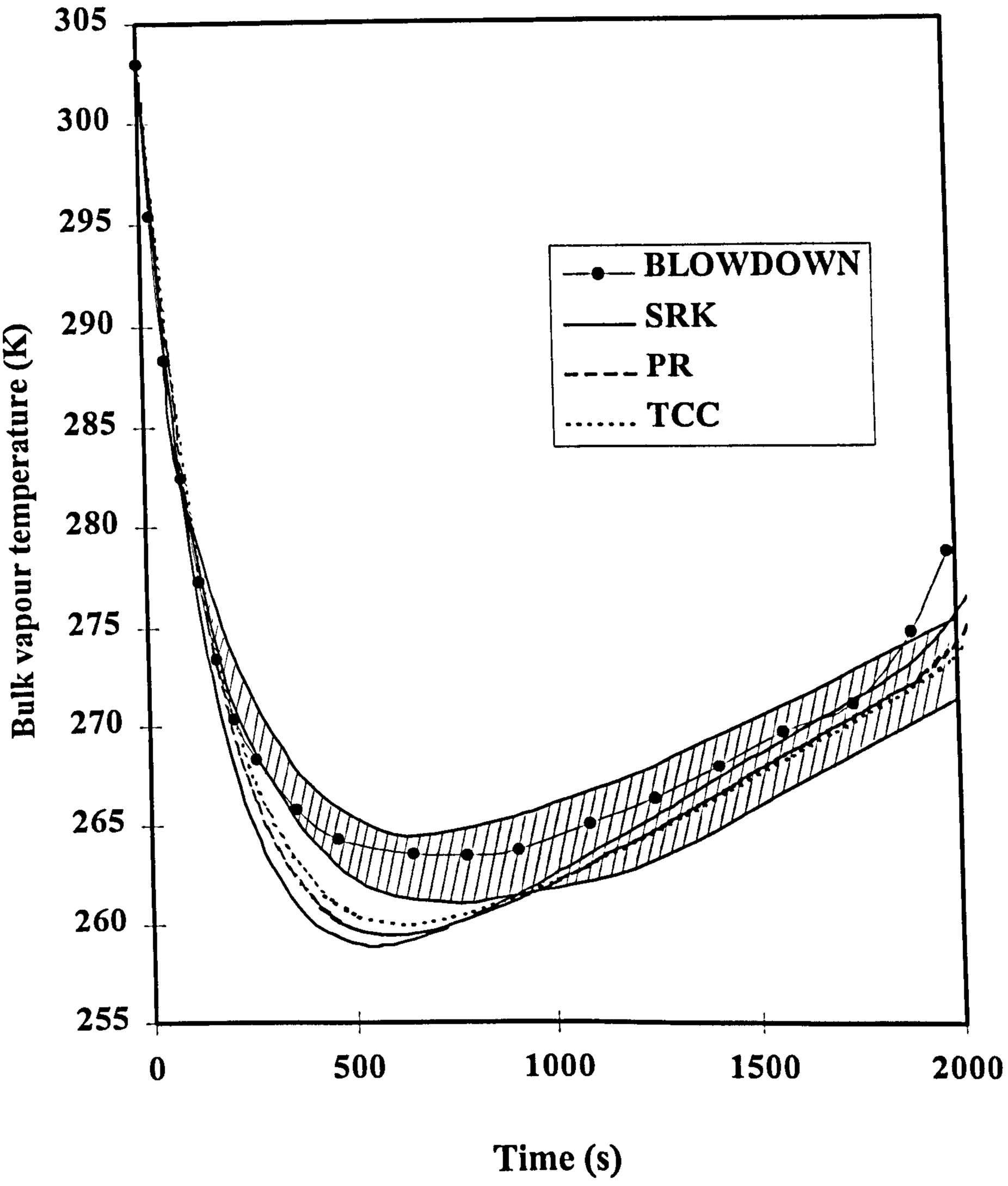

Figure 6.3 **Comparison between measured (shaded area) and predicted bulk vapour temperature/time profiles from BLOWDOWN and BLOWSIM based on SRK, PR and TCC CEOS for non-condensable gas mixture (91 mole % C_1 and 9 mole % C_2).**

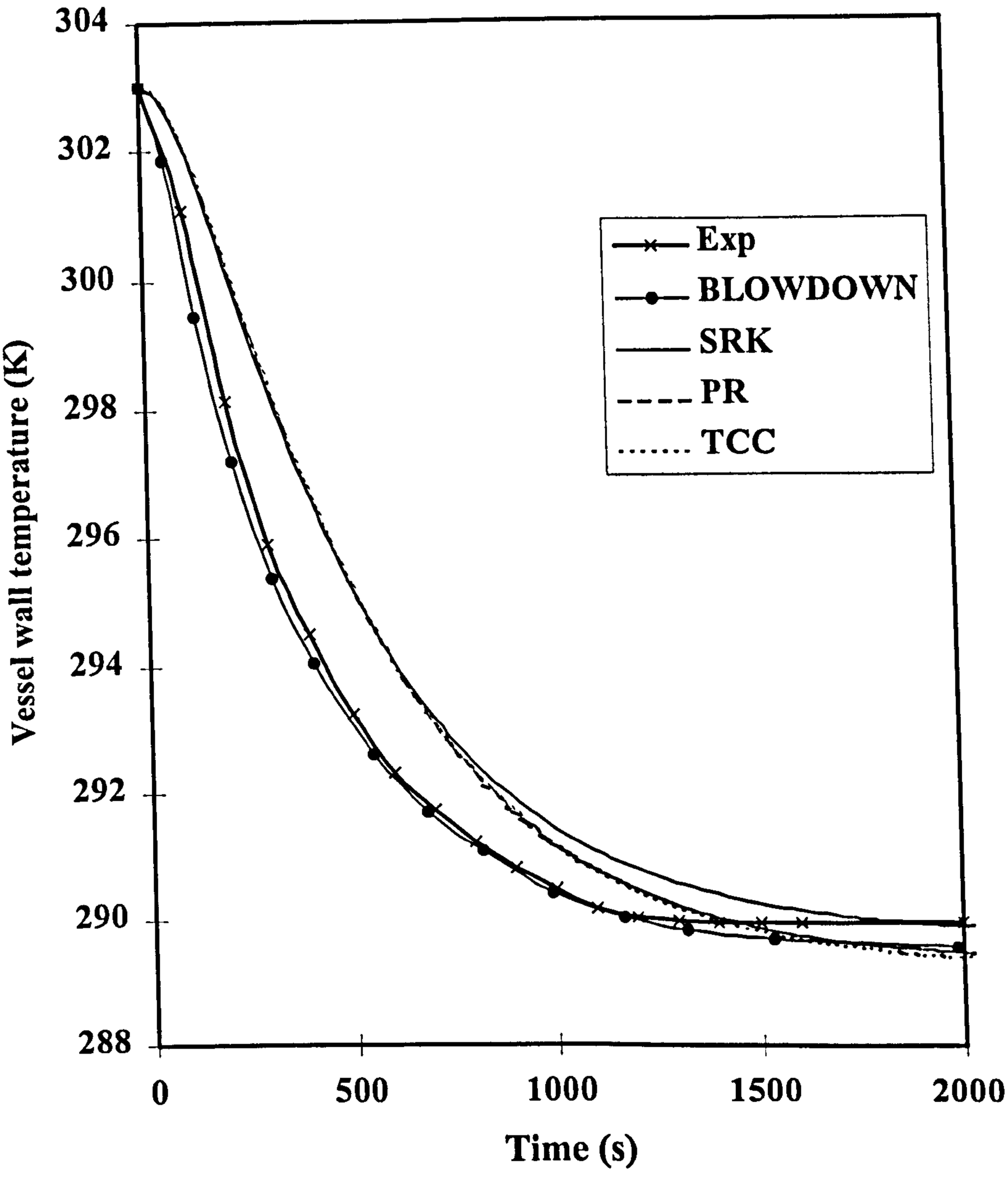

Figure 6.4 Comparison between measured (Exp) and predicted vessel wall temperature/time profiles from BLOWDOWN and BLOWSIM based on SRK, PR and TCC CEOS for non-condensable gas mixture (91 mole % C_1 and 9 mole % C_2).

6.2.4 Condensable Gas and Two-phase Mixture

In this section, the effect of considering or discounting work done by the liquid phase within the vessel during depressurisation of the condensable gas mixture (see table 6.1) on BLOWSIM's performance is investigated. The corresponding predictions based on BLOWDOWN which take into account of the work done by the liquid phase are also given. Both mathematical models employ Rohsenow's correlation (equation 4.2.22 in chapter 4) for predicting the boiling heat flux for the liquid phase within the vessel although, in the case of BLOWDOWN, the methodology for calculating the pseudo latent heat as well as the magnitudes of the required parameters in Rohsenow's correlation are not available.

On the other hand, the results of parallel simulations in conjunction with the two-phase mixture have indicated negligible effects on BLOWSIM's data when the work done by the liquid phase is accounted for. Hence, only the results considering work done by liquid phase within the vessel are shown.

Finally, the effect of assuming constant heat transfer coefficient between the liquid phase and vessel wall in the ranges suggested by Overa et al. [1994] on BLOWSIM's performance for both condensable gas and two-phase mixture is investigated.

6.2.4.1 Effect of Considering and Discounting Work Done by the Liquid Phase on Blowdown Simulations

Condensable gas (figures 6.5 - 6.9)

Figure 6.5 presents the predicted vessel pressure/time profiles for the condensable gas based on BLOWSIM (not accounting the work done by the liquid phase) and BLOWDOWN as compared with experimental data. Accounting for the work done by the liquid phase has negligible effect on BLOWSIM's pressure/time predictions and hence these data are not shown here.

The results indicate BLOWSIM's performance is relatively insensitive to the type CEOS used. Also, both mathematical models are capable of predicting pressure/time history relatively accurately.

Figures 6.6 a and b, show the corresponding bulk vapour temperature/time profiles. Once again, it is clear that accounting for the work done by the liquid phase (figure 6.6a) has little effect on BLOWSIM's predictions. Additionally, BLOWSIM's predictions which are rather insensitive to the type CEOS used, agree reasonably well with both BLOWDOWN and field data, except during the latter stages of depressurisation where BLOWDOWN incorrectly predicts a further reduction in temperature during the recovery period. Both models predict the minimum bulk gas temperature to ± 7K.

Figures 6.7 a and b show the predicted temperature/time profiles for the unwetted wall based on BLOWSIM and BLOWDOWN for the condensable gas mixture. The corresponding experimental data are represented by the shaded areas. Figure 6.7 a relates to the case where the effect of work done by the liquid phase in the BLOWSIM's simulation is taken into account whereas in figure 6.7 b, this effect is ignored.

Once again, BLOWSIM data are relatively insensitive to the choice of CEOS and whether the work done by the liquid is accounted for. The model over estimates the unwetted wall temperatures by ca. 4K. On the other hand, relatively accurate predictions are obtained from BLOWDOWN.

Figures 6.8 a and b show the corresponding data presented in terms of the predicted and measured bulk liquid temperatures for the same system. As before, both figures indicate that BLOWSIM's performance is insensitive to the choice of the CEOS used. However, during the early stages (0-600 s) of blowdown, when the rate of formation of the liquid is rapid, lower but more accurate liquid temperatures are predicted (figure 6.8 a) when the work done by the liquid is accounted for. Surprisingly, this trend is reversed during the latter stages of depressurisation. In the case of figure 6.8 b (when the work done for the liquid is not accounted for), better agreement in the results is obtained during the same period. In general, BLOWSIM performs better than BLOWDOWN.

It is interesting to note that the experimental data in the above figures indicate the formation of the liquid phase is nearly instantaneous while BLOWSIM and

BLOWDOWN predict liquid formation approximately 30 s and 100 s following blowdown respectively.

In figures 6.9 a and b, the measured time profiles for the wetted wall temperature are compared with the predicted profiles based on BLOWSIM and BLOWDOWN respectively. Interestingly, although liquid formation is instantaneous (figures 6.8 a and b) no wetted wall temperature is recorded until ca. 100 s after commencement of depressurisation.

On the basis of the data in figures 6.8 and 6.9, it is clear that BLOWSIM based on either one of the thermodynamic trajectories relating to the work done by the liquid phase predicts earlier formation of the liquid phase compared to BLOWDOWN. This is likely attributed to the following reasons :

1) the assumptions of instantaneous formation and immediate settlement of liquid droplets from vapour phase (see section 4.2.2.1) as soon as the two-phase boundary is crossed.

2) The application of CEOS may result in higher saturated pressure and temperature when compared to those predicted on the basis of the extended principle of corresponding states [Rowlinson & Watson, 1969] used in BLOWDOWN.

In order to investigate the effects associated with the nucleation time and settling velocity relative to the vapour in the vessel for liquid droplets formed just after the fluid entering the two-phase region, the nucleation time and settling velocity are estimated based on equations 3.4.6 and 3.4.7 (see chapter 3) respectively. Both equations are functions of equilibrium liquid mole fraction in the vapour phase. The equilibrium liquid mole fraction as estimated from TCC CEOS is 0.7. The estimated nucleation time and settling velocity relative to the vapour are 1.4 s and 2.2 m/s respectively. Additionally, the average gas velocity is 0.0097 m/s. Hence, the estimated absolute settling velocity of liquid droplets is 2.19 m/s.

The time required for the liquid droplets to settle gravitationally is determined by dividing the total height of the vessel by the settling velocity. The corresponding value is 1.4 s. The total time delay for formation of the liquid phase at the bottom of

the vessel is therefore 2.8 s (=1.4 + 1.4) which is comparatively small. In the absence of any other arguments, it is therefore likely that the earlier formation of liquid phase predicted from BLOWSIM as compared to BLOWDOWN is attributed to the use of different types of EOS.

Notably, both figures 6.9 a and b indicate all three CEOS lead to same predictions from BLOWSIM.

Returning to figure 6.9 a, BLOWSIM based on thermodynamic trajectory of considering work done by the liquid phase under estimates the wetted wall temperatures by 5K. Surprisingly, from figure 6.9 b, the same model but based on thermodynamic trajectory of discounting work done by liquid phase accurately predicts the field data.

Considering the overall performance, both BLOWDOWN and BLOWSIM produce reasonably accurate predictions of the wetted wall temperature.

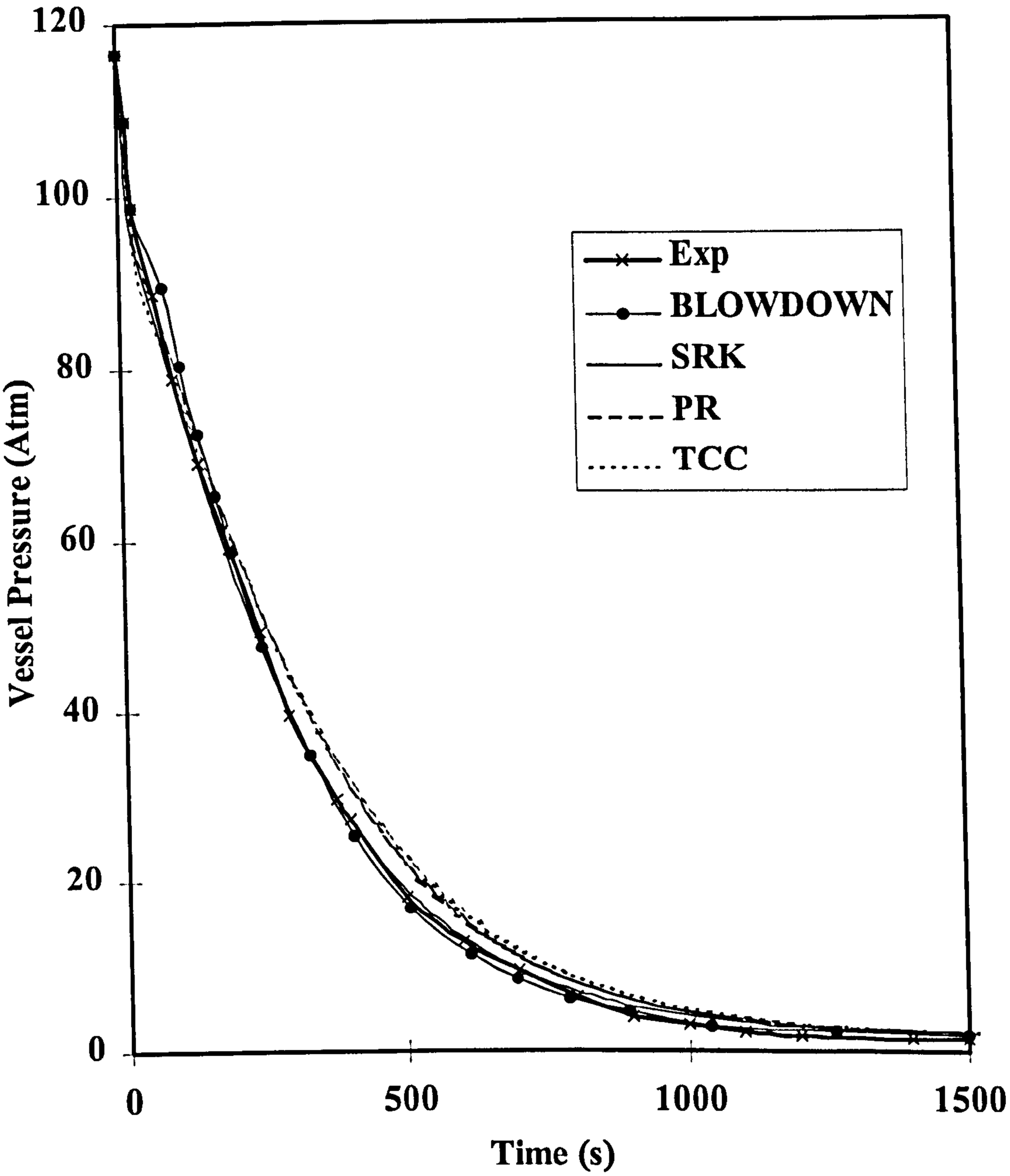

Figure 6.5 **Comparison between measured (Exp) and predicted pressure/time profiles from BLOWDOWN and BLOWSIM based on various CEOS (SRK, PR and TCC CEOS) in conjunction with thermodynamic trajectory of discounting work done by liquid phase within the vessel for condensable gas mixture (64 mole % C_1, 6 mole % C_2, 28 mole % n-C_3 and 2 mole % n-C_4)**

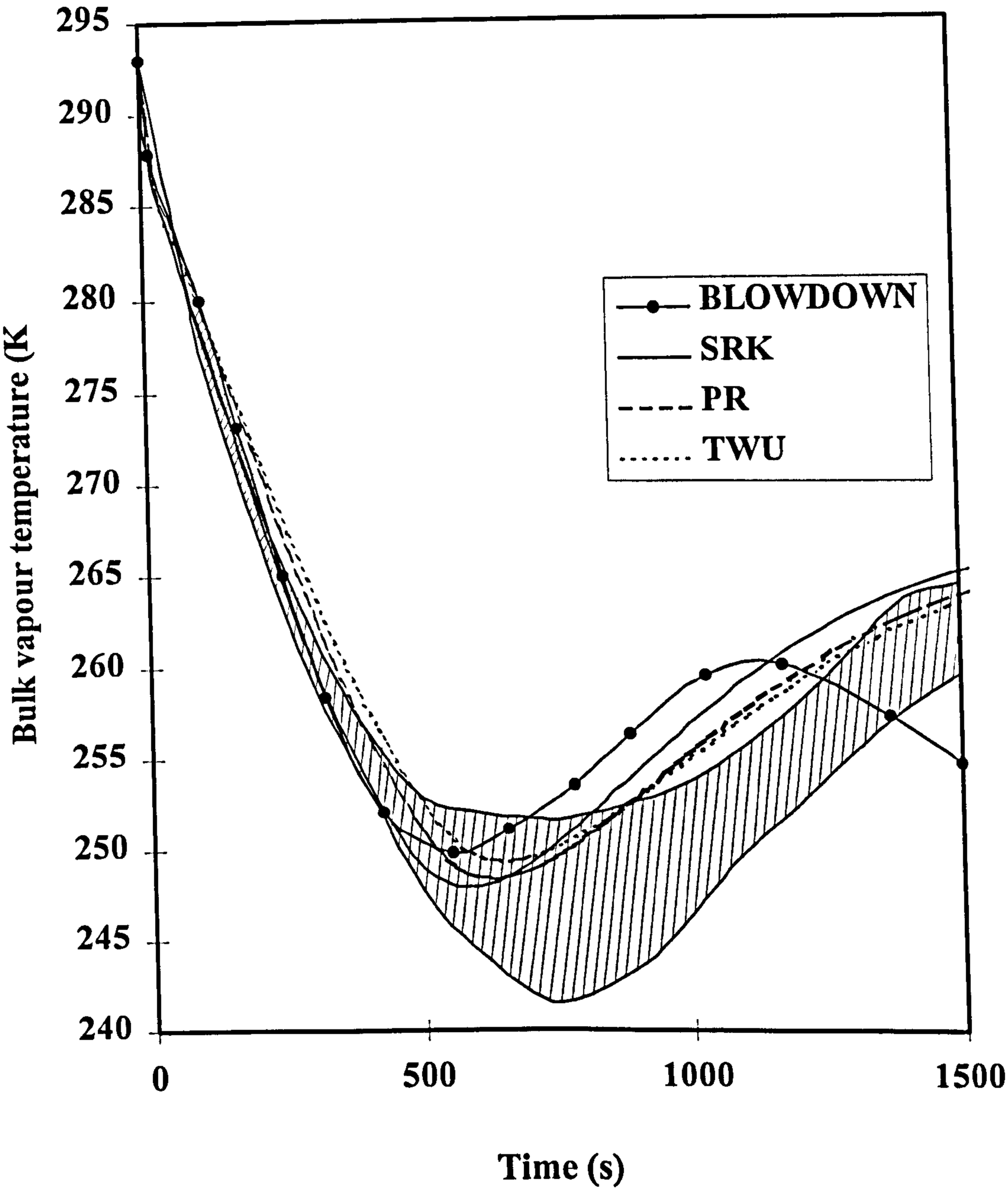

Figure 6.6.a **Comparison between measured (shaded area) and predicted bulk vapour temperature/time profiles from BLOWDOWN and BLOWSIM based on various CEOS (SRK, PR and TCC CEOS) in conjunction with thermodynamic trajectory of considering work done by liquid phase within the vessel for condensable gas mixture (64 mole % C_1, 6 mole % C_2, 28 mole % n-C_3 and 2 mole % n-C_4).**

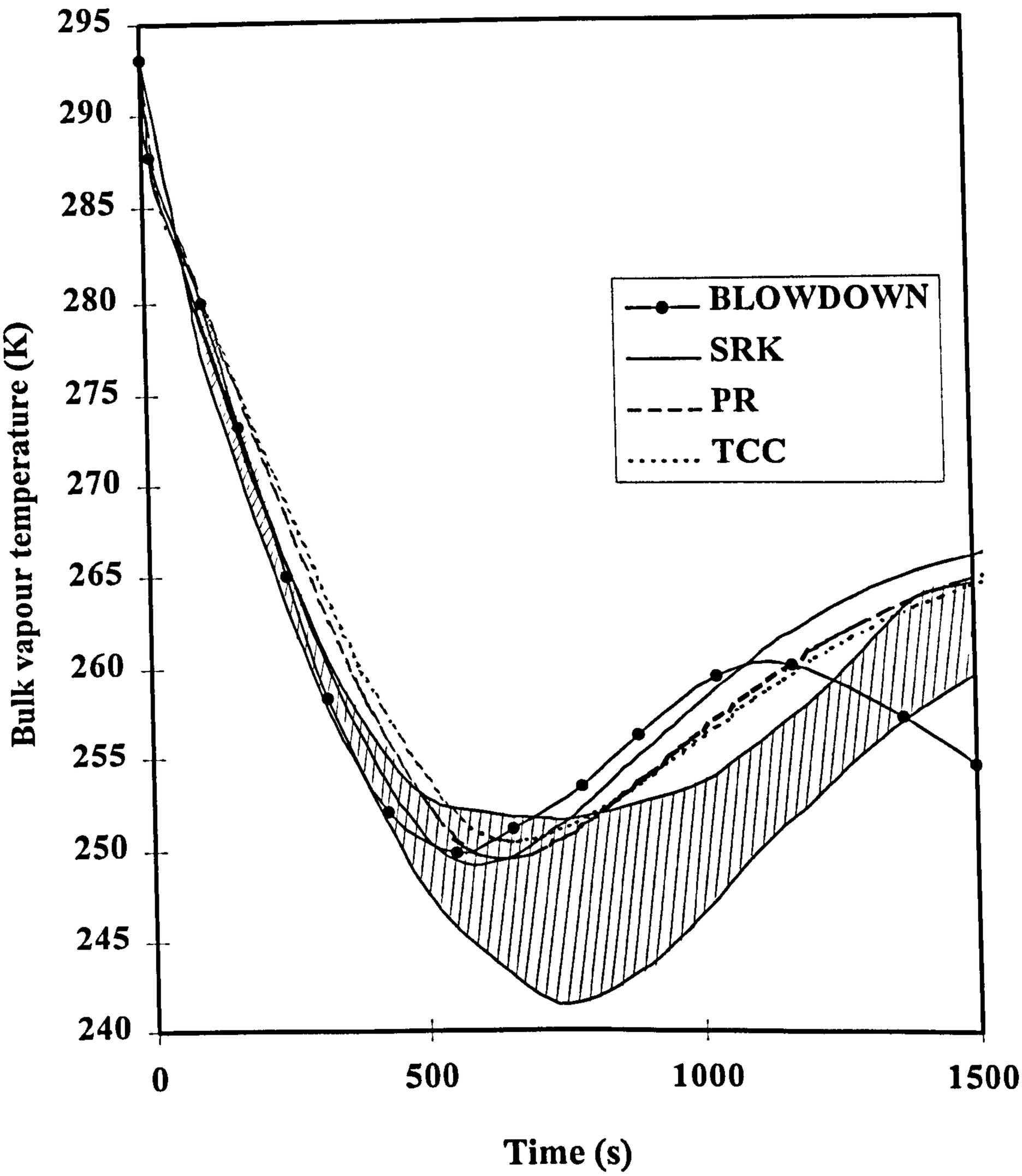

Figure 6.6.b **Comparison between measured (shaded area) and predicted bulk vapour temperature/time profiles from BLOWDOWN and BLOWSIM based on various CEOS (SRK, PR and TCC CEOS) in conjunction with thermodynamic trajectory of discounting work done by liquid phase within the vessel for condensable gas mixture (64 mole % C_1, 6 mole % C_2, 28 mole % n-C_3 and 2 mole % n-C_4).**

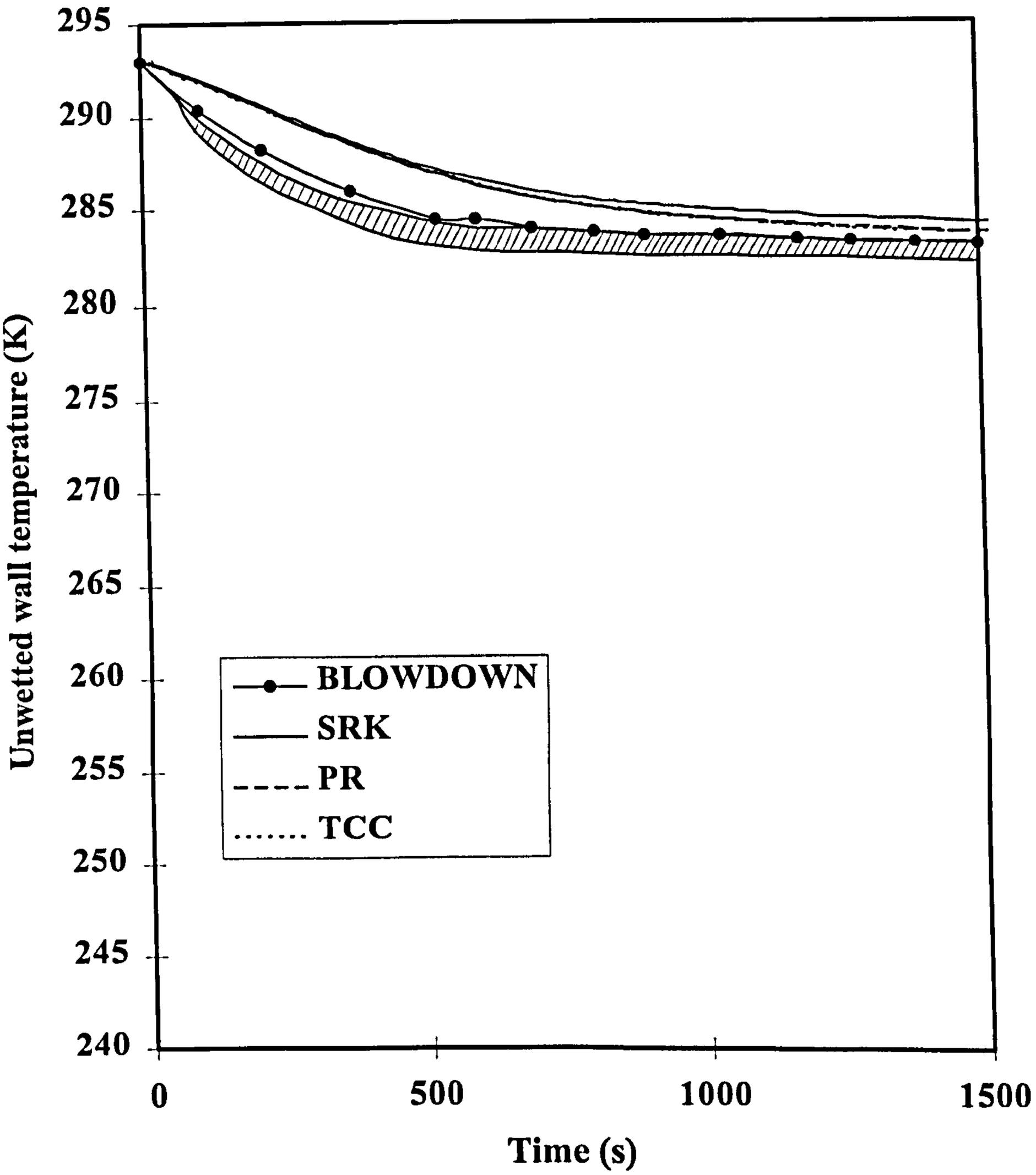

Figure 6.7.a **Comparison between measured (shaded area) and predicted unwetted wall temperature/time profiles from BLOWDOWN and BLOWSIM based on various CEOS (SRK, PR and TCC CEOS) in conjunction with thermodynamic trajectory of considering work done by liquid phase within the vessel for condensable gas mixture (64 mole % C_1, 6 mole % C_2, 28 mole % n-C_3 and 2 mole % n-C_4).**

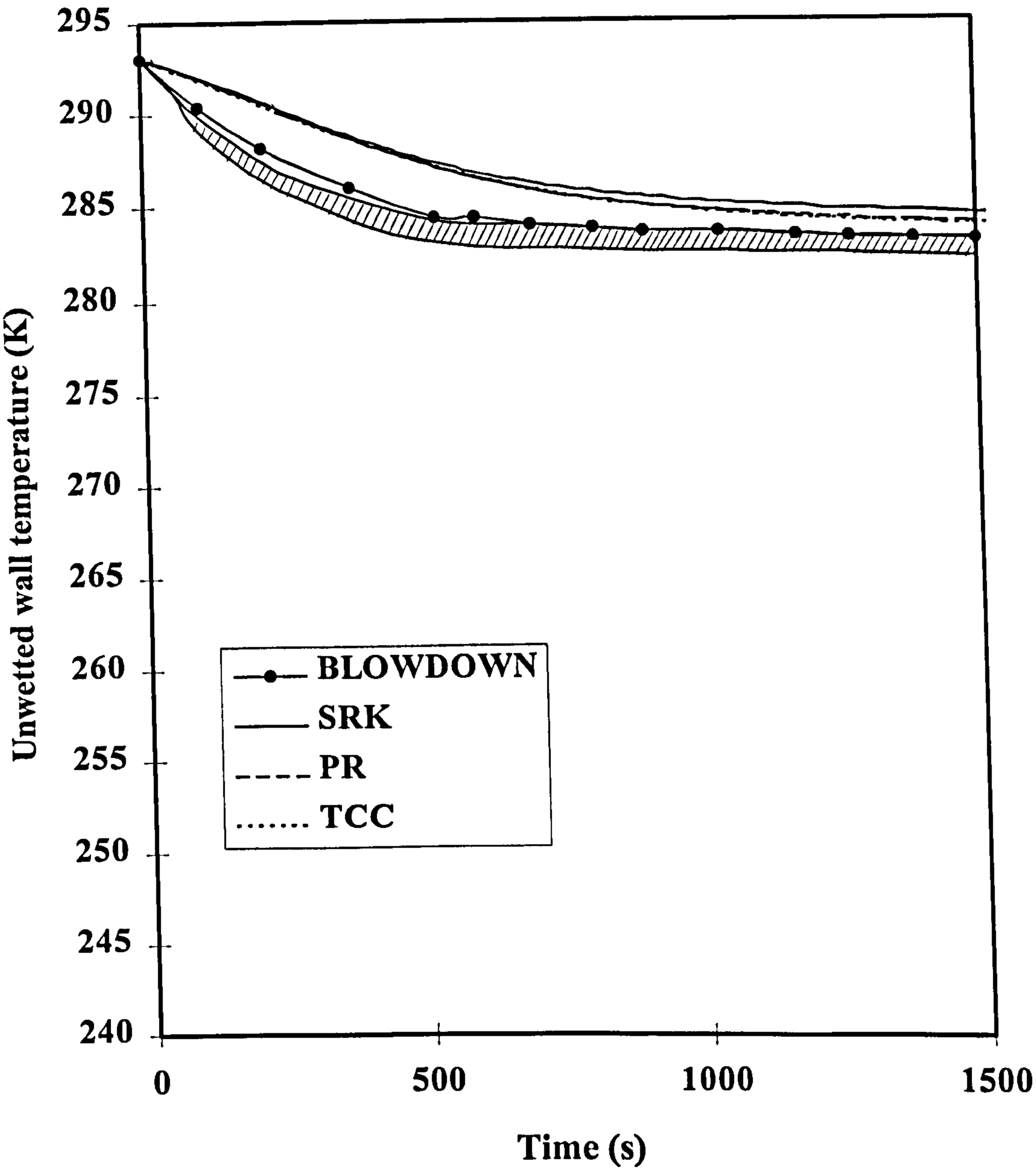

Figure 6.7.b **Comparison between measured (shaded area) and predicted unwetted wall temperature/time profiles from BLOWDOWN and BLOWSIM based on various CEOS (SRK, PR and TCC CEOS) in conjunction with thermodynamic trajectory of discounting work done by liquid phase within the vessel for condensable gas mixture (64 mole % C_1, 6 mole % C_2, 28 mole % n-C_3 and 2 mole % n-C_4).**

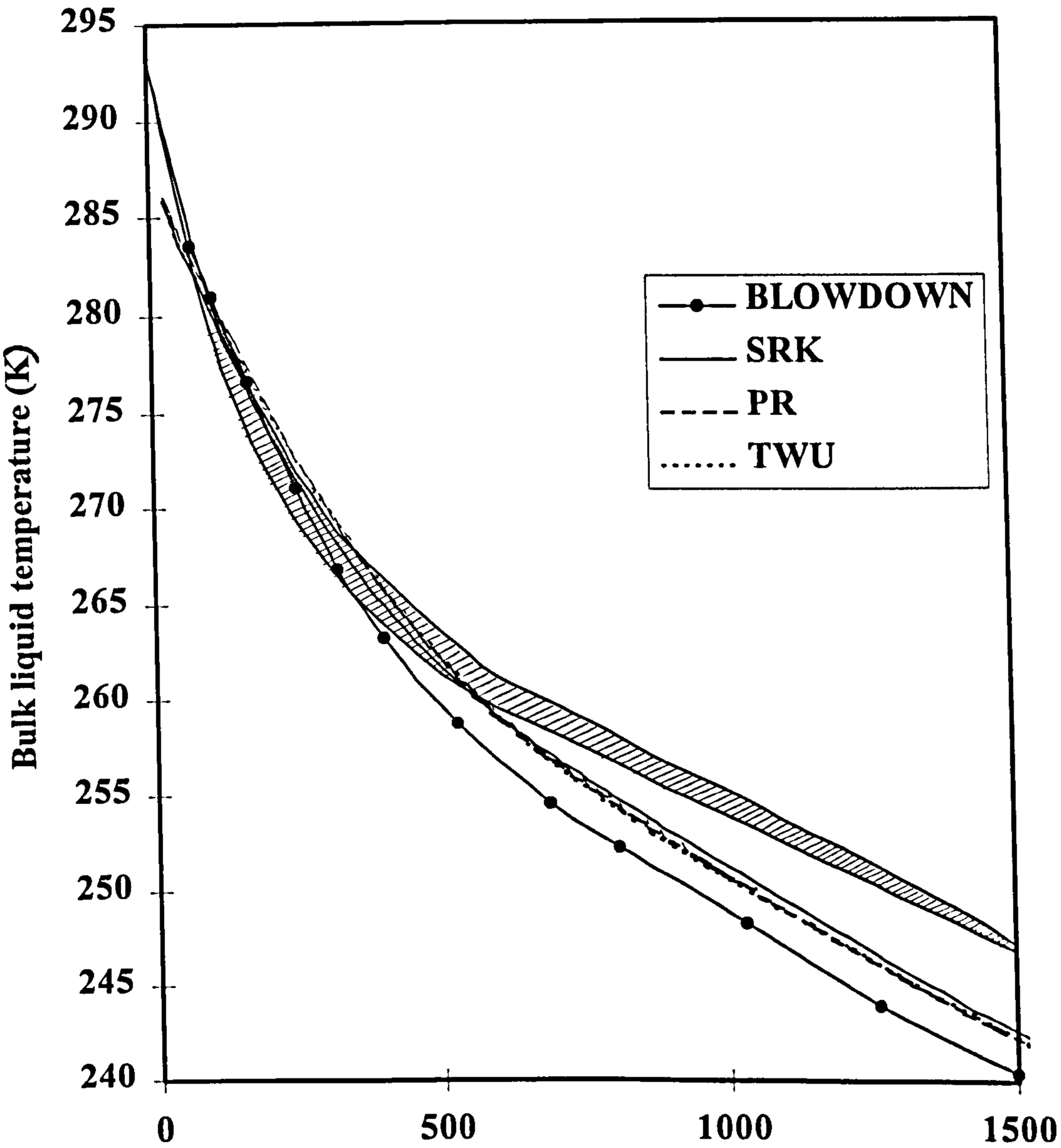

Figure 6.8.a **Comparison between measured (shaded area) and predicted bulk liquid temperature/time profiles from BLOWDOWN and BLOWSIM based on various CEOS (SRK, PR and TCC CEOS) in conjunction with thermodynamic trajectory of considering work done by liquid phase within the vessel for condensable gas mixture (64 mole % C_1, 6 mole % C_2, 28 mole % n-C_3 and 2 mole % n-C_4).**

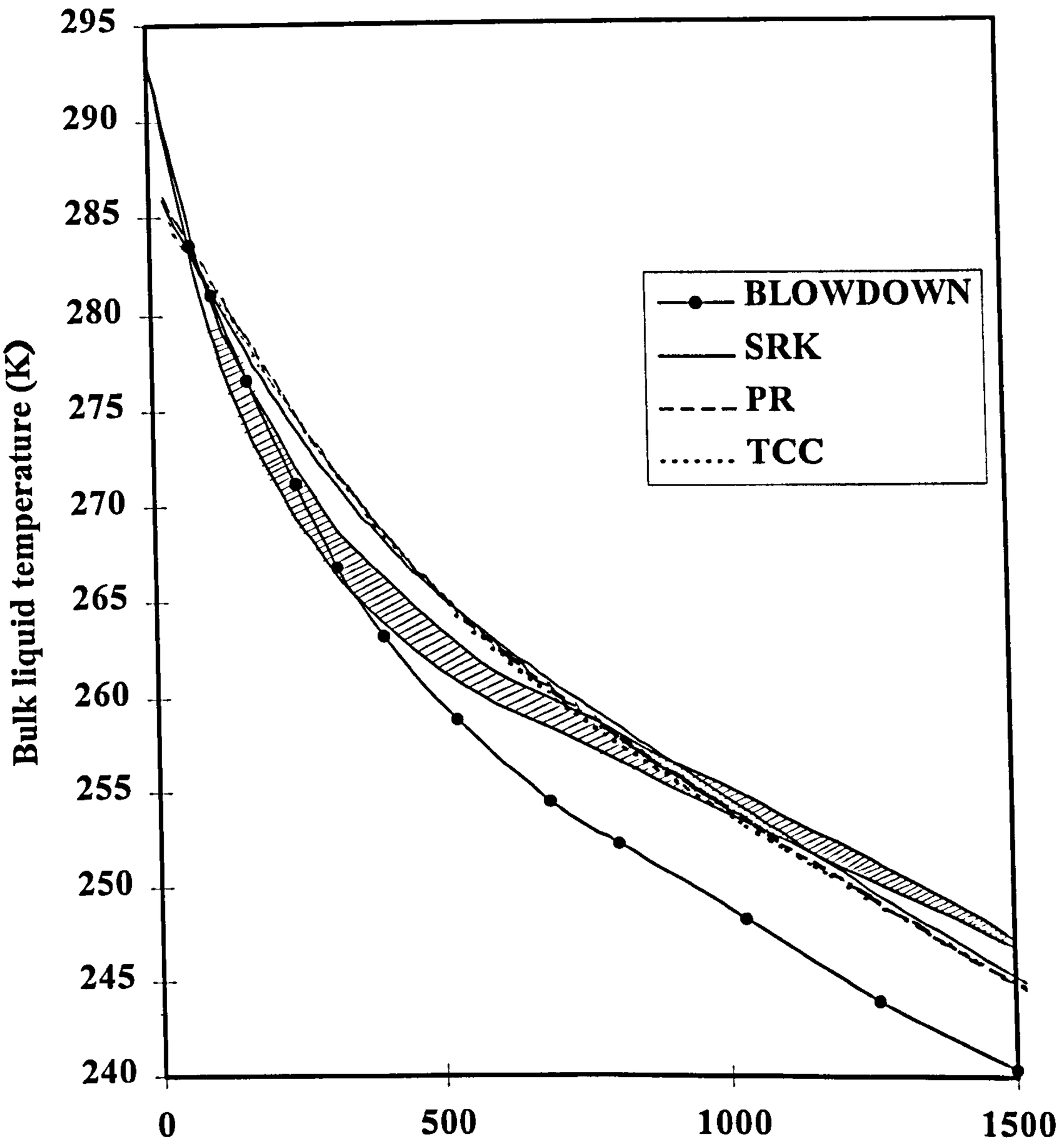

Figure 6.8.b **Comparison between measured (shaded area) and predicted bulk liquid temperature/time profiles from BLOWDOWN and BLOWSIM based on various CEOS (SRK, PR and TCC CEOS) in conjunction with thermodynamic trajectory of discounting work done by liquid phase within the vessel for condensable gas mixture (64 mole % C_1, 6 mole % C_2, 28 mole % n-C_3 and 2 mole % n-C_4).**

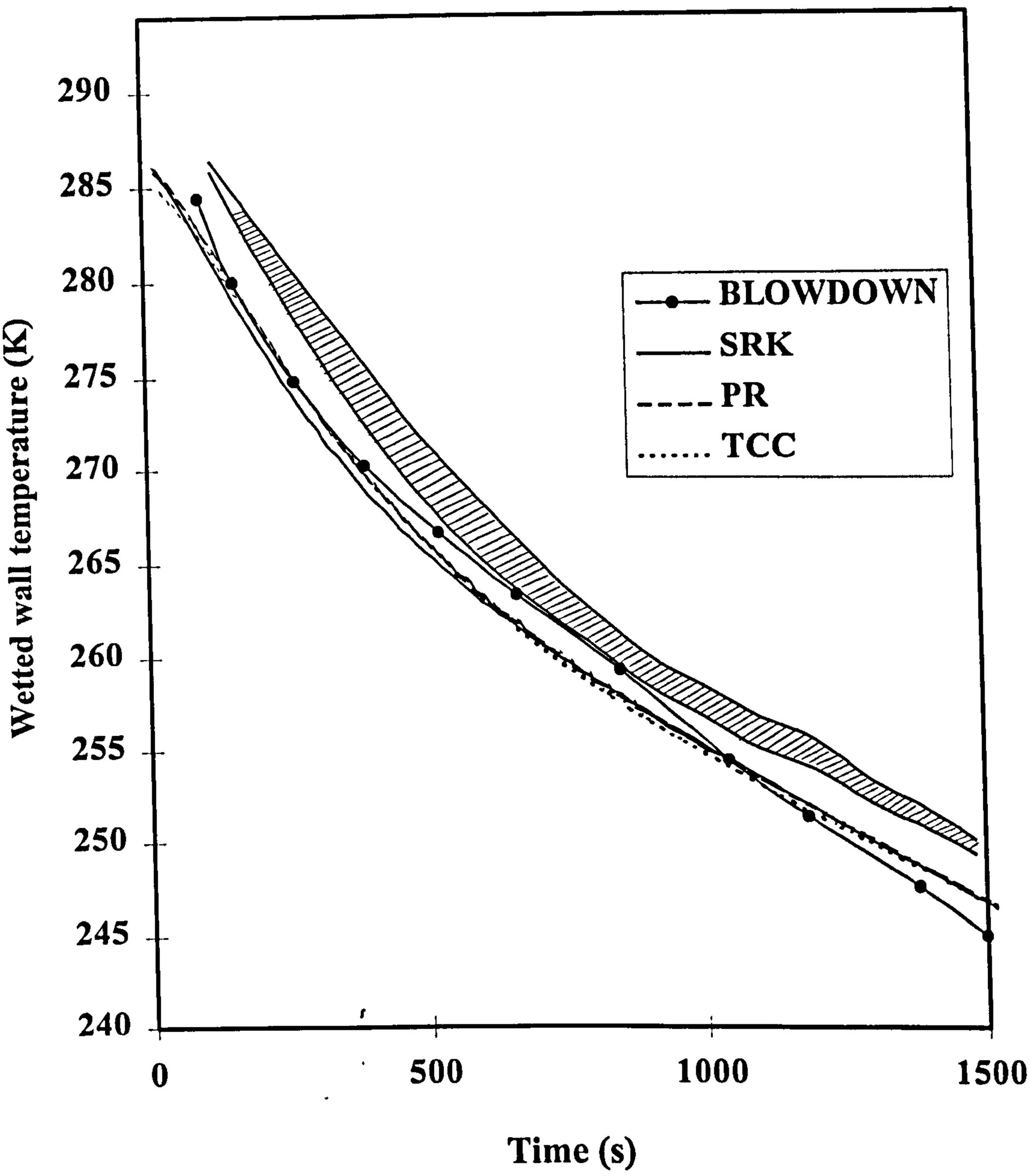

Figure 6.9.a **Comparison between measured (shaded area) and predicted wetted wall temperature/time profiles from BLOWDOWN and BLOWSIM based on various CEOS (SRK, PR and TCC CEOS) in conjunction with thermodynamic trajectory of considering work done by liquid phase within the vessel for condensable gas mixture (64 mole % C_1, 6 mole % C_2, 28 mole % n-C_3 and 2 mole % n-C_4).**

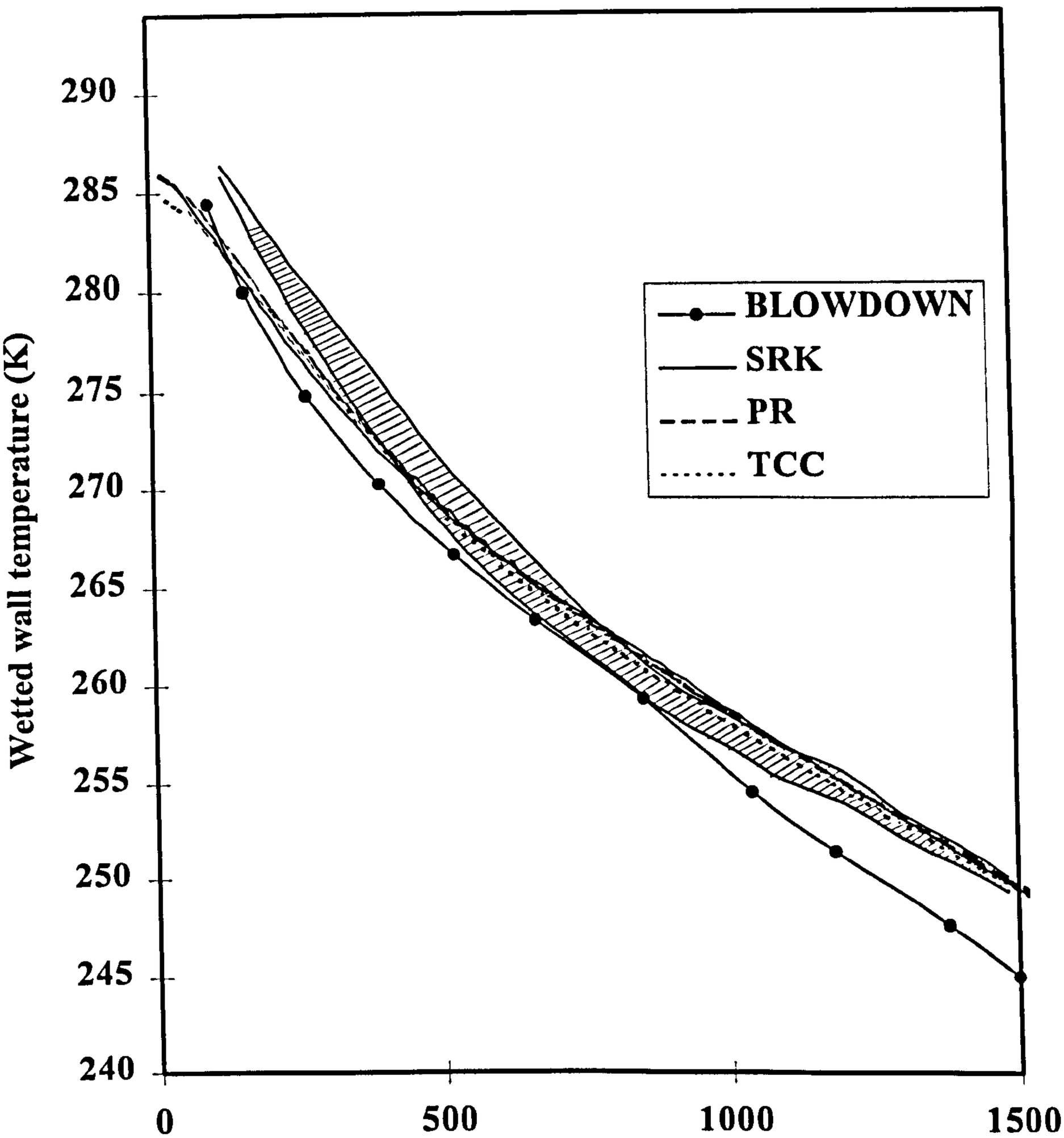

Figure 6.9.b **Comparison between measured (shaded area) and predicted wetted wall temperature/time profiles from BLOWDOWN and BLOWSIM based on various CEOS (SRK, PR and TCC CEOS) in conjunction with thermodynamic trajectory of discounting work done by liquid phase within the vessel for condensable gas mixture (64 mole % C_1, 6 mole % C_2, 28 mole % n-C_3 and 2 mole % n-C_4).**

Two-phase mixture (figures 6.10 - 6.13)

As mentioned earlier, in contrast to the condensable gas system, the work done by the liquid phase has negligible effect on blowdown results in the case of the two-phase mixture. This is probably because of the smaller pressure range at which this mixture is expanded as compared to that for the condensable gas (42 - 1 atm as compared to 116 - 1 atm) . The measured and BLOWDOWN predicted pressure/time profiles are not available.

Figure 6.10 shows the predicted bulk vapour temperature/time profiles based on BLOWSIM following the blowdown of the two-phase mixture. Also shown are the corresponding predictions based on BLOWDOWN. The experimental data only relate to the first 500 s of blowdown.

BLOWSIM predictions indicate that its performance is not too sensitive to the type of CEOS employed. Although BLOWSIM produces similar trends as the experimental as well as the predictions based on BLOWDOWN, it over-estimates the bulk vapour temperatures by a maximum of ca. 6 K. However, very similar values of minimum bulk vapour temperature are obtained from both models.

Figure 6.11 shows the corresponding temperature/time profiles for the unwetted wall. Once again the data indicate that the BLOWSIM's performance is insensitive to the chosen CEOS. In addition, the unwetted wall temperatures are predicted to ca. ± 2K using both models.

Figure 6.12 shows the predicted bulk liquid temperature/time profiles based on BLOWSIM in conjunction with all three CEOS as well as the results obtained based on BLOWDOWN. Unfortunately, no experimental data are available for comparison purposes. Both models predict similar trends whilst BLOWSIM estimates higher bulk liquid temperatures than BLOWDOWN with the maximum temperature difference being ca. 8K.

Figure 6.13 shows the comparison between measured wetted wall temperature/time profile for the last 500s of blowdown as compared to the predicted profiles from the two models. As before, BLOWSIM's performance is unaffected by the type of CEOS

employed. However, the model over estimates the wetted wall temperatures by ca. 8K. This is a direct consequence of the higher than expected bulk liquid temperatures predicted using this model (see figure 6.12).

The over estimations of both bulk liquid (figure 6.12) and wetted wall temperatures (figure 6.13) by BLOWSIM as compared to BLOWDOWN and/or experimental data are very likely attributed to the assumptions of instantaneous formation and immediate settlement of liquid droplets. In order to demonstrate the above, the estimated nucleation time and settling velocity related to the vapour within the vessel corresponding to the initial formation of liquid droplets are determined based on equations 3.4.6 and 3.4.7 respectively. The equilibrium mole fraction of liquid in the vapour phase based on TCC CEOS is 0.0098. The estimated nucleation time and settling velocity relative to the vapour are 102.04s and 0.06 m/s respectively. Additionally, the average gas velocity is 0.013 m/s. Hence, the estimated absolute settling velocity of liquid droplets is 0.047 m/s and the time required for the liquid droplets to settle gravitationally is equal to 68 s. The total time delay for formation of the liquid phase at the bottom of the vessel is therefore 170.04 s (=102.04 + 68). The mass ratio between vapour condensate and the liquid present at the bottom of the vessel is 0.12.

Ignoring the above delay results in predicting early addition of the heavier hydrocarbons to the liquid phase, especially during the early stage of blowdown. This in turn results in an over estimation of bulk liquid boiling point and hence higher than expected bulk liquid and wetted wall temperatures as observed in the case of BLOWSIM.

The liquid droplets formed during condensation are expected to be exposed to gravitational force, the effects of circulating motion of vapour (the corresponding flow pattern is given by figures 2.5 and 2.7) as well as the upward drag induced due to the motion of evaporating liquid (if liquid phase is present) and the discharging material through the orifice. With the exception of the gravitational force, when the amount of liquid droplets is small, the effect due to the above forces becomes

significant and most of the liquid droplets are likely to remain suspended in the vapour phase for a significant period of time during a given pressure increment.

In addition, the uncertainties associated with the method of determining the pseudo latent heat and the assumed parameters in Rohsensow's correlation (see equation 4.2.22 in chapter 4) may lead to inaccurate estimations of boiling heat flux for the liquid phase. If these fluxes are under estimated, then the wetted wall temperatures would be higher than expected.

However, it is important to note that the over estimation of BLOWSIM in predicting bulk liquid and wetted wall temperatures (figures 6.12 and 6.13) in conjunction with the two-phase mixture are not shown in the case of the condensable gas (figures 6.8 and 6.9). This is mainly because at the onset of condensation, the mass ratio between the amount of condensate in the vapour phase and the accumulated liquid at the bottom of the vessel is significantly higher in the case of the two-phase mixture. The data in figure 6.14 showing the variation of this ratio as a function of time during blowdown for the two systems confirm this. Hence the effects of ignoring any delay in the formation followed by settling of condensate into the liquid becomes especially important in the case of the two-phase mixture.

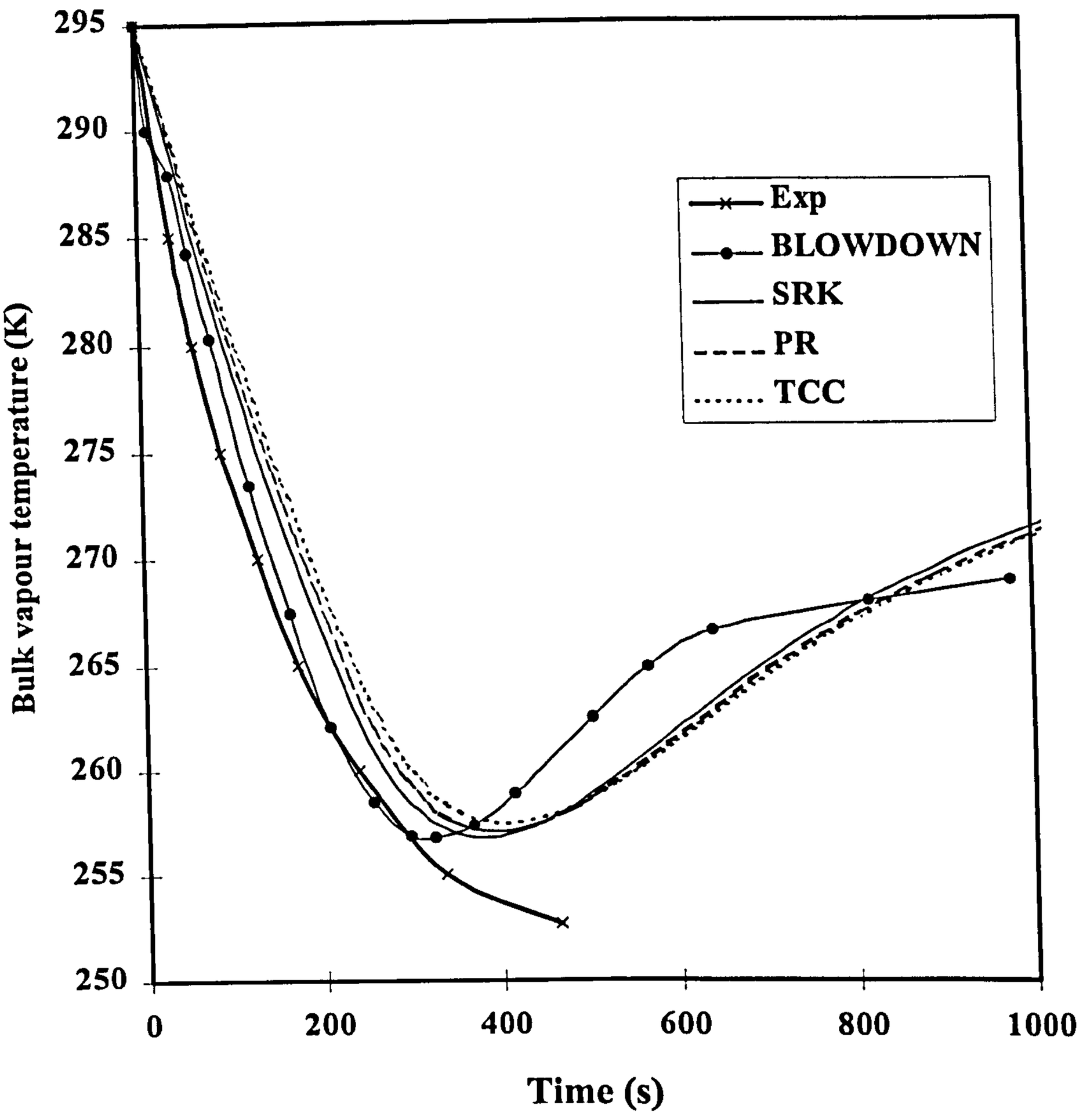

Figure 6.10 **Comparison between measured (Exp) and predicted bulk vapour temperature/time profiles from BLOWDOWN and BLOWSIM based on various CEOS (SRK, PR and TCC CEOS) in conjunction with thermodynamic trajectory of considering work done by liquid phase within the vessel for two-phase mixture (64 mole % C_1, 6 mole % C_2, 28 mole % n-C_3 and 2 mole % n-C_4).**

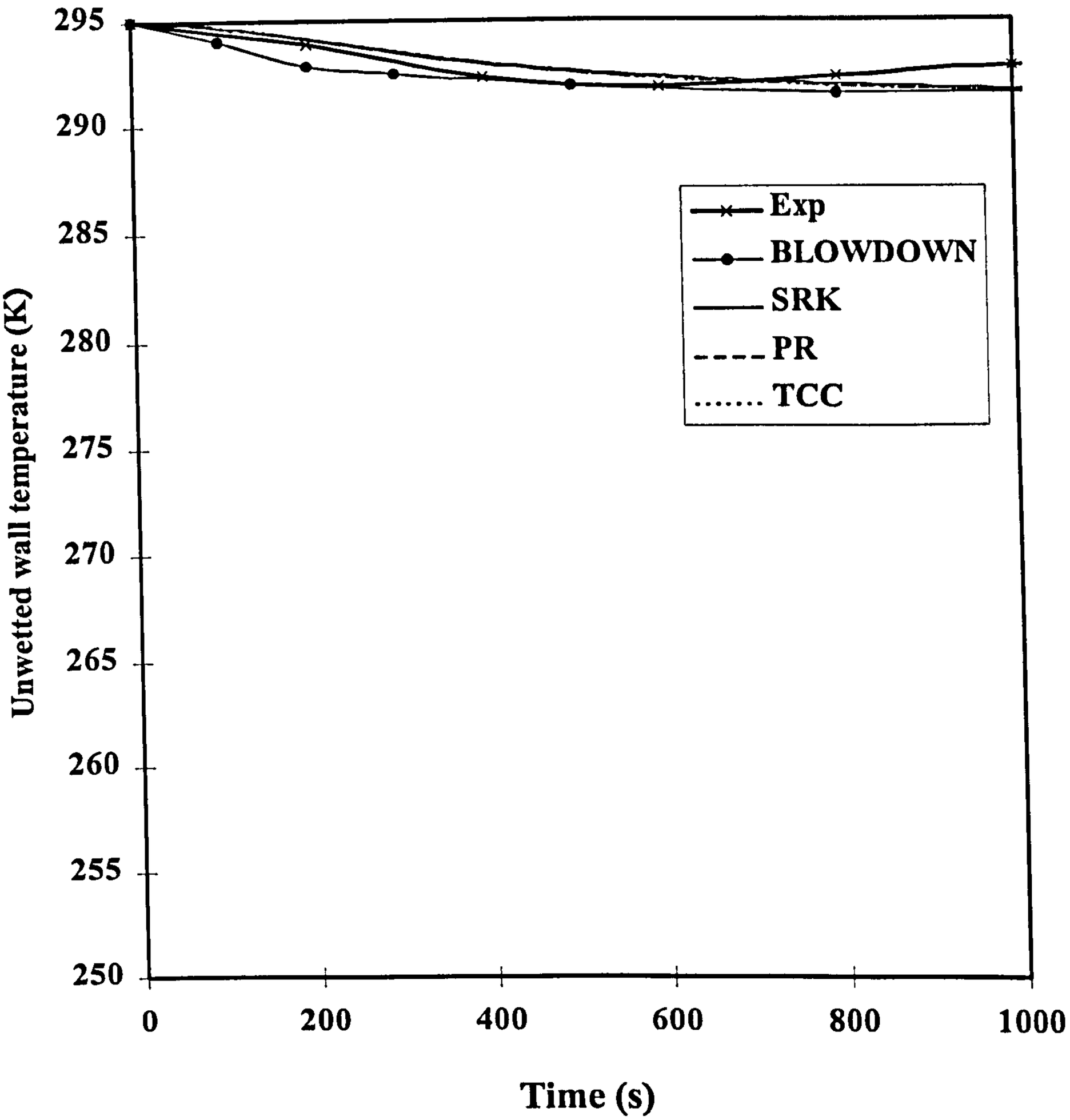

Figure 6.11 **Comparison between measured (Exp) and predicted unwetted wall temperature/time profiles from BLOWDOWN and BLOWSIM based on various CEOS (SRK, PR and TCC CEOS) in conjunction with thermodynamic trajectory of considering work done by liquid phase within the vessel for two-phase mixture (64 mole % C_1, 6 mole % C_2, 28 mole % n-C_3 and 2 mole % n-C_4).**

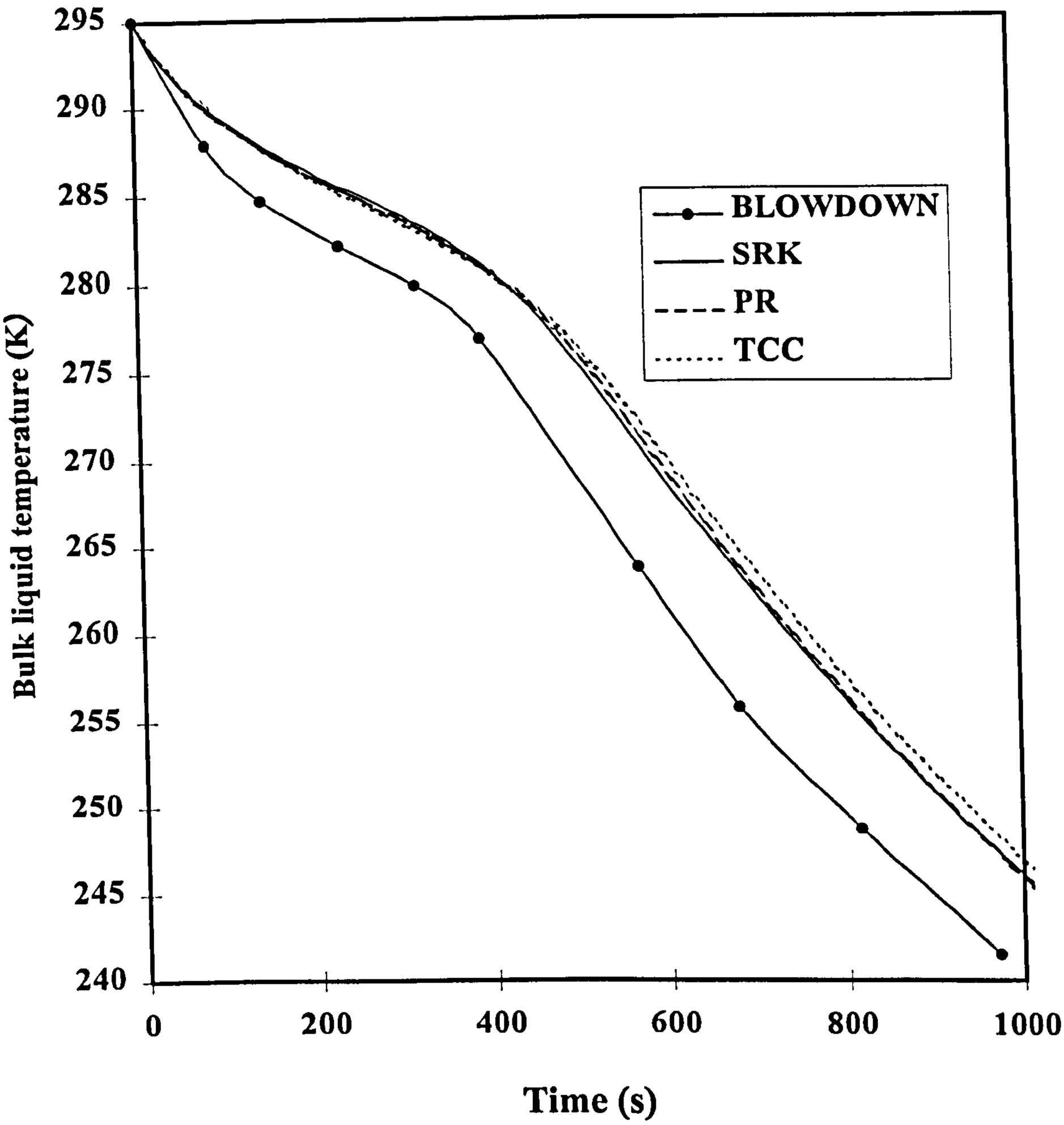

Figure 6.12 **Comparison between predicted bulk liquid temperature/time profiles from BLOWDOWN and BLOWSIM based on various CEOS (SRK, PR and TCC CEOS) in conjunction with thermodynamic trajectory of considering work done by liquid phase within the vessel for two-phase mixture (64 mole % C_1, 6 mole % C_2, 28 mole % n-C_3 and 2 mole % n-C_4).**

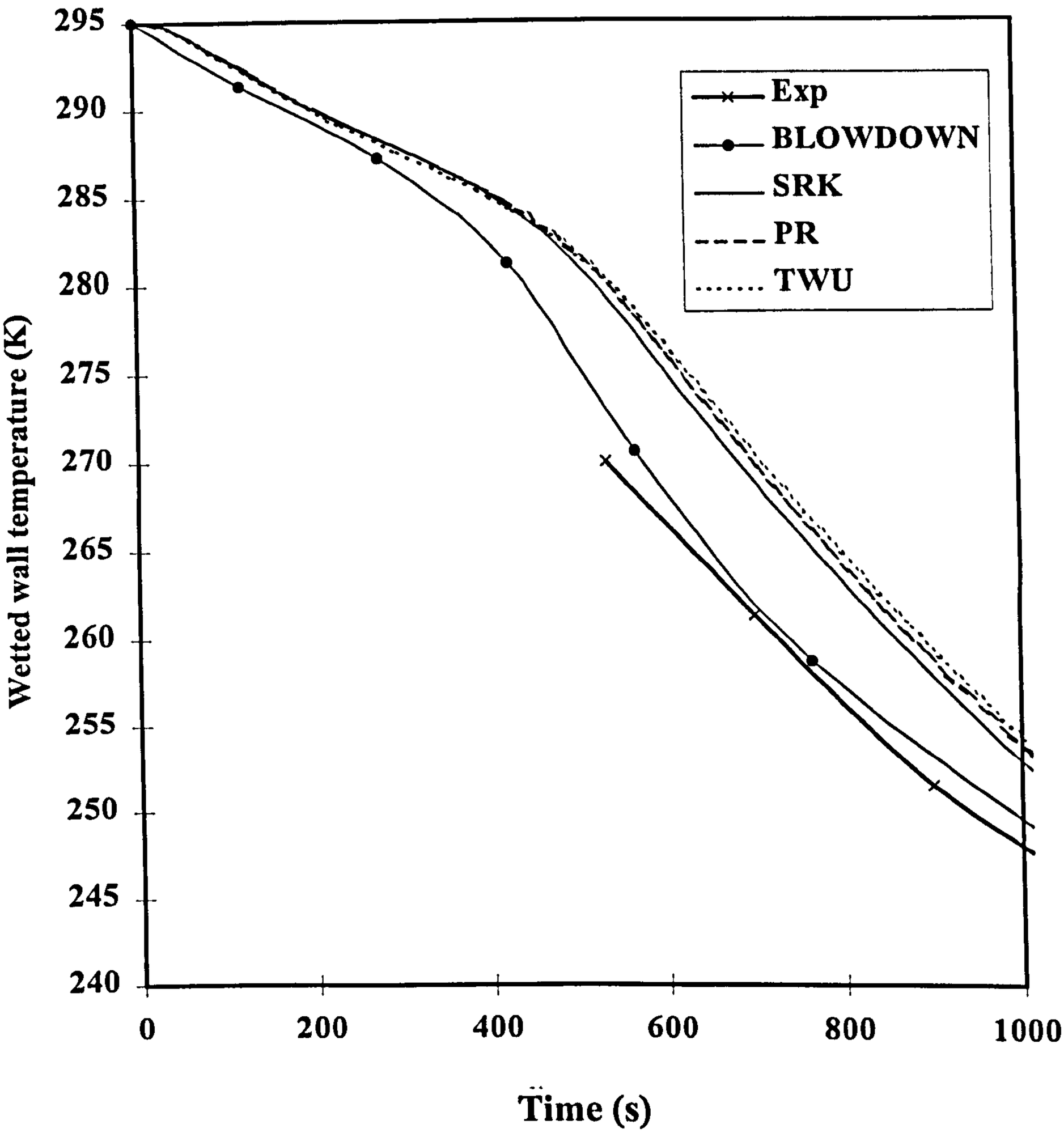

Figure 6.13 **Comparison between measured (Exp) and predicted wetted wall temperature/time profiles from BLOWDOWN and BLOWSIM based on various CEOS (SRK, PR and TCC CEOS) in conjunction with thermodynamic trajectory of considering work done by liquid phase within the vessel for two-phase mixture (64 mole % C_1, 6 mole % C_2, 28 mole % n-C_3 and 2 mole % n-C_4).**

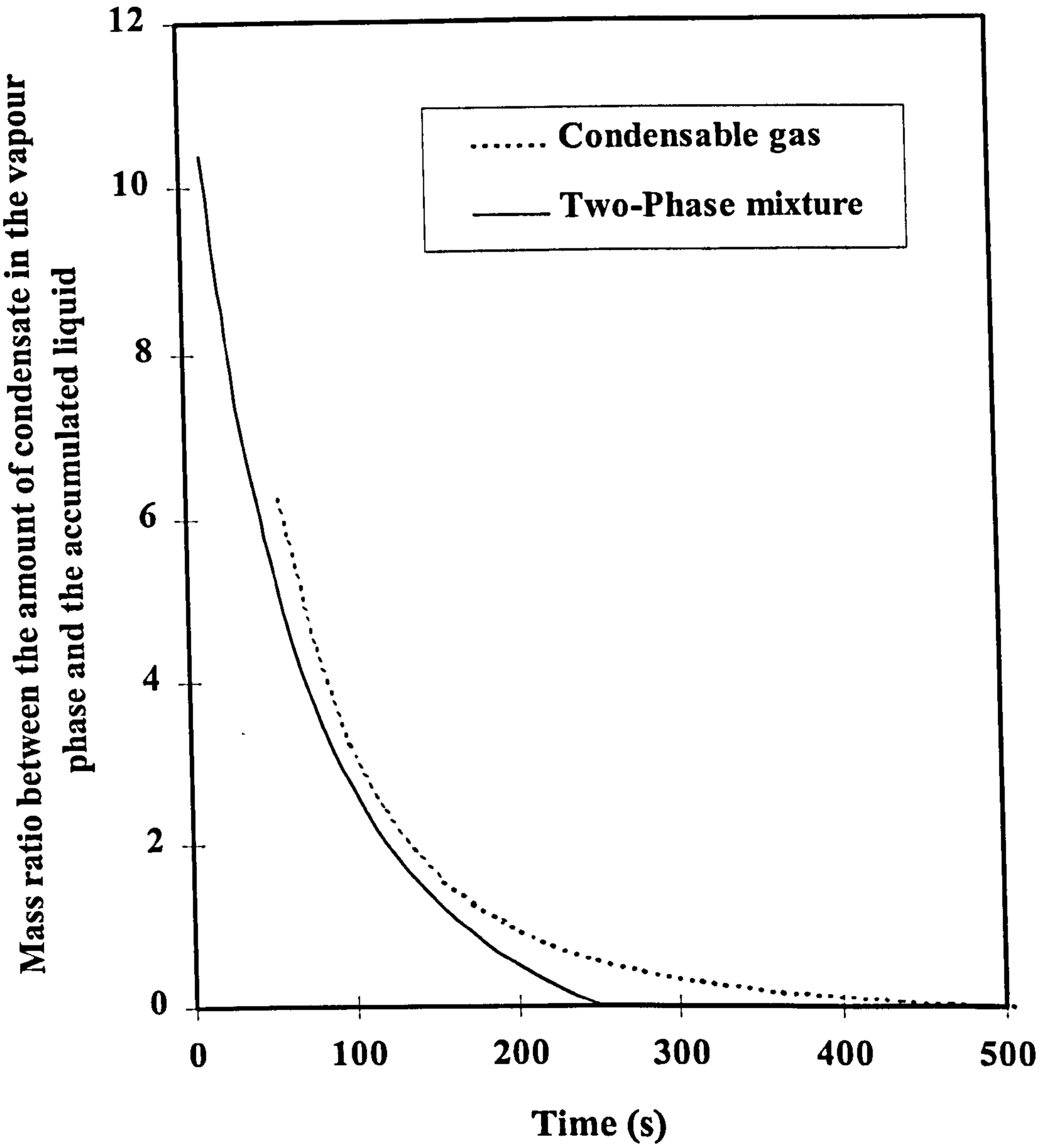

Figure 6.14 **Variations of mass ratio between the amount of condensate in the vapour phase and the accumulated liquid at the bottom of the vessel against time for two-phase mixture and condensable gas (64 mole % C_1, 6 mole % C_2, 28 mole % n-C_3 and 2 mole % n-C_4).**

6.2.4.2 Effect of Selecting Constant Heat Transfer Coefficients between Liquid and Wetted Wall on Blowdown Simulations

In this section, the effect of assuming constant values of heat transfer coefficients between the liquid phase and the vessel wall on BLOWSIM's performance are evaluated by comparison with field data as well as those predicted on the basis of Rohsenow's correlation presented in the previous section. The simulations are conducted in conjunction with the condensable gas and two-phase mixtures (see table 6.1) incorporating TCC CEOS and accounting for the work done by liquid phase within the vessel. Heat transfer coefficients in the ranges determined experimentally by Overa et al. [1994] are chosen.

Condensable gas (figures 6.15 - 6.19)

Figure 6.15 shows predicted vessel pressure/time profiles for the condensable gas based on constant heat transfer coefficients of 1000, 2000 and 3000 W/m^2K between the liquid phase and vessel wall. Also shown in the same figure is the experimental data and predictions from BLOWSIM based on Rohsenow's correlation. Analogous comparisons for temperature/time profiles of bulk vapour and unwetted wall together with bulk liquid and wetted wall are shown in figures 6.16 to 6.19 respectively.

The above figures demonstrate that in the case of the condensable gas mixture, within the ranges tested, BLOWSIM's performance is relatively insensitive to the magnitude of the chosen heat transfer coefficient. At any given time, despite a three fold increase in the heat transfer coefficient, the maximum difference in the predicted temperatures is only ca. 2K which is observed in the case of the wetted wall temperature response; figure 6.19.

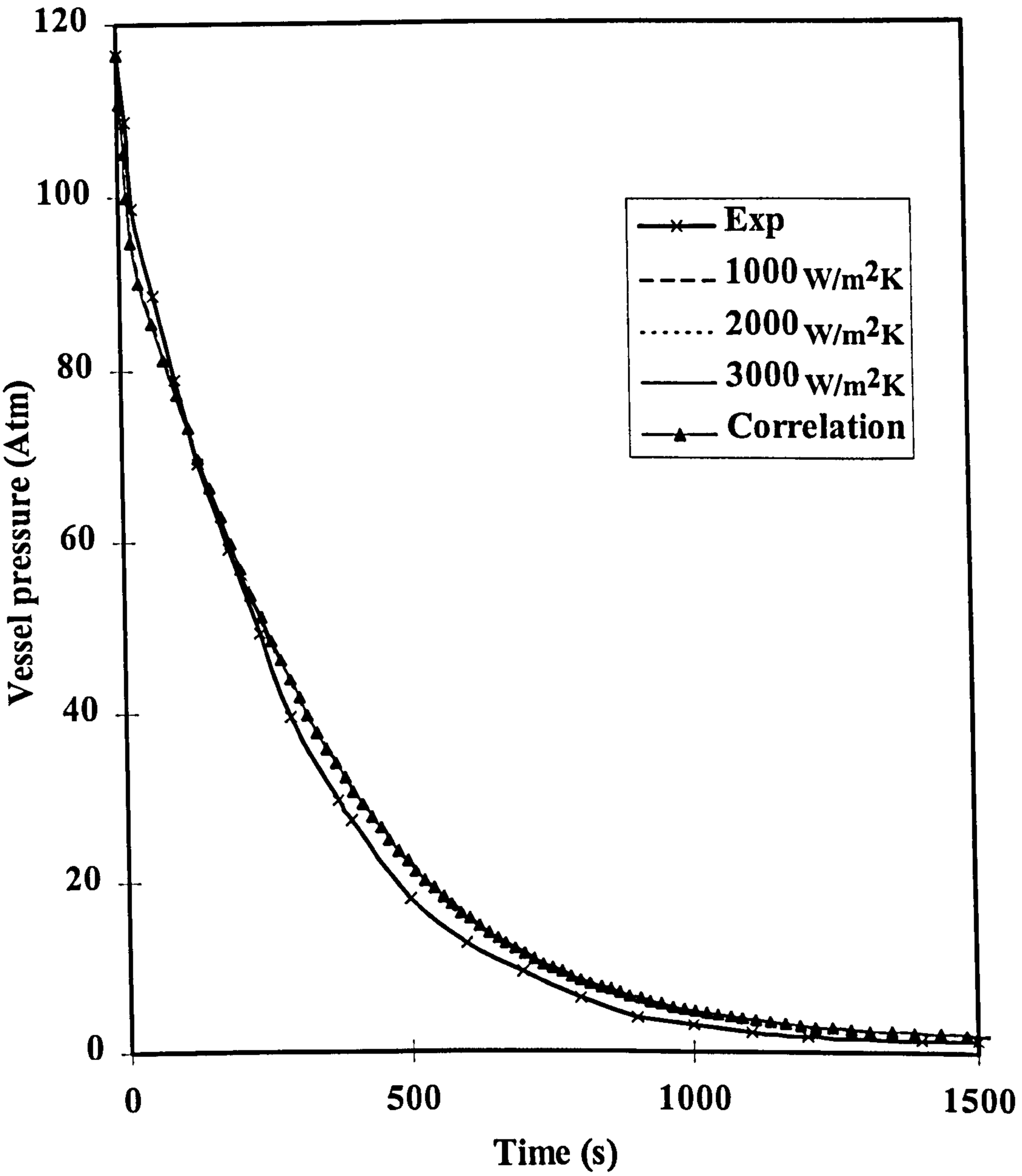

Figure 6.15 Comparison between measured (Exp) and predicted pressure/time profiles from BLOWSIM based on Rohsenow's correlation (Correlation) for predicting boiling heat flux of liquid phase and various constant heat transfer coefficients between liquid phase and vessel wall (1000, 2000 and 3000 W/m^{2}K) for a condensable gas mixture (64 mole % C_1, 6 mole % C_2, 28 mole % n-C_3 and 2 mole % n-C_4)

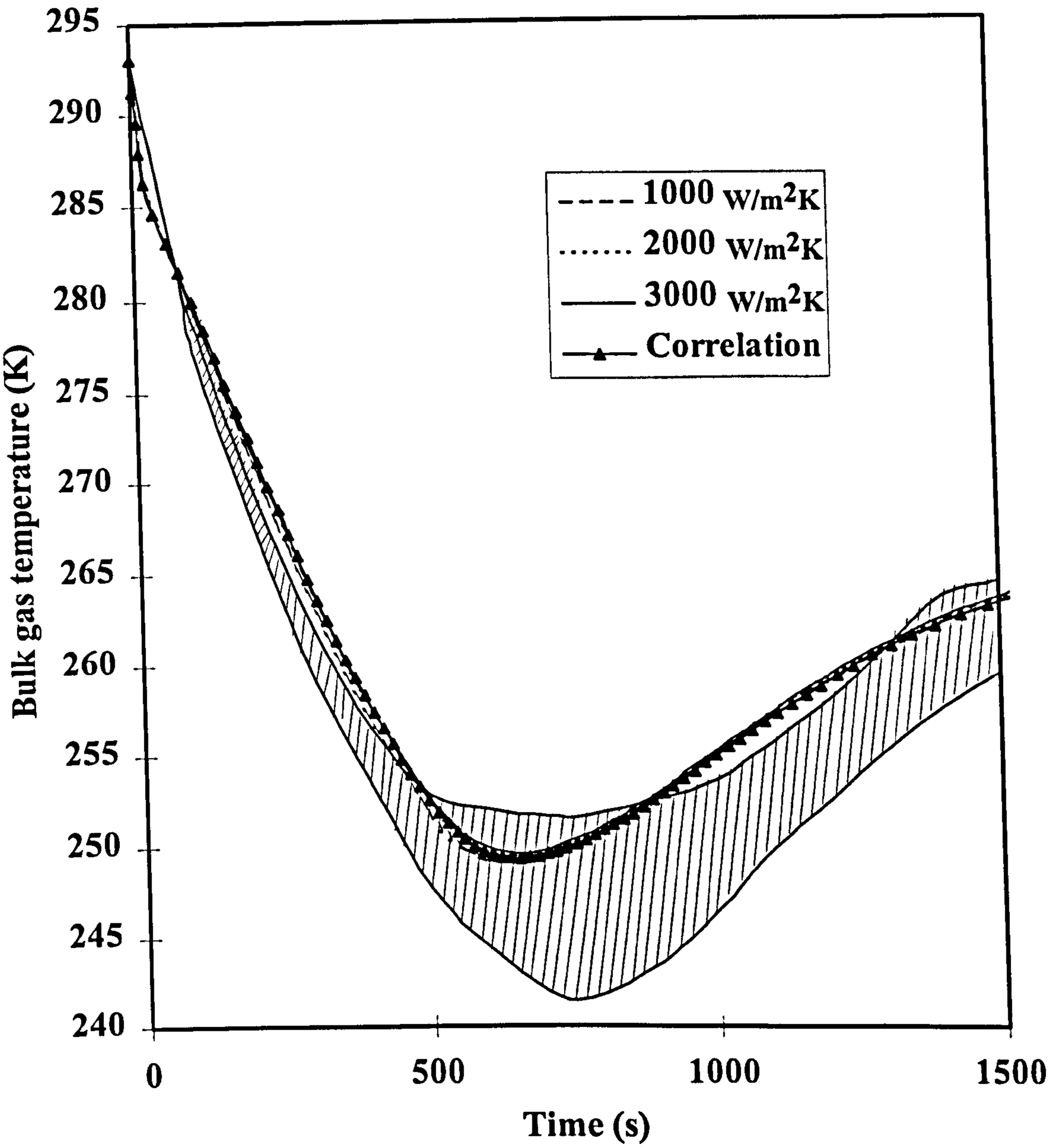

Figure 6.16 Comparison between measured (shaded area) and predicted bulk vapour temperature/time profiles from BLOWSIM based on Rohsenow's correlation (Correlation) for predicting boiling heat flux of liquid phase and various constant heat transfer coefficients between liquid phase and vessel wall (1000, 2000 and 3000 W/m^2K) for condensable gas mixture (64 mole % C_1, 6 mole % C_2, 28 mole % n-C_3 and 2 mole % n-C_4).

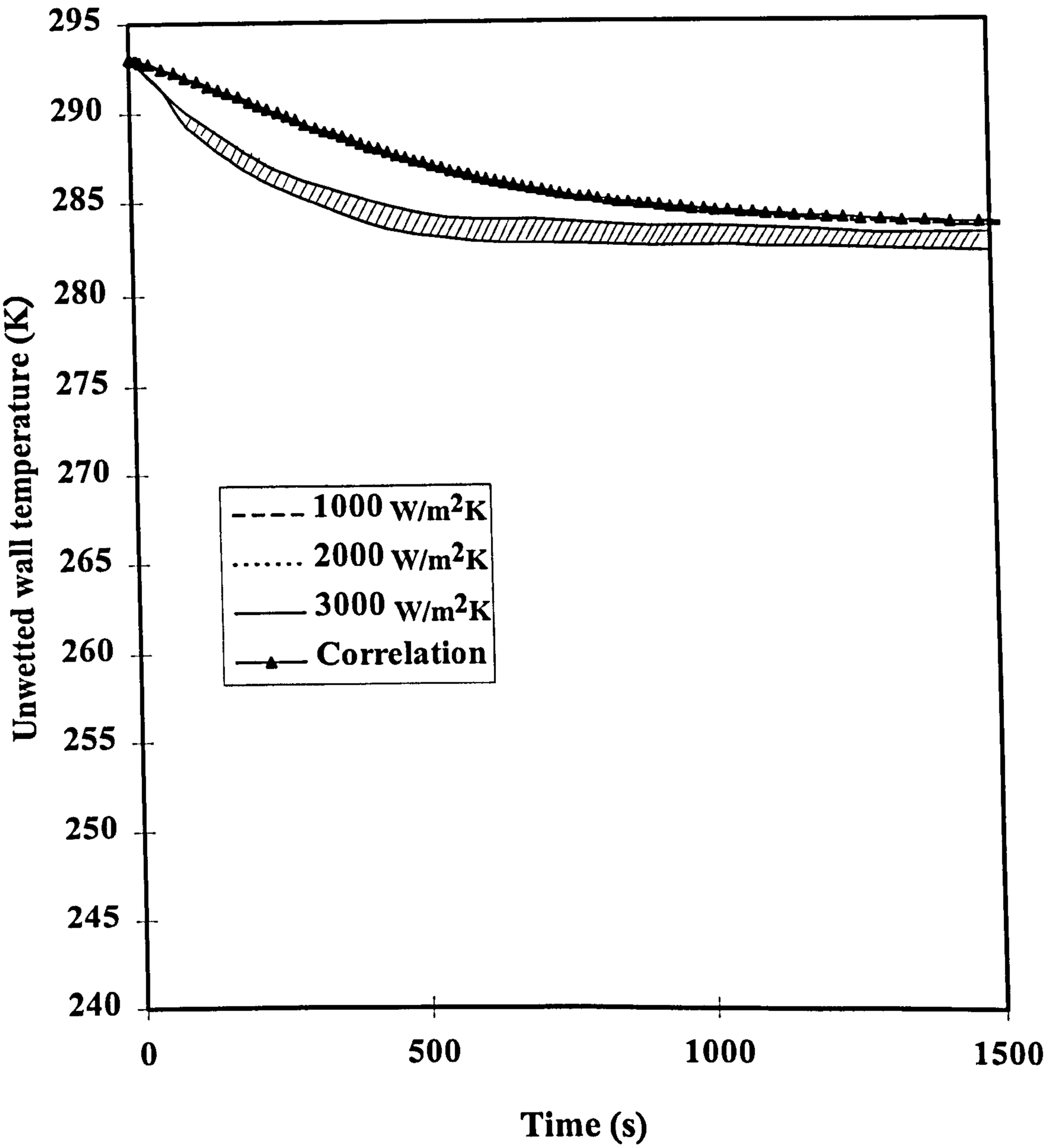

Figure 6.17 Comparison between measured (shaded area) and predicted unwetted wall temperature/time profiles from BLOWSIM based on Rohsenow's correlation (Correlation) for predicting boiling heat flux of liquid phase and various constant heat transfer coefficients between liquid phase and vessel wall (1000, 2000 and 3000 W/m^2K) for condensable gas mixture (64 mole % C_1, 6 mole % C_2, 28 mole % n-C_3 and 2 mole % n-C_4).

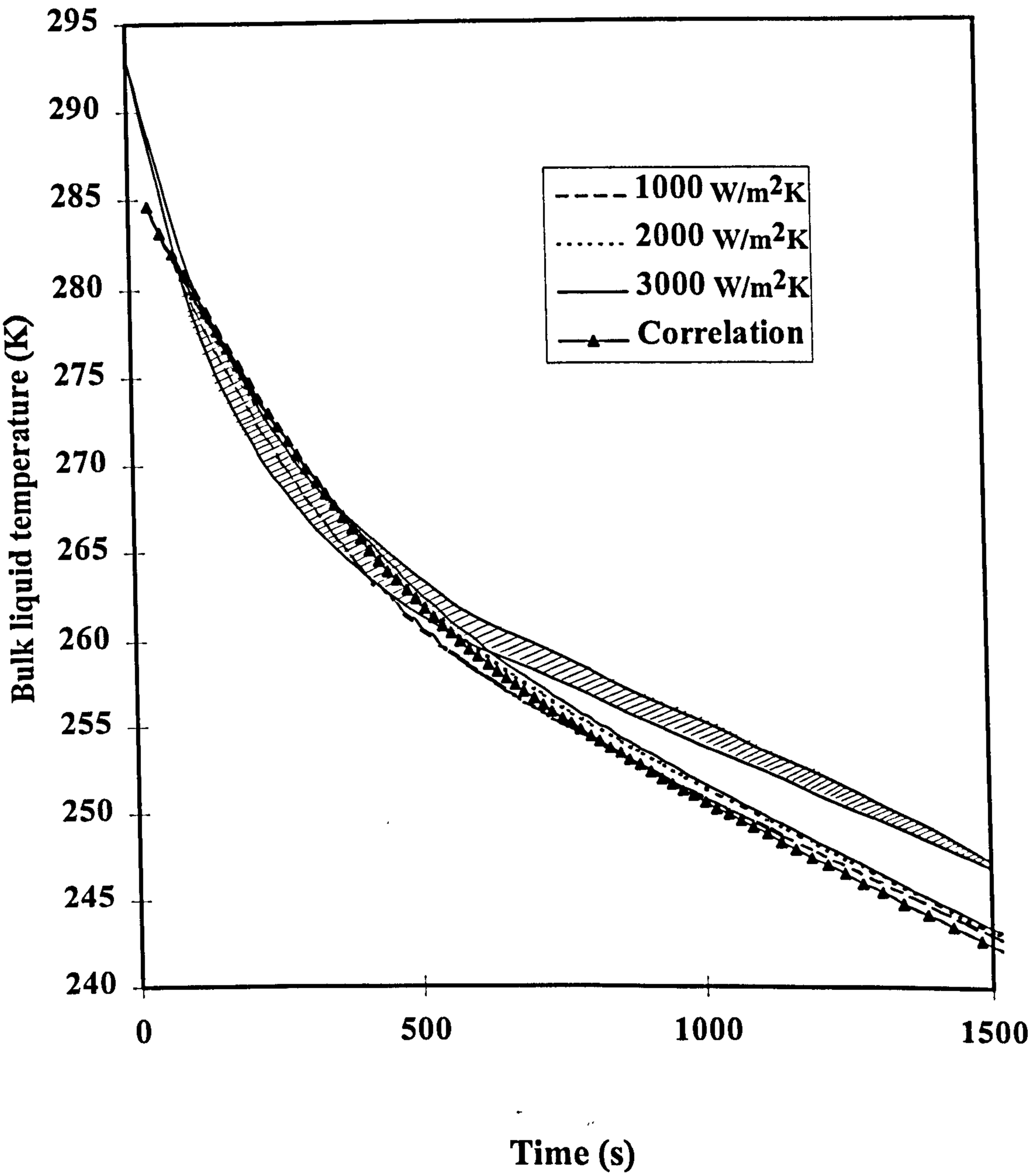

Figure 6.18 Comparison between measured (shaded area) and predicted bulk liquid temperature/time profiles from BLOWSIM based on Rohsenow's correlation (Correlation) for predicting boiling heat flux of liquid phase and various constant heat transfer coefficients between liquid phase and vessel wall (1000, 2000 and 3000 W/m^2K) for condensable gas mixture (64 mole % C_1, 6 mole % C_2, 28 mole % n-C_3 and 2 mole % n-C_4).

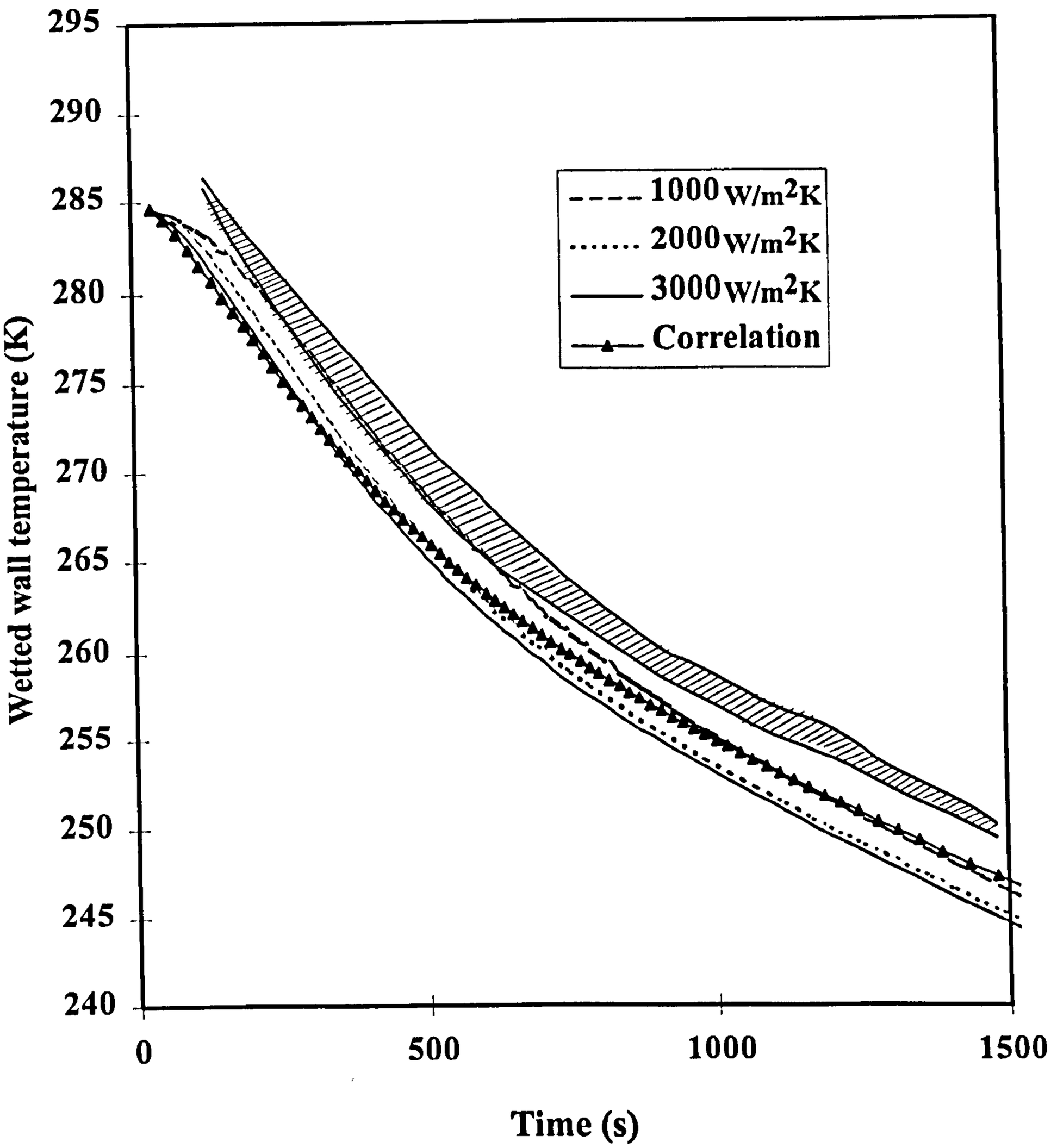

Figure 6.19 Comparison between measured (shaded area) and predicted wetted wall temperature/time profiles from BLOWSIM based on Rohsenow's correlation (Correlation) for predicting boiling heat flux of liquid phase and various constant heat transfer coefficients between liquid phase and vessel wall (1000, 2000 and 3000 W/m^2K) for condensable gas mixture (64 mole % C_1, 6 mole % C_2, 28 mole % n-C_3 and 2 mole % n-C_4).

Two-phase mixture (figures 6.20 - 6.23)

Figures 6.20 and 6.21 respectively show the predicted time/temperature profiles for bulk vapour and the unwetted wall following the blowdown of the two-phase mixture as compared to experimental data. Figure 6.22 on the other hand shows the corresponding data for the bulk liquid temperatures. In this case, due to the absence of the appropriate experimental results, these data are compared with those predicted from BLOWDOWN. The predicted and measured time/temperature profiles for wetted wall are shown in figure 6.23.

Referring to figures 6.20 - 6.22, it is clear that the use of various constant heat transfer coefficients between the liquid phase and vessel wall leads to very similar bulk gas, unwetted wall and bulk liquid temperature/time predictions. The closest agreement with the measured data is obtained for the bulk vapour temperature when using Rohsenow's correlation .

However, the data in figure 6.23 indicate that BLOWSIM's performance in predicting the wetted wall temperature is relatively sensitive to the magnitude of the heat transfer coefficient particularly during the latter stages of blowdown. In general, agreement between theory and experiment improves with an increase in the heat transfer coefficient, with the magnitude of the effect becoming less important as the heat transfer coefficient increases. In the limit, the results based on a heat transfer coefficient of 3000 W/m^2K converge with those based on Rohensenow's correlation.

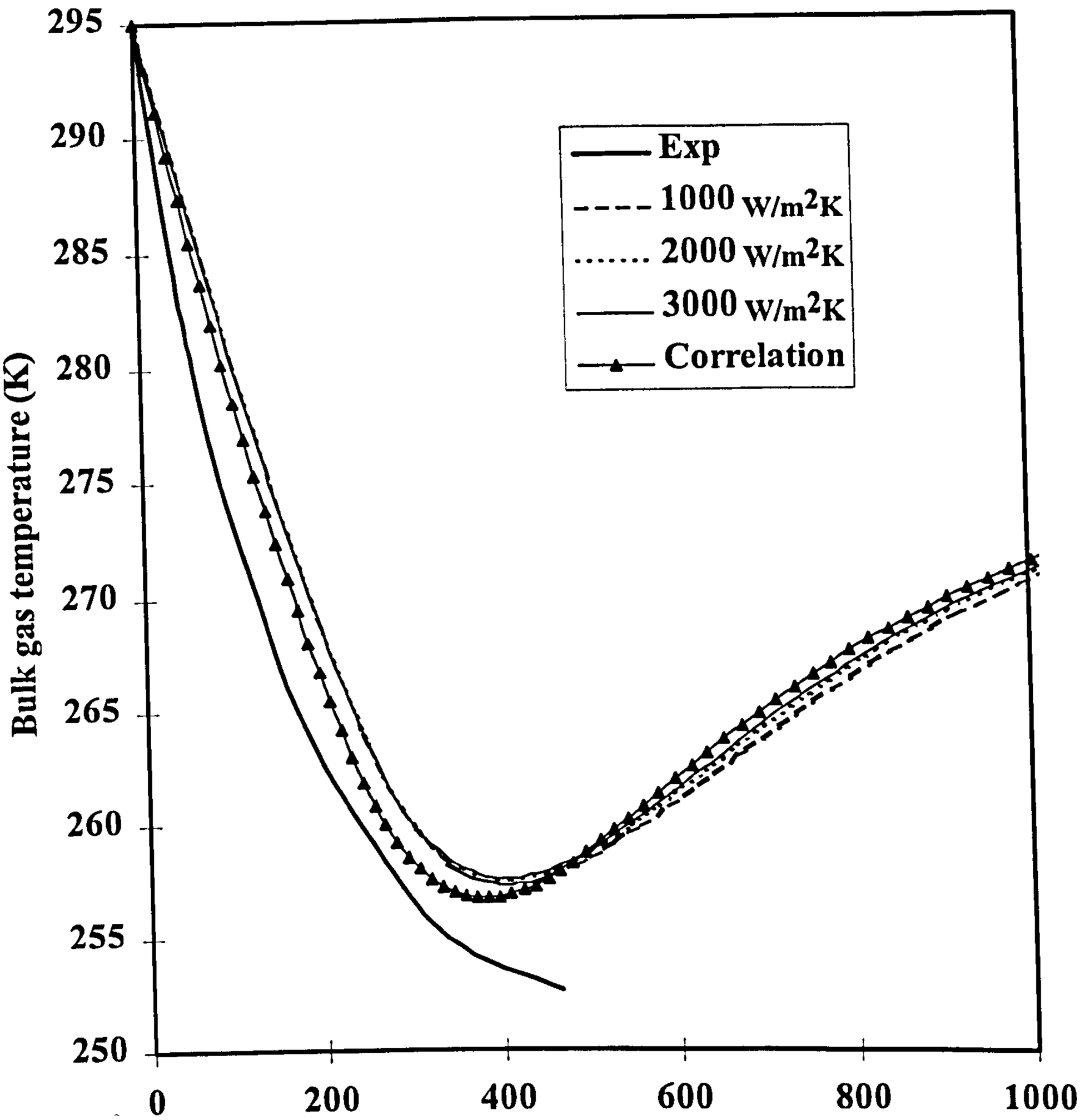

Figure 6.20 Comparison between measured (Exp) and predicted bulk vapour temperature/time profiles from BLOWSIM based on Rohsenow's correlation (Correlation) for predicting boiling heat flux of liquid phase and various constant heat transfer coefficients between liquid phase and vessel wall (1000, 2000 and 3000 W/m^{2}K) for two-phase mixture (64 mole % C_1, 6 mole % C_2, 28 mole % n-C_3 and 2 mole % n-C_4).

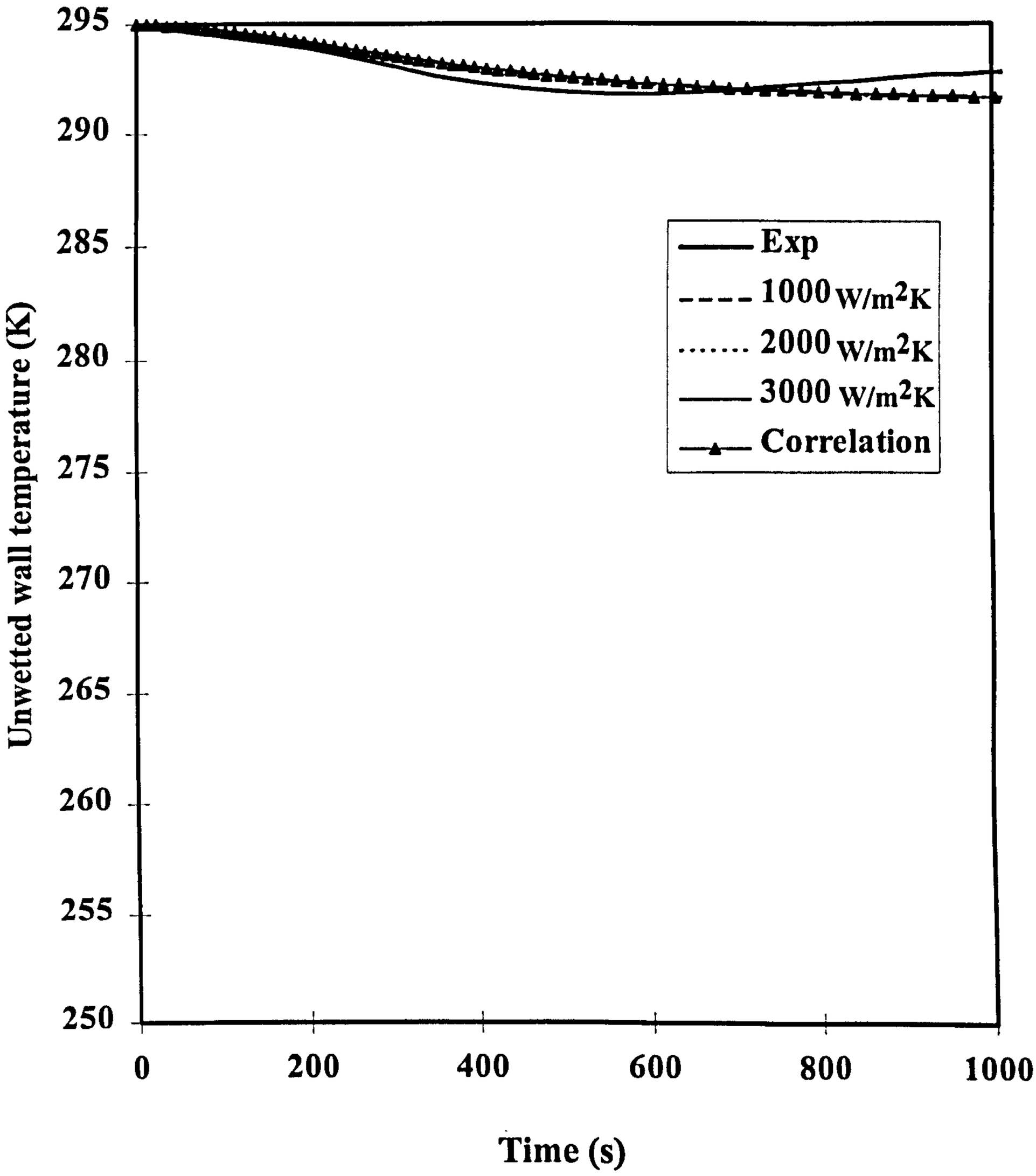

Figure 6.21 **Comparison between measured inner (Exp) and average unwetted wall temperature/time profiles from BLOWSIM based on Rohsenow's correlation (Correlation) for predicting boiling heat flux of liquid phase and various constant heat transfer coefficients between liquid phase and vessel wall (1000, 2000 and 3000 W/m^2K) for two-phase mixture (64 mole % C_1, 6 mole % C_2, 28 mole % n-C_3 and 2 mole % n-C_4).**

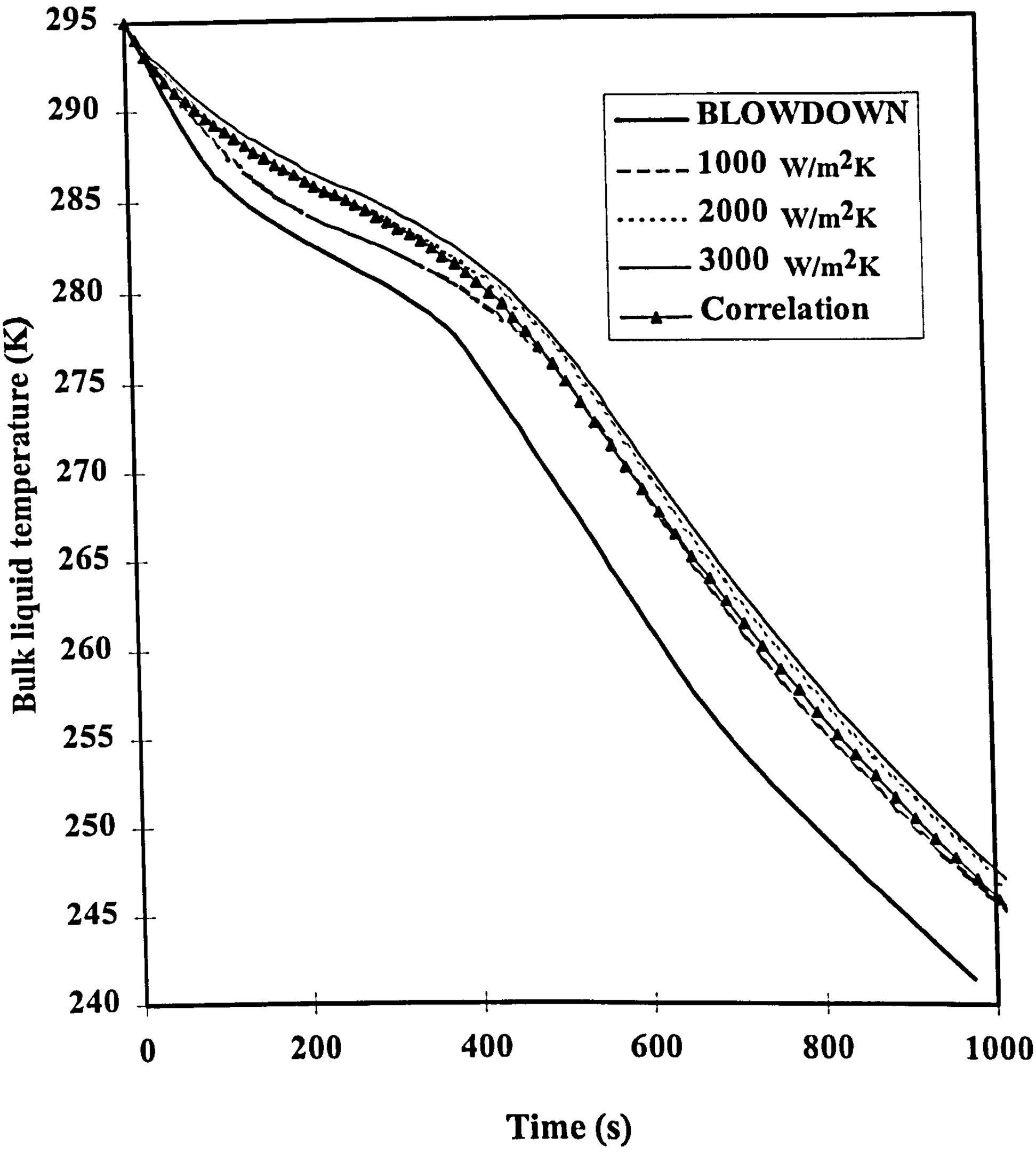

Figure 6.22 **Comparison between predicted bulk liquid temperature/time profiles from BLOWDOWN and BLOWSIM based on Rohsenow's correlation (Correlation) for predicting boiling heat flux of liquid phase and various constant heat transfer coefficients between liquid phase and vessel wall (1000, 2000 and 3000 W/m^2K) for two-phase mixture (64 mole % C_1, 6 mole % C_2, 28 mole % n-C_3 and 2 mole % n-C_4).**

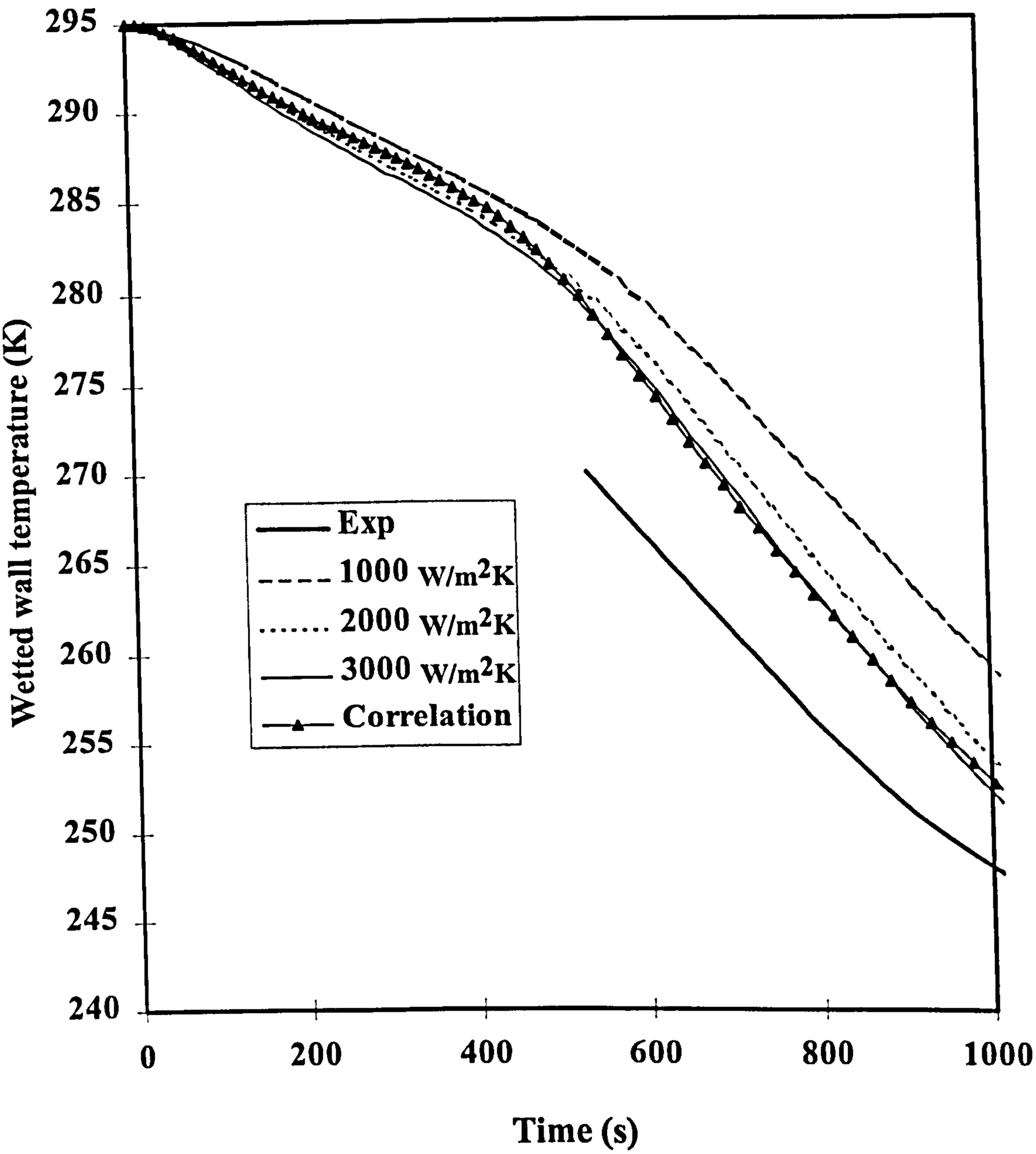

Figure 6.23 Comparison between measured inner (Exp) and average wetted wall temperature/time profiles from BLOWSIM based on Rohsenow's correlation (Correlation) for predicting boiling heat flux of liquid phase and various constant heat transfer coefficients between liquid phase and vessel wall (1000, 2000 and 3000 W/m^2K) for two-phase mixture (64 mole % C_1, 6 mole % C_2, 28 mole % n-C_3 and 2 mole % n-C_4).

6.2.5 Effects of Assuming Ideal Gas at the Orifice on Blowdown Predictions and Computational Efficiency

As mentioned in chapter 3, apart from BLOWDOWN, none of the models reviewed account for two-phase flow at the orifice during blowdown. In most cases, the fluid flowing through the orifice is assumed to remain in the vapour phase and the discharge rate is calculated on the basis of an ideal gas in conjunction with an estimated compressibility factor. Table 6.2 demonstrates the implications of the above in terms of predicting the minimum fluid, vessel wall and orifice temperatures for the non-condensable gas, two-phase and condensable gas mixtures. Also included in the table are the corresponding computational work loads (CPU time). The data were generated using BLOWSIM in conjunction with TCC EOS.

From the table 6.2 it is clear that ignoring two-phase flow at the orifice has negligible effect on the minimum temperatures associated with the fluid and vessel wall. There is also a significant reduction in CPU times. However, the minimum fluid temperatures at the orifice are consistently underestimated. The latter may give rise to engineering problems as well as leading to incorrect down-stream conditions.

Table 6.2 Predicted minimum temperatures and CPU time for the two-phase mixture, non-condensable and condensable gases from BLOWSIM based on ideal gas (Ideal) or real fluid (Real) approaches at the orifice

	Non-Condensable gas		Condensable gas		Two-Phase mixture	
	Ideal	Real	Ideal	Real	Ideal	Real
CPU time (s)	4.5	13.7	12.5	79.5	10.7	54.2
Min. vapour temp. (K)	258.7	260.0	248.6	249.3	256.6	257.4
Min. unwetted wall temp (K)	289.6	289.4	283.6	283.7	291.5	291.7
Min. liquid temp. (K)	N/A	N/A	245.3	242.7	245.5	247.9
Min. wetted wall temp (K)	N/A	N/A	248.1	247.1	253.0	255.3
Min. fluid temp. at orifice (K)	194.6	222.6	148.9	224.9	221.9	231.2

6.3 CONCLUSIONS

In this chapter, we evaluated the performance of BLOWSIM based on SRK, PR and TCC CEOS compared with predictions from BLOWDOWN and experimental data for a non-condensable gas, condensable gas and a two-phase mixture. In addition, the effects of the following on the performance of BLOWSIM in terms of predicting field data were investigated:

- ☞ discounting and accounting for the work done by the liquid phase within the vessel
- ☞ assuming constant heat transfer coefficient between the liquid phase and the associated section of vessel wall
- ☞ application of ideal gas assumption at the discharge orifice.

The important conclusions drawn based on the ranges tested are as follows :

- BLOWSIM's predictions are shown to be insensitive to the type of CEOS employed (SRK, PR and TCC CEOS). This is despite the fact that in chapter 5, it was shown that TCC CEOS performs very differently from SRK and PR CEOS in terms of predicting vapour and liquid speeds of sound at $P_r > 3$ and $T_r \leq 0.6$ respectively (see figures 5.4 - 5.9). Outside these ranges, similar predictions are obtained. In order to investigate the above, T_r and P_r for each fluid phase at the conditions within the vessel during the depressurisation process are determined. The estimated fluid composition and critical conditions are based on SRK CEOS. The results for all three blowdown systems are summarised in table 6.3 as follows.

Table 6.3 Predicted T_r and P_r from BLOWSIM based on SRK CEOS for each fluid phase in the vessel during blowdown of the two-phase mixture, non-condensable and condensable gases

Fluid	Vapour Phase		Liquid Phase	
	T_r	P_r	T_r	P_r
Non-condensable gas	1.03 - 0.88	1.24 - 0.01	N/A	N/A
Condensable gas	1.11 - 0.77	1.21 - 0.03	0.92 - 0.66	0.98 - 0.05
Two-phase mixture	1.04 - 0.79	0.43 - 0.02	0.82 - 0.64	0.71 - 0.04

On the basis of table 6.3, the insensitivity of BLOWSIM's performance on the type of CEOS employed is likely attributed to the fact that T_r and P_r, for a given fluid phase, are outside the conditions mentioned above.

- BLOWSIM predicts very accurate vessel pressure/time profiles. Also, the bulk vapour and unwetted wall temperatures are predicted to within 7K and 4K respectively. It appears that Overa et al.'s vapour phase thermodynamic trajectory is applicable to high pressure blowdown (ca. 120 atm). In addition, the effects due to temperature gradient across the thickness of the vessel wall and forced convection within the vapour phase can be ignored.

- In the case of the condensable gas, BLOWSIM, either discounting or accounting for work done by the liquid phase in the vessel, predicts the bulk liquid and wetted wall temperatures to ±5K. The earlier formation of liquid phase predicted from BLOWSIM as compared to BLOWDOWN is attributed to the use of different types of EOS rather than the assumptions of instantaneous formation and immediate settlement of liquid droplets condensed from the vapour phase employed in the former model.

- In the case of the two-phase mixture, BLOWSIM consistently over estimates the bulk liquid and wetted wall temperatures by maximum 8K. This is likely to be due to the assumptions of instantaneous formation and immediate settlement of liquid droplets condensed from the vapour phase. Consequently, similar errors are likely to be encountered when the amount of liquid formed prior to blowdown or at the first instant of condensation in the vessel is not sufficiently large to overcome the effects of subsequent condensation on the mass and energy balances of the liquid phase. Hence, the nucleation time and settling velocity for liquid droplets should be considered. Further investigations on the validity of Haque et al. [1992a] equations in predicting these two parameters for systems outside the range of correlation are required.

- The main mode of heat transfer between the liquid phase and vessel wall is nucleate boiling. The corresponding heat flux can be sufficiently represented by assuming the heat transfer coefficient between liquid and wall is constant. Hence,

it is not essential to use Rohsensow's correlation for predicting the corresponding heat flux. The recommended values of heat transfer coefficient are 2000 - 3000 W/m^2K.

- Based on the assumption of negligible temperature gradients across thickness of the vessel wall, we are able to obtain reasonably good predictions for both liquid and average wetted wall temperatures. However, nucleate boiling between the liquid phase and vessel wall is expected to result in rather a significant temperature difference across the vessel wall. By assuming boiling heat transfer coefficient of 3000 W/m^2K and steady-state conduction, we calculate that the maximum temperature differences across the wetted vessel wall for condensable gas and two-phase mixture are 10K and 16K respectively.

- For the condensable gas, the work done by the liquid phase should be considered. Conversely, the work done can be neglected in the case of the two-phase mixture.

- CPU time can be significantly reduced (by at least two thirds) by assuming ideal gas behaviour at the orifice without affecting accuracy in predicting the minimum fluid and wall temperatures. However, it is important to note that the minimum fluid temperatures at the orifice for all three mixtures are consistently underestimated. This may give rise to engineering problems as well as leading to incorrect down-stream conditions.

In conclusion, based on the limited amount of experimental data available, the CEOS tested are shown to be applicable for simulation of high pressure (ca. 120 atm) blowdown for hydrocarbon systems. For systems in which P_r of the vapour phase during blowdown is above 3, the application of TCC CEOS is recommended (see conclusions in chapter 5). However, for systems in which T_r of the liquid phase is likely to be below 0.6, SRK and PR CEOS should be used .

It is also important to note that the exact fluid composition prior to blowdown should be obtained when any of the above CEOS is used as the corresponding estimated fluid phase envelope is very sensitive to the fluid composition. The latter will directly affect blowdown data.

CHAPTER 7

CONCLUSIONS AND SUGGESTIONS FOR FUTURE WORK

7.1 CONCLUSIONS

This thesis describes the development of a mathematical model, BLOWSIM, for simulating vapour space blowdown of an isolated vessel containing single (vapour) or two-phase (vapour and liquid) hydrocarbon mixtures. The main incentive for this work has been the lack of a robust and readily available model for such simulations.

The work is in the main divided into two parts. The first part deals with an extensive evaluation of the performances of SRK, PR and the recently developed TCC CEOS in terms of predicting the required thermophysical properties for blowdown simulation. This is carried out by comparing predictions from the various CEOS against published experimental data for density and speed of sound for some typical multi-component hydrocarbon mixtures at a range of pressures and temperatures. This is the first time TCC CEOS has been validated against experimental data for these types of systems. On their own merit therefore, our findings under this heading have an additional important implication in terms of establishing the suitability of the TCC CEOS for process simulation. This is particularly so in view of the fact that the equation has been specifically developed in order to address some of the important shortcomings of the SRK and PR CEOS.

The development and validation of BLOWSIM in conjunction with the three CEOS as well as comparisons with the numerical predictions from BLOWDOWN [Haque et. al., 1992a] are described in the second part of the thesis.

Our major findings regarding the performances of the three CEOS may be summarised as follows :

- In general, even without the use of binary interaction parameters, all three CEOS are capable of accurately predicting vapour densities for multi-component mixtures mainly containing light hydrocarbons (C_1 to n-C_3) with small amounts of H_2S (< 7% mole) at elevated pressures (ca. 80 bar). With the exception of PR

CEOS, similar observations are made in the case of liquid systems containing mainly light hydrocarbons with moderate amounts of H_2S (< 25% mole) at the same pressure ranges.

- In terms of predicting vapour speeds of sound for vapour mixtures containing mainly C_1, TCC CEOS consistently performs better than the other CEOS at P_r >3 whilst PR gives the worst performance. On the other hand, at conditions outside the above region, all three CEOS perform equally well. This indicates that TCC CEOS is more effective at high reduced pressures for vapour hydrocarbon mixtures. However, at or near the critical region of the vapour mixtures, all three CEOS give rise to large errors. This seems to be an inherent problem associated with CEOS.

Different behaviour from the above are observed in terms of predicting speeds of sound for compressed liquid alkanes, C_1 to n-C_9. We find that:

- In the case of light alkanes, C_1 to n-C_4, both SRK and TCC CEOS generally perform reasonably well with PR CEOS giving the worst performance. Conversely, for heavier alkanes, n-C_5 - n-C_9, PR CEOS gives the best results whilst the worst performance is associated with TCC CEOS.

- As a function of reduced temperature (T_r), TCC CEOS gives rise to relatively large errors at $T_r \leq 0.6$ for all compressed liquid alkanes. For C_1 and C_2, this is because the predicted values of $\left(\frac{\partial P}{\partial v}\right)_T$ are too large compared with the corresponding values calculated from other CEOS. This is also very likely to be the main reason attributable to the poor performance of TCC CEOS at low T_r for other liquid alkanes.

- For saturated liquid alkanes (n-C_3 - n-C_5), TCC CEOS gives the best overall performance for n-C_3 and n-C_4. This is mainly due to the comparatively better capability of TCC CEOS in predicting the correct fluid state. All three CEOS give similar accuracy by predicting vapour-like behaviour for saturated liquid n-C_5.

The results of our evaluations on the performance of BLOWSIM compared to the numerical data from BLOWDOWN as well as experimental data relating to non-condensable gas, condensable gas and two-phase mixtures mainly containing methane, ethane and propane with trace amount of butane reveal that:

- For the vapour phase, for $P_r < 3$ and in the case of the liquid phase, for $T_r > 0.6$, all three CEOS lead to similar predictions from BLOWSIM. For vapour phase conditions corresponding to $P_r > 3$, we recommend the use of TCC CEOS. However, for systems in which T_r of the liquid phase is likely to be below 0.6, SRK or PR CEOS should be used.

- It is important to note that the exact fluid composition prior to blowdown should be obtained when any of the above CEOS are used as the corresponding estimated fluid phase envelope is very sensitive to the fluid composition. The latter will directly affect the blowdown prediction.

- Based on the results of comparison for all three hydrocarbon systems, the vapour thermodynamic trajectory used in SPLIT FLUID MODEL [Overa et al., 1994] is shown to be applicable to both vapour and liquid phases for simulating high pressure blowdown.

- In the case of the condensable gas, BLOWSIM satisfactory predicts (± 5 K) the bulk liquid and wetted wall temperatures.

- For all three systems tested, BLOWSIM predicts very accurate vessel pressure/time profiles. Also, the bulk vapour and unwetted wall temperatures are predicted to within 7K and 4K respectively

- In the case of the condensable gas, the earlier formation of liquid phase predicted from BLOWSIM as compared to BLOWDOWN is attributed to the use of different types of EOS rather than the assumptions of instantaneous formation and immediate settlement of liquid droplets condensed from the vapour phase employed in the former model.

- From the results of comparison for the two-phase mixture, the effects due to nucleation and gravitational settlement of liquid droplets condensed from the vapour phase, should be accounted for in blowdown simulation. Discounting such effects may lead to over estimation of the bulk liquid and wetted wall temperatures. This is with the exception of cases where the amount of liquid either present prior to blowdown or formed at the first instant of condensation is enough to overcome the effects of subsequent condensation on the mass and energy balances for the liquid phase.

- Based on the results of comparisons for all three hydrocarbon systems tested, the effects due to force convection within the vapour phase and heat transfer between the vessel and the surrounding can be discounted. However, under extreme conditions (e.g. under fire or extreme weather conditions), the heat flux between the vessel and the surrounding should be considered. The effects due to temperature gradient across the thickness of the vessel wall associated with either vapour or liquid phase can be ignored.

- The main mode of heat transfer between the liquid phase and vessel wall is nucleate boiling. The corresponding heat flux can be estimated by assuming a constant heat transfer coefficient between liquid and wall during blowdown. The recommended values of heat transfer coefficient are 2000 - 3000 W/m^2K. Similar estimations of the boiling heat flux are produced if Rohsensow's correlation is used.

- CPU time can be significantly reduced (by at least two thirds) by assuming ideal gas behaviour at the orifice without compromising the accuracy in predicting the minimum fluid and wall temperatures. However, it is important to note that the minimum fluid temperatures at the orifice for all three mixtures are consistently underestimated. This may give rise to engineering problems as well as leading to incorrect down-stream conditions.

- CEOS provide an efficient and satisfactory means of providing the necessary thermodynamic and VLE data required in blowdown simulation. The fact that such equations are being constantly developed in order to improve their accuracy

and range of applicability is an added important incentive for their use in conjunction with blowdown simulations.

In conclusion, we believe that the value of this study can be significantly improved by comparison of the results of our model with a wider range of experimental data and conditions. Such data would be important for validation as well as being directly useful for modelling purposes. The latter is because blowdown involves a large number of relatively complex processes which may be extremely difficult to model on a purely predictive basis. It is therefore inevitable that a robust mathematical model will rely, to some extent on empirical correlations.

Unfortunately experimental data of this nature are often difficult to obtain due to the high capital equipment costs involved as well as the associated safety implications. Industry seems to be the only source with sufficient resources to address this important issue. However, the limited data that are available are often proprietary. Our experience has been that even in the case of published data relating to the more sophisticated blowdown models, important information relating to the precise experimental conditions and mathematical formulation are either missing or in some cases are incorrect. Once again, the common explanation in such circumstances is restrictions due to industrial proprietary. In general we believe that the pace of progress for studies such as ours very much depends on a change of culture within the process engineering industry.

7.2 SUGGESTIONS FOR FUTURE WORK

Further investigations of TCC CEOS performance

So far, the results of our study indicate that the effect of the modifications introduced in TCC CEOS in order to address the shortcomings of the PR and SRK CEOS is particularly evident in terms of improving the prediction of vapour speed of sound for light hydrocarbon mixtures at conditions above critical temperatures and pressures. It would be useful to investigate the validity of the same argument at conditions below the critical temperatures and pressures. Similarly, additional experimental data are required in order to investigate if the poor performance of TCC

CEOS in predicting liquid speed of sound for pure alkanes at low T_r also applies in the case of multi-component hydrocarbon systems. A useful extension of this study would be undertaking of a similar exercise in conjunction with heavy hydrocarbons.

Use of multiple thermodynamic properties data for improving TCC CEOS performance

In chapter 5, we demonstrated the problems associated with just using saturated liquid densities for correlating the parameters in TCC CEOS. Although this approach produces relatively accurate values of fluid density, it gives rise to a poor estimates of liquid speed of sound at low reduced temperatures. The use of more than one thermodynamic property, rather than just density for producing the necessary parameters in TCC CEOS is expected to address this issue.

Haque et al. [1992a] correlations for determining the nucleation time and settling velocity of liquid droplets during blowdown

In chapter 6, we demonstrated the high sensitivity of blowdown predictions on the accuracy of predicting nucleation time and settling velocity of liquid droplets condensed from the vapour phase in the vessel. Further investigations on the validity of Haque et al's [1992a] empirical equations for determining these two parameters outside the range of correlation are required. If the equations are shown to be system dependent, additional experimental studies would be required for developing correlations for other systems.

The effect of using pseudo-components in conjunction with CEOS

In chapter 6, we demonstrated the importance of obtaining the exact fluid compositions for blowdown simulations. However, such information is not usually available during conceptual design. Consequently, the use of pseudo-components based on lumping hydrocarbon components is usually applied. Additional investigation on the effects of applying such techniques on blowdown simulations is required.

REFERENCES

API Recommended Practice 521, *Guide for Pressure-Relieving and Depressuring Systems*, 3rd edition, 19 (1990)

Aly, F.A., and Lee, L.L., *Self-Consistent Equations for Calculating the Ideal-Gas Heat-Capacity, Enthalpy and Entropy*, Fluid Phase Equilibria, **6**, 169-179 (1981)

Anderson, C., et. al., *The Effects of a Fire Environment on a Rail Tank Car Filled with LPG*, Ballistic Research Lab., US Army (1974)

Assael, M.J., Trusler, J.P.M., and Tsolakis, T.F., *Thermophysical Properties of Fluids, An Introduction to Their Prediction*, Imperial College Press., Chapter 6 (1996a)

Assael, M.J., Trusler, J.P.M., and Tsolakis, T.F., *Thermophysical Properties of Fluids, An Introduction to Their Prediction*, Imperial College Press., Chapter 9 (1996b)

Assael, M.J., Trusler, J.P.M., and Tsolakis, T.F., *Thermophysical Properties of Fluids, An Introduction to Their Prediction*, Imperial College Press., Chapter 10 (1996c)

Bejan, A., *Convection Heat Transfer*, John Wiley & Sons, 2nd edition, Chapter 4 (1995a)

Bejan, A., *Convection Heat Transfer*, John Wiley & Sons, 2nd edition, Chapter 10 (1995b)

Belinskii, B.A., and Ikramov, Sh.Kh., *Comprehensive Investigation of the Acoustical Parameters, Viscosity, and Density of n-Pentane over a Wide Pressure Interval*, Soviet Physics-Acoustics, **18 (No.3)**, 300 - 303 (1973)

Berenson, P.J., *Film-boiling Heat Transfer from a Horizontal Surface*, Trans ASME J. Heat Transfer, **83**, 351 - 358 (1961)

Bett, K.E., Rowlinson, J.S., and Saville, G., *Thermodynamics for Chemical Engineers*, Athlone, London, 196 (1975)

Boelhouwer, J.W.M., *Sound Velocities in and Adiabatic Compressibilities of Liquid Alkanes at Various Temperatures and Pressures*, Physica, **34**, 484 - 492 (1967)

Bransom, S.H., *Applied Thermodynamics*, D. Van Nostrand Company, 1st edition, 133 (1961)

Burmeister, L.C., Convective Heat Transfer, John Wiley & Sons , INC., 1st edition, Chapter 11 (1993)

Byrnes, W.R., Reid, R.C. and Ruccia, F.E., *Rapid Depressurization of a Gas Storage Cylinder*, I&EC Process Design and Development, **3**, 206 - 209 (July 1964)

ChemCAD III user guide, Chemstation Inc., 1993

Churchill, S.W., and Chu, H.H.S., *Correlating Equations for Laminar and Turbulent Free Convection from a Horizontal Cylinder*, Int J Heat Mass Transfer, **18**, 1049 - 1053 (1975)

Cullen, W.D., *The Public Enquiry into the Piper Alpha Disaster*, London:HMSO, 393 (1990)

Danesh, A., Xu, D.H., and Todd, A.C., *Comparative Study of Cubic Equations of State for Predicting Phase Behaviour and Volumetric Properties of Injection Gas-Reservoir Oil Systems*, Fluid Phase Equilibria, **63**, 259 - 278 (1991)

Daridon, J.L., Lagourette, B., *Ultrasonic Velocity Measurements at High Pressure for the Thermophyical Characterization of a Ternary Mixture*, Acustica, **82**, 32 - 38 (1996)

Eastop, T.D., and McConkey, A., *Applied Thermodynamics for Engineering Technologists*, Longman Scientific & Technical, 5th edition, Chapter 10 (1993)

Eggers, R., and Green, V., *Pressure Discharge from a Pressure Vessel Filled with CO_2*, J.Loss Prev. Process Ind., **3**, 59 - 63 (January 1990)

Ely, J.F., and Hanley, H.J.M., *Prediction of Transport Properties. 1. Viscosity of Fluids and Mixtures.*, Ind. Eng. Chem. Fundam., **20**, 323 - 332 (1981)

Ely, J.F., and Hanley, H.J.M., *Prediction of Transport Properties. 2. Thermal Conductivity of Pure Fluids and Mixtures.*, Ind. Eng. Chem. Fundam., **22**, 90 - 97 (1983)

Gundersen, Truls., *Numerical Aspects of the Implementation of Cubic Equations of State in Flash Calculation Routines*, Computers and Chemical Engineering, **6 (No.3)**, 245 - 255 (1982)

Haque, M.A., Richardson, S.M., Saville, G., and Chamberlain, G., *Rapid Depressurization of Pressure Vessels*, J. Loss Prev. Process Ind., **3**, 4 - 7 (1990)

Haque, M.A., Richardson, S.M., and Saville, G., *Blowdown of Pressure Vessels. I. Computer Model*, Trans IChemE Part B: Process Safety Environmental Protection., **70 (BI)**, 1 - 9 (1992a)

Haque, M.A., Richardson, S.M., and Saville, G., Chamberlain, G., and Shirvill, L., *Blowdown of Pressure Vessels. II. Experimental Validation of Computer Model and Case Studies*, Trans IChemE Part B: Process Safety Environmental Protection., **70 (BI)**, 10 - 17 (1992b)

Incropera, F.P., and De Witt, D.P., *Fundamentals of Heat and Mass Transfer*, John Wiley & Sons, 2nd edition, Chapter 5 (1985)

Incropera, F.P., and De Witt, D.P., *Fundamentals of Heat and Mass Transfer*, John Wiley & Sons, 4th edition, Chapter 9 (1996a)

Incropera, F.P., and De Witt, D.P., *Fundamentals of Heat and Mass Transfer*, John Wiley & Sons, 4th edition, Chapter 10 (1996b)

Incropera, F.P., and De Witt, D.P., *Fundamentals of Heat and Mass Transfer*, John Wiley & Sons, 4th edition, Appendix A (1996c)

Jhaveri, B.S. and Youngren, G.K., *Three-Parameter Modification of the Peng-Robinson Equation of State to Improve Volumetric Predictions*, SPE 13118 (1984)

Jordan, D.P., *Film and Transition Boiling, Advances Heat Transfer*, **5**, 55 - 128 (1968)

Kalra, H., and Robinson, D.B., *Vapor-Liquid Equilibrium in a Six-Component Simulated Sour Natural Gas System at Sub-Ambient Temperatures,* Fluid Phase Equilibria, **3**, 133 - 144 (1979)

Katz, D.L., and Lee, R.L., *Natural Gas Engineering - Production and Storage*, McGraw-Hill, 1st edition, Chapter 5 (1990)

Kreith, F., and Black, W.Z., *Basic Heat Transfer*, New York : Harper and Row, 1st edition (1980)

Lienhard, J.H., and Dhir, V.K., *Hydrodynamic Prediction of Peak Pool-Boiling Heat Fluxes from Finite Bodies*, Tran ASME J. Heat Transfer, **95**, 152 - 158 (1973)

Lagourette, B., Daridon, J.L., Gaubert, J.F., and Saint-Guirons, H., *High-Pressure Ultrasonic Speeds in a Ternary Condensate Gas : {0.880 CH_4 + 0.100 C_3H_8 + 0.020 $CH_3(CH_2)_6CH_3$} (g)*, J.Chem.Thermodynamics, **27**, 259 - 266 (1995)

Lagourette, B., Daridon, J.L., Gaubert, J.F., and Xans, P., *Experimental Determination of Ultrasonic Speeds in (Methane + Propane) (g) and in (Methane + Octane) (g) at High Pressures*, J.Chem.Thermodynamics, **26**, 1051 - 1061 (1994)

Mayinger, F., *The State of Knowledge of Thermohydraulic Pressure Release Phenomena*, German Chemical Engineering, **5**, 297 - 305 (1982)

McAdams, W.H., *Heat Transmission*, McGraw-Hill Book Company, 3rd edition, 172 (1954)

Michelsen, M.L., *The Isothermal Flash Problem. Part I. Stability*, Fluid Phase Equilibria, **9**, 1 - 19 (1982)

Millat, J., Dymond, J.H., and Nieto de Castro, C.A., *Transport Properties of Fluids - Their Correlation, Prediction and Estimation*, IUPAC, Cambridge University Press, 1st Edition, Chapter 8 (1996)

Montgomery, G., *How to Predict Temperatures During Gas Depressuring*, Hydrocarbon Processing, 85 - 88 (April 1995)

Moodie, K., Cowley, L.T., Denny, R.B., Small, L.M. and Williams, I., *Fire Engulfment Tests on a 5 Tonne LPG Tank*, Journal of Hazardous Materials, **20**, 55 - 71 (1988)

Niepmann, R., *Thermodynamic Properties of Propane and n-Butane 2. Speeds of Sound in the Liquid up to 60 MPa*, J. Chem. Thermodynamics, **16**, 851 - 860 (1984)

Norris III, H.L., *Single-Phase or Multiphase Blowdown of Vessels or Pipelines*, SPE 68th Annual Technical Conference, Houston, Texas, 519 - 528 (October 1993)

Norris III, H.L., *Hydrocarbon Blowdown from Vessels and Pipelines*, SPE 69th Annual Technical Conference and Exhibition, New Orleans, LA, 593 - 602 (September 1994)

Overa, S.J., Stange, E., and Salater, P., *Determination of Temperatures and Flare Rates During Depressurization and Fire*, Proceedings of 72th GPA Annual Convention., 235 - 247 (1994)

Peneloux, A., Rauzy, E., and Freze, R., *A Consistent Correction for Redlich-Kwong-Soave Volumes*, Fluid Phase Equilibria, **8**, 7 - 23 (1982)

Peng, D.Y., and Robinson, D.B., *A New Two-Constant Equation of State*, Ind. Eng. Chem. Fundam., **15**, 59 - 64 (1976)

Perry, R.H., and Chilton, C.H. (editors), *Chemical Engineers' Handbook*, McGraw-Hill, New York, 5th edition, 10-10 to 10-12 (1973a)

Perry, R.H., and Chilton, C.H. (editors), *Chemical Engineers' Handbook*, McGraw-Hill, New York, 5th edition, 10-12 to 10-15 (1973b)

Picard, D.J., and Bishnoi, P.R., Calculation of the Thermodynamic Sound Velocity in Two-Phase Multicomponent Fluids, Int. J. Multiphase Flow, **13 (No. 3)**, 295-308 (1987)

Press, W.H., Teukolsky, S.A., Vetterling, W.T., and Flannery, B.P., *Numerical Recipes in FORTRAN 77 : The Art of Scientific Computing*, Cambridge University Press, 2nd edition, Chapter 9 (1992)

Potter, J.H., and Levy, M.J., *The Free Expansion of Dry and Moist Air,* Journal of Engineering for Industry, **83**, 97 - 100 (February 1961)

Ramskell, P.K., *Discharge Rate Calculation Methods for Use in Plant Safety Assessments*, SRD/HSE/R35L (February 1987)

Ramskill, P.K., *A Description of the ENGULF Computer Codes - Codes to Model the Thermal Response of an LPG Tank Either Fully or Partially Engulfed by Fire*, J. of Hazardous Material, **20** (1988)

Redlich, O. and Kwong, N.S., *On the Thermodynamics of Solutions. V: An Equation of State. Fugacities of Gaseous Solutions*. Chem. Rev. **44**, 233 (1949)

Reid, R.C., Prausinitz, J.M., and Sherwood., T.K., The Properties of Gases and Liquids., McGraw-Hill Book Company., 3rd Edition, 629 (1977)

Reid, R.C., Prausinitz, J.M., and Sherwood., T.K., The Properties of Gases and Liquids., McGraw-Hill Book Company., 4th Edition, 642 (1986)

Reynolds, W.C., and Kays, W.M., *Blowdown and Charging Processes in a Single Gas Receiver with Heat Transfer*, Trans ASME., **80**, 1160 - 1168 (July 1958)

Richardson, S.M., *Private conversation* (February 1997)

Richardson, S.M., *Private conversation* (April 1998)

Richardson, S.M., and Saville, G., *Release the Pressure*, The Chemical Engineer, **617**, 14 -16 (15 August 1996)

Rohsenow, W.M., *A method for Correlating Heat-Transfer Data for Surface Boiling of Liquids*, Trans ASME, **74**, 969 - 976 (1952)

Rowlinson, J.S., and Watson, I.D., *The prediction of the Thermodynamic Properties of Fluids and Fluid Mixtures , I. the Principle of Corresponding States and its Extensions*, Chem. Eng. Sci., **24**, 1565 - 1574 (1969)

Saville, G. and Szczepanski, R., *Methane-Based Equations of State for a Corresponding States Reference Substance*, Chem. Eng. Sci., **37**, 719 - 725 (1982)

Schulz-Forberg, B., Droste, B., Charlett, H., *Failure Mechanisms of Propane-Tanks under Thermal Stresses Including Fire Engulfment*, Budesanstalt fur Materialprufung, Berlin, Germany (1983)

Shapiro, A.H., The Dynamics and Thermodynamics of Compressible Fluid Flow, The Ronald Press Company, 1st edition, Chapter 4 (1953)

Soave, G., *Equilibrium Constants from a Modified Redlich-Kwong Equation of State,* Chem. Eng. Sci., **27**, 1197 - 1203 (1972)

Straty, G. C., *Velocity of Sound in Dense Fluid Methane*, Cryogenics, 367 - 370 (July 1974)

Szczepanski, R., *Simulation Programs for Blowdown of Pressure Vessels*, IChemE SONG Meeting 12 April 1994

Thomas, L.H., *Comm Pure Math*, **7**, 195 (1954)

Tsonopoulos, C., and Heidman, J.L., *High-Pressure Vapor-Liquid Equilibria with Cubic Equations of State,* Fluid Phase Equilibria, **29**, 391 - 414 (1986)

Tsumura, R., and Straty, G.C., Speed od Sound in Saturated and Compressed Fluid Ethane, Cryogenics, 195 - 200 (April 1977)

Twu, C.H., *Private conversation* (15 March 1997a)

Twu, C.H., *Private conversation* (26 November 1997b)

Twu, C.H., Bluck, D., Cunningham, J.R., and Coon, J.E., *A Cubic Equation of State with a New Alpha Function and a New Mixing Rule.*, Fluid Phase Equilibria, **69**, 33 - 50 (1991)

Twu, C.H., Coon, J.E., and Cunningham, J.R., *A New Cubic Equation of State.*, Fluid Phase Equilibria, **75**, 65 - 79 (1992)

Twu C.H., Coon, J.E., and Cunningham, J.R., A New Generalized Alpha Function for a Cubic Equation of State Part 1. Peng-Robinson Equation, **105**, 49 - 59 (1995a)

Twu C.H., Coon, J.E., and Cunningham, J.R., A New Generalized Alpha Function for a Cubic Equation of State Part 2. Redlich-Kwong Equation, **105**, 61 - 69 (1995b)

Welty, J.R., Wicks, C.E., and Wilson, R.E., *Fundamentals of Momentum, Heat and Mass Transfer*, Wiley, 3rd edit., Chapter 21 (1984)

White, F.M., *Fluid Mechanics*, McGraw-Hill, 3rd edit., Chapter 9 (1994)

Wilson, A., Overa, S., Stange, E., and Majeed, A., Developing , *Implementing and Verifying an Engineering Tool*, 69th Annual GPA Convention (March 11 - 12, 1991)

Ye, S., Lagourette, B., Alliez, J., Saint-Guirons, H., and Xans, P., *Comparison with Experimental Data of Ultrasound Velocity in Pure Hydrocarbons Calculated from Equations of State*, Fluid Phase Equilibria, **74**, 157 - 175 (1992)

Younglove, B.A., and Frederick, N.V., *Sound Speed Measurements on Gas Mixtures of Natural Gas Components Using a Cylindrical Resonator*, International Journal of Thermophysics, **11**, No. 5, 897 - 910 (1990)